Predicting variations in the areas of circular leaks in water pipes due to changes in pressure

Prepared by:
Rene Nsanzubuhoro

For supervisor:
Prof. J. E. van Zyl

And co-supervisor:
Prof A Zingoni

In partial fulfilment of the requirements for:
Master of Science in Engineering

Submission Date: 25 Fèbuary 2016
Institution: University of Cape Town
Faculty: Engineering and the Built Environment
Department: Civil Engineering

Plagiarism Declaration

1. I know that plagiarism is wrong. Plagiarism is to use another's work and to pretend that it is one's own.

2. I have used the Harvard Convention for citation and referencing. Each significant contribution to and quotation in this report form the work or works of other people has been attributed and has been cited and referenced.

3. This report is my own work

4. I have not allowed and will not allow anyone to copy my work with the intension of passing it as his or her own work.

Student number: NSNREN001

Name: Rene Nsanzubuhoro

Date: 25 February 2016

Signature: R. Nsanzubuhoro

Abstract

Leak openings in water distribution system pipes are not static, but have areas that vary with pressure. These changes in area affect the way that leakage respond to changes in pressure, and was thus important for municipal engineers to understand.

This study focussed on round hole leak openings that can exist as pipe failures. In this study, a finite element analysis (FEA) study was carried out to model the behaviour of round holes in pipes with varying pressure under elastic conditions. It was found that the areas of the holes vary as linear functions of pressure in the pipe. The slope of this linear function, also referred to as the head-area slope *m*, was identified as a critical element to investigate because this head-area slope essentially gives an indication of the extent to which the leak area is sensitive to pressure.

The FEA was then used to better understand the factors that affect the head-area slope *m*. In order to understand which parameters affect the head-area slope *m*, a parametric study was conducted. This parametric study was done by varying each parameter in turn to study the effect of that parameter on the head-area slope of the pipe.

The parameters investigated in the study include the pipe material (elastic modulus, Poisson's ratio and longitudinal stress), pipe geometry (wall thickness and internal diameter) and hole diameter. It was found in this study that of the five aforementioned geometric and material parameters, the elastic modulus, wall thickness and internal diameter had the most significant effect on the head-area slope *m*. The extent to which these parameters influenced *m* depended on the hole diameter. It was found that as the hole diameter increased the effect of the parameter was more significant.

Solid mechanics theory was then used to develop an equation to predict the head-area slope of round holes in different pipes and materials. Various techniques were used in the development of the equation. To calibrate and validate this equation the head-area slopes calculated from the equation were compared and plotted against the finite element head-area slopes.

A reasonable expression was found that can be used in further research and practice. The head-area slopes *m* obtained from this equation was compared to the head-area slopes *m* obtained in the FEA analysis. It was found that this expression predicts the finite element model analysis reasonably well, producing trends that are similar to those found from the finite element models.

Acknowledgements

I would like to express my sincerest gratitude and thank the following people who have assisted me in different ways throughout this research project.

First and foremost, my supervisor, *Prof. J. E. van Zyl*, for his continuous support, guidance, motivation, enthusiasm, and vast knowledge. He has been a great supervisor.

My co-supervisor *Prof Alphose Zingoni* for his advice and guidance in the project.

The *Mandela Rhodes Scholarship* for sponsoring my tuition.

Xochiwe Jere, my fiancè, for her moral support, motivation and encouragement throughout my research.

Finally, and most importantly I wish to thank my family; my parents *Emmanuel Nsanzubuhoro* and *Martha Nsanzubuhoro* for raising me, supporting me, teaching me and loving me. To them I dedicate this thesis.

Table of Contents

List of Figures

List of Tables

1 Introduction

1.1 Background of Study

Leakage in water distribution systems, for many years, has been drawing much attention to the water industry. Leakage is a serious cause of concern because only less than 1% of the earth's water is suitable for human consumption (WISA, 2009) and therefore interventions need to be in place to avoid losses of this limited resource. Water losses from distribution systems can be real losses (through leaks, sometimes referred to as physical losses) or apparent losses (water theft, billing inaccuracies or even metering inaccuracies) (Vermersh & Rizzo, 2008).

Farley (2001) indicated that the bulk of water loss is due to real losses. In South Africa for example, a study done by Mckenzie, et al., (2012) which entailed analyzing 62 systems, showed that on average 31% of water supplied to urban systems or 670 million cubic meters of water per annum is lost through leakages in pipes. Shingo Adachi (2014) also highlighted that leakage does not only cause water losses; it also causes economic losses, water contamination risks, excessive environmental load in terms of water resources and operational energy consumption Leakage, therefore, is a great concern for South Africa and the international community at large.

Van Zyl, et al., (2008) indicated that the water distribution systems leakage is highly sensitive to the systems pressure. In 2007, van Zyl and Clayton proposed four factors that may be responsible for the high sensitivity of leakage to pressure, and these were; leak hydraulics, pipe material behaviour (variation of leak area as a function of pressure), soil hydraulics and water demand.

May (1994) was first to suggest that the leak area in a pipe increases as the pressure in the pipe increases. In light of this, significant developments have been made in the understanding of the relationship between leakage and pressure.

For example, Cassa & Van Zyl's (2011) study investigated the relationship between pressure and leak area in pipes with longitudinal, circumferential and spiral cracks using finite element analysis. Cassa & Van Zyl's (2011) study focused on elastically deforming materials. Their study showed that the leak area was linearly proportional to the pressure in the pipe. This linearity, however, is only true for linear elastic behaviour and does not necessarily represent the behaviour of all the leaks that can be found in distribution systems. For example, Ferrante et al (2011) showed that plastic pipe materials are sometimes subject to hysteresis, and therefore do not adhere to the assumption of elastic behaviour. For the purposes of this study all leaks are limited to linear elastic behaviour.

The slope of the linear line linking the leak area and the pressure was referred as the pressure-area slope in Cassa & Van Zyl's (2011) study, but will be referred to as the head-area slope throughout this study. This head-area slope m was investigated using a parametric study,

where material and geometric parameters were varied in order understand the effect each parameter has on this gradient.

Understanding the head-area slope is a useful development because the head-area slope can show how sensitive the systems leakage is to pressure. With this in mind, Cassa and van Zyl (2011) developed empirical equations for predicting the head-area slope for crack defects on the pipe. These equations assist in formulating mathematical formulas that predict the head-area slope response of the different cracks to variations in material and geometric properties of a system.

These empirical equations currently exist only for the cracks Cassa and van Zyl (2011) investigated, namely: spiral, longitudinal and circumferential. However, cracks are not the only type of leak defects that occur in water distribution pipes. Round holes for example are another common occurrence when it comes to defects in pipe materials (JM. Rodriguez, 2012). This study will therefore focus specifically on round holes and develop understanding of the head-area slope of round holes.

In light of what is known about round hole leaks and their behavior, semi-empirical equations that can be used to predict the head-area slopes for round holes will be developed. Solid mechanics theory will be used to develop an equation to predict the head-area slope of round holes in different pipes and materials. Various techniques will also be used in the development of the equation, and a reasonable expression for the head-area slope of round holes will be presented. This expression can be used in further research and practice.

1.2 Goals and Objectives

This study presents an analysis of leakage behaviour, particularly through round holes, in water distribution system pipes with variation of pressure under elastic conditions. The objectives of this dissertation are to:

- Provide a literature review of current understanding of relevant pipe materials used in water distribution networks and investigate factors affecting leakage in these pipe materials.
- Provide a literature review of previous work done in developing theoretical analyses on round hole deformation within pressurised pipes.
- Develop a theoretical analysis for the head-area slope with an equation that helps predict the response of the head-area slope of a round hole leak for different material and geometric properties.
- Conduct a Finite Element Analysis (FEA) study on round holes to determine the relationship of pressure and leakage for different round holes, and the behaviour of the head-area slope that results from this.
- Conduct a parametric study to investigate how material and geometric properties affect the head-area slope m of round holes.
- Compare the results of the theoretical head-area slope m model and the FEA head-area slope m.
- Determine the implication of results for leakage through round holes.

1.3 Limitation and Scope of the Investigation

This study is limited to round holes that undergo elastic deformations only. The theoretical equation developed is derived from elastic solid mechanics theory. The finite element models used for the FEA are simulated as purely elastic. Because of these conditions, failure modes beyond elastic deformation, which leaks may undergo are not included (i.e. creep, plastic deformation, fracture or any other irreversible deformation). However, the elastic limit assumption is a reasonable assumption because, in practice, the system pressures typically do not exceed the elastic limits of the pipe material.

1.4 Layout of this Dissertation

This study will divide the chapters as follows:

The literature review analysis is presented in Chapter 2. The literature review gives some background on the various pipe materials used in water distribution systems. The failure mechanisms of the pipe materials are outlined using the stress and strain analyses of the material. Finally a discussion on the finite element product to be used in the study is provided.

Chapter 3 is a short chapter that explains how mathematical models were used to validate some of the assumptions found in literature. In particular, the assumption that circular holes deform into elliptical holes once the pipe is pressurised.

Chapter 4 entails the methodology on how the finite element models were setup and simulated. Finite element simulations are run, and comparisons are done with an experimental study.

Chapter 5 shows the results obtained from the finite element analysis for the head-area slope for different round holes

Chapter 6 describes the two data processing techniques examined to obtain an expression for the head-area slope of different round holes. The dimensional analysis and regression analysis are the techniques adopted here.

Chapter 7 then attempts to develop an expression that can predict the head-area slope for round holes using a more theoretical approach.

Chapter 8 follows with a comparison of the head-area slopes m obtained from the derived theoretical expression and the head-area slope obtained from the finite element model results.

Chapter 9 contains the conclusions and recommendations for further studies.

Chapter 10 is the final chapter and contains all the Appendices.

2 Literature Review

This review begins by looking into various pipe materials, used in industry, understanding their various properties and failure mechanisms. The review then unfolds how these materials behave under pressurised conditions. This is then followed by developing an understanding of what causes the occurrence of the leaks found in these pipe materials, specifically the round hole leaks, and how these leaks behave.

The concept of leakage being linked to the systems pressure is explored in detail. Various pressure–leakage relationships are looked at, and the factors affecting these relationships are highlighted.

2.1 Pipe Materials

This section deals with various pipe materials that are used in industries, as well as the various failure mechanisms that occur in these pipes. The main pipes that will be explored are plastic, steel and cast iron. These pipe materials will be explored by investigating their stress and strain behaviour. Understanding the stress-strain behaviour of the materials helps unfold how the material behaves under various loading conditions (in the case of a pipe, this includes internal pressure). In addition to this, different potential failure modes can be highlighted from the material stress-strain behaviour profile.

Farshad (2006) cited by Cassa (2011) describes a 'failure event' in a pipe or pipeline as a situation where its function has been hindered, its configuration has changed, its integrity jeopardised and where potential harm to the environment exists. For example, the occurance of a leak causes the fluid contained in the pipe to escape and, thus, hindering the function of the pipe.

A good understanding of the behaviour of pipe materials is important in order to understand conditions that lead to pipe failure. This section goes on to develop literature around the various pipe materials and their failure mechanisms.

2.1.1 Polymers and Plastics

Plastics are composed of very large molecules called polymers. These large molecules are constructed from monomers which are much smaller molecular fragments that are joined together, as shown in Figure 2-1. Polymerisation is the process by which monomers react to form polymers.

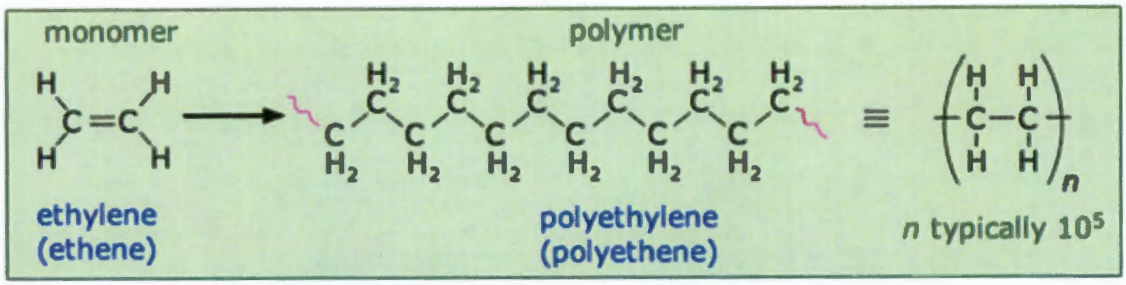

Figure 2-1: Polymerisation Process (gcsescience, 2015)

As can be seen from Figure 2-1, polymers are primarily made up of carbon and hydrogen. Sometimes other elements such as oxygen, nitrogen, chlorine and fluorine can exist.

In the water industry synthetic polymers include polyvinyl chloride (PVC), polyethylene, polypropylene and polystyrene. Polymers emerged in the early twentieth century. Chemists' engineered them to yield a desired set of properties and, because of this, plastics play many roles in the modern industrial economy (Lower, 2009). This study will focus mainly on the synthetic polymers.

Synthetic polymers are generally divided into three distinct groups: thermoplastics, thermosetting and elastomeric polymers. The thermoplastics can be heated and reformed over and over once formed. The thermosetting polymers cannot be remoulded or reformed once formed. These two differ in that heating the thermosetting results in a three dimensional network that can no longer allow the long chains to flow freely past one another. Finally, the elastomer, which are generally polymers with weak cross-linking, and are capable of large recoverable strains (Farshad, 2006).

2.1.1.1 Stress Strain Behaviour of Polymers

The stress-strain behaviour of solid polymers can be grouped into three behavioural classes: brittle behaviour, yield behaviour and rubber-like behaviour. Brittle behaviour is characterised by no yield point (see Figure 2-2), brittle materials show little or no plastic deformation before fracture. For yield behaviour, there is a maximum in the stress strain curve, which is typically followed by yielding deformation (see Figure 2-2). This is usually associated with ductile failure and typically demonstrates large amounts of plastic deformation before catastrophic failure occurs. Finally, the rubber like behaviour is characterised by the absence of a maximum yield point but does exhibit a plateau on the stress strain curve (see Figure 2-2).

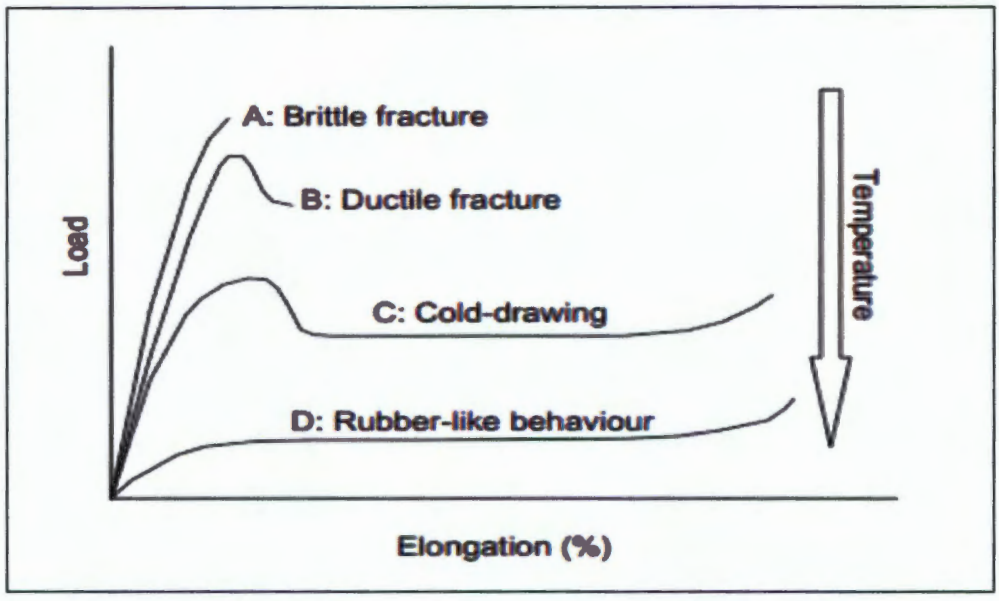

Figure 2-2: Load Elongation Curves for Polyethylene at Different Temperatures (Cassa & Van Zyl, 2011)

Depending on the temperature and time scale of measurement all three types of behaviour can be exhibited in a single polymer (Ward, 1971). Figure 2-2 showed how a polyethylene polymer has different load-elongation curves at different temperatures. It can be seen that at temperatures that are below the glass transition (curve A), brittle fracture occurs and the load rises linearly, with increasing strains, until rupture occurs at low strains. At high temperatures (Curve D), the polymer behaves like a rubber and the load rises to a breaking point with an S-curve relationship to the elongation, in which case the rapture occurs at very high strains. In an intermediate temperature range that is below the glass transition (Curve B), the load in this regime resembles that of a ductile polymer, which shows a maximum load at the yield point just before rupture occurs. At some higher temperature (Curve C), it can be seen that, although it is still under the glass transition regime, the phenomenon of necking (deformation where relatively large amounts of strain localise disproportionally) and cold-drawing (process of reducing the cross-sectional area) occurs.

2.1.2 Steel Pipes

Steel pipes are metal alloys made primarily of iron and carbon. The amount of carbon in the alloy controls various properties of the steel; these properties include the tensile strength, the elasticity, ductility and the hardness of the steel.

In practice steel pipes are formed by welding them longitudinally, spirally or circumferentially. Through progressive forming of hot rolled steel plates into a cylindrical shape the required diameter can be obtained. Using what is referred to as the double submerged welding process (DSAW) also known as electric fusion welding, the seam of the pipe is welded internally and externally (Midstate Steel, 2015).

2.1.2.1 Stress–Strain Behaviour of Steel

The behaviour of any given material can be investigated once tension or compression tests are performed on the material specimen and only, thereafter, can the stress–strain diagrams be drawn (SHARMA, 2015). In order to develop an understanding of this concept of stress-strain relationships, a diagram for a mild steel specimen is shown in Figure 2-3. Note that this diagram below is not to scale but is a good proxy of the stress strain behaviour of this specimen.

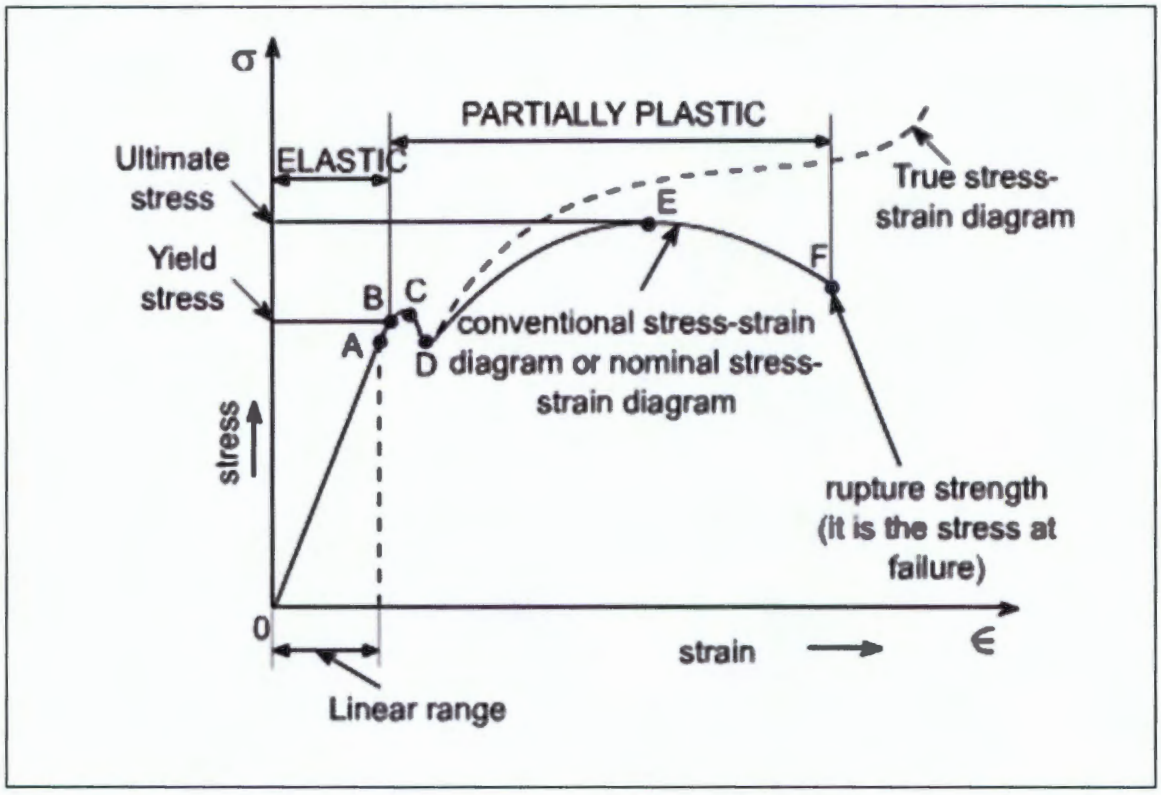

Figure 2-3: Stress-Strain Diagram for Mild Steel in Tension (not to scale) (SHARMA, 2015)

From Figure 2-3 it can be seen that, in the first region, the strain or elongation is proportional to the load applied and the linear range denoted by Point (A). This is known as the elastic region of the material and in this region, once the applied loading is removed, the material returns to its original form. The slope of this line is the elastic modulus or Young's modulus, E, where the $E = \sigma/\varepsilon$. This is known as Hooke's Law. The units for E are similar to the stress because the strain denominator is unit-less. For a short period beyond Point A, the material may still behave elastically because the deformations are recovered when the load is removed. The limiting Point B is termed as the elastic limit. Beyond the elastic limit (between (C) and (D)), plastic deformation begins to occur and strains are not totally recoverable. Thus, there will be permanent deformation when the load is removed. The two Points (C) and (D) are termed upper and lower yield points, respectively. The yield strength is the stress at the yield point (Point B).

A further increase in the load will result in further marked deformation in the volume of the metal. The maximum load, which the specimen can withstand without experiencing catastrophic failure, is called the ultimate strength (Point E). Beyond (E) the specimen begins

to experience necking. During necking there is a clear reduction in the area of the specimen and a pronounced necking of the specimen results. Thereafter, the specimen will stretch further and will be accompanied by reduced load, until eventually fracture occurs at Point F, where the material will fracture or experience catastrophic failure (Hibbeler, 2008).

2.1.3 Cast Iron

Cast iron pipes exist in two forms: pit cast and centrifugal/spun cast pipes. These two forms have different graphite flakes, flake sizes and metallic matrices. These distinct differences account for the differences in mechanical properties, where one finds that, generally, the larger flake sizes found in pit cast pipes produce weaker materials (Cassa & Van Zyl, 2011).

Previous work has made little differentiation between the mechanical properties of pit and spun cast iron water pipes. Makar (2007) conducted mechanical tests on coupons from spun and pit cast samples and showed that spun cast iron has mechanical properties that fall between those of pit cast iron and ductile iron pipes, often with marked similarities to ductile iron.

2.1.3.1 Stress-Strain Behaviour of Cast Iron

The stress-strain behaviour of cast iron shows that there is no yield point because of its brittle characteristics, therefore, consisting of an abrupt fracture at failure. A cast iron specimen under loading indicates that there is no completely elastic behaviour for any applied stress, because the cast iron undergoes, simultaneously, an amount of plastic strain under the application of the incremental loads. Therefore, for any given stress value the total load strain constitutes both an elastic and plastic component. Figure 2-4 shows a typical stress-strain curve for the pit cast and spun cast irons.

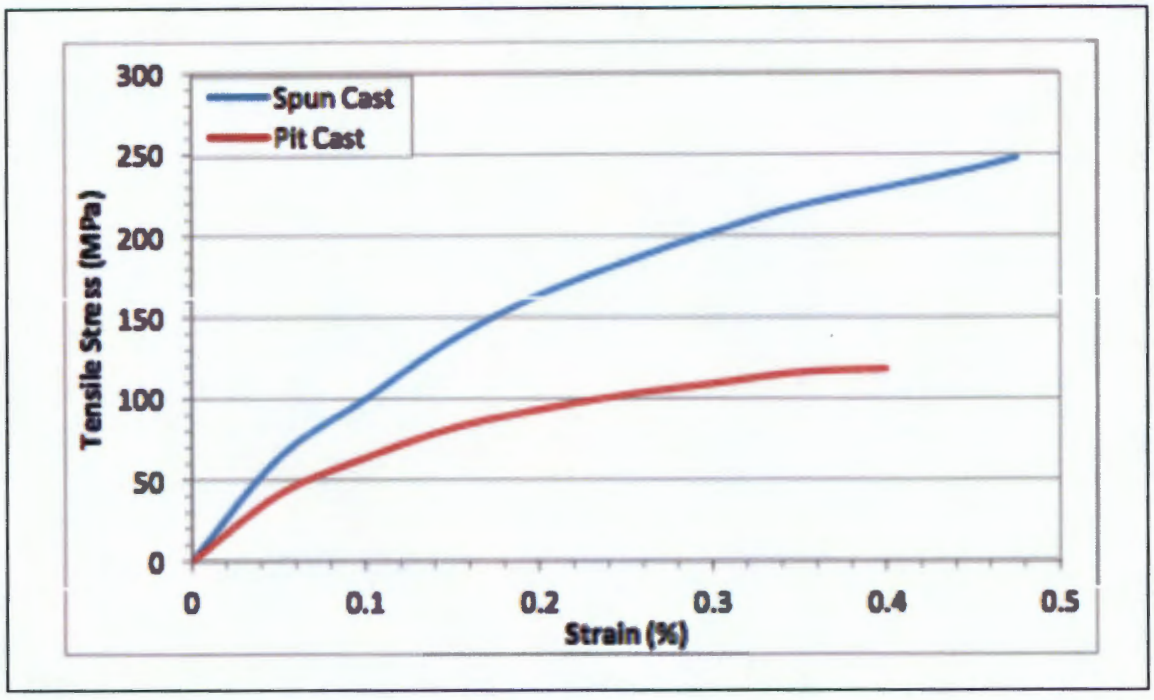

Figure 2-4: Typical Stress-Strain Curves for Cast Iron (Cassa, 2011)

From Figure 2-4 it can be seen that there is an abrupt fracture that occurs at very low strains and this is an indication of the brittle behaviour such a material possesses. The non-linear curvature that can be seen is an indication of the inelastic behaviour of the material. In addition, it can be seen that the spun cast iron shows approximately 50% increase in strength compared to the pit cast. This is attributed to the following reasons: quick solidification, uniformity of the cross section and the fact that impurities are isolated during the manufacturing process (Molnar, Finno, & Rossow, 2005) as cited by Cassa, 2011.

2.2 Understanding the Elastic Behaviour of Pressurised Pipes

Pipes that are used for water distribution systems typically operate under pressurised conditions. It is, therefore, necessary to develop an understanding of how the pipes behave under pressurised conditions. This section will look at the material behaviour of a typical pipe under pressure, in terms of the stress and strains, and how this behaviour affects round hole leaks in the pipe that result in leakage.

2.2.1 Stresses in Pressurised Pipes

Pressurised pipes, such as those used as water pipes, are classified as cylindrical pressure vessels. Fluid pressure, from water flowing in a pressurised cylinder or pipe, presses against the perpendicular interface all around the pipe or cylinder.

To analyse the behaviour of a pressurised pipe, consider a circular pipe AB that is subjected to an internal pressure shown in Figure 2-5 (a). A stress element is shown on the wall of the pipe with its parallel and perpendicular faces to the axis of the pipe. The membrane stresses in the wall are denoted by the normal stresses σ_1 and σ_2 on the stress element. There are no shear stresses because of the symmetry of the pipe and the loading orientation; therefore, the two normal stresses σ_1 and σ_2 are principle stresses.

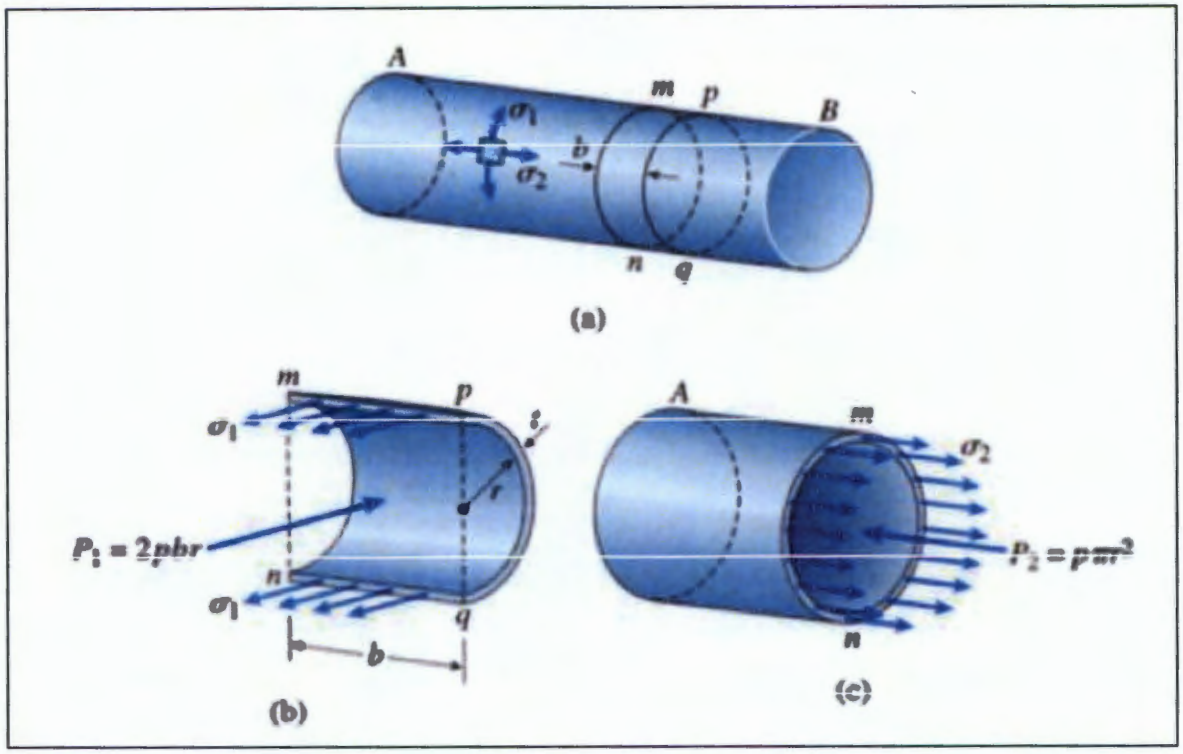

Figure 2-5: Stresses in Cylindrical Pressure Vessels (Gere, 2001)

Because of the directions, σ_1 is called the circumferential stress, or the hoop stress, and σ_2 is called the longitudinal stress, or the axial stress. These stresses can be calculated from equilibrium by using free body diagrams, illustrated by Figure 2-5 (b) and (c).

2.2.1.1 Circumferential Stresses

To calculate the circumferential stress, Figure 2-5 (a) is sectioned into three cuts: mn and pq, which are perpendicular to the longitudinal axis at a distance b apart, and the third cut being a cross-section in the vertical plane through the longitudinal axis, resulting in Figure 2-5 (b). This diagram, therefore, depicts the half circular piece of the pipe with the fluid contained within the cuts. Both the circumferential stress σ_1 and the fluid internal pressure P act on the plane *mpqn*.

Using the equilibrium equations, and considering only the stresses and pressures acting in the circumferential direction, it can be shown that the resultant force of the circumferential stress that acts within the pipe wall is given by σ_1 (2bt) where t is the thickness of the pipe wall, and the resultant force, due to the internal pressure P_1, is given by 2pbr where r is the internal radius of the pipe. Thus, from equilibrium:

$$\sigma_1(2bt) - 2Pbr = 0 \qquad \text{Equation 2-1}$$

Therefore, solving for the circumferential stress σ_1 this stress becomes:

$$\sigma_1 = \sigma_c = \frac{Pr}{t} \qquad \text{Equation 2-2}$$

This stress is distributed uniformly over the thickness of the pipe.

2.2.1.2 Longitudinal Stresses

To calculate the longitudinal stress σ_2 , consider the free body diagram shown in Figure 2-5(c). The stress σ_2 acts longitudinally and has a resultant force σ_2 ($2\pi rat$), where r is the internal pipe radius. The resultant force due to this internal pressure P_2, is $p\pi r^2$. Thus, from equilibrium:

$$\sigma_2(2\pi rt) - P\pi r^2 = 0 \qquad \text{Equation 2-3}$$

Therefore, solving for the longitudinal stress, σ_2 becomes:

$$\sigma_2 = \sigma_l = \frac{Pr}{2t} \qquad \text{Equation 2-4}$$

From Equation 2-2 and Equation 2-4 it can be seen that the circumferential stress in a pressurised pipe, or cylindrical vessel, is two times the longitudinal stress and, hence, Equation 2-5 can be obtained:

$$\sigma_c = 2\sigma_l \qquad \text{Equation 2-5}$$

These formulas for stresses, in cylindrical vessels or pressurised pipes, are valid for pipes and cylinders in space where external parameters are ignored.

2.2.1.3 Summary of Derived Equation

The internal pressure P is given by ρgh where ρ is the fluid density, g is the acceleration due to gravity and h is the head of the fluid in meters. Substituting this in Equations 2-2 and 2-4, the circumferential and longitudinal stress become:

$$\sigma_c = \frac{\rho ghr}{t} \qquad \text{Equation 2-6}$$

$$\sigma_c = \frac{\rho ghr}{2t} \qquad \text{Equation 2-7}$$

2.2.1.4 Limitations of the Derived Equations

If there are any discontinuities, such as openings, points of support, ends, bends and fittings, that cause stress concentrations, this theory does not apply. This is because these discontinuities give rise to a stress variation which is not incorporated in equations 2-6 and 2-7 (Buckley, 2007).

The equations derived for the circumferential and longitudinal stress are derived for the case when the pipe is not surrounded by soil and there are no closed ends in the pipe. For the case when the pipes are buried in the ground, other loads need to be taken into account.

Various loadings induce different stresses and strains. For the case of buried pipes, the loadings can be categorised into two categories: internal pressure and external loads. The internal pressure comprises of the hydrostatic pressure and the surge pressure. The external

loads, on the other hand, are made up of external soil pressure and/or surface (live) loads. Other external loadings to be considered are differential settlements, longitudinal bending and shear loadings. Temperature–induced stresses may be considered to be caused by either internal or external effects (Mosner & Folkman, 2008) as cited by Cassa (2011). Again, these factors are not incorporated when using equations 2-6 and 2-7.

These additional loads will be explored further in a later chapter.

2.2.2 Stress States in Pressurised Pipes

Pressurised pipes, such as those used for water distribution systems, are classified as cylindrical pressure vessels. When a pressure vessel is pressurised from inside there are two different stress states that result, namely, the uniaxial and biaxial stress states. These two states exhibit the same circumferential stresses but differ in longitudinal stresses.

Theoretically, the circumferential stress will always exist once an internal pressure is applied, because the specimen will experience circumferential expansion. However, longitudinal stresses do not always exist. Reynold K and Loren R, (1999) suggest that there are three principle cases that lead to the occurrence of longitudinal stresses. Firstly, changes in temperature and pressure causing relative lengthening and shortening of the pipe with respect to the soil and thrust constraints. Secondly, interferences in the longitudinal direction, such as end caps, valves or bends, will induce an axial thrust. Finally, beam bending causes flexural stresses: the beam bending is typically caused by non-uniform settlement of bedding, massive soil displacements and placement of pipe sections on piers for vertical alignment.

In summary, if a pipe is subjected to an internal pressure, but there are no perpendicular interferences in the longitudinal direction, only the circumferential stress will exist. This stress state is called the uniaxial stress state. In the case where the longitudinal interferences exist, and all the three principles discussed above are true; the longitudinal stresses are developed and exist in conjunction with the circumferential stress. This stress state is called the biaxial stress state.

2.2.3 Strains in Pressurised Pipes

2.2.3.1 Hooke's Law

Assuming elastic deformation, many materials obey Hooke's Law (equation 2-8), to a reasonable approximation. Hooke's Law states that stress is proportional to strain with the constant of proportionality being the Young's Modulus or the elastic Modulus E (Roylance, 2001).

$$\sigma = \varepsilon E \qquad \text{Equation 2-8}$$

Where: σ is the stress
ε is the strain
E is the Elastic Modulus.

This law simply illustrates that as a material is stressed within its elastic limits, it elongates elastically and the stresses and strains induced have a linear relationship (Hibbeler, 2008). This is also shown in Figure 2-6, where the stress and corresponding strain have a linear relationship in the elastic region.

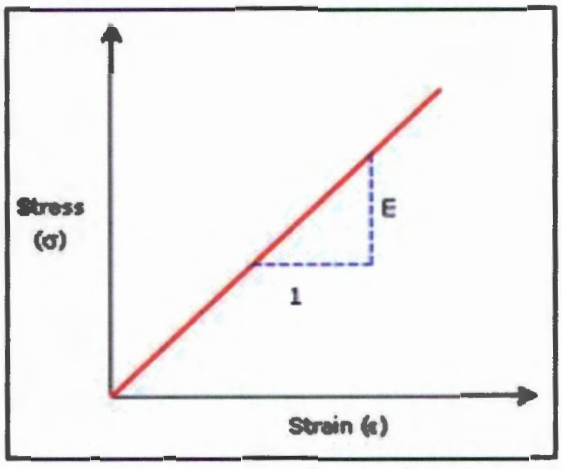

Figure 2-6: Stress against Strain for Elastic limit Source (scu.edu)

Figure 2-6 shows that Hooke's Law is only valid in the linear elastic region of a material, and E is the slope of the linear line between the stress and the strain of the material. It takes on the units for stress because the strain is unit-less.

2.2.3.2 Poisson's Ratio

The Poisson's ratio gives the ratio of lateral strain ε′ to the axial strain ε at any point in the material (see equation 2-9).

$$\upsilon = \frac{lateral(strain)}{axial(strain)} = \frac{\varepsilon'}{\varepsilon} \qquad \text{Equation 2-9}$$

For linear elastic conditions the lateral strain is proportional to the axial strain at that same point. The Poisson's ratio definition contains a minus sign to compensate the fact that the lateral strains and axial strains normally have opposite signs (Hibbeler, 2008), and is expressed as:

$$\varepsilon_l = \varepsilon_c \upsilon = -\frac{\sigma_c}{E}\upsilon \qquad \text{Equation 2-10}$$

Figure 2-7 shows a pressurised pipe that is super-imposed over an unpressurised pipe to illustrate Poisson's ratio of contraction applied to pipes.

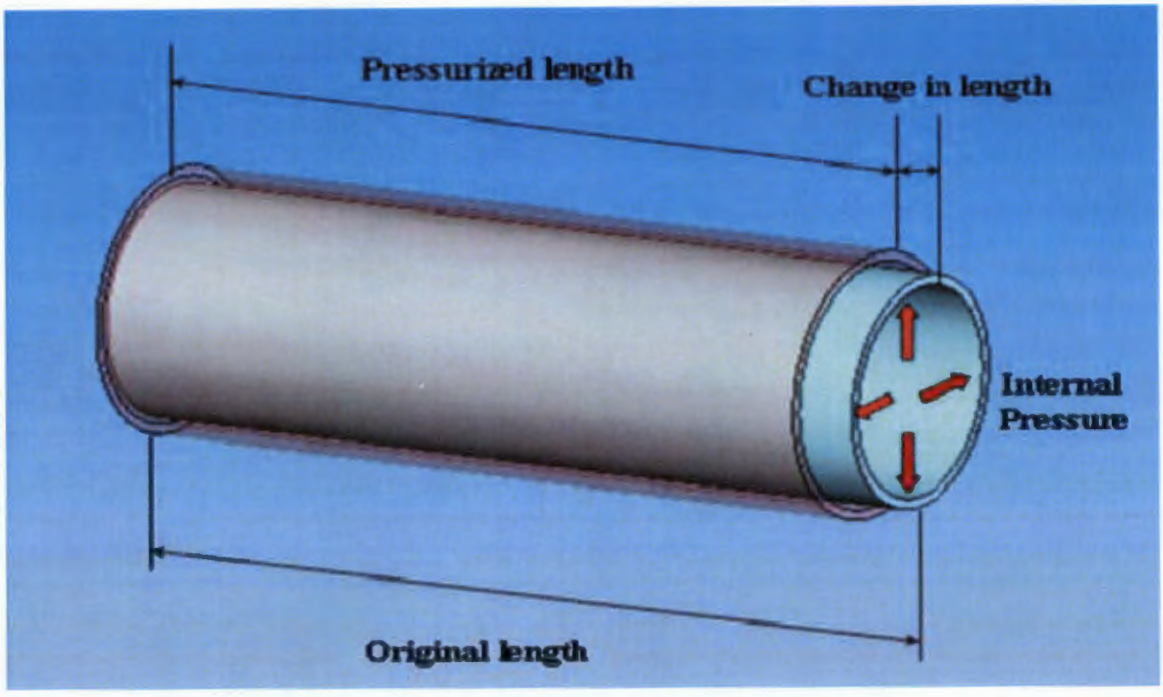

Figure 2-7: Pressurised Pipe Super-imposed Over an Unpressurised Pipe Illustrating Poisson's Ratio (Buckley, 2007)

2.2.3.3 Circumferential and Longitudinal Strains in a Pressurised Cylinder under Uniaxial Stress

Consider a uniaxial stress state, where only circumferential stress (σ_c) exists and longitudinal stress (σ_l) is equal to zero. Hooke's Law confirms that the strain in the material will be obtained from: $\varepsilon_c = \sigma_c/E$. Substituting the circumferential stress of Equation 2-6, the corresponding circumferential strain can be obtained as a function of material properties, geometrical variables and fluid properties. This circumferential strain is expressed as:

$$\varepsilon_c = \frac{\sigma_c}{E} = \frac{\mathrm{Pr}}{tE} = \frac{\rho ghr}{tE} \qquad \text{Equation 2-11}$$

This circumferential strain is the axial strain.

Equation 2-12 shows the lateral strain i.e. the longitudinal strain (ε_l) and is described as:

$$\varepsilon_l = -\varepsilon_c \upsilon = -\frac{\sigma_l}{E}\upsilon = -\frac{\rho ghr}{tE}\upsilon \qquad \text{Equation 2-12}$$

The negative longitudinal strain implies that the fluid pressure causes the pipe to expand in the circumferential direction, thereby resulting in a longitudinal contraction, again, as shown in Figure 2-7.

2.2.3.4 Circumferential and Longitudinal Strain in a Pressurised Cylinder under Biaxial Stress

Consider a biaxial stress state where both circumferential and longitudinal stresses exist. The strains that result in the circumferential and longitudinal directions are a result of the two stresses acting circumferentially and longitudinally, simultaneously. These strains are

presented in the equations that follow as presented by Benham, Crawford, and Armstrong, (1996):

Circumferential strain:

$$\varepsilon_c = \frac{\rho g h r}{tE} - \frac{\rho g h r}{2tE}\upsilon = \frac{\rho g h r}{2tE}(2-\upsilon) \qquad \text{Equation 2-13}$$

Longitudinal strain:

$$\varepsilon_l = \frac{\rho g h r}{2tE} - \frac{\rho g h r}{tE}\upsilon = \frac{\rho g h r}{2tE}(1-2\upsilon) \qquad \text{Equation 2-14}$$

The Equations 2-13 and 2-14 show the strain in the pipe material related to the change in length in the circumferential and longitudinal direction of the hole. These equations can be used to calculate the amount of material expansion or contraction in either the circumferential or longitudinal direction.

2.3 Development of Leaks in Water Distribution System Pipes

Pipe failures can cause severe problems in water distribution systems. These failures may include ruptures, orifices and other effects of internal and external corrosion. Many studies have been carried out to understand the consequences of pipe failures, associated with surrounding soils and existing ground water that induce diverse internal and external forces on pipes. Studies, such as Rodriguez (2012), have also looked at the interaction of pipes with these environments.

JM Rodriguez *et al.,* (2012) presented a study of the relationship of failures, defects and resulting water losses that exist in water distribution pipes in order to establish an approach that can capture the actual physical characteristics of pipe failures. The objective of the study was to determine the failure process, which was found to be dependant on material, age, type of surrounding, water quality, pressure and handiwork. After the different failures were studied, the research then aimed to connect all topics in order to present an integrated anlysis that was, primarily, based on certain hydraulic characteristic parameters.

This section gives an overview of the different ways in which pipe defects occur and their formation for different pipe materials.

2.3.1 An Overview of Leaks and Defects for Different Pipe Materials

Ranjani and Kleiner (2001), cited by JM Rodriguez *et al.,* (2012), consider three main aspects that must be looked at when investigating the mechanisms that generate pipe failures (see Figure 2-8):

- The pipe's structural properties, the pipe material, the interaction between the soil and the pipe, and the facility quality;
- Internal loads that exists due to the operational pressure and external loads, accidental or intentional damage and, finally;

- The deterioration of the pipe material due to internal and external chemical environments.

Ranjani and Kleiner (2001), cited by JM Rodriguez *et al.,* (2012), further classified pipe deterioration into two categories: the first being the structural deterioration and the second being the inner surface deterioration. In structural deterioration, the pipe's structural resistance (elasticity), and the ability to support active tensions and loads, are diminished. During the pipe inner surface the hydraulic capacity is diminished by the deterioration, the water quality is degraded, and in the case of severe internal corrosion, the structural resistance reduces.

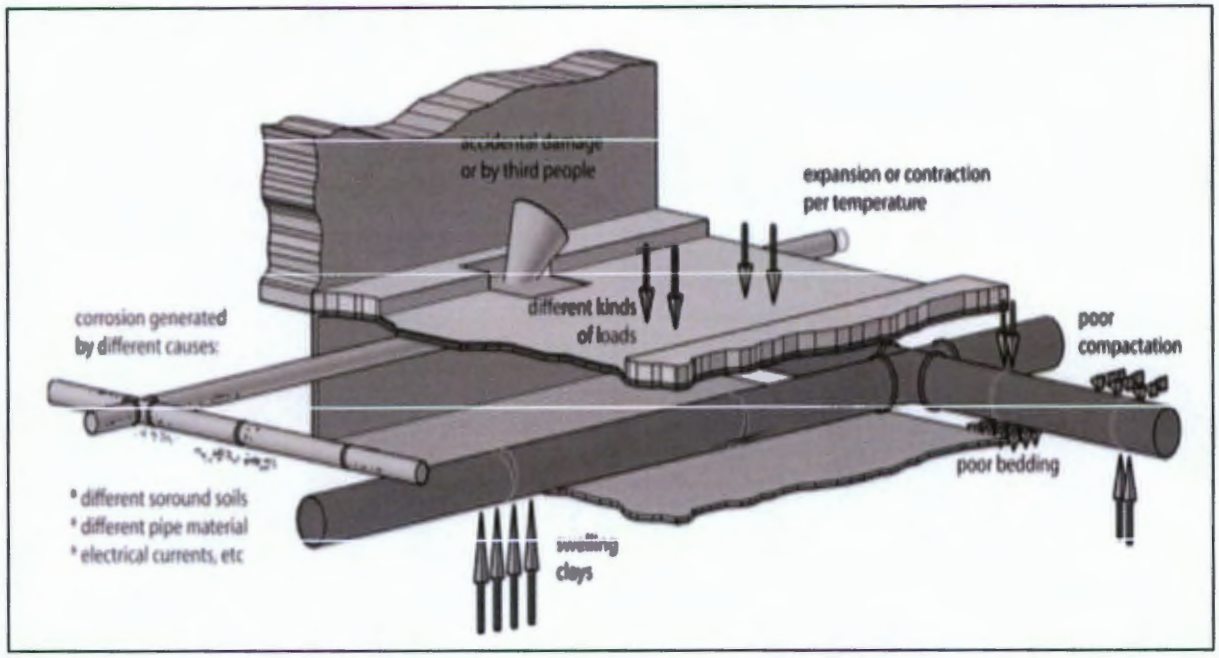

Figure 2-8: Some Mechanisms that Generate Failures in Buried Pipes (JM. Rodriguez, 2012)

The different deterioration mechanisms for different pipe materials will follow.

2.3.1.1 PVC

PVC deterioration mechanisms include both mechanical and chemical degradation. In general, this type of pipe produces relatively smaller rates of failure in comparison to other pipe materials. The failures that have been reported to occur in PVC-U pipes are attributed, mainly, to the following reasons: defective facilities, excessive operating conditions and damages that are induced by external factors and, in other cases, it was found to be a result of poor manufacturing quality (Davis, 2007).

2.3.1.2 Polyethylene

Because HDPE pipes are often delivered in much longer lengths, compared to PVC, they require smaller amount of joints making them better leak resistance. However, due to its higher coefficient of thermal expansion, when compared to other plastic pipes, when used above ground without sufficient anchoring or support design the pipe is subject to significant

temperature swings leading to eventual failure. Other areas identified to lead to failure in in PE pipes are the joint qualities. The general mode of failure reported for PE pipe is brittle, slow crack growth through the pipe wall. The driving force of crack opening in PE pipes is the circumferential stress in the pipe wall. (Staff, 2011)

Visually, these brittle cracks are typically smoothed, featureless and usually devoid of any yielding and deformation.

2.3.1.3 Cast Iron

The predominant deterioration mechanism of exterior cast iron is the electro-chemical corrosion, which commonly produces damages such as holes. For cast iron, the damage normally appears as graphitisation: these are graphite-like flakes that begin to appear in the iron pipe that has been affected by corrosion.

The soil that surrounds the pipe has significant impact on the deterioration of the pipe; there some factors that are responsible for accelerating the corrosion of metal pipes and these factors include: electrical current stray, soil characteristics such as humidity, chemical and micro-biological content, electrical resistivity, aeration and redox potential. Typically, metal pipe interiors are susceptible to incrustations. Erosions and cracks that result due to corrosion reduce the inner diameter and can allow bacterial growth. An illustration of this is shown in Figure 2-9.

Figure 2-9: Cast Iron Pipe, Corrosion, Graphitisation and Incrustation ((JM. Rodriguez, 2012)

2.3.1.4 AC Pipes and Concrete

AC pipes and concrete pipes are susceptible to chemical processes and these processes result in deterioration. The main factors affecting concrete corrosion are the presence of organic and inorganic alkaline acids or sulphates that exist in the soil. Hu and Hubble (2007) as cited by (JM. Rodriguez, 2012), identified some factors that cause bursts in AC pipes and these include: pipe age, diameter, climate, clayey soil, construction and maintanance methods. It is also noted that chemical factors associated with the transported water and soil humidity negatively affect the structural integrity of these types of pipe.

Hu and Hubble, (2007) classified AC pipe failures in the following five categories: circumferential, longitudinal, holes, joints and other cracks oriented in various directions on the pipe wall.

2.3.2 Modes of Failures and Failure Consequences

Generally, pipe failures occur when environmental and operating tensions jeopardise the structural integrity. This jeopardisation occurs in the form of corrosion, degradation, inadequate installation or manufacture defects (Almeida & Ramos, 2010). As documented in Ashton and Hope, (2001), failures in water pipes have environmental and economic consequences.

O'Day *et al.*, (1986), cited by JM Rodriguez, (2012), classified the different modes of failure into three categories:

- circumferential breaks that are caused by longitudinal tension;
- longitudinal breaks that are caused by cross-sectional tension (radial tension); and
- cracks that develop in union primarily caused by a cross-sectional tension in the pipe union.

The different failure categories arise as a consequence of certain causes, which will be discussed next. Circumferential breakage, that result from the longitudinal tension, arises because of: (1) thermal contraction due to low water temperature in the pipe and its surrounding soil, (2) tension by flexion due to differentials in ground movement (clayey soil), or simply a result of poor bed installation, (3) inadequate supporting beds and ditches also contribute to this type of failure, and finally (4) other external factors, such as vandalism or accidental breakage. The fluid pressure in the pipe applies an internal pressure which contributes to the longitudinal tension and causes an increase in the risk of circumferential failure when it exists, concurrently, with one or two more external tensions (Rajani & Kleiner, 2001).

Longitudinal failure, due to cross-sectional tension, normally occurs as a result of the following factors: (1) internal pressure in the pipe that induces radial tensions, (2) cross-sectional tension that exists due to ground loads, (3) cross-sectional tension due to other live loads such as traffic etc. and, finally, (4) the increasing of cross sectional loads whenever there is expansion by frozen water in the soil (Rajani & Kleiner, 2001).

Figure 2-10 shows these classifications of failure that can occur in pipes that have been discussed above.

Figure 2-10: Types of Failures in Pipes (O'Day *et al.*, (1986)).

It is inevitable that the presence of an initial failure will tend to increase the possibility of additional failures in a pipe. This is very likely to happen due to the imbalance of pressures and forces that exist in the surrounding soil, which appear because of the initial failure (Hu & Hubble, 2007).

As indicated by Stewart *et al.,* (1999) the primary economic loss, due to leakage, is the cost of the raw water, its treatment and its transportation. Inevitably, leakage also results in secondary economic loss that occurs in the form of the damaged pipes network itself. Besides the obvious environmental and economic losses that are caused by leakage, leaking pipes are a health hazard, because every leak presents a potential entry point for contaminants, if a pressure drop occurs in that system. Therefore, water leakage is not only a costly problem but also a public health risk.

2.3.3 Holes in Pressurised Pipes, Vessels and Cylinders

Section 2.3.2 showed the different types of failures that can occur in pipes. This study will focus, particularly, on round hole defects. An understanding of how round holes behave within pressurised systems will be developed in this section. The section will begin by looking at the effects of a round hole in a plate, to understand the typical stress distribution expected when investigating round hole defects in materials.

2.3.3.1 Stress Concentrations Around the Hole

As stated previously, water pressures induce stresses in the pipe walls. The stress distribution in the pipe walls is affected by a leak opening or discontinuity. Consider a thin plate with a hole in it, as shown in Figure 2-11 below. Timoshenko and Goodier (1951) were able to show that the effect of the hole in the plate is localised, and stresses become more uniform the

further away you are from the edge of the hole. In the experiment that was conducted, they subjected a thin plate to uniform tension at its edges as illustrated in Figure 2-11.

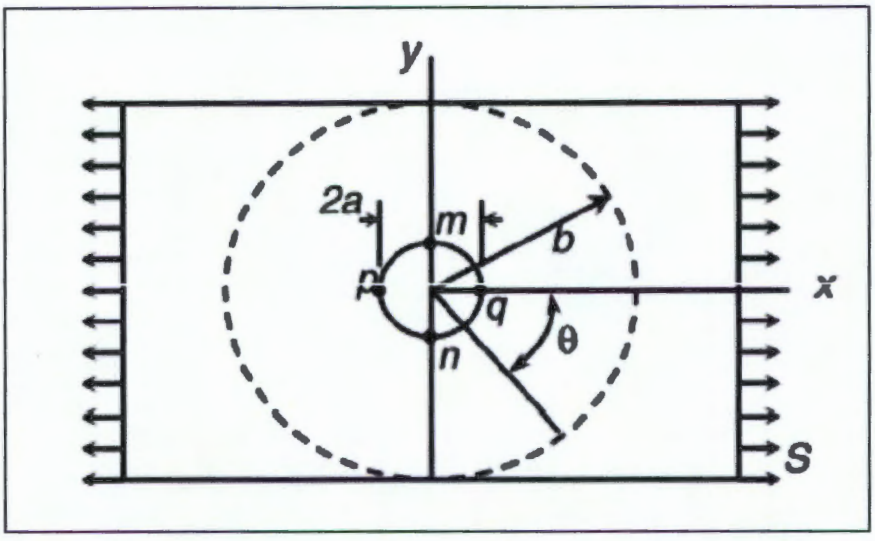

Figure 2-11: Plate With Hole Subject to Uniform Tension (Timoshenko and Goodier (1951))

From Figure 2-11, it can be shown that if a concentric circle of radius b is considered, with b larger than the radius of the hole, the stresses found at the large circle are effectively the same as those found in a plate with no hole. Timoshenko and Goodier (1951) also showed that the only stresses present are in the circumferential direction. It was also shown, theoretically, that the circumferential stress found at the edge of the hole is given by the equation that follows:

$$\sigma_\theta = S - 2S\cos(2\theta) \qquad \text{Equation 2-15}$$

Where σ_θ is the circumferential stress, θ is as shown in Figure 2-11, and S is the stress applied at the edge of the thin plate.

It can be seen from Equation 2-15 that at points *p* and *q*, where $\theta=180°$ and $\theta=0°$ respectively, there exists compressive stresses of the magnitude S. This further justifies the deformation of round holes to elliptical shapes, as observed in previous research e.g. Cassa *et al.*, (2010) etc. The stress distribution across the centre of the thin plate is illustrated by Figure 2-12.

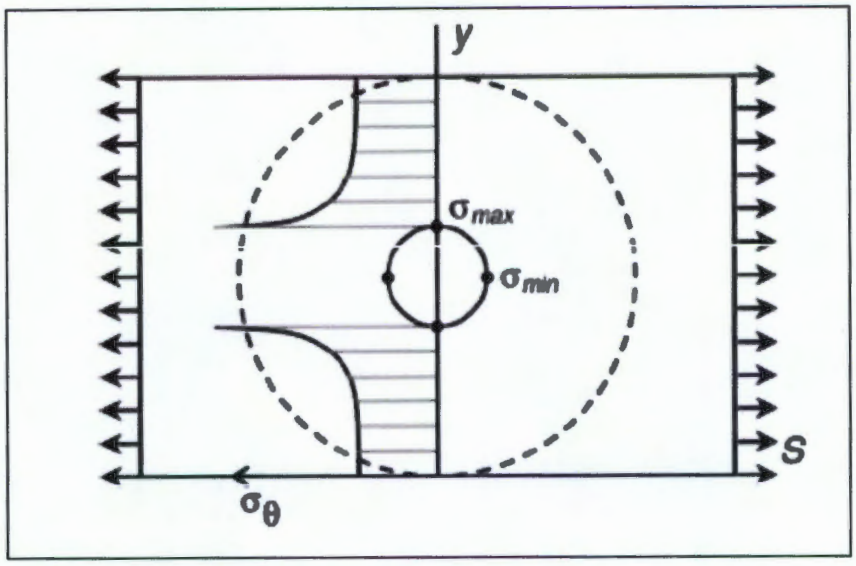

Figure 2-12: Stress Distribution Around a Hole in a Plate Showing Location of Maximum and Minimum Stresses (adapted from Timoshenko 1951)

The maximum stress that occurs around a leak opening is usually significantly higher than stresses found in the rest of the pipe wall. The effect of the hole, or any other discontinuity on the material behaviour, can be expressed by the use of a stress concentration factor *K*. This factor *K* is usually expressed by the ratio of maximum stress to the nominal stress experienced in all other parts which are significantly away from the hole (Gere, 2001):

$$K = \frac{\sigma_{max}}{\sigma_{nom}} \qquad \text{Equation 2-16}$$

Mechanics of material handbooks by Gere (2001) and Benham *et al.*, (1996) indicate that the stress concentration factor *K*, shown in Equation 2-16, remains constant within the elastic range of the material. For a flat plate with a round hole, the theoretical value of K would be 3, however, for a pipe, this is likely to differ due to the curvature associated with the pipe, and also the presence of longitudinal stresses. Figure 2-13 shows the stress concentration factors for different plates. It can also be seen that the maximum stress concentration factor for a round hole is three.

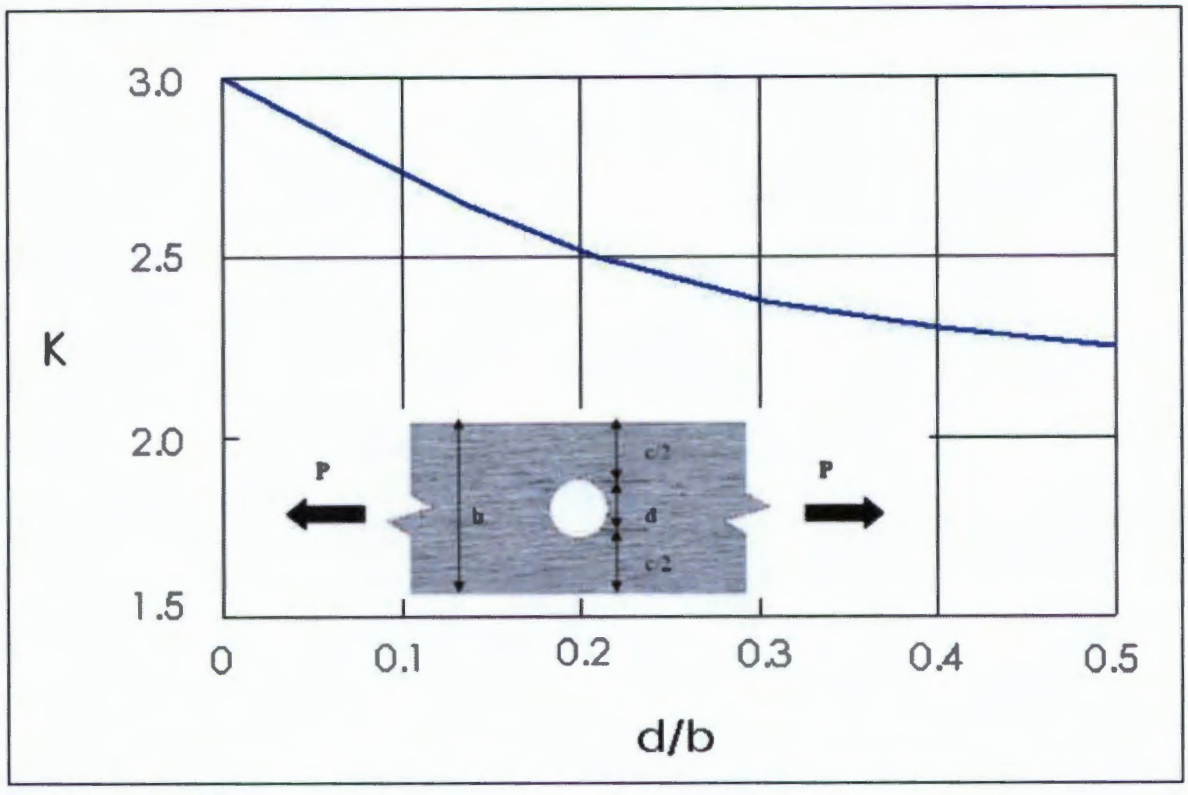

Figure 2-13: Stress Concentration Factor K for Flat Plates with Circular Holes (Buckley, 2007)

A study by Nsanzubuhoro & van Zyl, (2013) that used the finite element modelling approach to investigate the effect of round holes in pressurised pipes, also confirmed that the highest stresses occurred at the inside lip of the hole, as can be seen in Figure 2-14. As suggested by Timoshenko and Goodier's (1951) experimental study, this was at the furthest edges along the length of the pipe. The lowest stresses were found to occur in the transverse direction at the furthest edges, as shown in Figure 2-14.

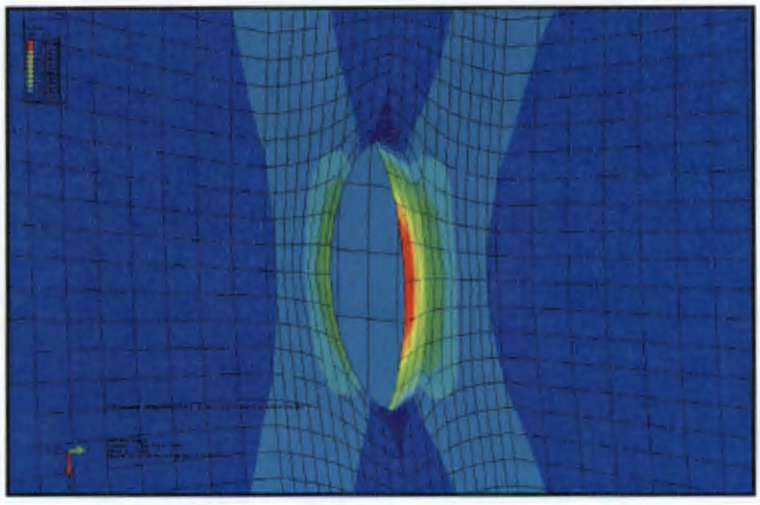

Figure 2-14: Von Mises stress distribution around the 8mm hole (Scale 40) (Nsanzubuhoro & van Zyl, 2013)

Cassa, van Zyl, & Laubscher, (2010) further suggest that the shape of the round hole after deformation can be assumed to be elliptical shaped as a result of the uneven stresses in the

pipe material. This can also be seen in Figure 2-14. Similar stress distributions were observed from all pipes and holes. Figure 2-15 shows the relationship between the stress concentration factor around a hole in the pipe and the hole size. This was done for different pipe materials. A linear trend line was fitted to the data points and the different equations were obtained for the various materials investigated by Cassa *et al.*, (2010).

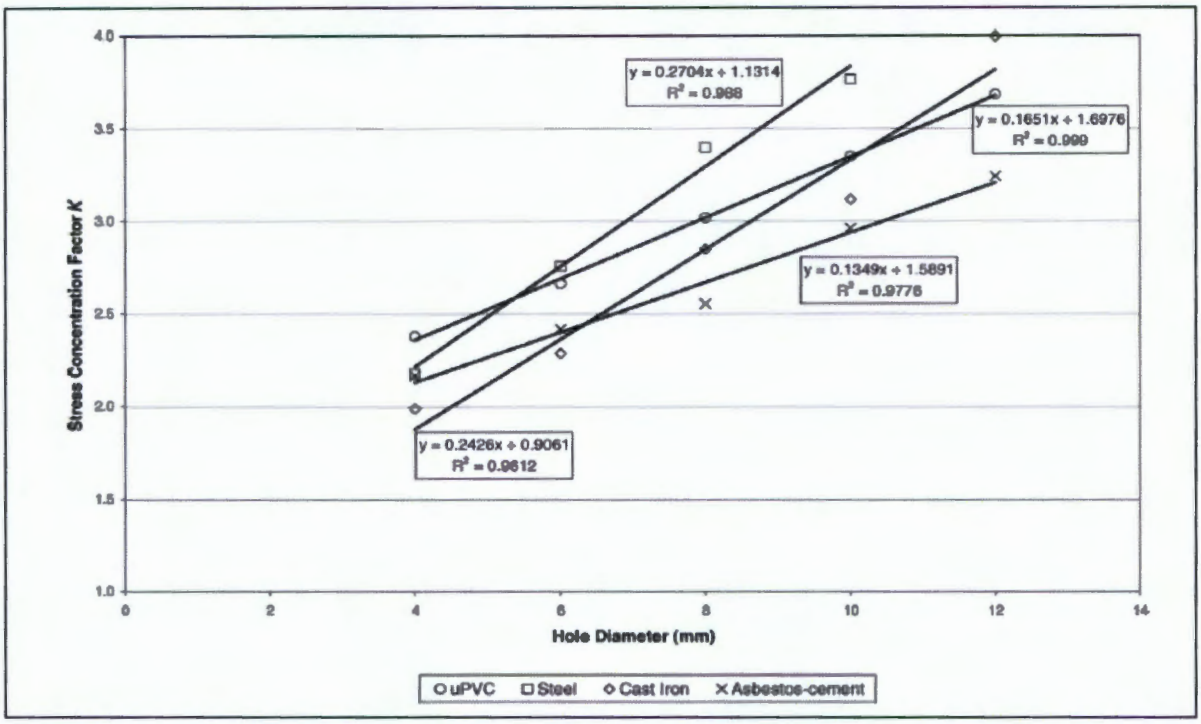

Figure 2-15: Stress Concentration Factor K, vs Circular Hole Size for a Class 6 uPVC Pipe (Cassa, van Zyl, & Laubscher, 2010)

Figure 2-15 shows that the stress concentrations for the different pipes increases somewhat linearly with increasing hole size. Cassa (2005) showed that for smaller holes (<3.4mm) uPVC and AC pipes had the lowest stress concentration, while for larger holes (> 10.2mm) steel and CI had the highest stress concentration. Linking this information back to the plate analogy, which showed the theoretical stress concentration to be 3, in Figure 2-15 the K of 3 is found in the 6-11mm hole diameter range.

2.4 Theoretical Behaviour of Round Hole Leak Areas in Pipes Under Pressure (Buckley, 2007)

2.4.1 Round Holes

To simulate the distortion of a round hole through a material, consider a small outer section of an infinitely long pressurised pipe away from any discontinuities, as shown in Figure 2-16.

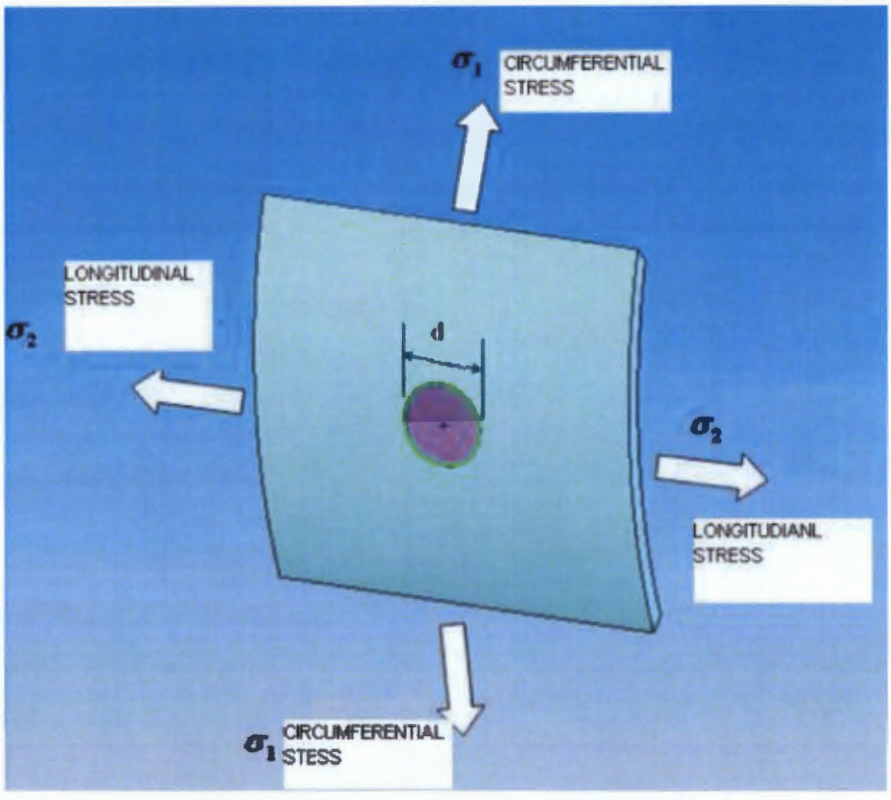

Figure 2-16: Stress Orientations for a Section from a Pressurised Pipe Wall (Buckley, 2007)

To simulate the distortion, a perfect circle with a diameter of *d* is placed in the middle of the small outer section of the pipe. Assuming elastic deformation, Hooke's Law can be incorporated to understand how the round hole will deform, with respect to the induced stresses and strains, as a result of an applied pressure. Assuming that the original length of the hole is *d* (the diameter), taking the change in length after deformation occurs, divided by the original length, will yield the new deformed strain. As mentioned previously, because of the different stresses, i.e. circumferential stresses are twice the longitudinal stresses; the strains will not be the same in both directions. This, therefore, implies that the hole will deform elliptically, as is shown in Figure 2-17.

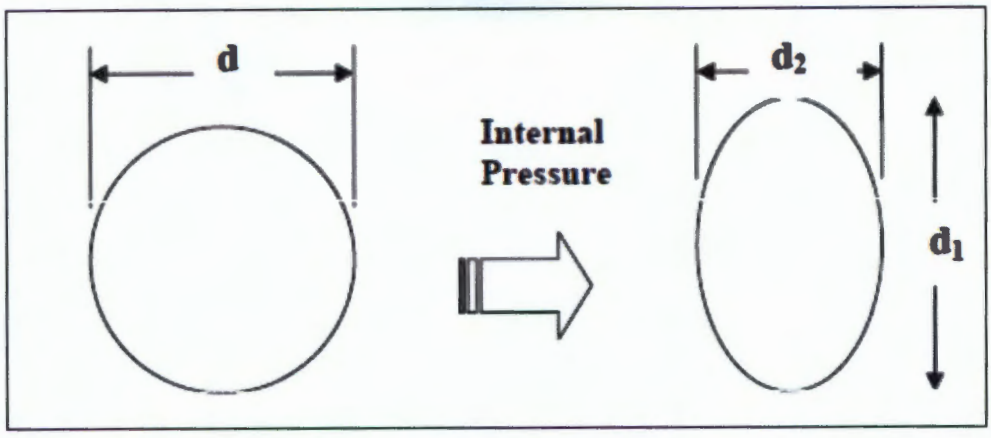

Figure 2-17: Effect of Pressure on Round Holes (Buckley, 2007)

The diameters d_1 and d_2 (shown in Figure 2-17) were calculated by adding the original diameter to the change in diameter in the respective direction, resulting in the diameters expressed as a function of pressure head, shell geometry and material properties. With these new diameters the area of an ellipse was determined and, thus, the area could be expressed as a function of pressure head and other material properties. This procedure is illustrated in the proceeding sections.

2.4.2 Theoretical Investigation into the Behaviour of Round Holes

This section explains Buckley's (2007) uniaxial and biaxial round hole leak behaviour derivation. The derivation assumes that a round hole, located on the wall of a pipe material, will distort elastically under an internal pressure. Both the uniaxial and biaxial stress states will be investigated, in order to obtain an area as a function of pressure for both states. The areas obtained for the two stress states will be substituted in the orifice equation and simplified further to yield a relationship of leakage and pressure. The method assumes that the round hole deforms into an elliptical shape and this was incorporated into the derivation.

2.4.2.1 Leakage Derivation through a Round Hole in a Uniaxial Stressed Pressurised Pipe

Consider a finite element section of a pipe material, with a round hole in it, representing the uniaxial stress state, as shown in Figure 2-18.

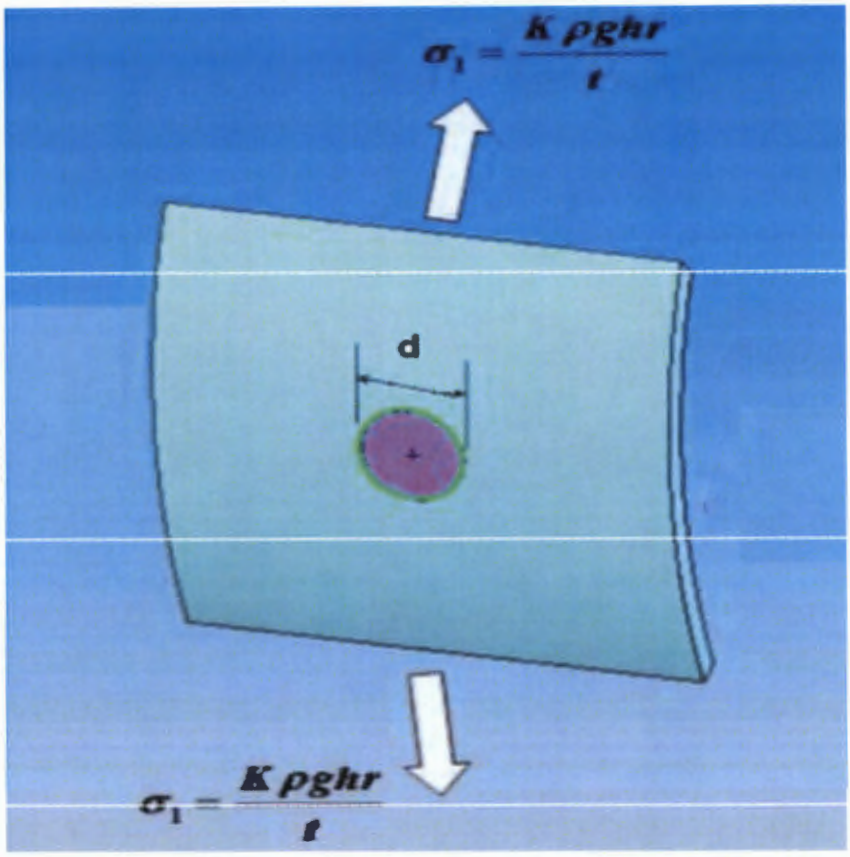

Figure 2-18: Uniaxial Stress State Represented on a Finite Element of a Pipe (Buckley, 2007)

As can be seen from Figure 2-18, for a uniaxial stress state, the pressurised pipe will experience the circumferential stress. Therefore, the stress conditions in the element can be expressed as: $\sigma_z = 0$, $\sigma_2 = 0$, and from Equation 2-6 $\sigma_1 = K\rho ghr/t$. From Hibbeler (2008) the stress in the z direction is zero because we assume plane stress, i.e. the wall is thin in the z direction compared to all other directions. Strain is a function of the change in length over the original length, assuming that the original length in the circumferential and longitudinal direction is the diameter of the hole d. Using Hooke's Law (σ = i.e.) the change in length in these directions can be calculated, recalling the strains in a uniaxially stressed pressurised pipe, as was shown in Equations 2-11 and 2-12 (repeated below):

$$\varepsilon_c = \frac{\sigma_c}{E} = \frac{\mathrm{Pr}}{tE} = \frac{\rho ghr}{tE}$$

$$\varepsilon_l = -\varepsilon_c \upsilon = -\frac{\sigma_l}{E}\upsilon = -\frac{\rho ghr}{tE}\upsilon$$

The longitudinal and circumferential strains, with the stress factor included, can be deduced and presented as:

$$\varepsilon_c = \frac{\sigma_c}{E} = \frac{K\rho ghr}{tE} = \frac{\Delta d_c}{d} \qquad \text{Equation 2-17}$$

$$\varepsilon_l = -\varepsilon_c \upsilon = -\frac{\sigma_c}{E}\upsilon = -\frac{K\rho ghr}{tE}\upsilon = \frac{\Delta d_l}{d} \qquad \text{Equation 2-18}$$

The new diameters d_c and d_l of the ellipse can be obtained by adding the original d_0 to Δd_c and Δd_l, which are attainable from re-arranging equations 2-17 and 2-18. The values of d_c and d_l then become:

$$d_c = d_0 + \Delta d_c = d_0 + d_0 \frac{K\rho ghr}{tE} = d_0\left(1 + \frac{K\rho ghr}{tE}\right) \qquad \text{Equation 2-19}$$

$$d_l = d_0 + \Delta d_l = d_0 - d_0 \frac{K\rho ghr}{tE}\upsilon = d_0\left(1 + \frac{K\rho ghr}{tE}\right) \qquad \text{Equation 2-20}$$

The area of an ellipse is given by the following equation:

$$A = \frac{\pi}{4} d_c d_l \qquad \text{Equation 2-21}$$

Substituting equations 2-19 and 2-20 into equation 2-21, and doing some mathematical simplification, the area of the ellipse, as a function of material properties and the pressure head, is obtained as:

$$A = \frac{\pi}{4} d_0^2 \left(1 + \frac{K\rho ghr}{tE}\right)\left(1 - \frac{K\rho ghr}{tE}\upsilon\right) \qquad \text{Equation 2-22}$$

$$A = \frac{\pi}{4} d_0^2 \left[1 + \frac{K\rho ghr}{tE}(1-\upsilon) - \left(\frac{K\rho ghr}{tE}\right)^2 \upsilon\right] \qquad \text{Equation 2-23}$$

Equation 2-23, therefore, represents the area of a round hole defect on the side wall of a pressurised pipe in the uniaxial stress state.

The orifice equation given as $\left(q_{actual} = C_d A\sqrt{2gh}\right)$ gives the actual flow through the hole area given by equation 2-23. Thus, when equation 2-23 is substituted in the orifice equation the flow through the round hole is obtained as:

$$q_{actual} = \frac{\pi}{4} d_0^2 C_d \sqrt{2g}h^{0.5}\left[1 + \frac{K\rho ghr}{tE}(1-\upsilon) - \left(\frac{K\rho ghr}{tE}\right)\upsilon\right] \qquad \text{Equation 2-24}$$

Finally, by multiplying the pressure head into the square brackets, the actual flow can be re-written as follows:

$$q_{actual} = \frac{\pi}{4} d_0^2 C_d \sqrt{2g} \left[1 + \frac{K\rho g h^{0.5} r}{tE}(1-\upsilon) - \left(\frac{K\rho g r}{tE} \right) h^{2.5} \upsilon \right] \qquad \text{Equation 2-25}$$

2.4.2.2 Leakage Derivation through a Round Hole in a Biaxially Stressed Pressurised Pipe

This section will go through the derivation of a leak through a hole in a finite element section of a pressurised pipe in the bi-axial stress state, as shown in Figure 2-19.

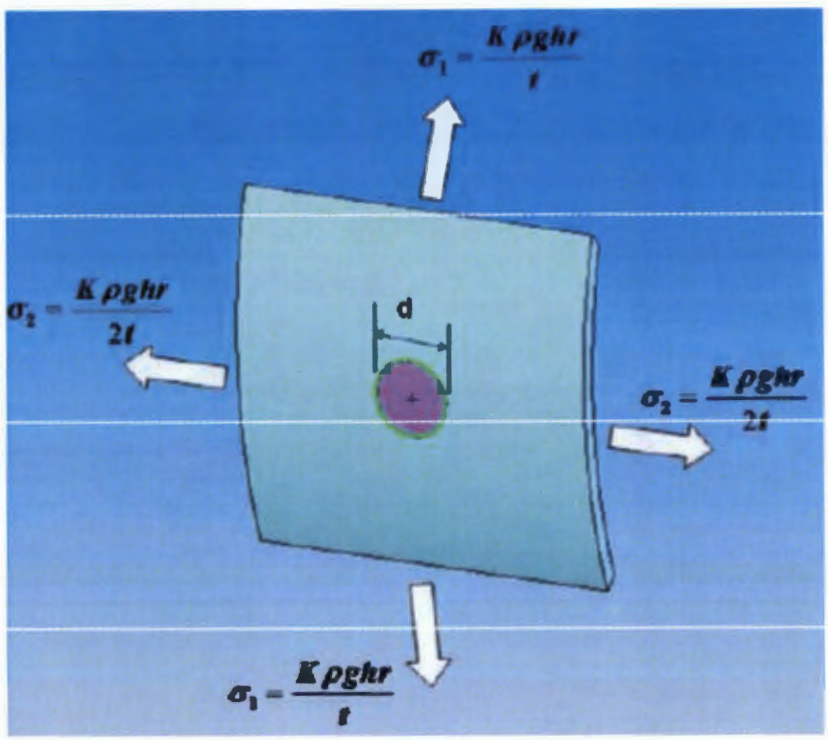

Figure 2-19: Biaxial Stress State Represented on a Finite Element with a Round Hole (Buckley, 2007)

The derivation of the bi-axial stress state will follow very closely to that carried out in Section 2.4.2.1. However, in this section, the stress conditions in the material do present themselves differently. The conditions are given as follows: $\sigma_z = 0$, from equation 2-6 $\sigma_1 = K\rho ghr/t$, and from equation 2-7 $\sigma_2 = K\rho ghr/2t$. Once again, plane stress is assumed because the pipe wall is very thin in the z-direction and, therefore, the stress in this direction can be assumed to be zero (Hibbeler, 2008). All other directions exhibit some form of stress because ultimately the bi-axial stress states implies that stresses exist, simultaneously, in two perpendicular directions.

Once again, the strain induced in any direction is a function of the change in length over the original length. Assuming that the original length, in the circumferential and longitudinal direction, is *d*, the change in length in both these directions can be calculated using Hooke's Law ($\sigma = \varepsilon.E$) and the strains for a bi-axial stress state can be expressed as was shown in equations 2-13 and 2-14 in Section 2.2.3.4. These equations are recalled here:

Circumferential strain:

$$\varepsilon_c = \frac{\rho ghr}{tE} - \frac{\rho ghr}{2tE}\upsilon = \frac{\rho ghr}{2tE}(2-\upsilon)$$

Axial strain:

$$\varepsilon_l = \frac{\rho ghr}{2tE} - \frac{\rho ghr}{tE}\upsilon = \frac{\rho ghr}{2tE}(1-2\upsilon)$$

To determine the strains with the associated stress and stress intensity factor K, Equations 2-13 and 2-14 can be re-written as follows:

$$\varepsilon_c = \frac{\sigma_c}{E} = \frac{K\rho ghr}{2tE}(2-\upsilon) = \frac{\Delta d_c}{d} \qquad \text{Equation 2-26}$$

$$\varepsilon_l = \frac{\sigma_l}{E} = \frac{K\rho ghr}{2tE}(1-2\upsilon) = \frac{\Delta d_l}{d} \qquad \text{Equation 2-27}$$

The new diameters d_c and d_l of the deformed round hole can be obtained by adding the original diameter of the undeformed hole ,d_0, to Δd_c and Δd_l, respectively, where Δd_c and Δd_l are attainable by re-arranging equation 2-26 and equation 2-27. These dimensions become:

$$d_c = d_0 + \Delta d_c = d_0 + d_0\frac{K\rho ghr}{tE}(2-\upsilon) = d_0\left[1 + \frac{K\rho ghr}{2tE}(2-\upsilon)\right] \qquad \text{Equation 2-28}$$

$$d_l = d_0 + \Delta d_l = d_0 + d_0\frac{K\rho ghr}{tE}(1-2\upsilon) = d_0\left[1 + \frac{K\rho ghr}{2tE}(1-2\upsilon)\right] \qquad \text{Equation 2-29}$$

Using the equation for an ellipse given by equation 2-21, and substituting the circumferential and longitudinal diameters obtained in equations 2-28 and 2-29, the area of a deformed hole, that is under a bi-axial stress state, is deduced as follows:

$$A = \frac{\pi}{4}d_0^2\left[1 + \frac{K\rho ghr}{2tE}(2-\upsilon)\right]\left[1 + \frac{K\rho ghr}{2tE}(1-2\upsilon)\right]$$

$$A = \frac{\pi}{4}d_0^2\left[1 + \frac{K\rho ghr}{2tE}(1-2\upsilon) + \frac{K\rho ghr}{2tE}(2-\upsilon) + \left(\frac{K\rho ghr}{2tE}\right)^2(2-\upsilon)(1-2\upsilon)\right]$$

$$A = \frac{\pi}{4}d_0^2\left[1 + \frac{3K\rho ghr}{2tE}(1-\upsilon) + \left(\frac{K\rho ghr}{2tE}\right)^2(2-\upsilon)(1-2\upsilon)\right] \qquad \text{Equation 2-30}$$

Equation 2-30 gives the area of the orifice on the side of a biaxially stressed pressurised pipe. Substituting this equation into the orifice equation, given as $\left(q_{actual} = C_d A\sqrt{2gh}\right)$, gives the actual flow through an orifice. This flow can, therefore, be represented as follows:

$$q_{actual} = \frac{\pi}{4} d_0^2 C_d \sqrt{2g} h^{0.5} \left[1 + \frac{3K\rho ghr}{2tE}(1-\upsilon) + \left(\frac{K\rho ghr}{2tE} \right)^2 (2-\upsilon)(1-2\upsilon) \right] \quad \text{Equation 2-31}$$

By multiplying the pressure head into the brackets, the actual flow through a round orifice, that is located within a biaxially pressurised pipe, is obtained:

$$q_{actual} = \frac{\pi}{4} d_0^2 C_d \sqrt{2g} \left[h^{0.5} + \frac{3K\rho ghr}{2tE}(1-\upsilon) + \left(\frac{K\rho gr}{2tE} \right)^2 h^{2.5} (2-\upsilon)(1-2\upsilon) \right] \quad \text{Equation 2-32}$$

2.5 Pressure–Leakage Relationships of Individual Leaks

Several studies have shown that water distribution system leakage is highly sensitive to the systems pressure (Van Zyl, et al., 2008). Van Zyl and Clayton (2007) proposed four factors that may be responsible for the sensitvity of leakage to pressure, i.e. leak hydraulics, pipe material behaviour (variations in leak area as a function of pressure), soil hydraulics and water demand. These will be discusse in more detail.

As a result engineers have been paying particular attention to the relationship between pressure and leakage from the moment they realised that the water loss in their systems can no longer be ignored (Thornton, 2002).

A recent report by IWA International, cited by Thornton (2003), indicated that proactive pressure management was practiced in very few countries - most countries do not practice pressure management as a strategy to manage leakage.

In part, this can be attributed to the fact that leakage management practice has not been traditionally associated with measuring operating pressures or taking account of pressure when analysing leakage data. Many practitioners still believe, incorrectly, that system leakage is relatively insensitive to presssure, and most of them feel that the prediction of the effects of pressure management can not be made with any degree of certainty. However, in recent times, there has been notable advances in analysing diverse sets of experimental and field test data, and also in developing an understanding of pressure-leakage relationships. There have been some success stories, such as the savings of 24MLD of unwanted demand and leakage in Khayelitsha Township in South Africa, through the installations of numerous prerssure reducing valves, and in Sao Paulo, Brazil, which saved 260MLD, as well as various numerous single installations in individual systems (Thornton, 2003).

According to Franchini and Lanza (2013), being able to define a relationship capable of linking the leakage from a pipe to the internal system pressure head, is of considerable importance in order to devise management rules that are aimed at controlling leaks and limiting breakages in water distribution systems. Therefore, in recent years significant developments in the understanding of the relationship between pressure and leakage based on the results of theoretical, numerical, experimental and field studies (van Zyl J. E., 2014)

This section will explore the different methods and developments that exist pertaining to how pressure relates to leakage discharge. The first development looks into the orifice flow equation, derived from the Torricelli equation, which sets the basis of leakage calculations. The second development will explore the conventional equation or the power equation that is well established in practice. Finally, the Fixed and Variable Area Discharge concept, which forms the basis of this study, will be explored.

2.5.1 Orifice Flow Equation

Leakage is a discharge and many researchers have used the orifice equation to define the hydraulics around the leak (van Zyl J. E., 2014). According to Urquhart (1977) "an orifice is a hole of regular form through which water flows". Orifices come in many forms; circular, square rectangular or any other regular form (Urquhart, 1977).

To understand the derivation of the orifice flow equation, consider a tank with a leak (orifice) on the side, with the tank's area much greater than the leak area as shown in Figure 2-20

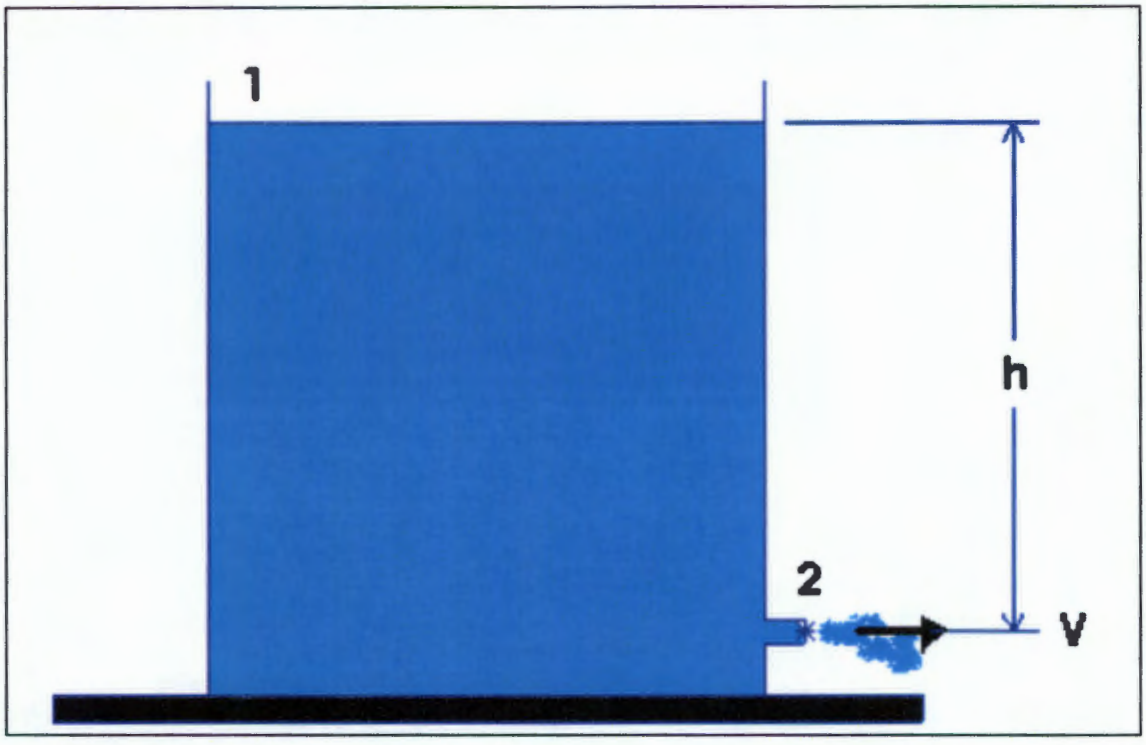

Figure 2-20: Water jetting from a large tank through a well-rounded opening (Buckley R. , 2007)

Writing the Bernoulli equation for any point in the tank and another point being located at the leak area (the vena contractor), under the assumption of zero energy loss, will result in the Torricelli's equation. Orifice hydraulics is generally based on the Torricelli's equation, which essentially states that the velocity through an orifice can be described by:

$$v = \sqrt{2gh} \qquad \text{Equation 2-33}$$

Where v is the velocity, g is the acceleration due to gravity and h is the pressure head at the orifice. The pressure head is a fundamental function of the orifice equation and is defined as

the depth of water above the centre line of the orifice producing the discharge, and the discharge is known as the jet. There are horizontal and vertical orifices, depending on the orientation of the plane that the orifice lays.

The well-known orifice flow equation is derived from the Torricelli's equation. This orifice equation describes the leakage through a round hole, and is given as follows:

$$Q = C_d A\sqrt{2gh} \qquad \text{Equation 2-34}$$

Where Q is the flow rate, C_d is the discharge coefficient (which will be explored further in the next section), g is the gravitational acceleration, and h is the pressure head.

2.5.1.1 Discharge Coefficient in the Torricelli equation

The reason why the discharge coefficient is introduced into the Torricelli equation is because it takes into account the fact that, in real life, the effective area of the orifice is reduced by the fluid jet that contracts downstream of the orifice. It can be determined experimentally by measuring the volume, or weight of water, discharged under a given head in a known time. Three factors that affect the discharge coefficient will be explored: pressure head, type of leak area and type of flow (i.e. Reynolds number).

Different experiments reported in Lea, (1908) and Brater and King, (1976), cited by Schwaller, (2012), showed that the values of the discharge coefficients decrease with increasing pressure and decreasing area. The values found by Bovey (1909), cited by Brater & King, (1976), showed that the shape of the orifice also has an influence on the variation of discharge coefficient. Bovey found that the shape with the greatest C_d is the rectangle orifice and the lowest C_d was the circular orifice - see Figure 2-21.

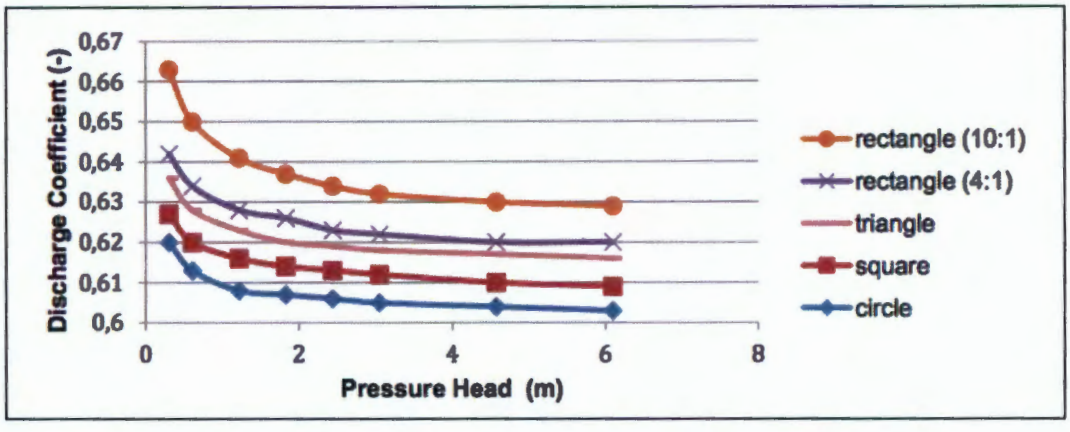

Figure 2-21: Discharge Coefficient Plotted against Pressure Head for Orifices with Same Area but Different Shape (adapted from (Brater & King, 1976))

From Figure 2-21 it can be seen that all orifices exhibit a common trend in behaviour, showing a somewhat exponential relationship, when it comes to discharge coefficient against pressure head. Interestingly, the lowest discharge coefficient is exhibited by the circular orifice.

Other previous studies, shown in Figure 2-22 have also shown how the area of various orifices influences the discharge coefficient. For the constant pressure head of 15m, the resulting behaviour was found and shown in Figure 2-22.

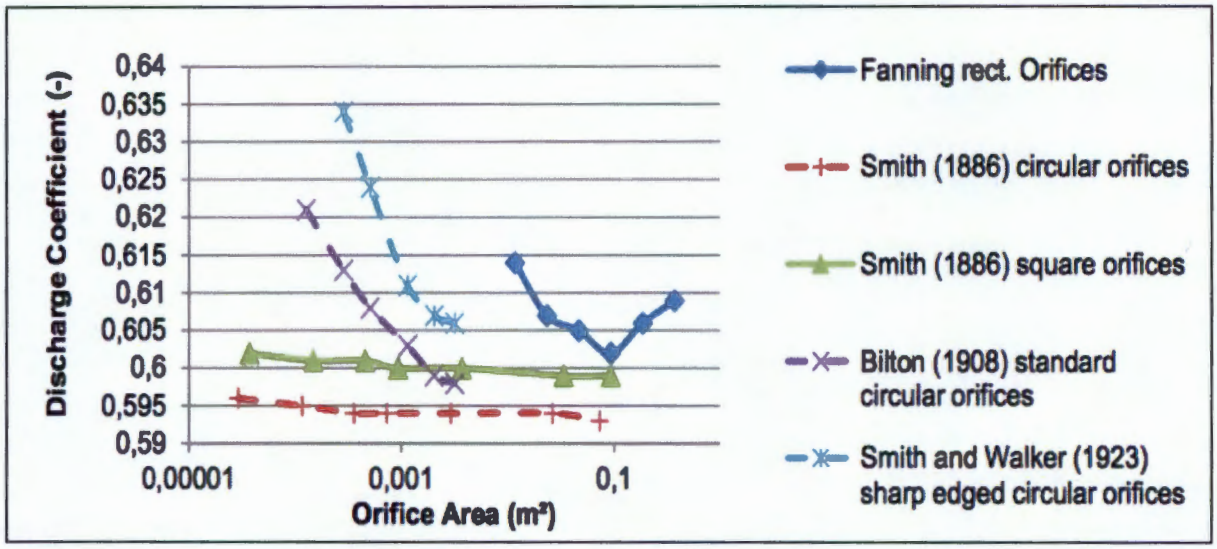

Figure 2-22: Discharge Coefficient Plotted against the Orifice Area for a Pressure Head of Approximately 15m (adapted from (Brater & King, 1976))

Finally, some experimental work conducted testing the orifice equation has shown that the square root relationship between the flow rate and the pressure head is only valid for turbulent flows, i.e. flows with Reynolds number greater than 4 000. For laminar flows, with Reynolds numbers less than 10, the discharge coefficient also becomes a function of the pressure head. Figure 2-23 below shows the relationship between C_d and Reynolds number for discharges through a 1mm diameter orifice that is drilled into the side of a 15mm diameter copper pipe.

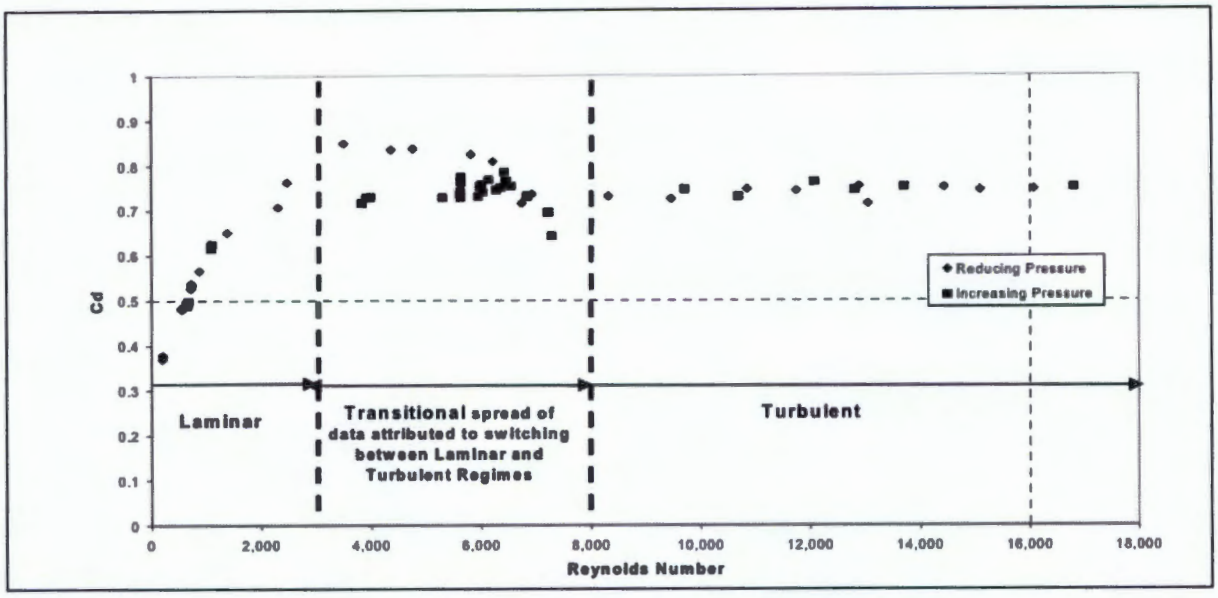

Figure 2-23: Discharge Coefficient of 1mm Diameter Orifice vs Reynolds Number ((Lambert, 2001)

From Figure 2-23 it can be seen that, for this particular set of test data, in the laminar flow range (R<3000), C_d rises rapidly to about 0.8 as R increases. This implies that discharge rates of small leaks may be very sensitive to changes in pressure because of changes in C_d. In the fully turbulent flow range (R>8 000), C_d remains steady at around 0.75, and in the transitional flow range, C_d oscillates between 0.7 and 0.85.

Leak openings in distribution systems can be considered as orifices and, thus, should adhere to the orifice equation (Equation 2-34). However, in practice, this equation has proven not to be a satisfactory model for the behaviour of leaks in pressurised systems. International data analysed by Lambert in 2001 on pressure leakage relationships, has demonstrated that leakage in distribution systems is generally much more sensitive to pressure than would be predicted by the square root relationship, with different components of the leak responding differently to pressure. As a result there has been alternative leakage equations adopted by leakage practitioners, namely: the *power equation* and the *FAVAD equation*. These will be discussed in detail next.

2.5.2 Power Equation

The power equation is often referred to as the conventional approach, by practitioners in industry, to give an indication of leakage in a pressurised system. This approach of modelling leakage behaviour is also derived from the original orifice equation. It was adopted by leakage practitioners, even as far back as 1881 (Lambert, 2001). This power equation is presented in the form:

$$Q = Ch^{N1} \qquad \text{Equation 2-35}$$

Where Q is the leakage flow rate, h is the pressure head in the system, C is the leakage coefficient and $N1$ is the leakage exponent.

There has been great focus on the leakage exponent in efforts to characterise the behaviour of system leaks with pressure. Field tests, such as those conducted by Greyvenstein and Van Zyl's, (2007), have found system leakage exponents substantially higher than 0.5, which the orifice equation suggests.

Van Zyl and Greyvenstein's (2007) study showed that the leakage exponent, N1, of individual leaks can be substantially higher than 0.5 and sometimes even lower than 0.5. Their study proposed four factors that may be responsible for these high variations in N1. These were: leak hydraulics, pipe material behaviour, soil hydraulics and water demand. Of these factors, van Zyl & Clayton (2005) suggest that the pipe material behaviour, meaning that the variation of leak area with pressure, is the most important. Each of these factors will be discussed in greater detail in Section 2.6.

2.5.3 Fixed and Variable Area Discharge Approach

May (1994) was the first to propose the concept of fixed and variable leaks. May's paper became very influential as it explained the wide range of pressure and leak flow relationships measured internationally. This led to the development of the fixed and variable area discharges (FAVAD) concept, which was then adopted and recommended for international use. May (1994) suggested that some leaks have fixed areas (with an exponent of 0.5), while others have variable areas (with an exponent of 1.5). The proposed leakage equation by May (1994) was in the form:

$$Q = k_1 h^{0.5} + k_2 h^{1.5} \qquad \text{Equation 2-36}$$

Cassa and Van Zyl (2010) investigated this concept by testing three 60mm long crack leaks in a 110mm class 6 uPVC pipe. These cracks were oriented differently: longitudinally, spirally and circumferentially. Using finite element models they investigated, for a purely elastic state, how the crack area would vary with an increasing pressure head. The findings of the study are shown in Figure 2-24.

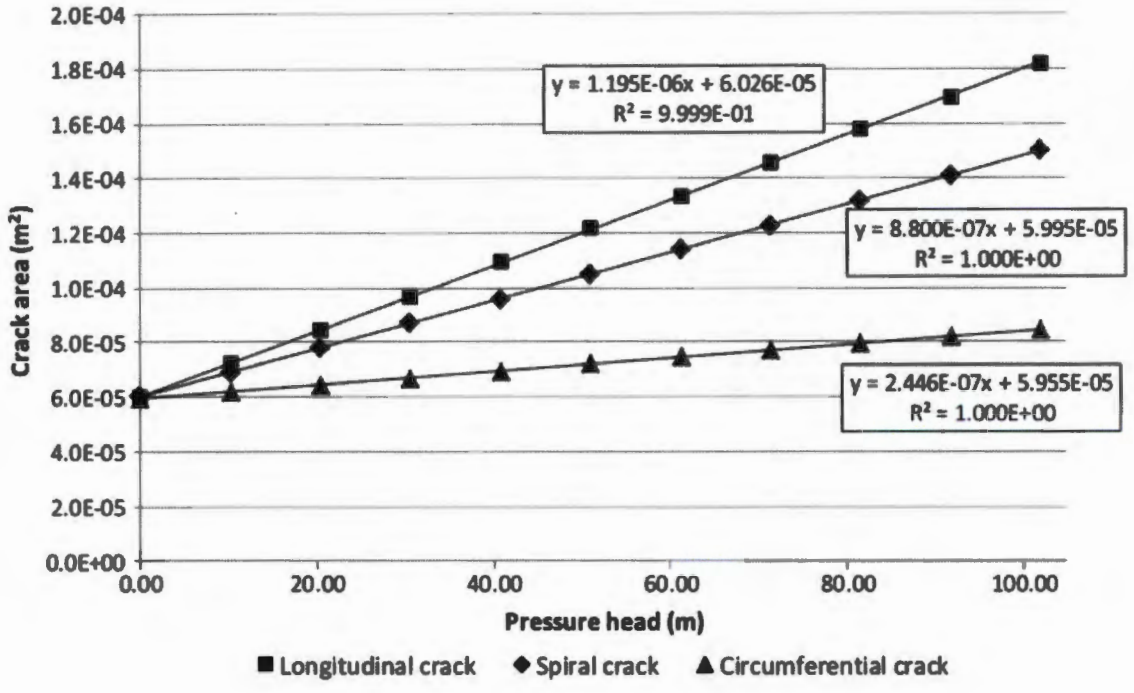

Figure 2-24: Areas of 60mm Long Cracks in a Class 6 uPVC Pipe as a Function of Pressure Head as Determined by Finite Element (Cassa and Van Zyl, (2010))

From Figure 2-24 it can be seen that leak areas expanded linearly irrespective of the crack orientation. This linear relationship can be expressed with the equation:

$$A = A_0 + mh \qquad \text{Equation 2-37}$$

Where h is the pressure head, A_0 is the initial leak area and m is the head-area slope. The FAVAD concept is also developed from the orifice equation. The orifice equation is based on Torricelli's equation, which states that the velocity of flow through an orifice is given by:

$$Q = C_d A\sqrt{2gh} \qquad \text{Equation 2-38}$$

As previously mentioned, the orifice equation is not a good indicator of leak behaviour in pressurised systems. The inaccuracies that pertain to this equation are usually because it does not consider other properties, such as material deformation, affecting the leakage behaviour. For example, rigid materials usually have lower exponents, compared to the fixed value of 0.5 that the orifice equation suggests (Greyvenstein, 2007). These inaccuracies have resulted in various efforts to improve the orifice equation.

With this, Cassa and van Zyl (2010) introduced a new interpretation of the FAVAD equation. Their study showed that, indeed, a leak is made up of a fixed and variable area (See Figure 2-25). The FAVAD equation, proposed by Cassa and van Zyl (2010), was developed by replacing Equation 2-37 into the area variable of Equation 2-38, which then yields:

$$Q = C_d\sqrt{2g}\left(A_0 h^{0.5} + mh^{1.5}\right) \qquad \text{Equation 2-39}$$

Where Q is the flow rate, C_d is the discharge coefficient, g is the acceleration due to gravity, A_0 is the initial leak area at zero pressure head, m is the head-area slope and h is the pressure head. Figure 2-25 shows the fixed leak area and the variable leak area.

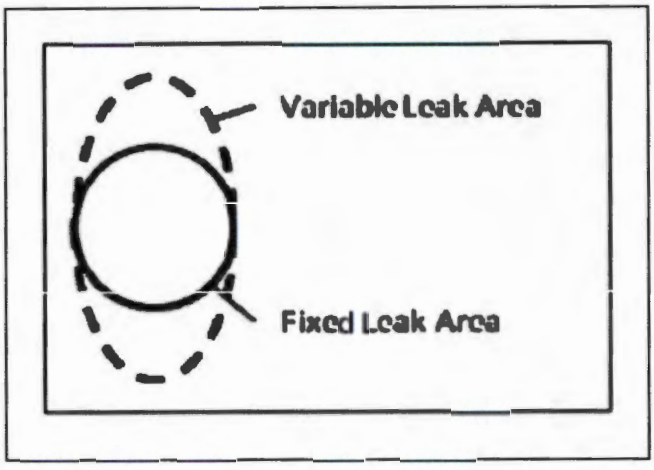

Figure 2-25: Fixed and Variable Leak Areas (Schwaller, 2012)

While Equation 2-39, proposed by Cassa and van Zyl (2010), seems identical to the Equation 2-36 that May (1994) proposed, it has some distinct interpretive differences in that leaks are not either fixed or variable, while all leaks are considered variable to some degree. In other words, as pressure in a system increases, so does the area of the leak. For leaks with very small head-area slopes (m), it can be seen that the first term ($Q_{fixed} = C_d\sqrt{2g}A_0 h^{0.5}$) of Equation 2-39 will dominate, thus resulting in an effective leakage exponent of 0.5. Conversely, for the more flexible leaks with high head-area slopes, the second term ($Q_{expanding} = C_d\sqrt{2g}mh^{1.5}$) becomes more dominant, thus resulting in a leakage exponent of 1.5.

2.5.3.1 Leakage Number

The fixed leaks are generally defined by the first term and the second term defines the variable or expanding leak. By comparing the ratio of the fixed leak to the variable leak, a new term called the leakage number, L_N, can be found (Cassa & Van Zyl, 2011).

$$L_N = \frac{Q_{expanding}}{Q_{fixed}}$$

$$L_N = \frac{C_d\sqrt{2g}mh^{1.5}}{C_d\sqrt{2g}A_0h^{0.5}}$$

$$L_N = \frac{mh}{A_0} \qquad \text{Equation 2-40}$$

The relationship between the leakage number and the leakage exponent can be obtained by calculating the leakage number for different values of head-area slope m, and initial leak area A_0, at different pressure heads h. The leakage number can then be plotted against the leakage exponent and the result is shown below in Figure 2-26.

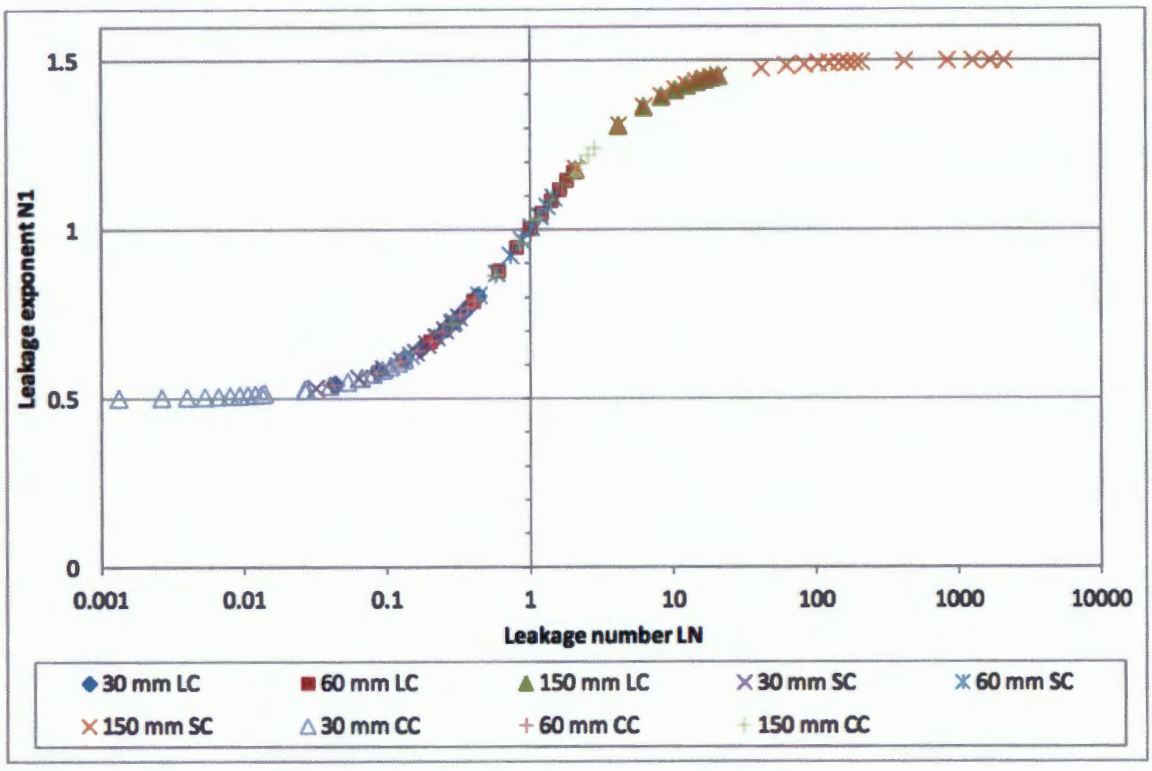

Figure 2-26: Relationship between Leakage Exponent N1 and Leakage Number Ln (Cassa & Van Zyl, 2011)

Figure 2-26 also shows that, regardless of what the head-area slope and the initial leak area is the relationship between the $N1$ and the leakage number L_N will plot on the same curve. The curve limits are 0.5 and 1.5, which are the same limits as the FAVAD equation. Also, it can be seen that when the leakage number L_N is 1, the leakage exponent $N1$ is also equal to 1; when the leakage number L_N is less than 1, the leakage exponent $N1$ is also less than 1: and when the leakage number L_N is greater than 1, then the leakage exponent is also greater than 1. From Figure 2-26 a relationship can be drawn between the leakage number L_N and the leakage exponent $N1$, because the curves are asymptotic to 0.5 and 1.5.

$$L_N = \frac{(N1 - 0.5)}{(1.5 - N1)}$$ Equation 2-41

$$N1 = \frac{(1.5L_N + 0.5)}{(1 + L_N)}$$ Equation 2-42

2.6 Factors Affecting Pressure–Leakage Relationship

Van Zyl and Clayton (2005) published some work that discussed possible factors that could be accountable for the observed high sensitivity of leakage to pressure. These factors included leak hydraulics, pipe material behaviour, soil hydraulics and, water demand. These will be discussed in this section.

2.6.1 Leak Hydraulics

In Section 2.5 various techniques on how to relate pressure and leakage were explained in some detail. It was shown that all adopted techniques were derived from the orifice equation, because one can always consider that a leak opening in a pipe is hydraulically equivalent to an orifice on the side of a tank. The reason why the orifice equation does not reflect, correctly, this relationship between leakage and pressure, is due to the fact that the leakage exponent of a constant diameter for the orifice equation is accepted as 0.5. This implies that the discharge coefficient c is not constant. As a result, it is plausible to model leaks differently, using a fixed discharge coefficient and allowing the exponent to vary.

An important feature, when looking into the leak hydraulics, is the type of flow which, typically, is associated with a linear relationship between head losses and flow rate. The different types of flow regimes are dependent on the Reynolds number. Subsequently, the Reynolds number for a typical leak opening or orifice can be expressed as:

$$R_e = \frac{4vR}{\upsilon} = \frac{4Q}{\upsilon P}$$ Equation 2-43

Where R_e is the Reynolds number, v is the velocity, ◆ is the kinematic viscosity of the fluid, and R the hydraulic Radius. Laminar flow through any orifice occurs when the Reynolds number is below 10 and turbulent flow occurs when Re is above 4 000 to 5 000. The transitional zone is represented with Re values that are intermediary. For these intermediate Re values the leakage exponent can vary from 1 (usually at the boundary of laminar/transition) and 0.5 (usually at the boundary of transitional/turbulent).

It is possible to find an expression for the maximum laminar and transitional flow, through different types of leak openings, for pressures that are typically found in water distribution systems. Firstly, the flow rate is written as the product of the velocity and area of an opening and this is given by:

$$Q = Av = \frac{\pi d^2}{4} v$$ Equation 2-44

Where d is the diameter of the leak opening. Writing the Reynolds equation (Equation 2-43) in terms of the hole diameter and replacing it with the orifice equation into equation 2-44, this yields:

$$q = \frac{\pi (vR_e)^2}{4C_d \sqrt{2gh}}$$ Equation 2-45

Figure 2-27 that follows illustrates the calculated maximum laminar and transitional flow for various types of leak openings. The openings representing cracks are depicted by a rectangular opening with the large l/b ratio.

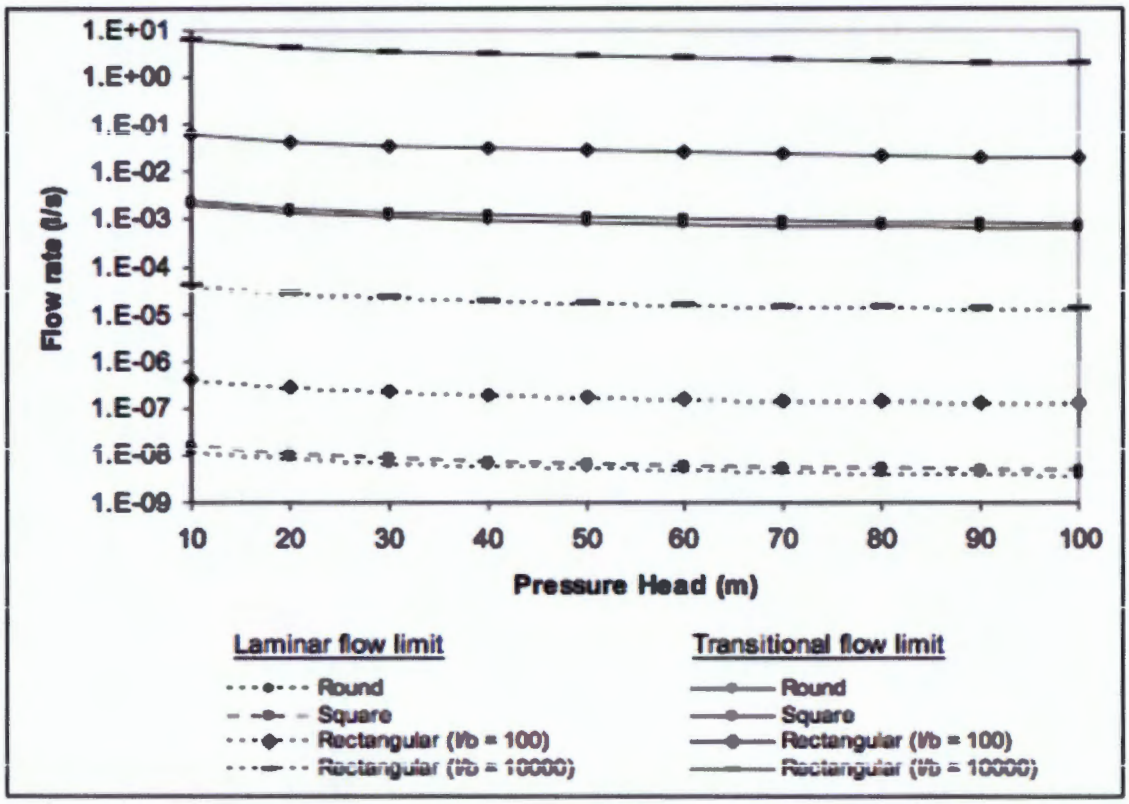

Figure 2-27: Maximum Laminar and Transitional Flow Rates for Different Types of Leak Openings (Van Zyl and Clayton (2005))

From Figure 2-27 it can be seen that the cracks (referred to as rectangular in the figure) portray a much higher laminar and transitional flow rate when compared to squares or round hole openings. Van Zyl & Clayton (2005) suggest that this can be attributed to their larger wetted perimeters.

As a result of the small flow rates' resulting from laminar flow it is most likely not going to play a significant role in leakage. Transitional flow rate, however, can be important because of background leakage and, thus, can contribute to leakage exponents that are greater than 0.5

(although not above 1.0 because the flow rate is not high enough), leakage exponents greater than 1 are usually caused by turbulent flows with higher flow rates (van Zyl & Clayton 2005).

2.6.2 Water Demand

It is often extremely challenging to separate legitimate water consumption from leakage measured when in the field. It is, therefore, crucial to understand the relationship between pressure and consumer demand, i.e. the behaviour of water demand as a function of pressure. According to Van Zyl, Haarhoff and Husselmann (2003) the effect of pressure on water demand Q_{demand} can be expressed as:

$$Q_{demand} = Ch^{\beta} \qquad \text{Equation 2-46}$$

Where C is a constant coefficient and β represents the elasticity of water demand with respect to pressure. There is a clear resemblance between the equation for demand elasticity, which shows the responsiveness of the quantity of water demanded, and the power equation for leakage. The water demand elasticity comprises of the effects of human behaviour; one example of this is monitoring how users react to increased pressures by opening taps less to obtain the same flow rate.

In a study done by (Bartlett, 2004) on water consumption patterns, at a student village at the University of Johannesburg, he found the indoor demand elasticity for pressure to be approximately 0.2. For outdoor use the elasticity was expected to be higher, because outdoor activities are typically time-based, rather than volume-based. However, the elasticity for outdoor activity water demand is unlikely to exceed 0.5.

According to van Zyl and Clayton (2005) it is possible that the minimum measured night flows will include some legitimate consumption in large systems. Since the combined leakage exponent for outdoor and indoor consumption is likely to be less than 0.5, it is plausible to conclude that systems with demand are likely to under-estimate the true leakage exponent of the system. This is true, provided that the levels of demand in the measured night flows do not differ significantly.

2.6.3 Soil Hydraulics

A simplistic geotechnical seepage theory that states, if head losses through the pipe orifice are neglected, the flow rate should be linearly proportional to the head of the water in the pipe at the leak (Walski et al., 2009). Following Darcy's Law, the flow rate q, that is in the soil for any given head on the orifice water-soil boundary, will be given as:

$$q = Fkh \qquad \text{Equation 2-47}$$

Where F is known as the form factor for the soil flow region, and k is the coefficient of permeability of the soil. However, it is important to note that the equation is under-pinned by assumptions which are not valid for seepage around a leaking water pipe.

Van Zyl and Clayton (2005) concluded that the interaction between a leaking pipe and its surrounding soil is rather complex. They are of the opinion that this relationship is unlikely to be linear as a result of interaction of soil particles with the orifice, the turbulent flow in the soil, the changing geometry of the unconfined flow regime, hydraulic fracturing and piping.

Some theoretical considerations suggest that continuous leaks, that are small enough from pipes, can easily drain away without any trace into the underlying granular soils. However, in places with lower permeability, soils such as clays and silts, and where hydraulic fracture is likely to occur, leaks become more visible as wet patches or even burst at the surface of the ground.

2.6.4 Pipe Material

Pipe material plays the most important role when it comes to factors that affect the pressure and leakage relationship. As a result of varying material properties, pipes of different materials will always fail in unique characteristic ways. The water pressure induced inside the pipe by the flowing water is taken up by the stresses in the pipe wall, and this may be the factor in failure and leakage behaviour. As a result of an increase in internal pressure the following effects can be observed:

i. New leaks are created by opening up of small cracks or fractures that do not leak at low pressures.
ii. The existing leak area in the pipe increases as the stresses in the pipe wall increase.
iii. The frequency of pipe bursts increases with a corresponding increase in maintenance costs.

Using experimental setups of failed pipes taken from the field and artificially induced leaks, (Greyvenstein & Van Zyl, 2007) measured the leakage exponents of both types of pipe. The study included round holes, longitudinal and circumferential cracks in uPVC, steel and asbestos cement pipes. All the flows were made turbulent and were exposed to the atmosphere. The resulting leakage exponents varied from 0.42-2.4.

A theoretical study carried out by (Buckley R. , 2007) at the University of Johannesburg, developed a model using basic mechanical and fluid principals, for the flow rate through a round hole in an elastic pipe:

$$q_{actual} = \frac{\pi}{4} d_0^2 C_d \sqrt{2g} \left[h^{0.5} + \frac{K\rho g r}{tE}(1-\upsilon)h^{1.5} - \left(\frac{K\rho g r}{tE}\right)^2 \upsilon h^{2.5} \right]$$

Where q is the leakage flow rate, d_0 is the original hole diameter, r is the pipe internal radius, t is the pipe wall thickness, E is the Elasticity modulus, C_d is the discharge coefficient, g is the acceleration due to gravity, υ is the Poisson's ratio, K is the concentration factor, ρ is the fluid density and h is the pressure head. This relationship also confirms that the processes involved in expanding leak area are not depicted correctly by the simple power relationship that is normally used to describe leakage. Buckley's equation contains three different leakage exponents of: 0.5, 1.5 and 2.5, respectively, which almost complements some of the field and

experimental observations. However, it was found that when Buckley's equation was used to measure leakage from typical pipes under normal pressure conditions the terms with the exponents 1.5 and 2.5 did not contribute much.

2.7 Previous Investigations of Pressure-Leakage Relationships

Previous investigations, that will help to build a more comprehensive understanding of the pressure leakage relationship, will be discussed in this section. These investigations include finite element models of the effects of elastic material behaviour on the leakage and practical experiments with PVC pipes.

2.7.1 Experimental Investigations

Greyvenstein (2004) conducted an experimental investigation into the pressure-leakage relationship of some failed water pipes, in Johannesburg. It was found that different failure modes and leak orientations result in different leakage rates and pressure relationships.

The Greyvenstein (2004) investigation included testing three pipe materials, namely, asbestos cement, steel and PVC with four different forms of failure. Longitudinal cracks, circular cracks, round holes and corrosion clusters were tested. A summary of typical results for the leakage exponent (N1) are shown in Table 2-1 below:

Table 2-1: Different Leakage Exponents (N1) Found in Greyvenstein's Study

Material	Leakage exponent (N1)
Asbestos-cement pipe with longitudinal crack	0.78-1.04
Steel pipe with corrosion cluster	1.90-2.30
uPVC pipe with longitudinal cracks	1.50-1.85
uPVC pipe with circular cracks	0.40-0.52

2.7.2 Numerical Studies

Numerous numerical studies have been conducted. Cassa (2010) conducted a numerical investigation of the behaviour of leak openings in PVC pipes under pressure. Pressurised pipes with defects were modelled using finite element methods in order to investigate the effects of material behaviour on the leakage exponent *N1*. It is important to note that for this investigation linear elastic behaviour was assumed throughout the study.

Finite element analysis enabled Cassa (2010) to observe the results of a pipe with a defect under internal pressure. The software used was ABAQUS, and pipes were modelled in a CAD program, after which they were assessed with the finite element analysis package. This investigation covered circular holes, longitudinal and circumferential cracks for various engineering materials.

The findings showed that, under linear elastic assumption, leak areas increased linearly with pressure, as is shown by Figure 2-28:

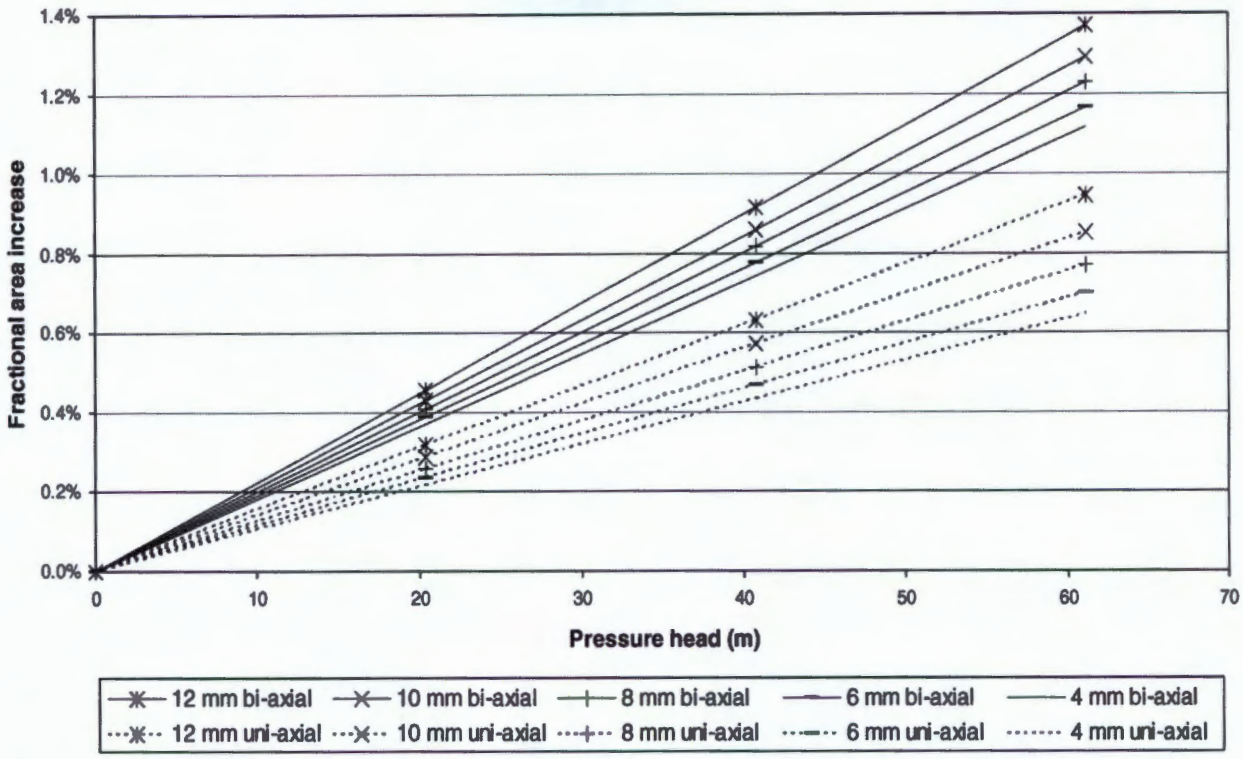

Figure 2-28: Fractional Increase in Area of Different Diameter Round Holes as a Function of Pressure in PVC Pipes

Figure 2-28 above illustrates the behaviour of a leak opening, characterised by the slope of the area vs pressure head line, which is called the head-area slope or *m*.

Using the FEA data from the finite element analysis, Cassa (2011) derived some empirical equations that can predict the head-area slope *m* for longitudinal, spiral, and circumferential cracks. However, head-area slope *m* equation for round holes was not defined. This study will, therefore, look at techniques to estimate the head-area slope *m* for round holes, by using the finite element method technique to investigate all the parameters involved in the pipe and, thereby, formulate an equation that can predict this head-area slope. The finite element method will be used to model the pipes and the hole leaks.

Given that the finite element analysis is a critical aspect of this study, the final section of the literature review will give an overview of the finite element method, how it works, its application and the software used in this study.

2.8 Theory of Finite Element Method

This chapter will give insight into the finite element method that is used in this study. The chapter will cover what the finite element method is, how it works, its applications and how it is applied in this study.

2.8.1 The Finite Element Analysis

The finite element method (FEA) is a method for numerical solution of field problems. FEA breaks down or cuts a structure into several elements (in this study the structure is classified as the pipe material). The cut elements of the structure are then reconnected at "nodes".

These nodes act as if they were pins or drops of glue that hold the cut elements together (Olivier de Weck & IL Yong Kim, 2004).

When working with FEA there are generally two types of analysis that can be carried out: 2-D modelling, and 3-D modelling. The 2-D method of analysis conserves simplicity and also allows the analysis to be run on a relatively normal computer; however, it tends to yield less accurate results. 3-D modelling, on the other hand, produces much more accurate results, but requires much more computing power. This study conducted a 3-D modelling analysis.

Within each of these modelling schemes, the user is allowed to insert numerous types of algorithms, which make the system being analysed behave either linearly or non-linearly. As expected, linear systems are less complicated and generally do not take into consideration plastic deformation of the system. Non-linear systems, on the other hand, do take into consideration plastic deformation, and sometimes are capable of testing the material all the way until fracture happens (Widas, 1997). In this study the systems were set to behave linearly, as linear elastic deformation was the material state being investigated.

2.8.2 How the Finite Element Method Works

The finite element method uses a complex system of elements and nodes, as was briefly explained above. These elements and nodes make up a grid that is called a mesh. The mesh is programmed in the FEA software to contain the properties, both material and structural properties, which then define the behaviour of the structure when subjected to certain loading conditions.

Depending on the anticipated stress levels of a particular area, the nodes will be assigned at certain densities throughout the material. Higher node densities are usually assigned to the regions that will receive the highest amounts of stress, and those areas that receive very little or no stress, the assigned node densities are also less. In many cases points of interest may consist of the following: fracture points (e.g. a crack in a pipe), induced holes, fillets, corners, and complex details.

The mesh created acts like a spider web in that in each node, a mesh element extends to each of the adjacent nodes. Many elements are then created by the web vectors which carry the material properties to the object.

Some of the steps of the finite element formulation are described below:

- mesh generation which is part of the pre-processing;
- a system of equations is assembled, in order for the elemental matrices and vectors to be evaluated;
- boundary condition must be applied;
- solving the linear system of equation and, finally;
- Post-processing.

2.8.3 Application of the Finite Element Method

FEA provides engineering information about a structure/component which cannot always be obtained by using traditional analysis methods. This information includes stress/strain, deformation, natural frequencies etc. Any design concept can be simulated in order to determine the concepts of real world behaviour under any desired environmental condition, therefore, allowing a better understanding of the concepts behaviour.

The finite element method can be divided into three, depending on the nature of the problem. These three categories are: steady state problems, Eigenvalue problems and transient problems (Fagan, 1992).

The most common use of the finite element analysis is solving steady state problems. Elastic problems in equilibrium can be analysed and distortions can be calculated. The stresses and strains experienced by the body can be obtained from the calculated displacements.

Eigenvalue problems are an expansion of the steady state problems; they involve the calculation of fundamental characteristics of the entire system. The FEA can be used to determine the buckling loads of structural elements, the natural frequencies and mode of vibration of solids and fluids.

Transient problems have a time dimension, in addition to the steady state and the Eigenvalue problem. The loads can be functions of time, and the forced response of the body can be determined using the finite element method.

Like any other approximate numerical method, the solution that is produced by the finite element analysis contains a certain amount of error. The magnitude of this error depends on the type, the size, and accuracy of the model that is used for the analysis. This is why not all finite element models are created equal. Sensitivity analyses are usually done in order to build the most suitable model.

2.8.4 Finite Element Analysis Software and Process used in this Study

The commercial finite element software used in this study is ABAQUS. There are many other finite element software packages. However, ABAQUS was the software of choice because the research edition license is available to students at the University of Cape Town to conduct finite element related research.

The ABAQUS software was written to support a nonlinear solution approach to structural mechanics. ABAQUS has an extensive library tools that can model almost any geometry and material that the user may desire to model. Most engineering materials include: metals, rubber, polymers, soils and rocks, as well as composites (Hibbit, 2004). A complete analysis usually consists of the stages shown in Figure 2-29.

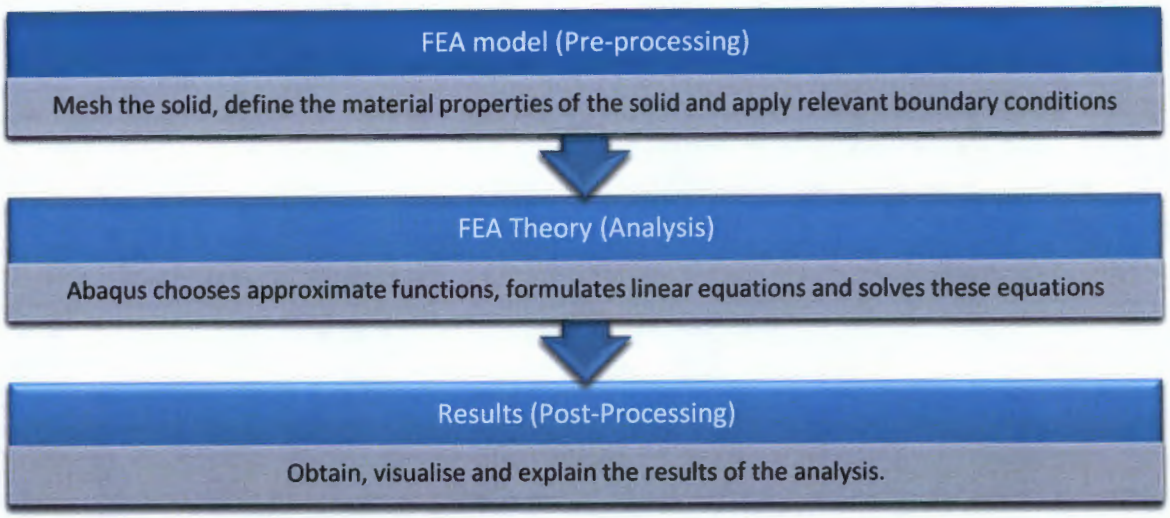

Figure 2-29: General Procedure of the Finite Element Analysis

From Figure 2-29 there are three main stages of an ABAQUS analysis: pre-processing, analysis and the post-processing (Hibbit, 2004).

2.8.5 Sensitivity Analysis

In order to determine the optimum element size for the different geometric properties analysed in this study, various sensitivity analyses must be carried out. This is done by varying the element size and plotting the stresses which correspond to the element size. Eventually the stresses converge and from this point of convergence the optimum element size can be determined.

The accuracy of the base model increases as the element size of a model decreases. This is because when an element represents a smaller area of the model part, there is a better indication of the stresses, strains and displacements which will occur at each node. However, elements which are too small reduce the computational speed, taking longer to simulate the model, and often require larger processing power.

The main focus of this study is to monitor changes in stress and deformations around the leak hole, in order to understand how the hole deforms with induced internal pressure. Therefore, it is critical that around the hole there must be a large number of elements at a small element size. As explained previously, the main reason for using a smaller element size for the local mesh around the hole area, is because this would result in greater accuracy in the results obtained about the hole deformation. As a result, there are two different sensitivity analyses that must be carried out for the base models; one sensitivity analysis must be done in order to determine the optimal element size around the hole, and the second sensitivity analysis must be done in order to determine the optimum element size for the rest of the base model, i.e. the

global size. The sensitivity analysis procedure will be explained in greater details in the proceeding chapter.

3 Mathematical Model Developed to Understand Round Hole Deformation in Pressurised Pipes

This chapter begins with developing a technique to understand how a round hole leak behaves in a pressurised pipe. This is particularly significant because, in deriving the equation for the head-area slope *m,* it is important to know what the final shape of the hole will be, after an internal pressure is applied to the pipe. From previous literature, it is always assumed that all leak holes deform into an elliptical shape once the pressure is applied in the pipe. In order to unpack this, and investigate the true deformation behaviour of a round hole, an excel model is developed. This model shows how the hole will deform under various pressures. The results obtained from the model are compared to a known shape, in this case an ellipse, in order to prove whether the hole becomes an ellipse or just an oval-like shape.

3.1 Understanding Behaviour of Round Holes in Pressurised Pipes

A mathematical formulation is used to confirm the resulting shape of a hole in a pressurised pipe. Previous research has always assumed an elliptical shape. This model will not assume any shape but instead uses mathematical techniques to understand the form of shape that results after a pressure is applied.

It is also noted that this method does not take into account the fact that, by virtue of the hole being in a pipe, it exists on a curved surface (pipe geometry). However, the pipe curvature was ignored, on the assumption that the holes were small compared to the pipe diameter and, therefore, the curvature has little effect on the hole geometry. Consequently, the assumption presumes that the hole is on a flat surface.

Consider the initial leak area as a round hole defect on a pipe. The original hole size is chosen to be described, as shown in

Figure 3-1.

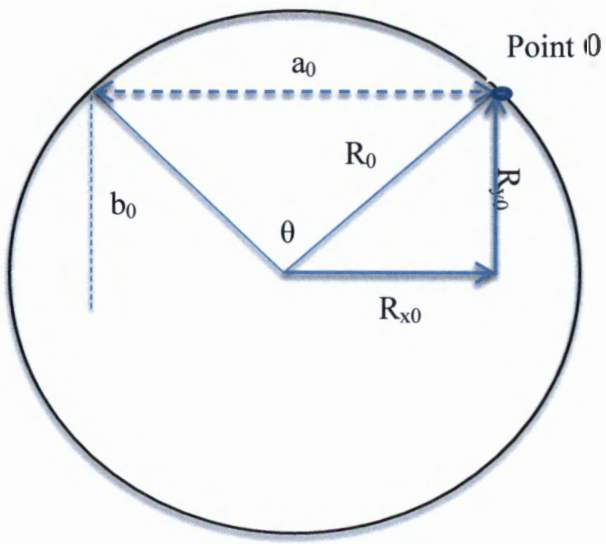

Figure 3-1: Geometry of round hole

Letting R_0 be the radius of the round hole, a_0 the cord length, and b_0 the vertical distance from horizontal (running through the centre) to the coordinate "Point 0". Then the radius R_0 has two components that can be defined as:

$$R_{x0} = \frac{a_0}{2} = R\sin\left(\frac{\theta}{2}\right)$$

$$R_{y0} = b_0 = R\cos\left(\frac{\theta}{2}\right)$$

$$\text{For } \{0 < \theta < 4\pi\}$$

These two components (R_{x0} and R_{y0}) plot the coordinate of any point on the circumference of the hole. For the given range of θ a full set of points can be plotted along the circumference to form the hole. R_{x0} and R_{y0} here are taken as lines along the longitudinal and circumferential axis respectively (see

Figure 3-1). Assuming Hooke's law, when an internal pressure (P), resulting in a stress (σ), is applied in the pipe, the lines R_{x0} and R_{y0}, experience a change in length, ΔR_x and ΔR_y respectively. The circumferential strains (ε_c) and longitudinal (ε_l) strains, resulting from the applied stresses, causing the changes in length, are given as:

$$\varepsilon_c = \frac{\sigma_c}{E} = \frac{K\rho ghr}{tE} = \frac{\Delta R_y}{R_{y0}}$$

$$\varepsilon_l = \frac{\sigma_l}{E} = \frac{K\rho ghr}{tE} = \frac{\Delta R_x}{R_{x0}}$$

Where the internal pressure P, has been expanded into the following parameters:

- ρ = Density of water (1 000 kg/m^3)
- g = Acceleration due to gravity (9.81m/s^2)
- h = Internal pressure (m)
- K = Stress concentration (Assumed to be 3 for round holes).
- σ_c = Circumferential stress
- σ_l= Longitudinal stress

Due to Poisson's ratio effect, υ, there are also associated strains in other directions. In other words, longitudinal strains result in circumferential strains and vice-versa - this can be illustrated as follows:

Longitudinal strains that are due to the circumferential stresses:

$$\varepsilon_l = -\varepsilon_c \upsilon = -\frac{\sigma_c}{E}\upsilon = -\frac{K\rho ghr}{tE}\upsilon = \frac{\Delta R_x}{R_{x0}}$$

Circumferential strains due to longitudinal stresses:

$$\varepsilon_c = -\varepsilon_l \upsilon = -\frac{\sigma_l}{E}\upsilon = -\frac{K\rho ghr}{2tE}\upsilon = \frac{\Delta R_x}{R_{x0}}$$

The effect of these additional strains can be incorporated by relating them to their respective stress states. For the uniaxial stress state, the strains that result from the circumferential stresses would cause longitudinal strains. For the biaxial case the longitudinal stress that exists will cause both longitudinal and circumferential strains and, similarly, the circumferential stresses will cause circumferential strains, as well as longitudinal strains. The super-position of these strains, in each direction, for the two stress states, is shown below.

Uniaxial:

$$\varepsilon_c = \frac{\sigma_c}{E} = \frac{K\rho ghr}{tE}$$

$$\varepsilon_l = -\varepsilon_c \upsilon = -\frac{\sigma_c}{E}\upsilon = \frac{K\rho ghr}{tE}\upsilon$$

Biaxial:

$$\varepsilon_c = \frac{K\rho ghr}{tE} - \frac{K\rho ghr}{2tE}\upsilon = \frac{K\rho ghr}{2tE}(2-\upsilon)$$

$$\varepsilon_l = \frac{K\rho ghr}{2tE} - \frac{K\rho ghr}{tE}\upsilon = \frac{K\rho ghr}{2tE}(1-2\upsilon)$$

These equations can be applied to the area expansion of a round hole, where the strains can be set to determine the change in R in the x and y directions, as follows:

$$\varepsilon_c = \frac{\Delta R_y}{R_{yo}}$$

$$\varepsilon_l = \frac{\Delta R_x}{R_{x0}}$$

The new coordinates R_x and R_y of the circle can be obtained by adding the original R_{y0} to ΔR_y and the original R_{x0} to ΔR_x which are attainable from re-arranging:

$$R_{new} = R_{original} + \Delta R$$

Therefore, the new deformed coordinates $R_{x\text{-}new}$ and $R_{y\text{-}new}$ for the uniaxial and biaxial state is given by the following equations:

Uniaxial:

Equation 3-1

$$R_{y-new} = R_{y0} + \Delta R_y = R\cos\left(\frac{\theta}{2}\right) + R\cos\left(\frac{\theta}{2}\right)\varepsilon_c = R\cos\left(\frac{\theta}{2}\right)(1+\varepsilon_c) = R\cos\left(\frac{\theta}{2}\right)\left(1+\frac{K\rho ghr}{tE}\right)$$

Equation 3-2

$$R_{x-new} = R_{x0} + \Delta R_x = R\sin\left(\frac{\theta}{2}\right) + R\sin\left(\frac{\theta}{2}\right)\varepsilon_l = R\sin\left(\frac{\theta}{2}\right)(1+\varepsilon_l) = R\sin\left(\frac{\theta}{2}\right)\left(1+\frac{K\rho ghr}{tE}\upsilon\right)$$

Biaxial:

Equation 3-3

$$R_{y-new} = R_{y0} + \Delta R_y = R\cos\left(\frac{\theta}{2}\right) + R\cos\left(\frac{\theta}{2}\right)\varepsilon_c = R\cos\left(\frac{\theta}{2}\right)(1+\varepsilon_c) = R\cos\left(\frac{\theta}{2}\right)\left(1+\frac{K\rho ghr}{tE}(2-\upsilon)\right)$$

Equation 3-4

$$R_{x-new} = R_{x0} + \Delta R_x = R\sin\left(\frac{\theta}{2}\right) + R\sin\left(\frac{\theta}{2}\right)\varepsilon_l = R\sin\left(\frac{\theta}{2}\right)(1+\varepsilon_l) = R\sin\left(\frac{\theta}{2}\right)\left(1+\frac{K\rho ghr}{tE}(1-2\upsilon)\right)$$

For $0 < \theta < 4\pi$ the new coordinates for R_x and R_y can be plotted for the uniaxial and the biaxial stress state. These coordinates plot the shape of the new hole. The area of the new hole can be obtained using Riemann sums. This will be explained further in the following section of this chapter.

3.1.1 Area Calculation of Round Holes

The deformed hole areas that are obtained from plotting the coordinates $R_{x\text{-}new}$ and $R_{y\text{-}new}$ are calculated using the Riemann sum. In mathematics, a Riemann sum is defined as an approximation of the area that is under a curve. Using Excel an interval of $\theta = \pi/36$, equivalent to 5 degrees, is generated. Substituting for the pipe parameters of the base model the equations above for $R_{y\text{-}new}$ and $R_{x\text{-}new}$ plot 72 points along the original hole circumference and also the deformed hole circumference. The 5 degrees interval is used in order for the leak hole to be divided into a series of trapezoidal regions, as shown in Figure 3-2. Theoretically, the sum of the area of all the trapezoids should approximate the area of the hole, i.e., the Riemann Sums method. For illustration purposes Table 3-1 below shows the calculated coordinate points for the original and deformed hole shown in Figure 3-2.

The area of the original hole is calculated using the Riemann sum and the value that was obtained was compared to the area of a circle, given by the mathematical equation, $A = \pi r^2$. In order to test the accuracy of this technique, the original area of the hole found using the Riemann sum is compared to the area found using the mathematical equation. The percentage difference between the two results is in the range of 0.13%, which is sufficiently accurate, given that the Riemann sum technique is an approximation technique, and is used to validate the actual area of the hole.

Table 3-1: Showing How the Coordinate Points Were Plotted

		Original		Deformed (New)	
Degrees	Radians	R_x (mm)	R_y (mm)	R_x (mm)	R_y (mm)
0	0.000	0.000	2.000	0.000	2.059
5	0.087	0.174	1.992	0.175	2.051
10	0.175	0.347	1.970	0.348	2.027
15	0.262	0.518	1.932	0.518	1.989
20	0.349	0.684	1.879	0.685	1.935
25	0.436	0.845	1.813	0.846	1.866
30	0.524	1.000	1.732	1.001	1.783
35	0.611	1.147	1.638	1.149	1.686
40	0.698	1.286	1.532	1.287	1.577
45	0.785	1.414	1.414	1.416	1.456
50	0.873	1.532	1.286	1.534	1.323
55	0.960	1.638	1.147	1.640	1.181
60	1.047	1.732	1.000	1.734	1.029
65	1.134	1.813	0.845	1.815	0.870
70	1.222	1.879	0.684	1.882	0.704
75	1.309	1.932	0.518	1.934	0.533
80	1.396	1.970	0.347	1.972	0.357
85	1.484	1.992	0.174	1.995	0.179
90	1.571	2.000	0.000	2.002	0.000
95	1.658	1.992	-0.174	1.995	-0.179
100	1.745	1.970	-0.347	1.972	-0.357
105	1.833	1.932	-0.518	1.934	-0.533
110	1.920	1.879	-0.684	1.882	-0.704
115	2.007	1.813	-0.845	1.815	-0.870
120	2.094	1.732	-1.000	1.734	-1.029
125	2.182	1.638	-1.147	1.640	-1.181
130	2.269	1.532	-1.286	1.534	-1.323
135	2.356	1.414	-1.414	1.416	-1.456
140	2.443	1.286	-1.532	1.287	-1.577
145	2.531	1.147	-1.638	1.149	-1.686
150	2.618	1.000	-1.732	1.001	-1.783
155	2.705	0.845	-1.813	0.846	-1.866
160	2.793	0.684	-1.879	0.685	-1.935
165	2.880	0.518	-1.932	0.518	-1.989
170	2.967	0.347	-1.970	0.348	-2.027
175	3.054	0.174	-1.992	0.175	-2.051
180	3.142	0.000	-2.000	0.000	-2.059
185	3.229	-0.174	-1.992	-0.175	-2.051
190	3.316	-0.347	-1.970	-0.348	-2.027

195	3.403	-0.518	-1.932	-0.518	-1.989
200	3.491	-0.684	-1.879	-0.685	-1.935
205	3.578	-0.845	-1.813	-0.846	-1.866
210	3.665	-1.000	-1.732	-1.001	-1.783
215	3.752	-1.147	-1.638	-1.149	-1.686
220	3.840	-1.286	-1.532	-1.287	-1.577
225	3.927	-1.414	-1.414	-1.416	-1.456
230	4.014	-1.532	-1.286	-1.534	-1.323
235	4.102	-1.638	-1.147	-1.640	-1.181
240	4.189	-1.732	-1.000	-1.734	-1.029
245	4.276	-1.813	-0.845	-1.815	-0.870
250	4.363	-1.879	-0.684	-1.882	-0.704
255	4.451	-1.932	-0.518	-1.934	-0.533
260	4.538	-1.970	-0.347	-1.972	-0.357
265	4.625	-1.992	-0.174	-1.995	-0.179
270	4.712	-2.000	0.000	-2.002	0.000
275	4.800	-1.992	0.174	-1.995	0.179
280	4.887	-1.970	0.347	-1.972	0.357
285	4.974	-1.932	0.518	-1.934	0.533
290	5.061	-1.879	0.684	-1.882	0.704
295	5.149	-1.813	0.845	-1.815	0.870
300	5.236	-1.732	1.000	-1.734	1.029
305	5.323	-1.638	1.147	-1.640	1.181
310	5.411	-1.532	1.286	-1.534	1.323
315	5.498	-1.414	1.414	-1.416	1.456
320	5.585	-1.286	1.532	-1.287	1.577
325	5.672	-1.147	1.638	-1.149	1.686
330	5.760	-1.000	1.732	-1.001	1.783
335	5.847	-0.845	1.813	-0.846	1.866
340	5.934	-0.684	1.879	-0.685	1.935
345	6.021	-0.518	1.932	-0.518	1.989
350	6.109	-0.347	1.970	-0.348	2.027
355	6.196	-0.174	1.992	-0.175	2.051
360	6.283	0.000	2.000	0.000	2.059

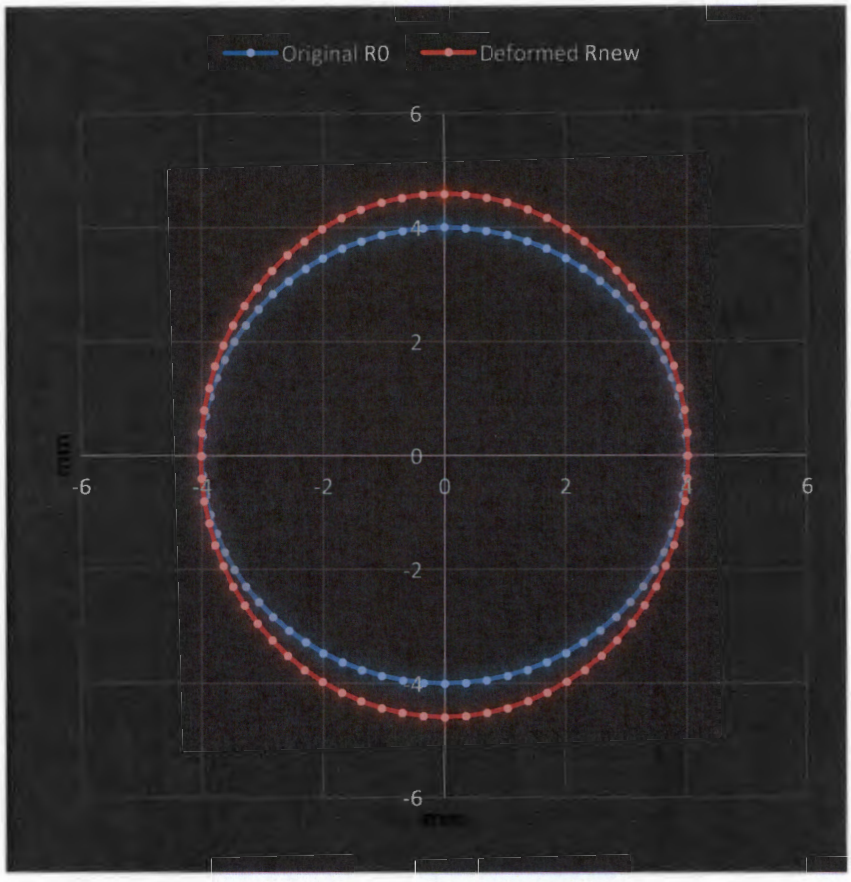

Figure 3-2: Showing How the Holes Were Divided in Excel

Using the Excel model, various pressures are applied and the hole deformation is monitored. Indeed, it is clear that an oval-like shape results when the internal pressure is applied. Buckley (2007) assumed, in his analytical derivation, that after applying an internal pressure to the pipe, the leak hole deforms and becomes an ellipse, and his theoretical analysis was based on this assumption. This study investigates this assumption, and seeks to validate what the true deformed area of the leak hole becomes. Appendix D shows how these models were setup for each hole on Excel.

Figure 3-3 shows the 6mm original leak hole (In blue), compared to the deformed hole after the pressure is applied (In red). It can be seen that the deformed shape takes on an "oval-like" shape. This oval-like shape area will be compared to the equivalent elliptical area to see how well they compare.

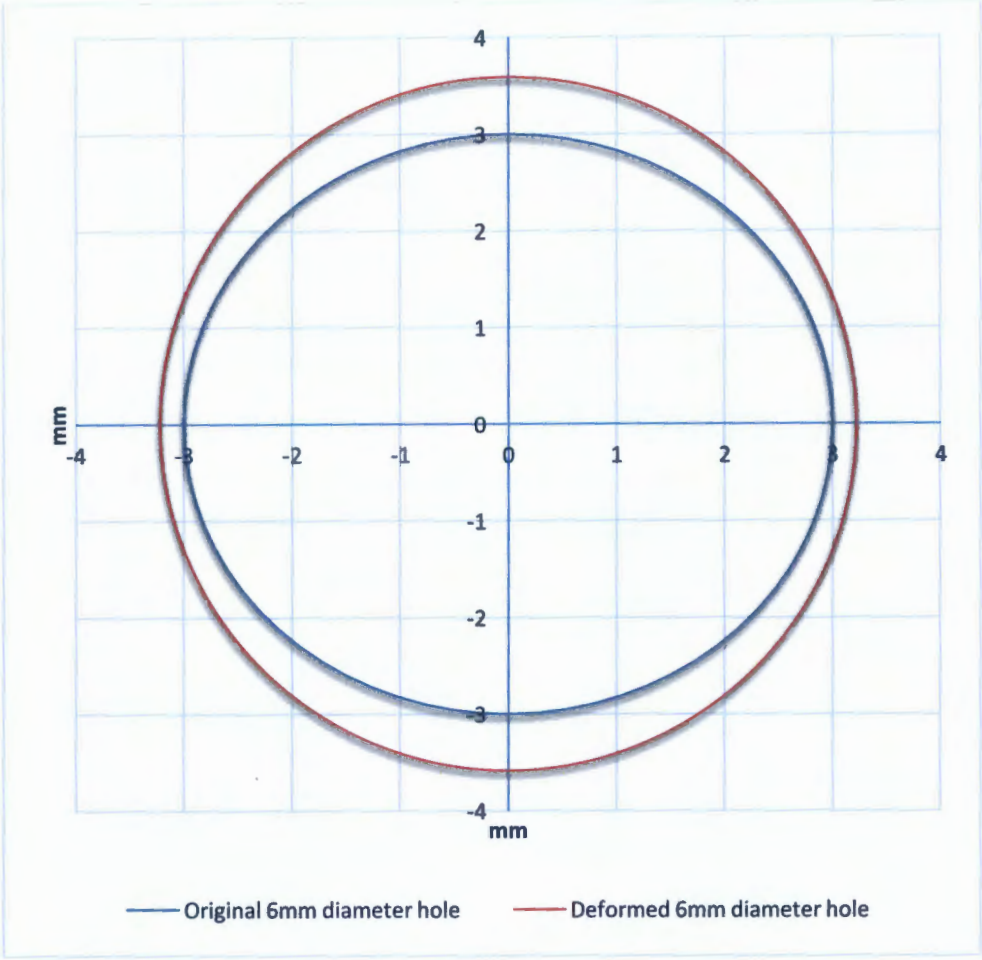

Figure 3-3: Illustration of Original Area and Deformed Area

The Riemann sum technique is used to calculate the area of both the original and the deformed holes. This was done in order to classify the "oval like" shape, and thereby validate whether indeed it is elliptical, as literature assumes. The areas calculated using the Riemman sum, were compared to the areas of equivalent ellipses to see how closely these matched. Table 3-2 shows how these compared.

Table 3-2: Table Indicating Resulting Hole Areas After Pressure is Applied

Hole diameter x 10^{-3} (m)	Deformed area (m^2) by Riemann sum	Equivalent ellipse area(m^2)	% Difference between area
2	12.78 x 10-6	12.79 x 10-6	0.08
4	50.29 x 10-6	50.35 x 10-6	0.12
6	115.03 x 10-6	115.17x10-6	0.12
8	204.50 x 10-6	204.75x10-6	0.12

Based on Table 3-2 it can be seen that the percentage error between the calculated deformed area and the deformed area calculated by the ellipse formula is insignificantly small. This exercise has validated the pre-assumed notion that a round hole leak will deform into an ellipse. This is an indication that the assumption that round holes become elliptical once the pipe is pressurised is valid.

4 Understanding Round Hole Deformation Using Finite Element Modelling Method

This section of the chapter describes the setup of the finite element models. The study was based on three round hole leak models. The finite element method that was adopted to investigate the behaviour of round hole leaks under different conditions. A base model of 110mm class 6 uPVC pipe was used for the three round holes. The hole's diameters were, 4mm, 6mm and 8mm. The geometric properties of the base model (internal diameter and wall thickness) are varied, as well as the material properties (elastic modulus, Poisson's ratio and longitudinal stress.

The finite element models were set up on ABAQUS, and this involved the selection of appropriate element type for the models, selecting the analysis type and the boundary conditions. Boundary conditions were assigned to all the models in order to simulate how the pipe models would be held in reality. In order to ensure that appropriate model parameters were used, sensitivity analyses were carried out.

4.1 Setup of the Finite Element Models

This section will illustrate how the finite element base model was setup for the analyses. This was the standard procedure used for all other models, with the difference being only the geometric or material properties.

4.1.1 Geometry and Material Properties

The geometry of the pipe was created using ABAQUS.cae. The geometry of a model is described by elements and their nodes. The cross-section of the structural member (pipe) must be defined. The standard geometry of all pipes investigated in this study, and their cross-section, as sketched on Abaqus, is shown in Figure 4-1.

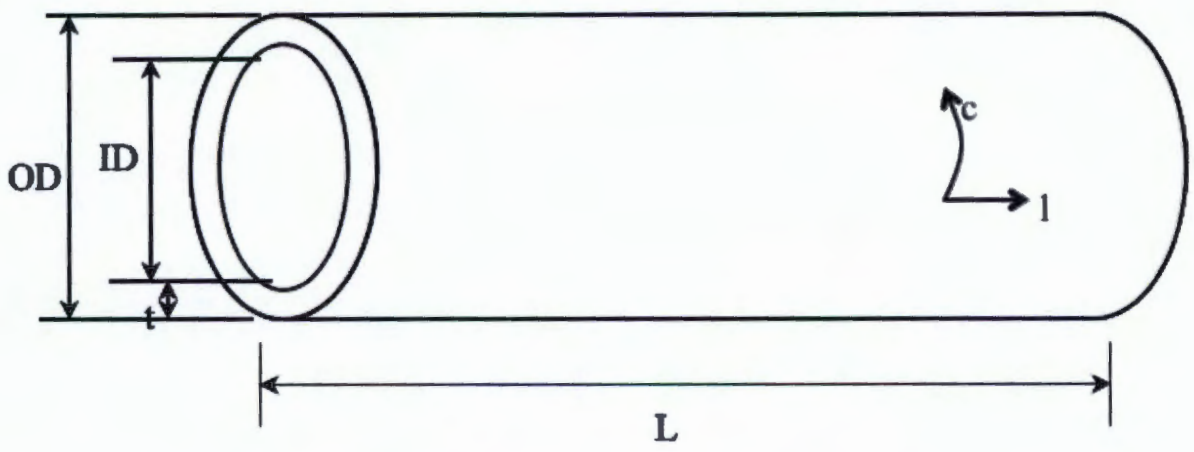

Figure 4-1: Showing the Geometry and Dimensions of the Standard Base Model (Cassa & Van Zyl, 2011)

Where ID is the internal diameter of the pipe, OD is the outer diameter, t the thickness of the pipe wall and L is the length of the pipe, *c* and *l* denote the circumferential and longitudinal

axes, respectively. A sensitivity analysis was conducted to determine the optimum pipe length: reducing the pipe length meant fewer elements and, thus, optimum simulation time. A material type must be associated with the geometry. ABAQUS has a material library, but for this study, only the linear elastic material model was used for analysis.

Table 4-1 below indicates the material parameters, as well as the geometric properties, that were varied in this study. These values were adopted from Cassa's (2011) study, and they were chosen to represent the typical range of parameters found in distribution systems.

Table 4-1: Material Properties of a Standard

Property or Dimension	Varied
Young's Modulus (MPa)	**3**, 10, 30, 90, 200
Poisson's ratio	0.17, 0.21, 0.29, **0.4**, 0.45, 0.5
Longitudinal stress (MPa)	0, 5.2, 10.4, 15.6, 20.8
Wall thickness (mm)	2, 2.5, **3**, 4, 5
Internal diameter (mm)	20,30,40,50,80,**110**,150,200,250,300,350
Hole diameter (mm)	2, 4, 6, 8
Pressure (kPa)	0,100,200,300,400,500,**600**,700,800,900,1000

The units used for the geometry were in SI units of mm. It followed that the rest of the units used in the model were required to follow the SI (mm) units. ABAQUS works in dimensionless units: this means that if one of the units shown in Table 4-2 is used, all the analyses should be consistent to that SI unit.

Table 4-2: ABAQUS System of Units (As Adapted from imechanica.org)

Quantity	SI	SI (mm)
Length	m	mm
Force	N	N
Mass	Kg	Tone (10^3 kg)
Time	S	S
Stress	Pa (N/m^2)	MPa (N/mm^2)
Energy	J	mJ (10^{-3} J)
Density	Kg/m^3	$Tonne/mm^3$

4.1.2 Load Applications

The distributed loading condition was used, because this is a good representation of the behaviour of fluid pressure inside a pipe. Therefore, the distributed load was the internal pressure applied on the inner surface of the pipe, as shown in Figure 4-2. After inputting the magnitude and direction of the internal distributed loading (internal pressure), and the induced associated circumferential stress in the finite element analysis is generated. However, in the case of the biaxial stress state where the longitudinal stress exists, the user must compute the resulting longitudinal stress and apply the load to the pipe ends.

It is known from literature that, for the biaxial stress state analysis, the applied internal pressure induces both the circumferential and longitudinal stresses and for the uniaxial stress state analysis, the applied distributed loading will induce only the circumferential stress. Figure 4-2 shows how the internal distributed loading is applied to the pipe model in ABAQUS. The arrows that can be seen inside the pipe illustrate the direction of the internal pressure.

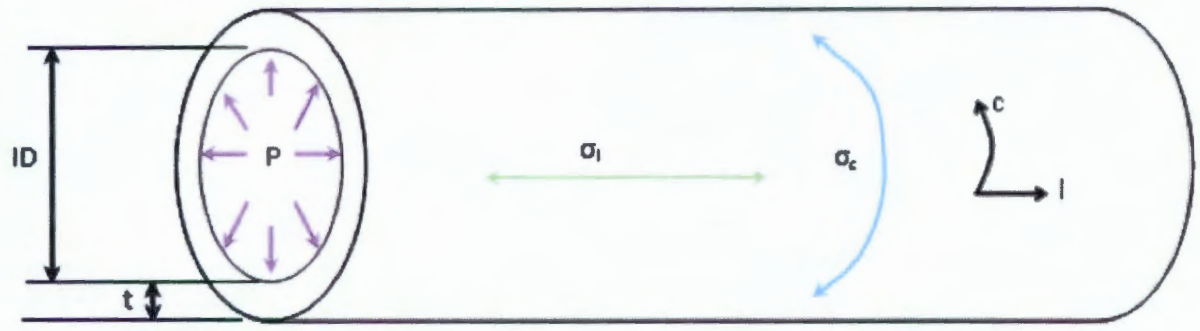

Figure 4-2: Pipe Showing Longitudinal and Circumferential Stresses (Cassa (2005))

Longitudinal and circumferential stresses can be calculated using Equation 2-2 and Equation 2-4 Gere (2001) which were discussed in the literature and are recited here:

$$\sigma_l = \frac{Pr}{2t}$$

$$\sigma_c = \frac{Pr}{t}$$

Cassa (2005) highlights that these equations are valid only when there is no induced stress concentration as a result of end conditions or discontinuities.

4.1.3 Application of Holes to Standard Base Pipe

Each pipe was modelled with a hole on the side. These holes were all positioned in the same place, along what is shown as the longitudinal axis in Figure 4-3. The hole diameter was varied accordingly, using add on geometrical functions in ABAQUS that allows the user to change the hole diameter whenever necessary. The outer diameter (OD), inner diameter (ID) and the thickness (t) were also adjusted accordingly. The length was fixed at 500mm.

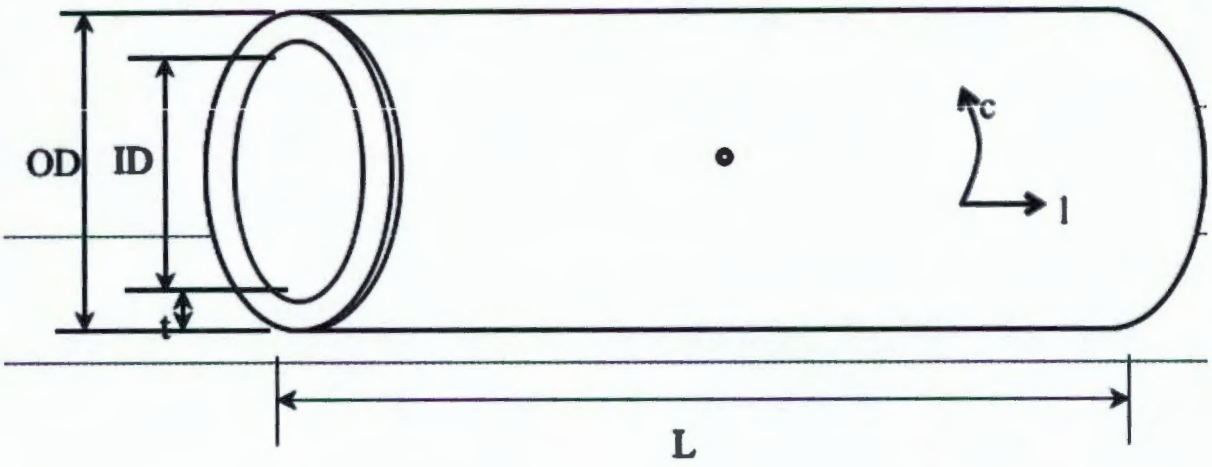

Figure 4-3: Showing How the Holes Were Positioned and the Direction of the Longitudinal and Circumferential Axis

4.1.4 Boundary Conditions

Boundary conditions were necessary in order to model the condition of a pipe that is laid underground. In this case, two main boundary conditions would be applied to the model: a clamped internal line and a clamped external point, as shown in Figure 4-4. Effectively, the clamped point meant that the pipe was clamped in the circumferential, longitudinal and radial direction. The internal line opposite the crack meant that the pipe was allowed to expand freely in the longitudinal direction only.

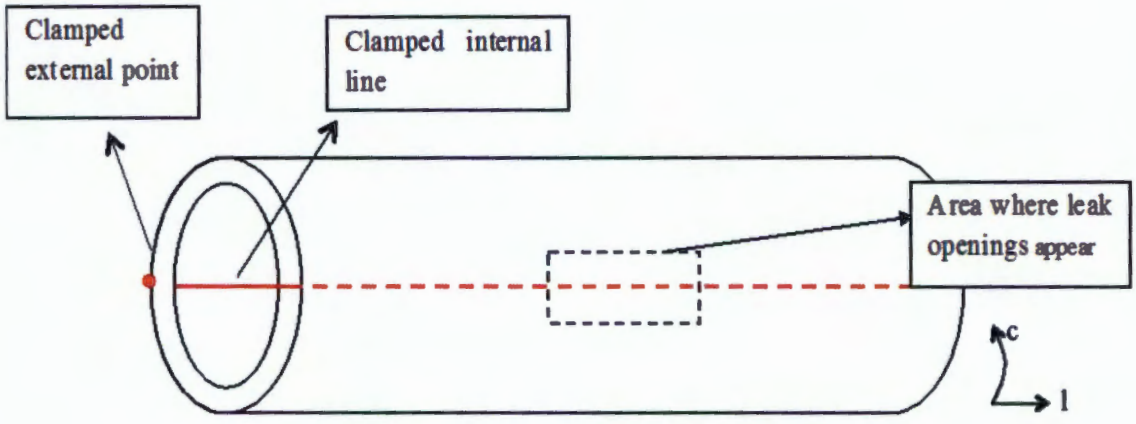

Figure 4-4: Boundary Conditions for Model Pipe (Cassa 2011)

4.2 Setup of Finite Element Model With a Hole in ABAQUS

This section will give an overview of the finite element process carried out in this study. As cited by Cassa (2005), Habbitt *et al.*, (2004), highlighted that the finite element model in ABAQUS consists of ten "modules" and these are: part, property, assembly, step, interaction,

load, mesh, job, visualisation and sketch. Each of these modules will be discussed in relation to the 8mm diameter hole base model. A similar process was undertaken for the 6mm and the 4mm diameter hole areas.

Part Module: Using this module on ABAQUS, the user can create different parts of the final model. The user may also choose to create the model using other compatible modelling softwares, and import the final product to ABAQUS. The models, investigated in this study, were all created using the ABAQUS part module with the 3D modelling space for a deformable part type and a solid shape. The final part created was as shown in Figure 4-5.

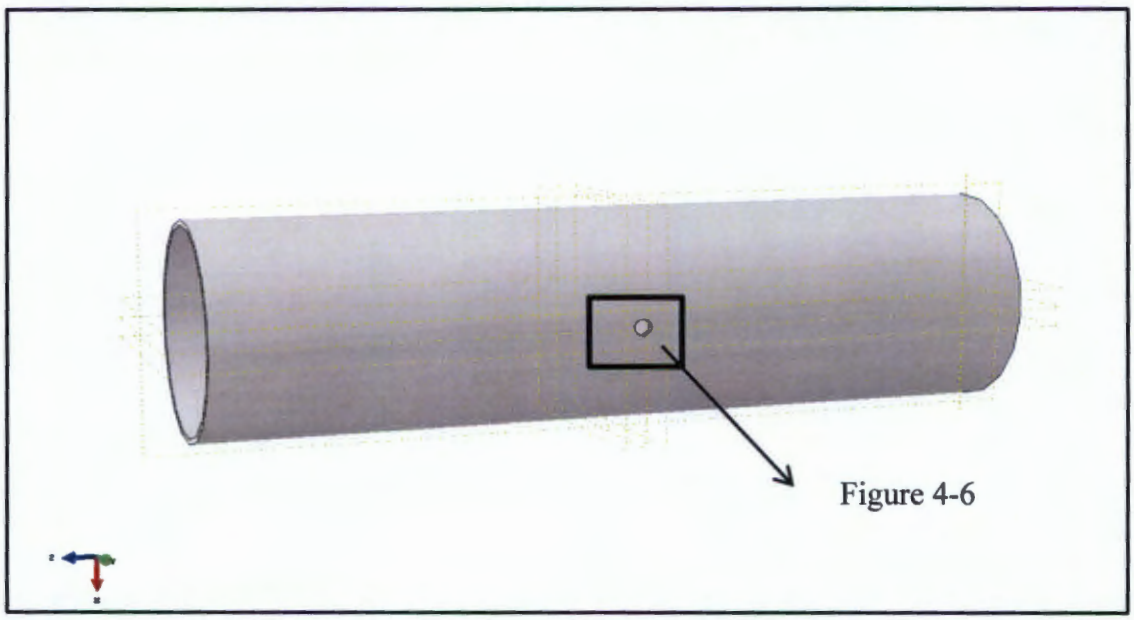

Figure 4-5 Part Model of a Base Model Pipe With a 8mm Hole Diameter

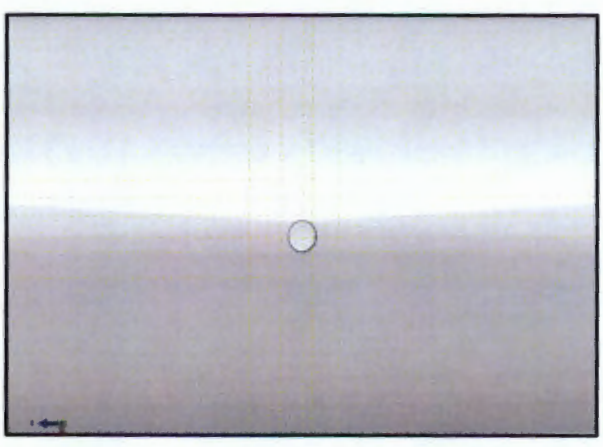

Figure 4-6 Detail of Part Model to Show Hole Leak

Property module: Using this module, the user can define the material properties and assign the sections of the part that has been created from the previous module. The assigned sections contained information about the property of the part. In this study the model parts were all set

as solid homogeneous, based on the assumption that the composition of the pipe part is uniform and solid throughout.

For example, for the 110mm PVC class 6 the elastic modulus was entered as 3 000 MPa and the Poisson's ratio was 0.4. The created solid homogeneous section is then assigned to the part. In the ABAQUS viewport the part model is highlighted, the material is defined and the section is assigned to it.

Assembly module: Each part that a user creates on ABAQUS is oriented in its own coordinate system and is independent of the other parts in the model. Even though a model can contain many parts, it usually contains only one assembly. By creating instances of a part and positioning the instance relative to each other in a global coordinate system, an instance may be independent or dependant. The difference between independent and dependant instances is that independent part instances are meshed individually, while for the dependant part instance the mesh is associated with the mesh of the original part. By default, the part instances were dependent and, therefore, the default setting was used for the linear elastic models.

Step Module: Various steps are used in the analysis of a simulation. ABAQUS/cae generates the initial step automatically, but the user must create the analysis steps required for analysis. In other words, given specific output requests at various stages in the analysis, this module enables the user to create steps that can isolate and capture changes in the model i.e. loadings and boundary conditions. In the case of the elastic simulation, only one step was needed, an instance was created and the pipe was then ready for the assigning of conditions. To fully analyse the models, a static stress analysis was used with a 3D stress field for the models.

Interaction Module: In this module the user can specify whether there may be interaction between the surfaces when one or more parts are assembled together in the assembly module. This module was not used for this study.

Load Module: Using the loading module all the loading conditions and the boundary conditions are set up. Each loading condition needs to be assigned a specific step because each loading condition is step dependant. For example, if a particular load was only required for the first step in a model and not the second, this was specified in this module.

As discussed in the literature, the application of an internal load within a pipe results in varying load situations, the uniaxial and the biaxial states. The working pressure of 600 kPa will be used for illustrative purposes. All other pressures followed the same procedure. The areas where the internal load is to be applied are selected and the load is created as a pressure. The magnitude was applied as 0.6 MPa, SI units. The longitudinal stresses are assigned the same way as the internal pressure (acting outwards) and the circumferential stresses are induced when the internal pressure is applied. The magnitudes of these stresses, resulting from the 0.6MPa internal pressure, are determined from Equation 1 and Equation 2 and are shown. A sample calculation is shown below:

Dimensions:
D= 110mm

$r = D/2 = 55mm$

P= 600 kPa

t= 0.3mm

Equations:

$\sigma_l = \frac{P(r-2t)}{2t}$ $\sigma_l = 54.7MPa$

$\sigma_c = \frac{P(r-2t)}{t}$ $\sigma_c = 109.4MPa$

Figure 4-7 below shows how the boundary conditions were assigned to the base models. The first one entailed clamping a point on the outside of the pipe; the objective here is to keep the pipe from moving as there are no external supports. Effectively, this meant that the pipe was clamped in the circumferential, longitudinal and radial direction by the external point in **Figure 4-7** (b). The second boundary condition was clamping an internal line (shown in **Figure 4-7** (a) opposite the crack; this meant the pipe was allowed to expand freely in the longitudinal direction only. In effect, this meant the pipe was only clamped in the radial and circumferential directions.

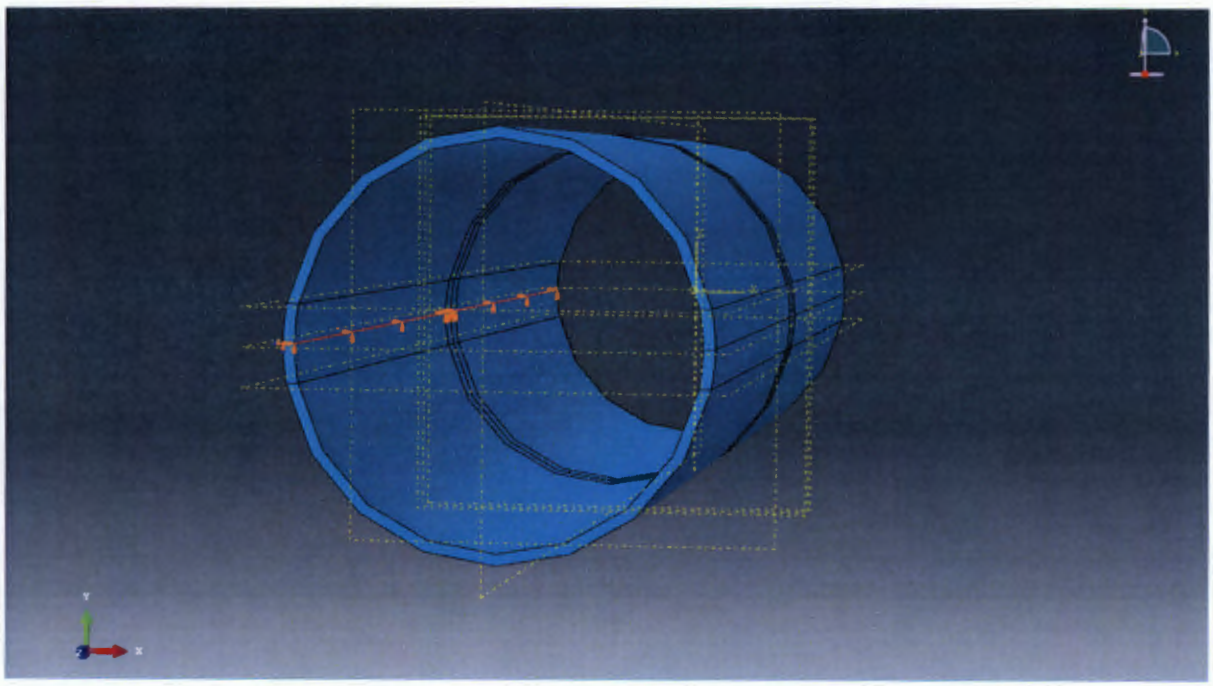

(a)

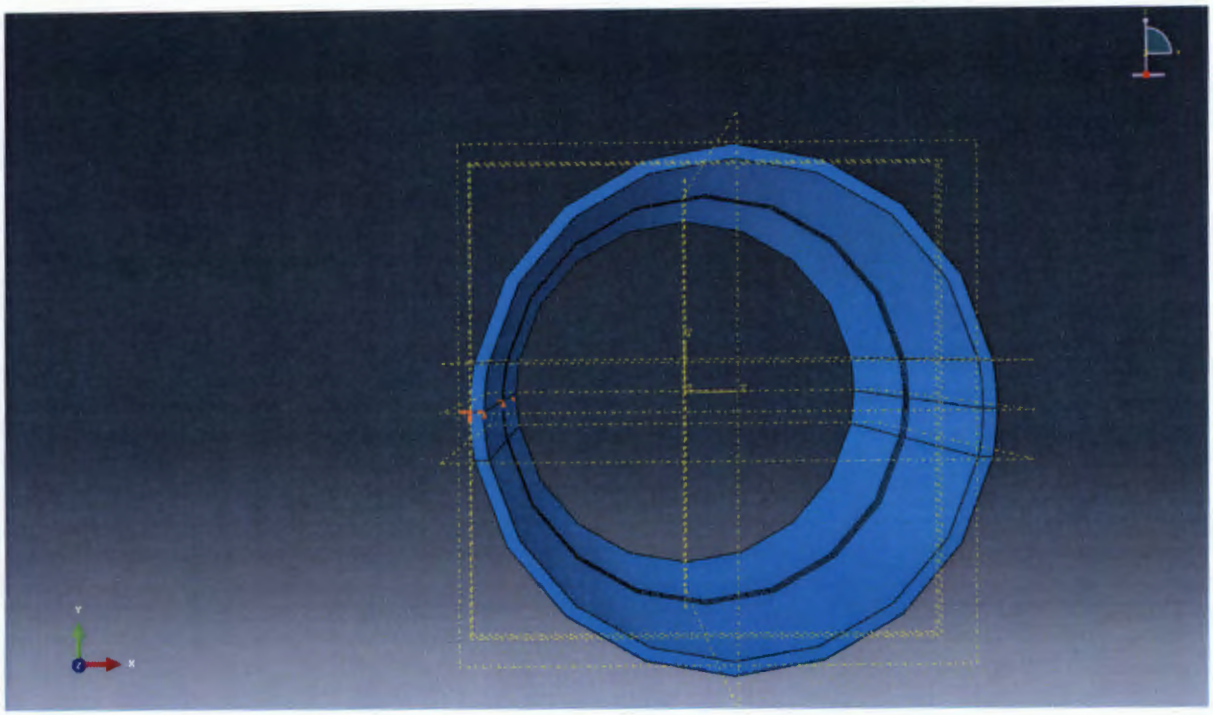

(b)

Figure 4-7 Showing How the Boundary Conditions Were Applied (a) line and (b) Point

Mesh Module: Using the mesh module, the user is able to generate the meshing on an assembly, which required the finite element analysis. Various types of mesh and elements exist that can be used. The mesh is created in such a way that it suits the particular model. If ABAQUS displays the model in orange, it cannot be meshed without assistance from the user. Before a mesh is selected, a sensitivity analysis is to be carried out. The sensitivity analysis will ensure that the optimal finite element sizes are used.

The pipe models were meshed using a C3D20R: A 20-node quadratic brick with reduced integration. However, before this was done, the part was partitioned into different mesh regions. Partitioning creates additional edges, which allows more control over local mesh density. Each mesh region can have different mesh controls. Partitioning and local mesh seeding allows you to refine the mesh in the area of a stress concentration. Even when the sensitivity analysis is being carried out, it is important to ensure that the element is small enough to ensure that there is enough detail. Too large elements would not provide the required accuracy, while too small elements could reduce the computational speed and, therefore, causing longer simulation time yet little accuracy gained. Figure 4-8 shows the partitioning technique employed; the pipe was partitioned in a symmetrical manner. It can also be seen that various partitions pass through the hole effectively dividing it into quarters. Full circles cannot be meshed if they are in a structured format in ABAQUS.

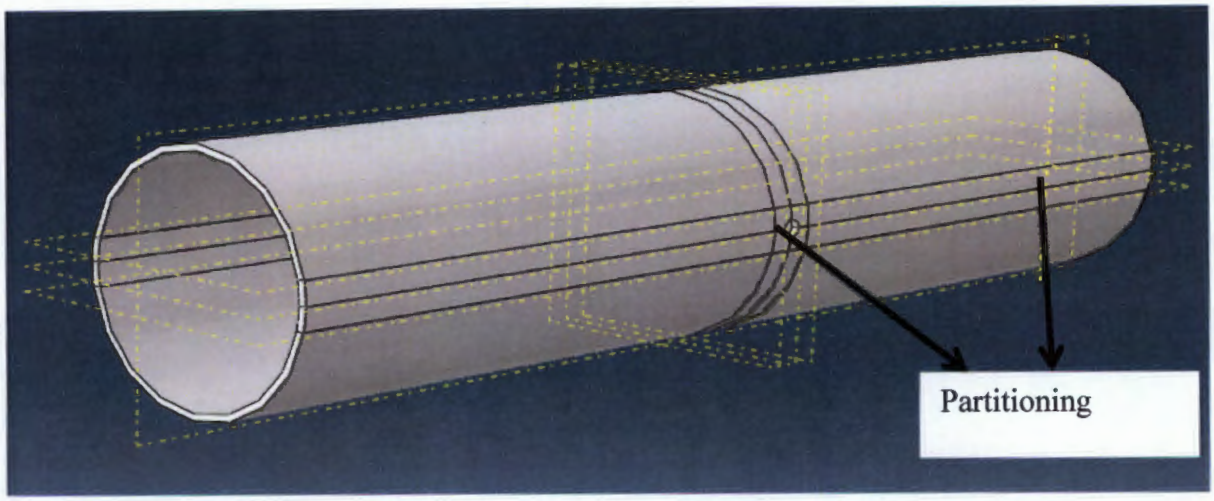

Figure 4-8 Partitioning Technique Adopted

Figure 4-9 shows a base model with an 8mm hole meshed. A more detailed look at the mesh, zoomed in, in the region of the hole is shown in Figure 4-10. The mesh was selected to be the hexahedral (hex) shape, instead of the tetrahedral (Tet) shapes that were used in Cassa's (2005) investigation, for reasons mentioned in the ABAQUS 6.12 documentation. According to the ABAQUS documentation, hex mesh is usually structured, so the cell co-ordinates can easily be transformed to the calculation matrix ABAQUS used for computation. The Tet, on the other hand, is usually unstructured and, thus, there is a need for a transformation matrix, which then introduces a new time step so the computational time is much longer. Based on the documentation, it was also recommended that quadratic elements are chosen over linear elements. Taking into account these factors, a 20 nodded quadratic brick was used in order to mesh the part of the pipe models.

The size of the element chosen in the model is of great importance because this determines the number of elements. For the pipe mesh there were different element sizes which were investigated. There was an outer mesh, which was sufficiently far away from the hole, and the centre mesh, which was made small enough to ensure that sufficient detail, regarding the circle, was obtained. These meshes which were chosen, as explained in the sensitivity analysis section, are still to come. An example of the mesh is shown in Figure 4-9.

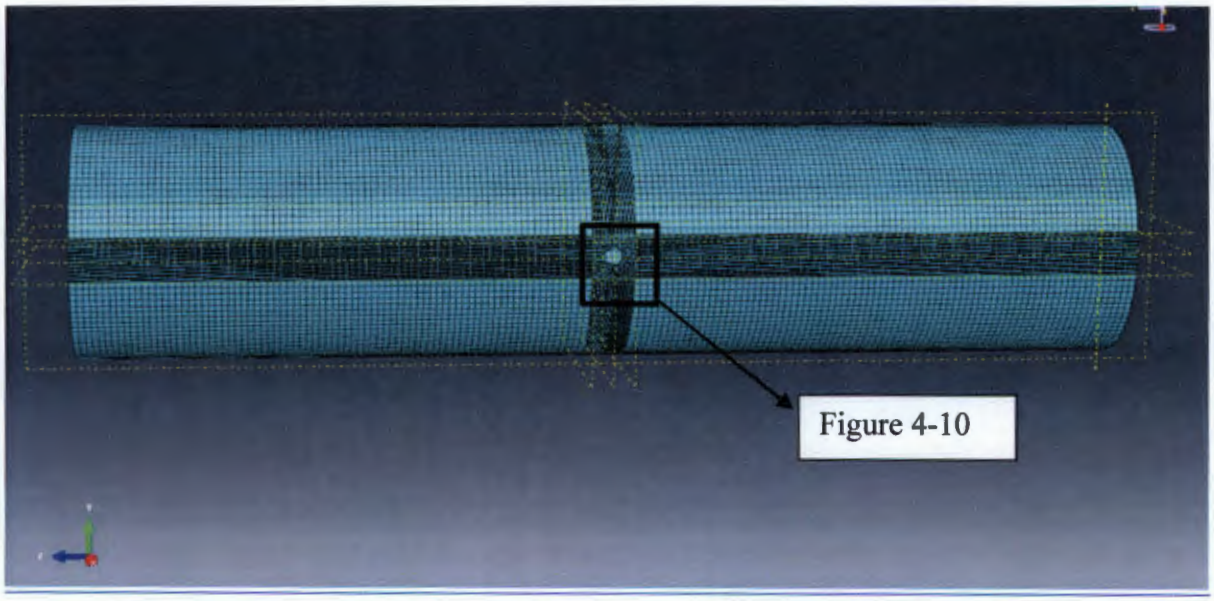

Figure 4-9: The Base Model Pipe With 8mm Diameter Hole

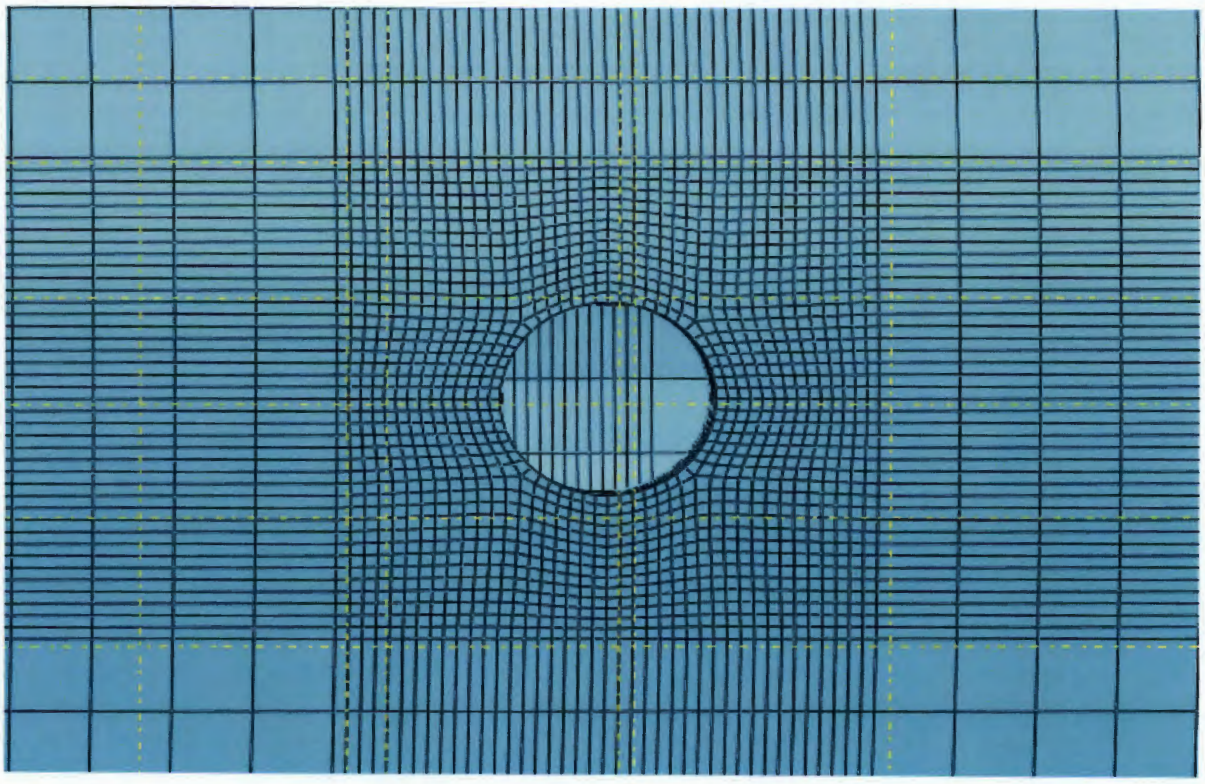

Figure 4-10 Showing a More Detailed Look at the Mesh Around the Different Holes

Job Module: In this module the analysis of the model takes place. The analyses are done in the form of jobs and they can be created, and their progress monitored, while the analysis is taking place. As soon as the job has been created it creates an input file. This input file contains all the information pertaining to the model. Basically, it will contain the geometry, i.e. the part, the assembly and the element type used in the model, the material properties, loading and boundary conditions, and all the analysis steps and field output requests that are needed to run the simulation successfully. Essentially, after inputting all other relevant

parameters in each module and specifying the mesh of the base models, a job was created and run.

Visualisation Module: The results of the pipe model can be viewed graphically in this module. The results obtained can be extracted and written to a file for the purposes of analysis. Different plots can be viewed in this module, i.e. deformed plot of the model, an un-deformed plot and each variable defined as a field output can also be graphically represented on the model to show the areas of interest. Should the user also want to present the results in video format, the deformation can be viewed as a video and captured. Figure 4-11and Figure 4-12 illustrate the various views of the stress distribution of the class 6 PVC pipe with an 8mm diameter hole. Figure 4-13 and Figure 4-14 show the deformed round hole which3e have been scaled up to a factor of 60 to show the deformation more clearly.

Sketch Module: This is the last module in ABAQUS, and this module enables the user to sketch a two-dimensional profile that can define a planar part (Hibbit *et al.*, 2004). This set up was repeated numerously for the various hole openings that were used throughout the study.

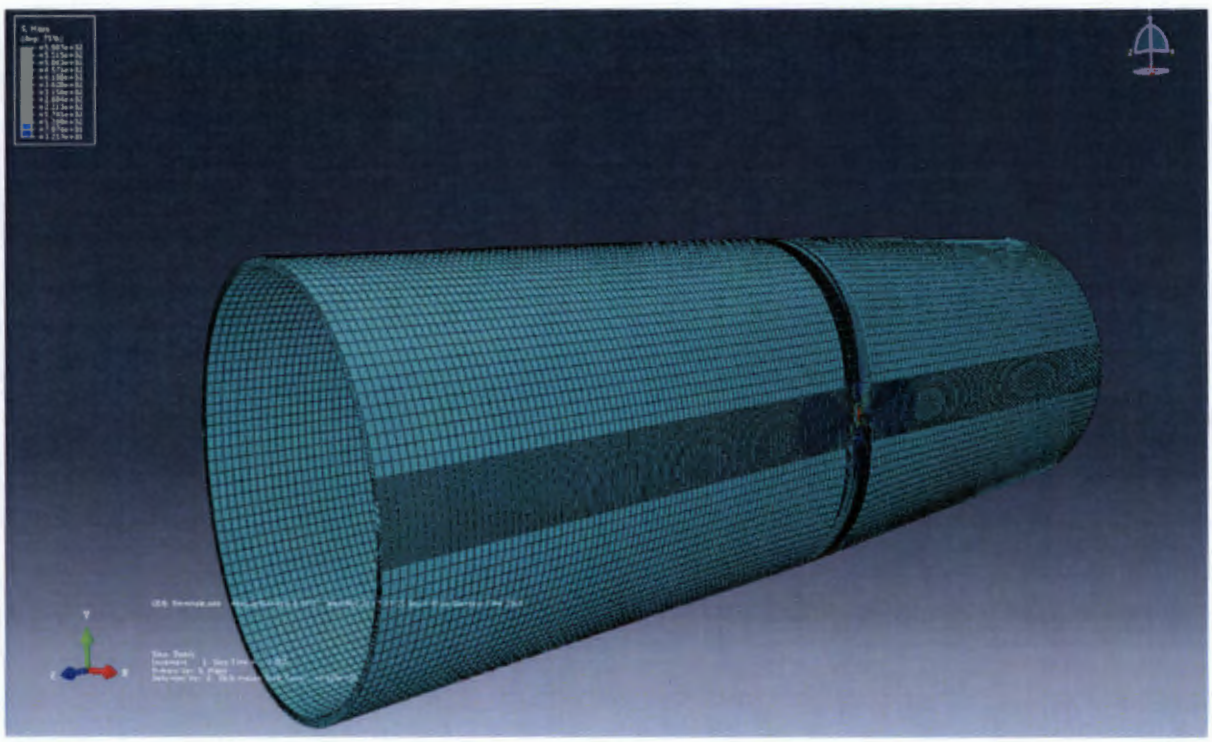

Figure 4-11: Von Mises Stress Distribution of a Class 6 PVC Pipe Deformed

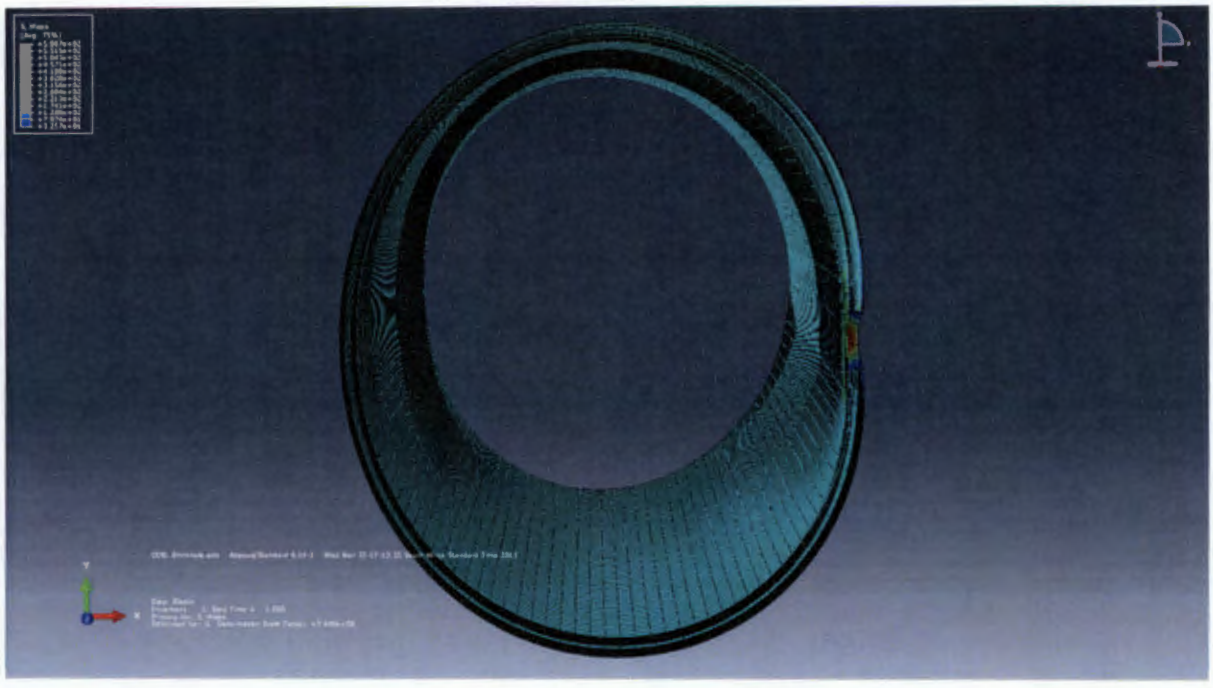

Figure 4-12: Von Mises Stress Distribution of a Class 6 PVC Pipe Deformed Side View

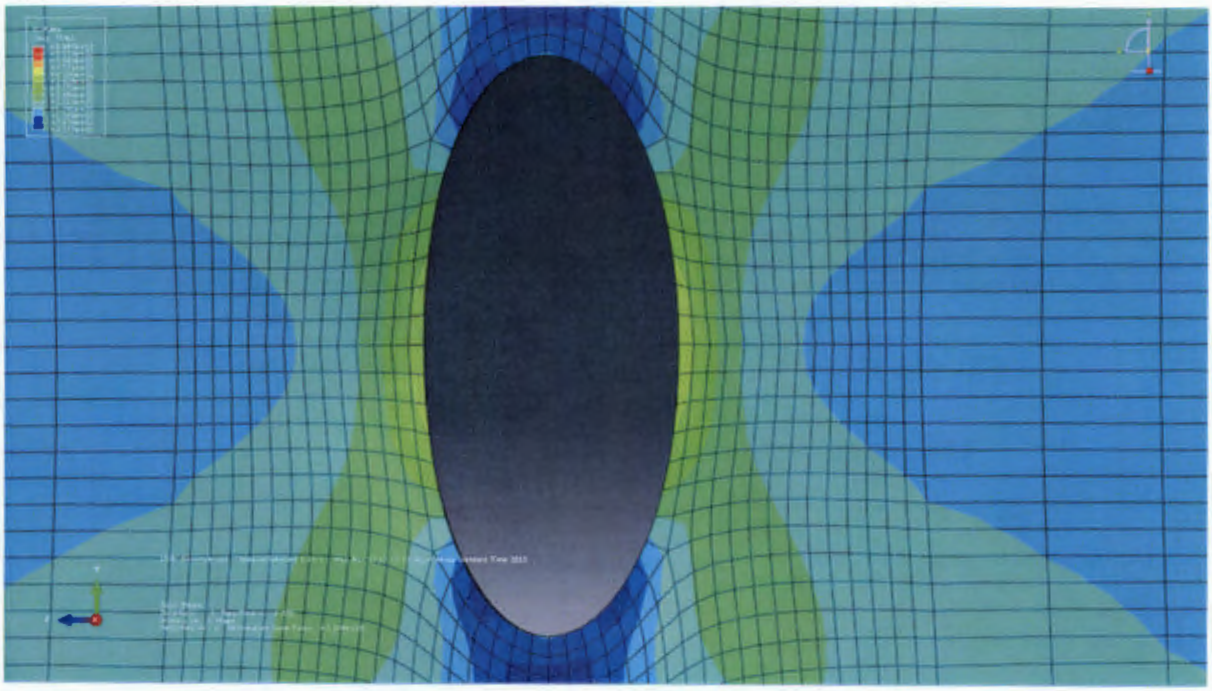

Figure 4-13: Close Up on Hole from the Front of a Class 6 PVC Pipe Deformed (Scale 60)

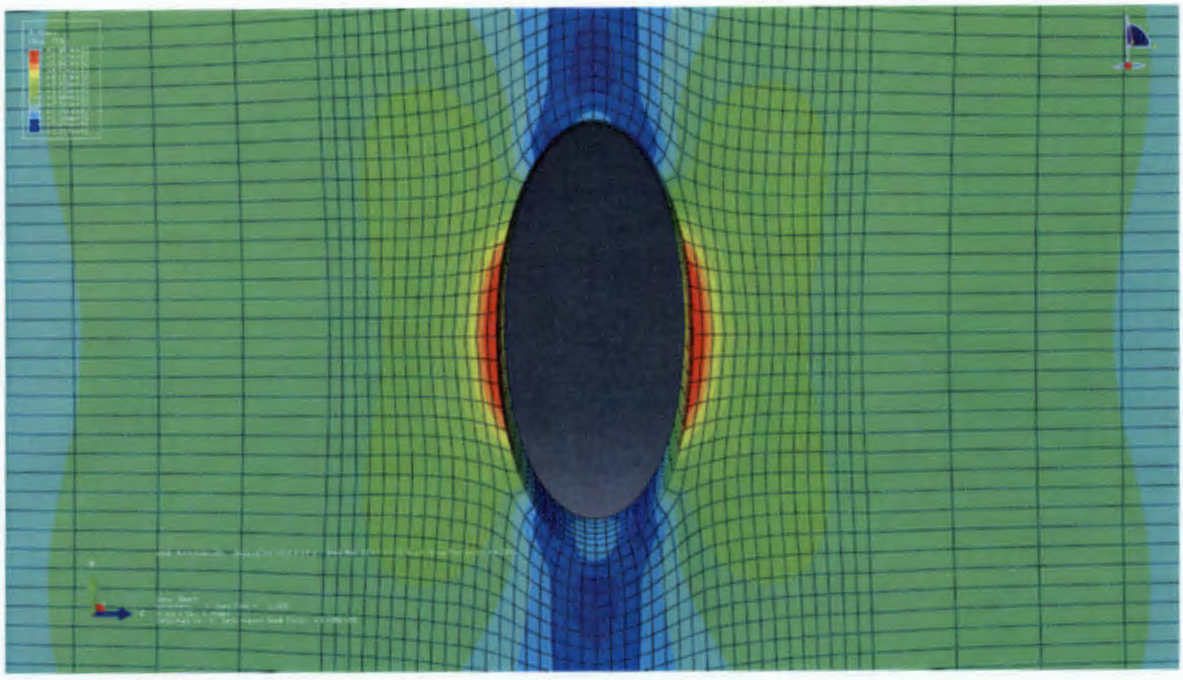

Figure 4-14: Close Up on Hole from the inside of a Class 6 PVC Pipe Deformed (Scale 60)

4.3 Sensitivity Analysis of the Finite Element Models

This section provides the sensitivity analyses that were carried out for various geometric parameters of the pipe models. The primary objective of the sensitivity analysis is to determine the optimum element size required for computation. A sensitivity analysis was done for five parameters: length of the pipe, global seed (element size of the pipe), local seed (for the element size around the leak hole), internal diameter, and wall thickness.

It is known from literature that the application of an internal pressure will cause the stress distribution around the leak hole to change. However, this change of stress distribution is negligible at distances along the pipe that are larger in comparison with the hole radius (Saint Venants Principle). Another factor that can influence the stress distribution is the edge effects in the pipe and the assigned boundary conditions. For these reasons, the leak hole was placed sufficiently far away from the edges of the pipe, as well as local positions where boundary conditions were assigned.

4.3.1 Setup of Sensitivity Analysis Procedure

The first sensitivity analysis that was done was to determine the optimum pipe length for the pipe models. A set was created on the geometry of the pipe in ABAQUS. This set consists of a point that is sufficiently far away from the hole and the edge of the pipe (see base point in Figure 4-5 (a) and (b)). This set was created to ensure that the selected base point remained constant no matter the mesh size or shape.

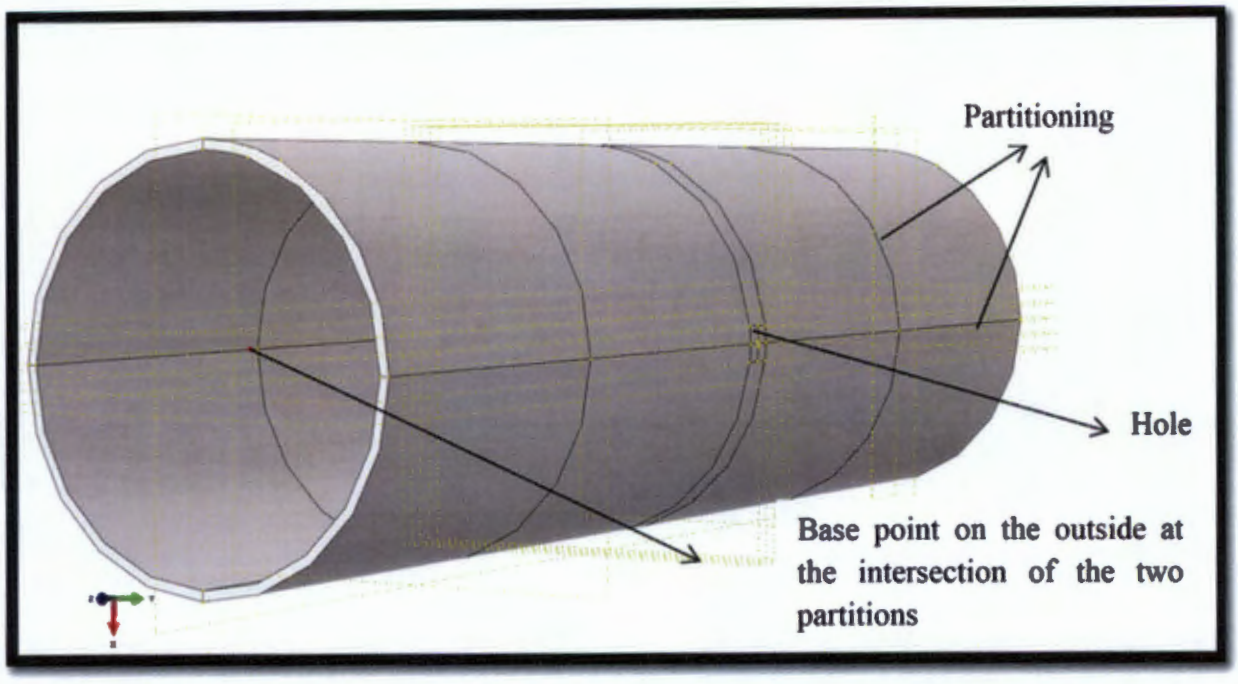

(a)

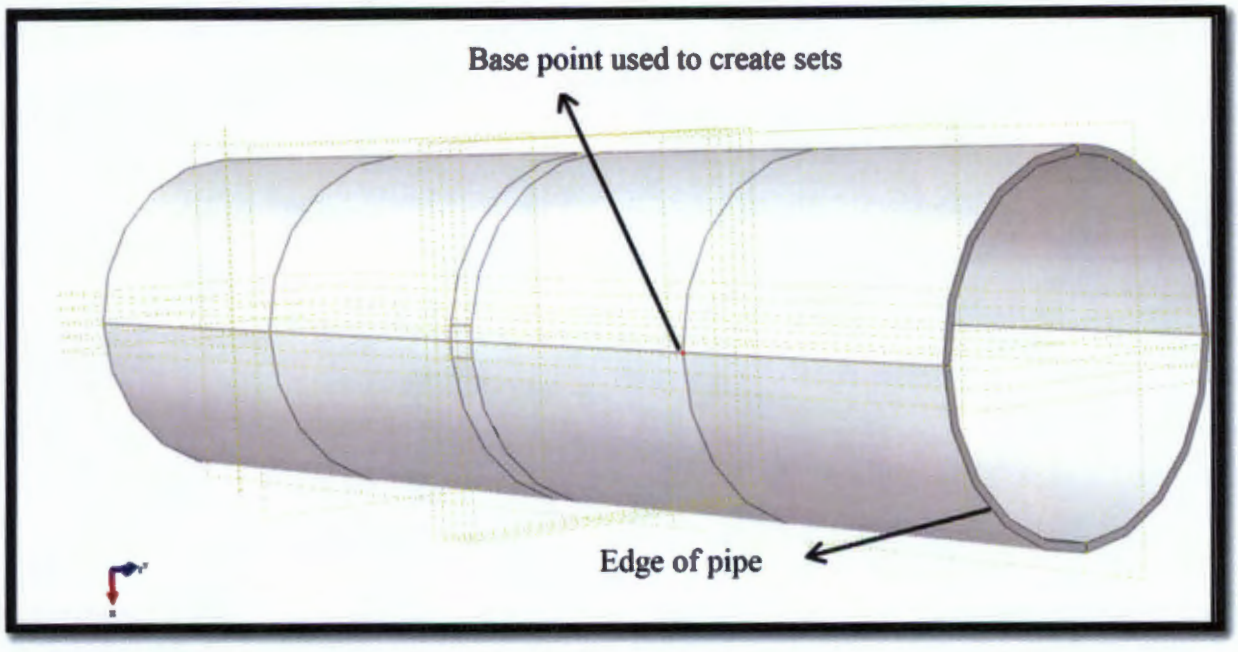

(b)

Figure 4-15: Representation of Leak Hole Location and Location of Base Point for Sets

As can be seen from Figure 4-15 (b) the partitioning played a critical role. This particular partitioning technique was necessary in order to locate the base point easily. This point was always at the intersection of the two partitioning lines. Also, this point was strategically chosen to be in-between the edge of the pipe and the leak hole. It was also chosen to be on the outer surface of the pipe, as can be seen from Figure 4-15 (b).

4.3.2 Determination of Pipe Length

The optimal pipe length for the analysis was the length of the pipe whose edges did not interfere with the stress distribution around the leak hole. In order to determine this optimum pipe length, different pipe lengths were applied to the base model, then reducing the element sizes of the entire pipe. Using the query probe node function, the stresses and strains were determined for each element size. The element sizes started at 20mm and were reduced to 2mm in size. The various stresses obtained were then plotted against the element size to see if convergence is achieved. Once the convergence of the stresses is achieved, the appropriate element size can be chosen for the model and used for further analysis. If this is done for different pipe lengths of the base model pipe, and the graphs converge with the stresses, one can conclude that the edge effects no longer play a role in the stress distribution around the round hole. The sensitivity analysis was done only for the 8mm leak hole, because it was the largest hole and, therefore, the results obtained would accommodate for the 6mm and the 4mm holes, as they are smaller leak holes. Figure 4-16 shows the sensitivity analysis that was done for a class 6 uPVC pipe with an 8mm hole.

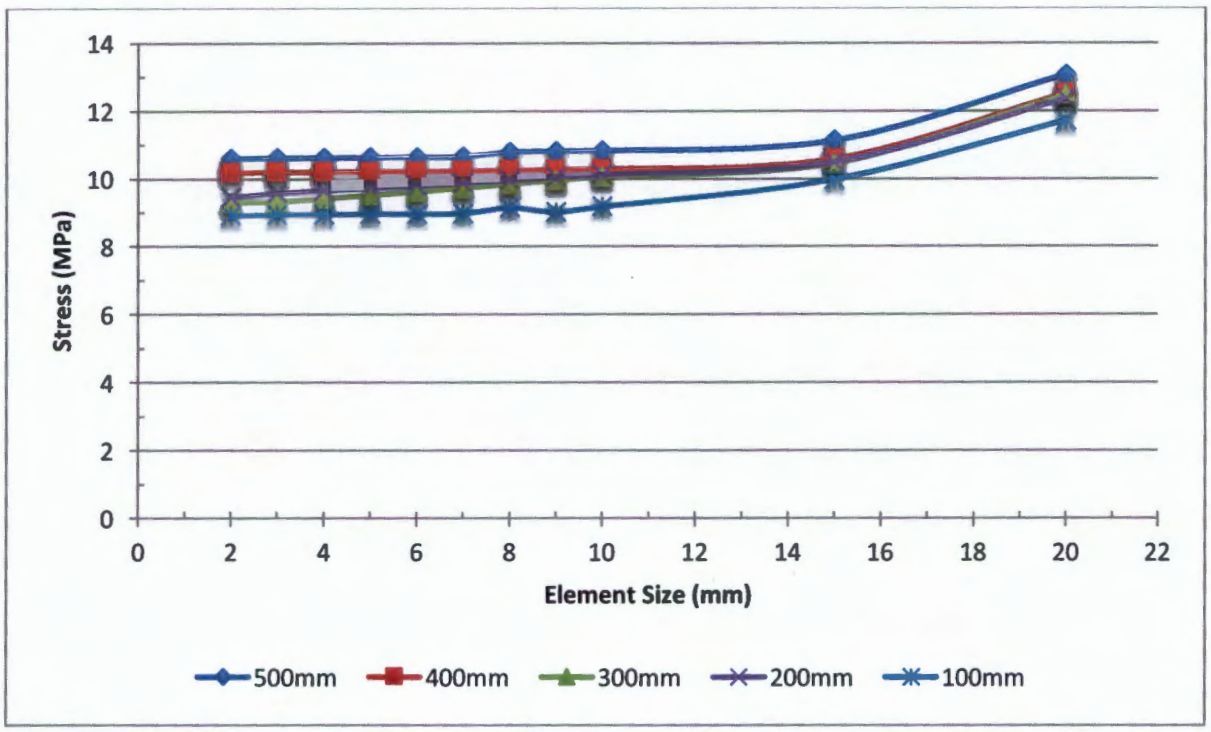

Figure 4-16: Sensitivity Analysis Graph of Stress for a Pipe With an 8mm Hole

Figure 4-17 that follows shows the sensitivity analysis for the strain of a class 6 uPVC pipe with a 8mm round hole leak, in order to determine the optimum length of the pipe for the base model.

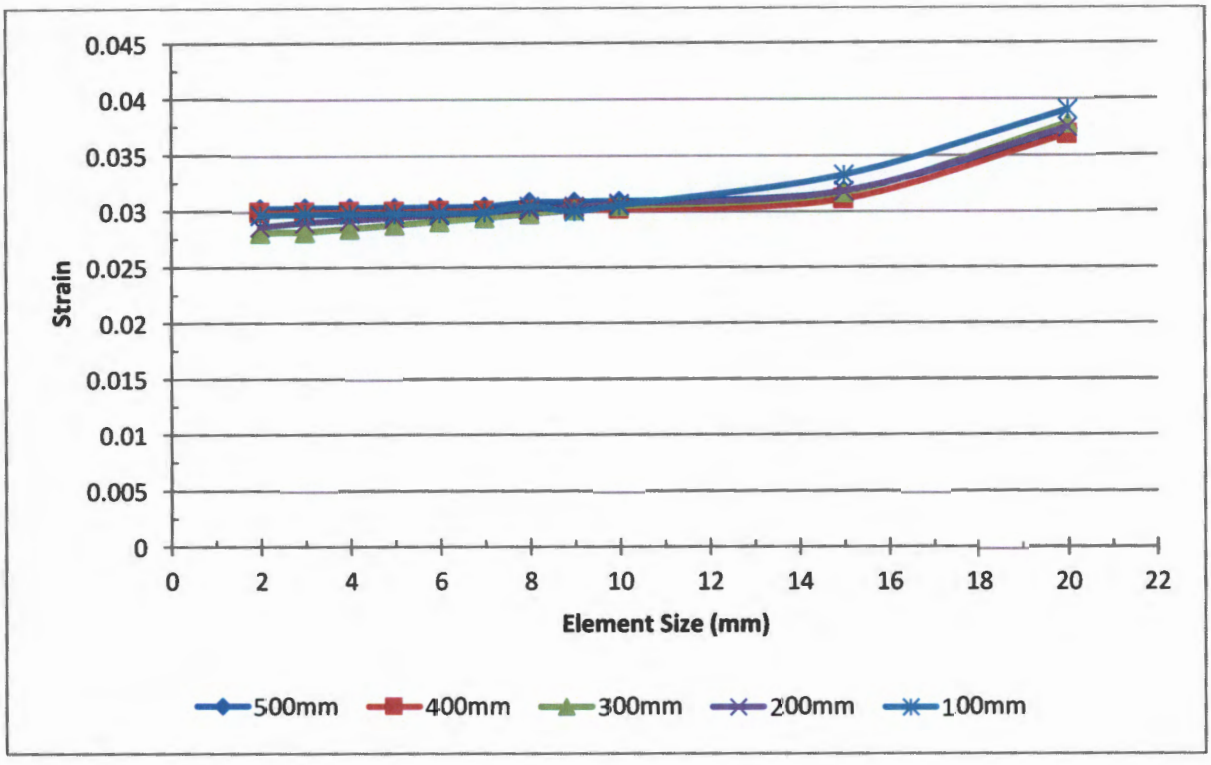

Figure 4-17: Sensitivity Analysis Graph of Stress for a Pipe With an 8mm Hole

From Figure 4-16 and Figure 4-17 it can be seen that, for all cases, convergence began around the 9mm element size mark. The graphs are also very close together and, therefore, the edge effects do not play a significant role with round holes. It is from this finding that a length of 500mm pipe was chosen.

4.3.3 Determination of the Pipe Element Size (Global Seed Size)

After the pipe length is determined, a second sensitivity analysis is done to determine the most appropriate element size of the entire pipe. A sensitivity analysis for the 500mm pipe model was conducted in order for the global element size to be determined. The same base point, shown in Figure 4-15 (b), was chosen for consistency and to ensure that the global element size is not affected by the pipe edge or the stresses experienced by the hole. Figure 4-18 shows the sensitivity analysis that was conducted for the 500mm pipe. The element sizes were varied from 1mm, 2mm, 3mm, 4mm, 5mm, 6mm, 7mm, 8mm, 9mm, 10mm, 15mm, 20mm and 25mm.

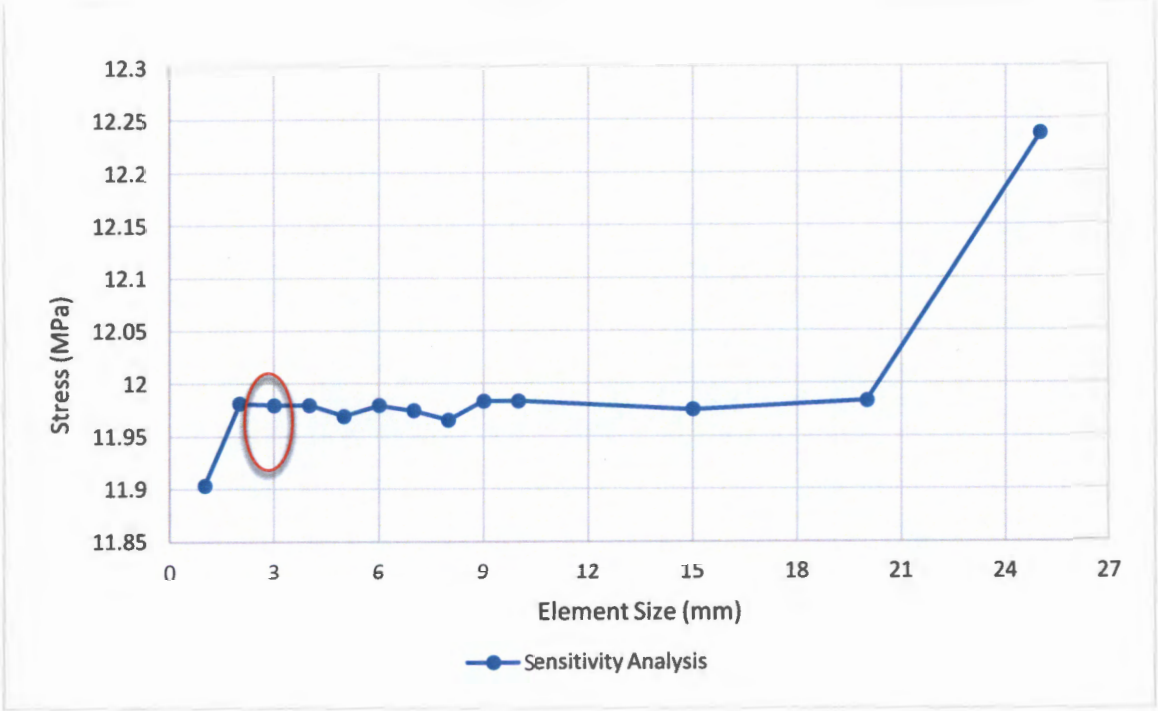

Figure 4-18 Sensitivity Analysis Graph for Global Seed Size

From Figure 4-18 it can be seen that the stress level starts converging at about the 8mm element size, up to the 2mm element size, i.e. the stress level remains relatively constant between the 8mm and 2mm element size. From this the 3mm element size was chosen because choosing this element size would ensure that some reasonable accuracy of the model is maintained yet, at the same time, computational processing time is optimised for the analysis.

4.3.4 Sensitivity Analysis for the Various Hole Sizes

Another important area that required a sensitivity analysis to be conducted was around the hole area. As was shown in Figure 4-10, the element size around the hole is less than the element size around the pipe. Figure 4-19 shows the sensitivity analyses carried out for the 4mm, 6mm and 8mm holes. The sizes of the elements started at 2.5mm and were reduced to 0.2mm in size.

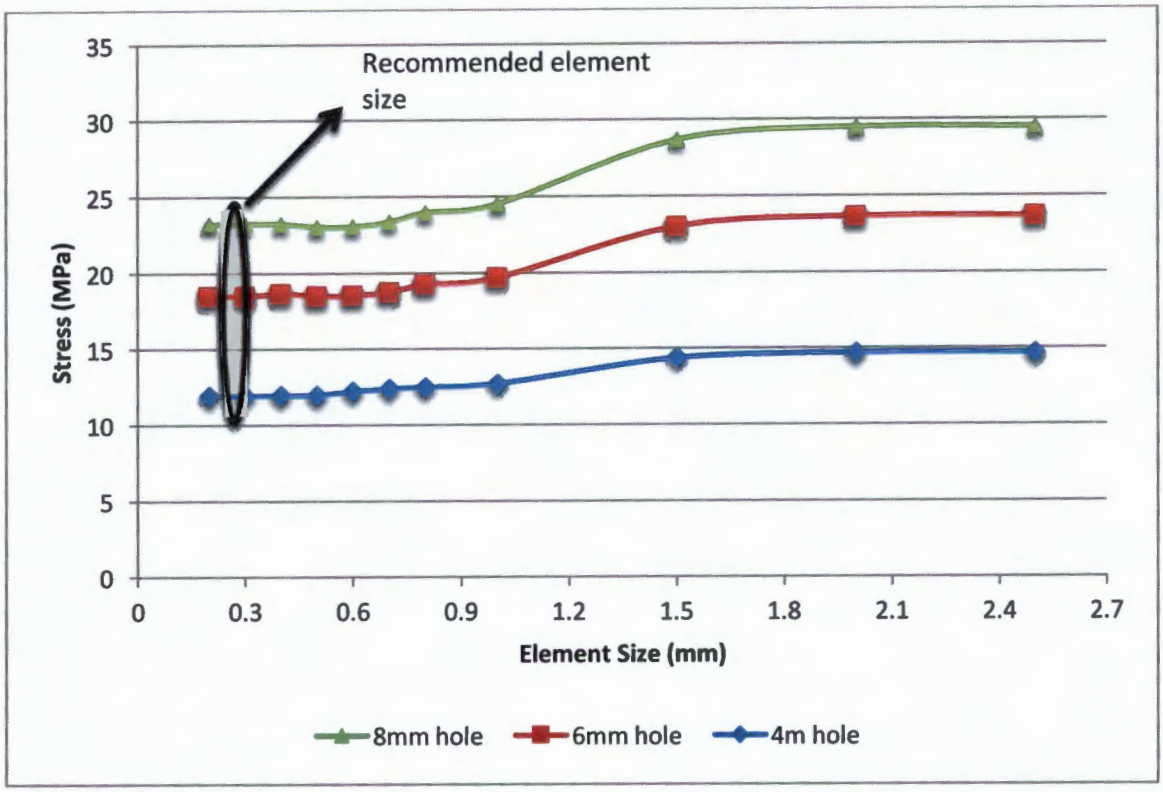

Figure 4-19 Sensitivity Analysis Graphs for a Class 6 uPVC Pipe with 4mm, 6mm, 8mm Diameter Leak Hole

Table 4-3 below shows the corresponding values and element sizes for the graph shown in Figure 4-19.

Table 4-3: Showing the Recommended Sizes and Results for the Base Model

Hole Diameter (mm)	Recommended Element Size (mm)	Stress (MPa)
8	0.3	23.23
6	0.3	18.45
4	0.3	11.90

4.3.5 Summary of Sensitivity Analyses

This section looked at the methodology used in setting up the pipe models. This study involves investigating the behaviour of round hole leaks in water pipes. The base model pipe is a 110mm class 6 uPVC which was used as the standard base pipe for analysis. This standard base pipe was used to create different base models according to the size of the hole that is applied to it. Three hole sizes were investigated, each with a diameter of 4mm, 6mm and 8mm, respectively. Due to the holes being the same (i.e. all investigated holes were round holes) and only differing in diametric size, the sensitivity analysis was done for the largest hole and, therefore, it was reasonable to assume that the sensitivity analyses results also applied to the smaller holes. The length of the pipe was chosen as 500mm, the global element size to be used was 3mm and the local element size around the hole was 0.3mm.

4.4 Area Measurement Using ABAQUS Scripts

In order to measure the various areas from ABAQUS a python script was used. Hellmut Bowles wrote this script. The script reads the co-ordinates of the set that is named "HolePerimeterOD". Before running the script, the user must create a boundary set of the hole in ABAQUS, and this is the set that must be named "HolePerimeterOD".

After creating the job and submitting it successfully, the user must open the job results to view the ODB file of the simulation. The script should then be run after the ODB file is visible in the viewport showing the deformed part. The script can be located from selecting a file and then run script; ABAQUS will request for the script location. The user then opens the scripts from the location it has been saved in and runs the script.

The script computes the area of the hole projected onto the Y-Z plane. ABAQUS then computes the area by triangulating the aperture with projected triangles and summing all their areas.

4.5 Effect of Pressure on Hole Area using finite element analysis

This section will look at the effect of pressure on the hole areas. The three holes, investigated in this study, are used to illustrate how the hole area expands due to increased pressure for different holes.

In order to illustrate how the hole areas change with varying pressure, finite element simulations are run for pipes with pressures ranging from 100 kPa to 1000 kPa. The hole areas ranged from 4mm, 6mm and 8mm in diameter. From the sensitivity analyses the appropriate element size is chosen for the various models.

The original area of the holes can be calculated using the mathematical formula for calculating a circle, according to a two-dimensional co-ordinate system. The areas obtained for the various pressures for the three holes are shown in Table 4-4.

Table 4-4: Showing How the Hole Leak Area Varied With Pressure Head

Hole diameter	Pressure (m)	Area (m^2)	% Opening
4mm	0	1.2566E-05	0.00%
	10.19	1.2577E-05	8.25%
	20.39	1.2587E-05	16.49%
	30.58	1.2597E-05	24.73%
	40.77	1.2608E-05	32.96%
	50.97	1.2618E-05	41.18%
	61.16	1.2628E-05	49.40%
	71.36	1.2639E-05	57.62%
	81.55	1.2649E-05	65.83%
	91.74	1.2659E-05	74.03%
	101.94	1.2670E-05	82.23%
6mm	0	2.8274E-05	0.00%
	10.19	2.8298E-05	8.25%
	20.39	2.8321E-05	16.49%
	30.58	2.8344E-05	24.73%
	40.77	2.8368E-05	32.96%
	50.97	2.8391E-05	41.18%
	61.16	2.8414E-05	49.40%
	71.36	2.8437E-05	57.62%
	81.55	2.8460E-05	65.83%
	91.74	2.8484E-05	74.03%
	101.94	2.8507E-05	82.23%
8mm	0	5.0265E-05	0.00%
	10.19	5.0307E-05	8.25%
	20.39	5.0348E-05	16.49%
	30.58	5.0390E-05	24.73%
	40.77	5.0431E-05	32.96%
	50.97	5.0472E-05	41.18%
	61.16	5.0514E-05	49.40%
	71.36	5.0555E-05	57.62%
	81.55	5.0596E-05	65.83%
	91.74	5.0638E-05	74.03%
	101.94	5.0679E-05	82.23%

Table 4-4 shows the relationship of area to pressure for the three round holes. A linear trend line was fitted to the FEA data points. As confirmed by Cassa (2010), the straight line fits the FEA data points almost perfectly. Figure 4-20 shows the relationship of area to pressure for the three holes investigated in this study.

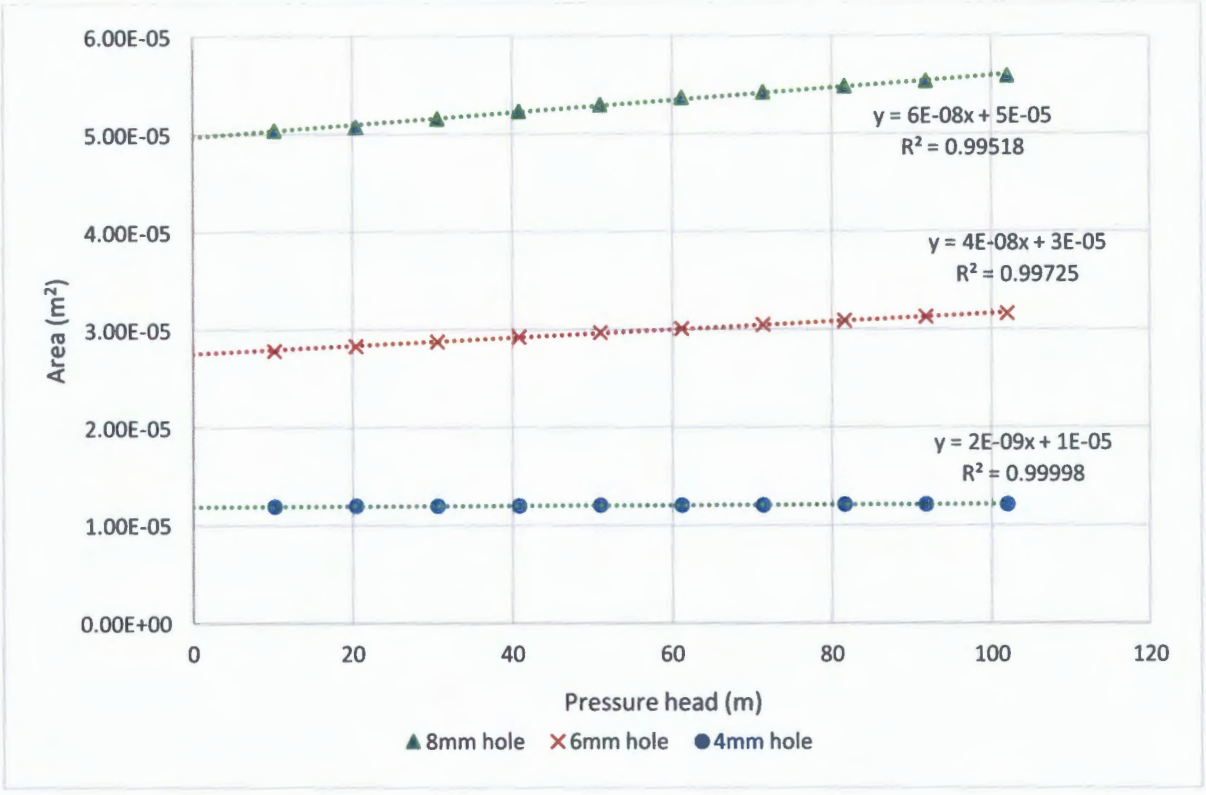

Figure 4-20 Showing the Relationship Between the Leak Area and the Pressure Head

From Figure 4-20 it can be seen that the leak area of a hole is linearly proportional to the pressure in the pipe. This linear relationship between pressure and leak area was also experimentally confirmed by other studies such as Malde, 2015. As Cassa & Van Zyl, 2011 concluded, it can also be seen that, irrespective of the hole size, the hole area increases linearly with increasing pressure, this finding yields Equation 2-37 explained in section 2.5.3 and is recited here:

$$A=A_0 + mh$$

Where A is the leak area, m is the head-area slope, and h is the pressure head. The head-area slope that is introduced in equation 2-37 is not yet well understood, especially for round hole defects. The head-area slope essentially gives an indication of the extent to which the leak area is sensitive to pressure. This study seeks to understand better what factors affect this parameter. A theoretical and a FEA approach will be developed and compared in the subsequent chapters.

4.6 Comparison of Experimental and FEA

This section briefly compares some finite element analysis (FEA) results to experimental work results. The experiments that were run by Malde & Van Zyl, (2015) are modelled and simulated in ABAQUS in order to compare the results.

4.6.1 Description of the experiment

The experiment focused on four pipe materials: Steel, uPVC, mPVC and HDPE. The experiment investigated the following crack types: Holes, Longitudinal, Circumferential and

Spiral. However, for the purposes of comparing results the FEA models focused only on the round hole and therefore only the round holes in the experimental results will be of interest.

In the experimental results all the pipes had an outer diameter of 110mm and a length of 800mm, with round hole leaks of 12mm in diameter. The thickness of the pipe wall varied depending on the material. The material parameters inserted for the FEA models were obtained from manuals found on the manufacturers' website, where Malde & Van Zyl (2015) ordered his pipe samples. The mPVC pipes material properties were not available on the website, because the mPVC properties depend on the specific type of pipe and the amount of modifier in the material. Due to the lack of this information the mPVC was eliminated in the simulation of the FEA models. The table below summarizes the parameters that were used to build the FEA model.

Table 4-5: summary of parameters inserted in the model

Material	Wall Thickness (mm)	Pipe Length (mm)	Elastic Modulus (MPa)	Poisson ratio
uPVC	4.54	500	3000	0.4
Steel	4.92	500	200000	0.3
HDPE	6.38	500	1035	0.425

The three pipe materials listed in Table 4-5were simulated in Abaqus as pipes with a round hole defect of 12mm in diameter. The internal pressures used in Abaqus were obtained from Malde & Van Zyl (2015) work. This was done in order to replicate the exact conditions of the experiment in the FEA models.

4.6.2 Comparison of leak area against pressure head

Table 4-6 shows the varying pressure heads Malde & Van Zyl, (2015) used and the corresponding leak area for the three materials: uPVC, Steel and HDPE compared. Figure 4-21 that follows shows graphically how the leak area varies with the pressure head for the FEA models simulating Malde's work. This is later compared to the experimental results obtained from (Malde & Van Zyl, 2015) work.

Table 4-6: Pressure head with the area expansion of the materials

	Area m^2		
Pressure head (m)	**uPVC x 10^{-4}**	**HDPE x10^{-4}**	**Steel x 10^{-4}**
18.42	1.13	1.14	1.12
24.70	1.13	1.15	1.12
32.00	1.14	1.17	1.12
32.39	1.14	1.16	1.12
32.42	1.14	1.17	1.12
36.65	1.14	1.17	1.12
40.93	1.14	1.18	1.12
55.40	1.15	1.20	1.12
55.57	1.15	1.20	1.12
56.02	1.15	1.20	1.12
58.15	1.16	1.20	1.12
67.62	1.16	1.21	1.12
67.84	1.16	1.21	1.12

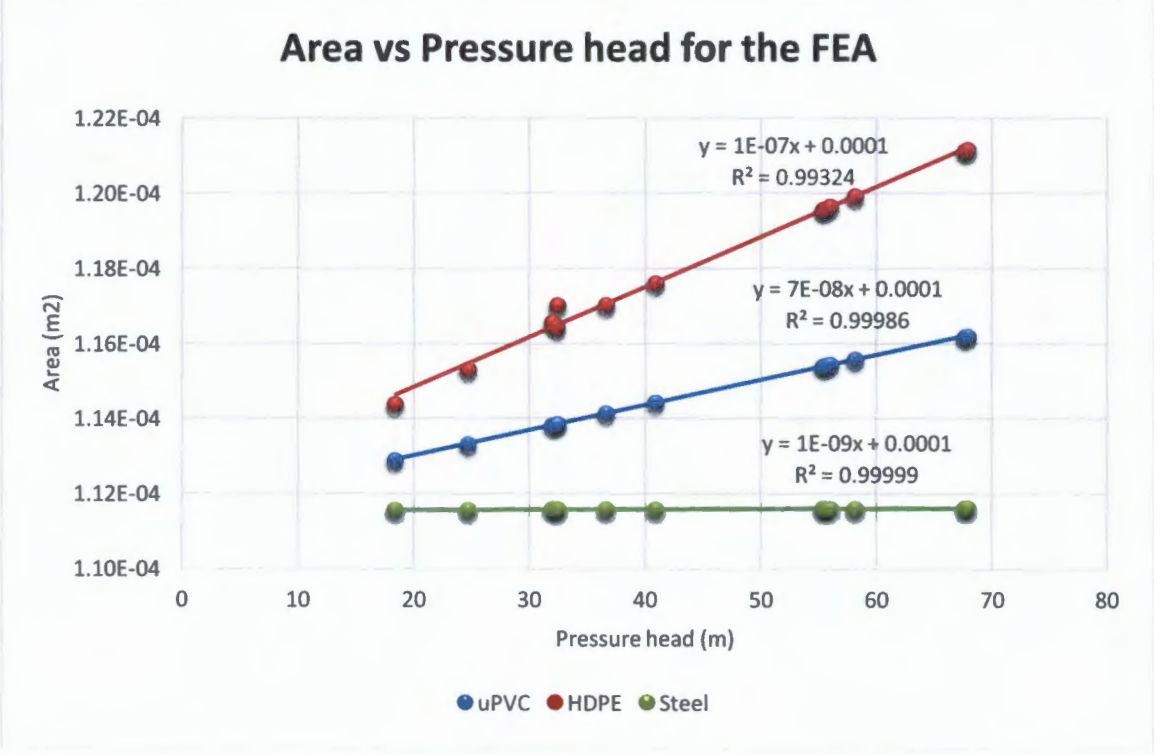

Figure 4-21: Head vs Area expansion from the FEA using ABAQUS

From Figure 4-21 it can be seen that the leak area changes differently for all the materials, with the HDPE showing the highest head-area slope, followed by the uPVC and finally the steel with the least head-area slope *m*. Despite the varying head-area slopes *m* all the

materials show a positive head-area slope. Figure 4-22 now shows (Malde & Van Zyl, 2015) experimental data of the area vs pressure head results. This is illustrated for comparison purposes. It can be seen that, for this range of pressures, the experimental data has a poor correlation (R^2) when compared to the FEA data that has R^2 of close to 1, implying .

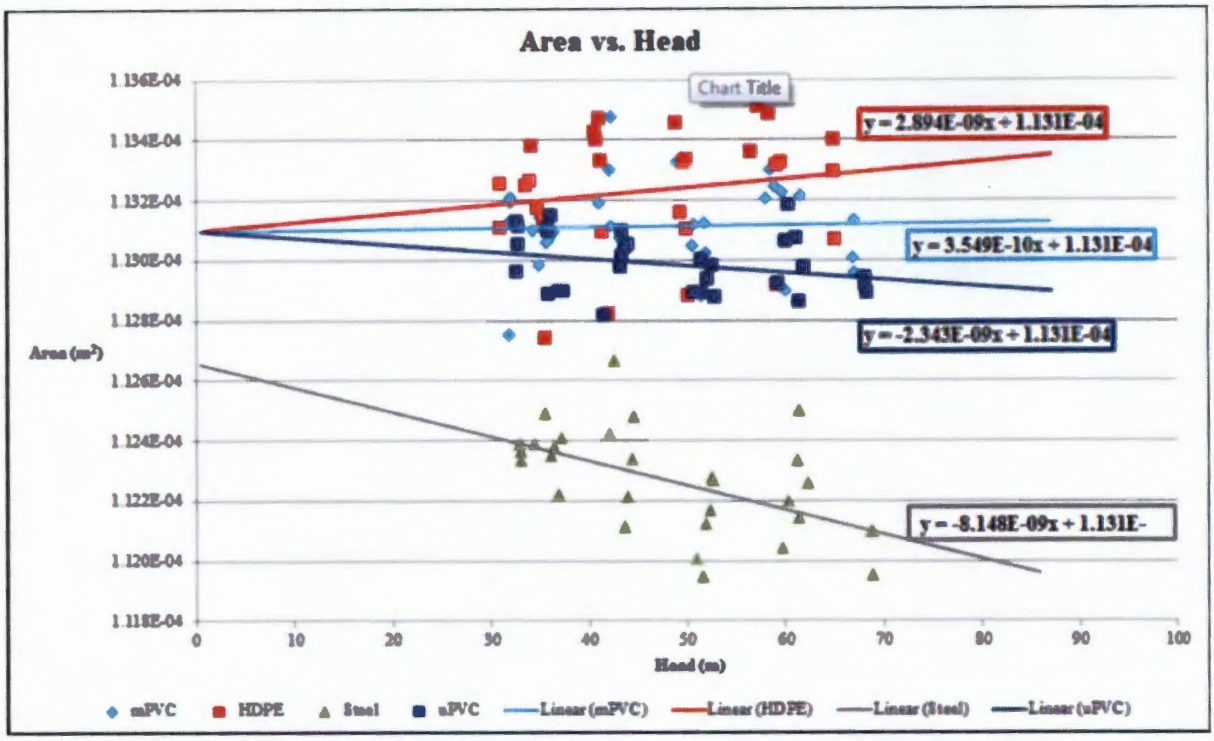

Figure 4-22: Leak area vs head for round hole leaks with 12 mm diameter (Malde & Van Zyl, 2015))

From Figure 4-22 it can be seen that only the HDPE and mPVC pipes portrayed a positive head-area slope, the steel and the uPVC both portrayed a negative head-area slope. This is in contrast to the FEA results (shown in Figure 4-21) where all pipe materials portrayed a positive head-area slope. Table 4-7 gives a summary of how the head-area slopes obtained for the three materials varied for the experimental results and the FEA results.

Table 4-7: Comparison of the head-area slope for the experimental and the FEA

	head-area slope	
Material	Experimental	FEM
uPVC	-2.34E-09	7.00E-08
Steel	-8.15E-09	1.00E-09
HDPE	2.89E-09	1.00E-07

There are a number of reasons why this discrepancy may exist. Firstly, the FEA models were assumed to behave as perfectly elastic materials, and therefore with increasing pressure the resulting material strain will always increase proportionally. The models do not take into account any plastic deformation that would occur in local regions of increased stress intensity as a result of the discontinuity of the hole. Also, in addition to the plastic deformation there is

a possibility that viscoelastic phenomenon may play a role, particularly in the plastic materials.

4.6.3 Comparison of leak flow rate against pressure head

Further analysis was done to compare the leak flow rates and the pressure heads. Figure 4-23 shows the results of the FEA models and figure 4 shows the experimental results from Malde & Van Zyl's (2015) work.

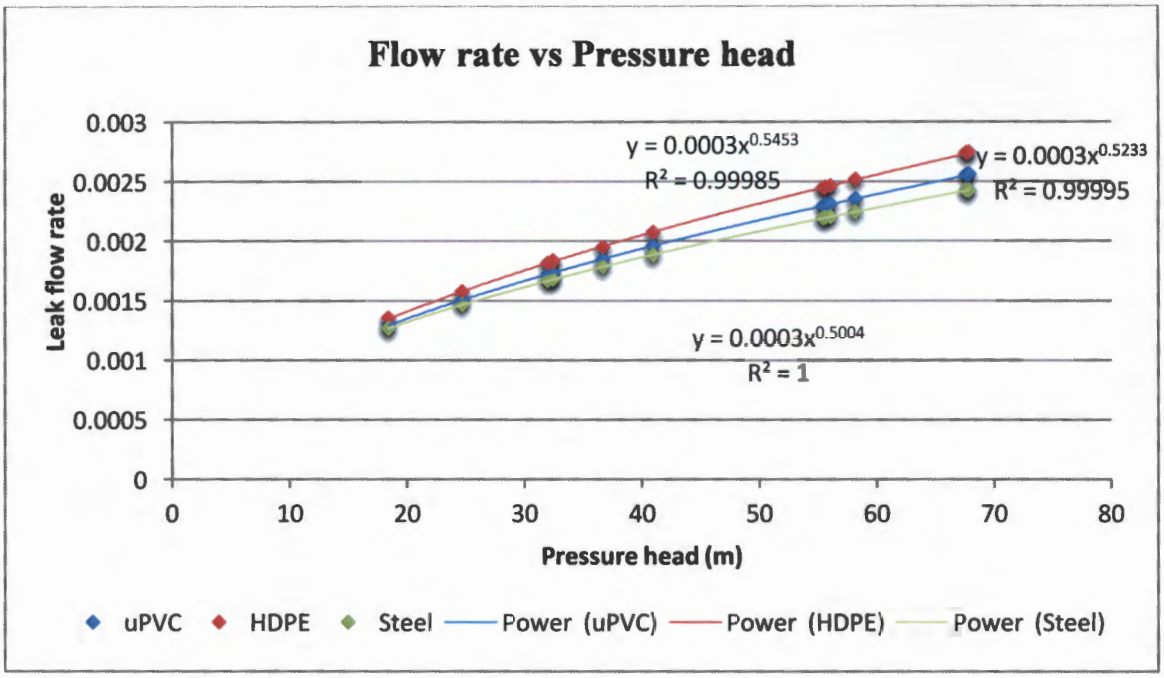

Figure 4-23: Leak flow rate vs head-area slope from FEA models

From Figure 4-23 it can be seen that the HDPE has the highest flow when compared to the other materials, flowed by the uPVC and lowest leak flow experienced with the steel sample. The corresponding *N1* values can be read off the graph, after plotting a power trend line through the data points.

In order to compare the FEA flow vs head to the experimental flow vs head, Figure 4-24 is shown to illustrate how the experimental samples behaved. From Figure 4-24 it can be seen that similar to the FEA results the HDPE had the highest flow, followed by the uPVC and the steel showing the lowest flow rate.

When comparing the two figures it is important to take into account the different scales used for the axis. However, it can be seen that the flow for all the materials typically ranged from $0.0014m^3/s$ to $0.00255m^3/s$.

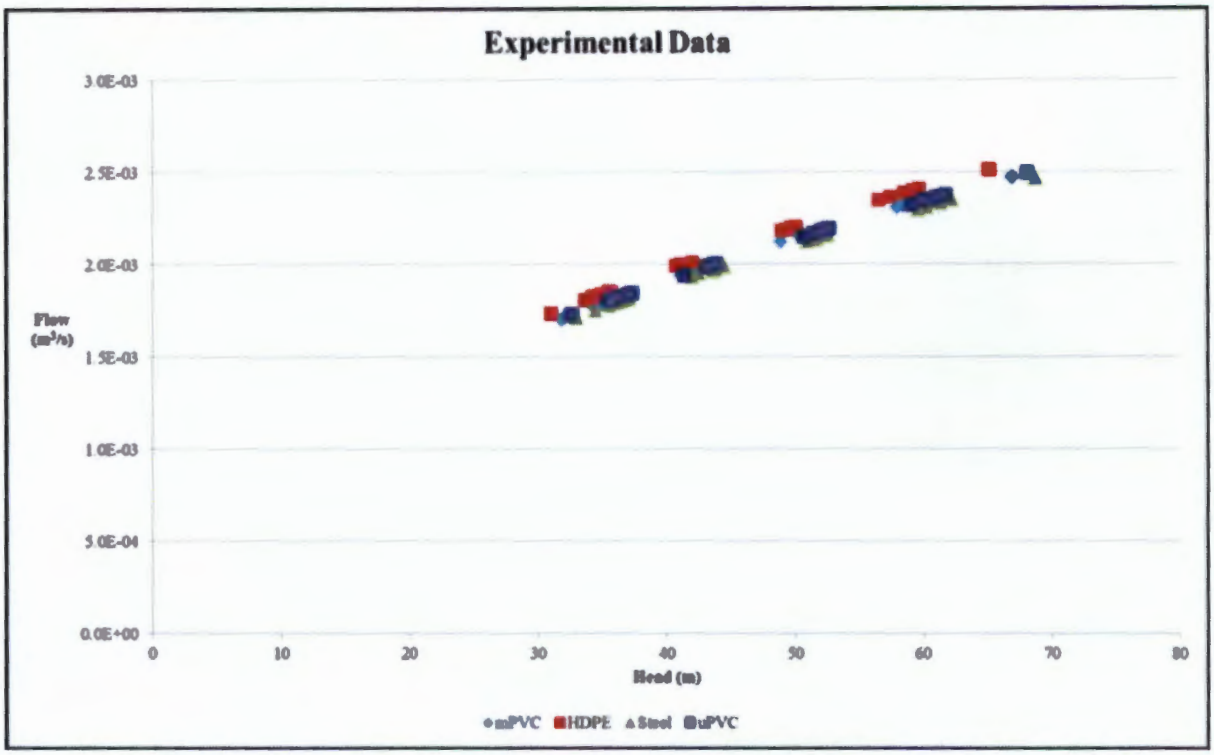

Figure 4-24: Experimental leak flow rate vs the head area for each pipe sample (Malde & Van Zyl, 2015)

4.6.4 Discussion on Comparison

It was clear that the experimental and the FEA results did not match very well. This could be accounted to a number of factors, which will are listed below:

The boundary conditions imposed on the FEA model might reflect the conditions the experimental results were calibrated too. This could interfere with the failure mode, particularly around the round hole defect

The FEA models were simulated as perfectly elastic materials; however, in reality this might not always be the case. Other phenomena, such as viscoelasticity and plasticity, may play a role in zones where stress intensity may supersede the yield strength of the material

4.7 Understanding the Head-Area Slopes

This section develops a methodology that helps to understand better the factors that affect the head-area slope *m*. In order to understand what these factors are, different geometric and material parameters are investigated to see what effect they might have on the head-area slope. The effect these parameters have on the head-area slope will give insight as to which factors play a role in influencing how the head-area slope behaves. In other words, a parametric study is carried out to determine what influence each parameter has on the head-area slope.

This parametric study was carried out by fixing all the identified parameters, except one parameter, which was allowed to vary. This is done for each parameter in turn to study the effect of that parameter on the head-area slope of the pipe. Table 4-8 shows how each

parameter varied. The base parameter's value (in bold) was constant, while varying the values of the parameter being investigated.

Table 4-8: Table Indicating the Parameters to be Varied Against the Head-Area Slope

Property or Dimension	Varied
Young's Modulus (MPa)	**3**, 10, 30, 90, 200
Poisson's ratio	0.17, 0.21, 0.29, **0.4**, 0.45, 0.5
Longitudinal stress (MPa)	0, 1.3, 2.6, 3.9, **5.2**
Wall thickness (mm)	2, 2.5, **3**, 4, 5
Internal diameter (mm)	20,30,40,50,80,**110**,150,200,250,300,350
Hole diameter (mm)	4, 6, 8
Pressure head (KPa)	0,10,20,30,40,50,**60**,70,80,90,100

Various graphs are compiled showing the head-area slope vs each of the parameters and these are discussed in the next chapter. The pressure is not varied with head-area slope; it remains constant at the working pressure of 60 KPa for all analyses.

5 Effect of Various Parameters on Head-Area Slopes for Different Hole Types

This chapter will explore the effect of changing various parameters on the head-area slope *m*. The parameters that will be varied are: elastic modulus, Poisson's ratio, wall thickness, pipe internal diameter and, finally, the longitudinal stress. This chapter is based on the simulations conducted on ABAQUS and the FEA head-area slope results that were obtained from this. It will end by showing which parameter plays the most significant role with regards to having an effect on the head-area slope *m* for round holes.

5.1 Effect of Elastic Modulus on the Head-Area Slope *m*

For materials assumed to behave elastically the modulus of elasticity is proportionality constant between stress and resulting strain. It is a property of the pipe material. In order to investigate the effect of the elastic modulus on the head-area slope, the simulation fixed the pressure at 600 kPa, the Poisson's ratio at 0.4, the longitudinal stress at 5.2 MPa, wall thickness at 3mm, and the internal diameter at 110mm and the parameter that was varied was the elastic modulus *E*.

The values for the elastic modulus ranged from 3, 10, 30, 90 and 200 GPa. This range of elastic moduli is particularly favourable because it represents the spread of elastic moduli for pipes that are commonly used in water distribution systems (Cassa, 2011).

In order to determine the head-area slope for each elastic modulus an *area vs pressure head graph* was plotted for the individual elastic moduli. Thereafter the slope of the *area vs pressure head* trend line was calculated by simply computing the gradient (i.e. $\Delta A/\Delta h$), (see Figure 5-1). The Δh was kept constant at 61.16 mm, i.e. 600 kPa for all analyses carried out. The hole area at 0 kPa or 0 m pressure head is assumed to be the original area, i.e. the hole area before any deformation occurs. These original areas were calculated to be: 50.27 mm^2, 28.27 mm^2 and 12.57mm^2 for the 8mm, 6mm and 4mm hole, respectively.

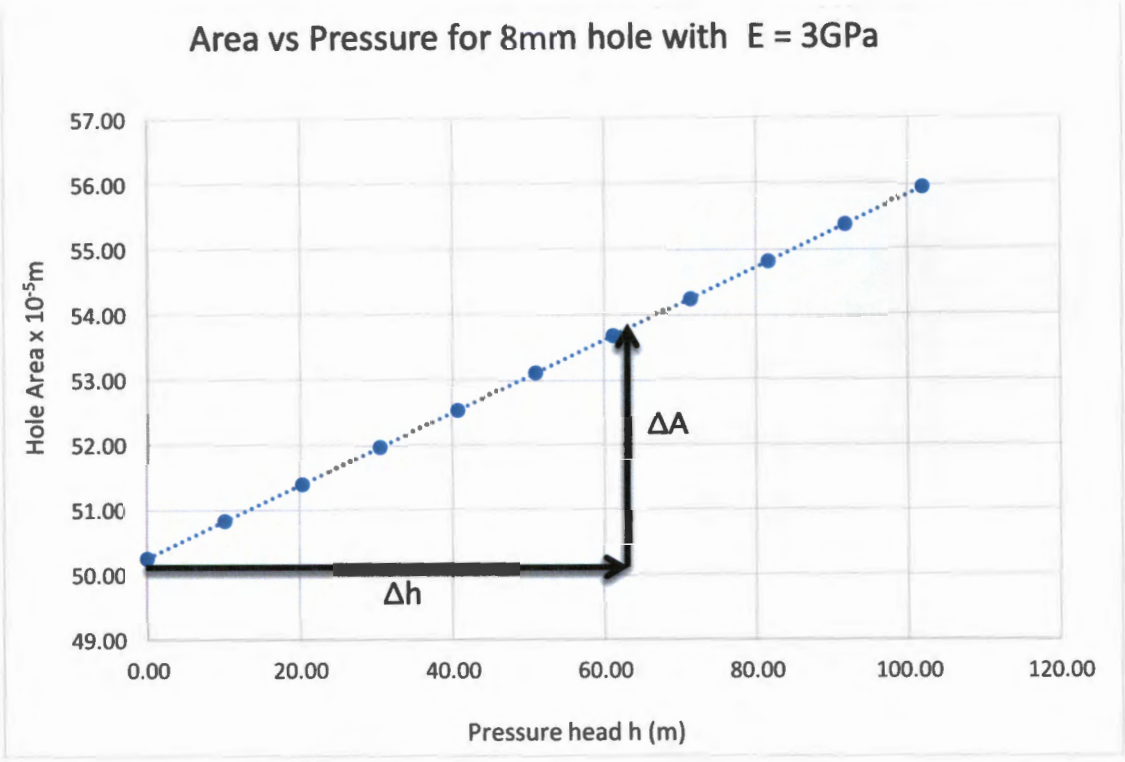

Figure 5-1: Pressure vs Area Graph for Pipe with E=3GPa

The calculation that follows illustrates how the head-area slope was calculated for the case shown in Figure 5-1. This calculation was carried out for each elastic modulus for all three holes.

$$m = \frac{\Delta A}{\Delta h} = \frac{(53.68 - 50.27)\times 10^{-6}}{(61.16 - 0)} = 5.58\times 10^{-8}\text{m}$$

Table 5-1 shows the head-area slope m results that were obtained from varying the elastic moduli of all three holes that were investigated.

Table 5-1: Areas of Holes at 600 kPa with Varying Elastic Modulus

Hole Diameter (mm)	Elastic Modulus (Pa) x 10^9	Area (m^2) x 10^{-5}	Head-Area Slope *m* (m) x 10^{-9}
8	3	5.37	55.8
8	10	5.07	7.23
8	30	4.97	-8.41
8	90	4.94	-13.8
8	200	4.93	-15.3
6	3	3.01	29.6
6	10	2.82	-0.81
6	30	2.76	-10.4
6	90	2.74	-13.7
6	200	2.74	-14.6
4	3	1.32	10.3
4	10	1.23	-4.24
4	30	1.20	-8.77
4	90	1.19	-10.3
4	200	1.19	-10.7

Figure 5-2 that follows shows the relationship between the head-area slope *m* and the elastic modulus.

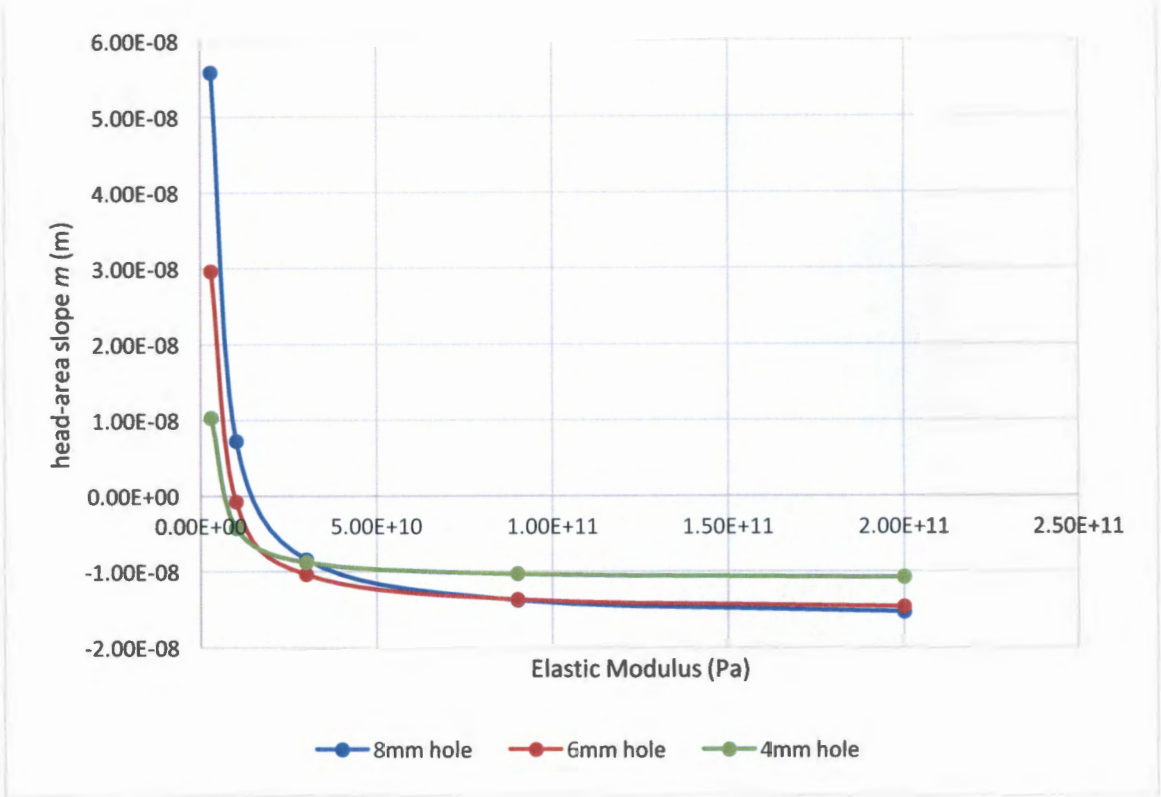

Figure 5-2: Pressure-Area Slope m for a Change in Young's Modulus E for Different Holes

From Figure 5-2 it can be seen that the three hole diameters maintain a similar trend. It can be seen that the head-area slope m has an inversely proportional relationship to the elastic modulus. In other words, as the pipe elastic modulus increases (i.e., increasing E) the change in hole area increases at a slower rate, with respect to an increase in pressure head. It is also important to note that negative head-area slopes were found. Mathematically, if $\Delta A = A_{deformed} - A_0$, then ΔA will be negative if$A_0 > A_{deformed}$, and thus from the formulation given for the head-area slope m, if ΔA is negative then this will result in a negative head- area slope. This phenomenon could be due to local deformation that occurs as a result of the inner material forces which concentrate around the hole. These forces create stress concentrators that tend to magnify the stress levels around the inside hole area, contracting the hole and, thus, resulting in a smaller hole area.

These results were also related to the conventional leakage exponent *N1*. This was done because the leakage exponent *N1* is commonly used in practice. The leakage number was first calculated and, thereafter, the *N1* was calculated from this. The leakage number is a function of the pressure at which it is measured - for this case two pressure heads were used to calculate the leakage number and, therefore, the leakage exponent. These were: 20 m and 100 m. Two pressure heads are used (one low and one high) because this would show how the leakage exponent varies at different pressures and the range of this variation. The calculation that follow illustrates how the leakage number L_N and N1 were calculated for the pipe model with an 8mm hole (A_0 =50.27x10^{-6}m^2) and an elastic modulus of 3 Pa, and a head-area slope m of 5.58x10^{-8}m.

Leakage number (L_N) and Leakage exponent (N1) at 20 m:

$$L_N = \frac{mh}{A_0} = \frac{5.58\times10^{-8}(20)}{50.27\times10^{-6}} = 2.22 \times 10^{-2}$$

$$N1 = \frac{(1.5\,L_N+0.5)}{(1+L_N)} = \frac{(1.5\,(2.22\times10^{-2})+0.5)}{(1+2.22\times10^{-2})} = 5.22\times10^{-1}$$

Leakage number (L_N) and Leakage exponent (N1) at 100 m:

$$L_N = \frac{mh}{A_0} = \frac{5.58\times10^{-8}(100)}{50.27\times10^{-6}} = 1.11 \times 10^{-1}$$

$$N1 = \frac{(1.5\,L_N+0.5)}{(1+L_N)} = \frac{(1.5\,(1.11\times10^{-1})+0.5)}{(1+1.11\times10^{-1})} = 6.00\times10^{-1}$$

These calculations were done for all the elastic moduli for all the three holes investigated. The results of these calculations are tabulated in Table 5-2.

Table 5-2: Illustrating the Leakage Number and Leakage Exponent Results

				20 m		100m	
Hole Diameter (mm)	Elastic Modulus (Pa)	Area (m^2)	Head-Area Slope *m* (m)	Ln	N1	Ln	N1
8	3.00E+09	5.37E-05	5.58E-08	2.22E-02	5.22E-01	1.11E-01	6.00E-01
8	1.00E+10	5.07E-05	7.23E-09	2.88E-03	5.03E-01	1.44E-02	5.14E-01
8	3.00E+10	4.97E-05	-8.41E-09	-3.35E-03	4.97E-01	-1.67E-02	4.83E-01
8	9.00E+10	4.94E-05	-1.38E-08	-5.49E-03	4.94E-01	-2.74E-02	4.72E-01
8	2.00E+11	4.93E-05	-1.53E-08	-6.08E-03	4.94E-01	-3.04E-02	4.69E-01
6	3.00E+09	3.01E-05	2.96E-08	2.10E-02	5.21E-01	1.05E-01	5.95E-01
6	1.00E+10	2.82E-05	-8.10E-10	-1.72E-03	4.98E-01	-2.86E-03	4.97E-01
6	3.00E+10	2.76E-05	-1.04E-08	-2.21E-02	4.77E-01	-3.69E-02	4.62E-01
6	9.00E+10	2.74E-05	-1.37E-08	-2.91E-02	4.70E-01	-4.85E-02	4.49E-01
6	2.00E+11	2.74E-05	-1.46E-08	-3.10E-02	4.68E-01	-5.17E-02	4.45E-01
4	3.00E+09	1.32E-05	1.03E-08	4.92E-02	5.47E-01	8.20E-02	5.76E-01
4	1.00E+10	1.23E-05	-4.24E-09	-2.02E-02	4.79E-01	-3.37E-02	4.65E-01
4	3.00E+10	1.20E-05	-8.77E-09	-4.19E-02	4.56E-01	-6.98E-02	4.25E-01
4	9.00E+10	1.19E-05	-1.03E-08	-4.92E-02	4.48E-01	-8.21E-02	4.11E-01
4	2.00E+11	1.19E-05	-1.07E-08	-5.13E-02	4.46E-01	-8.55E-02	4.07E-01

From Table 5-2 it can be seen that a negative head-area slope *m* will give a negative leakage number which, in turn, gives a leakage exponent less than 0.5. Malde's (2015) experimental results also showed that negative head-area slopes can occur for certain materials, with round hole leaks. Table 5-3 is taken from Malde's (2015) experimental work, and it illustrates some of the results of the experiment carried out in his study.

Table 5-3: Summary of Leakage Parameters Determined for a Round Hole Leak with a 12 mm hole (Malde (2015))

Pipe Sample	C_d	C	N1	m (m)	A_0 (m^2)
mPVC	0.6039	3.022×10^{-04}	0.5003	3.549×10^{-10}	1.131×10^{-04}
HDPE	0.6212	3.102×10^{-04}	0.5012	2.894×10^{-09}	1.131×10^{-04}
Steel	0.5960	3.015×10^{-04}	0.4965	-8.148×10^{-09}	1.131×10^{-04}
uPVC	0.6035	3.032×10^{-04}	0.4990	-2.343×10^{-09}	1.131×10^{-04}

It can be seen from Table 5-3 that a negative head-area slope *m* also resulted in a leakage exponent *N1* of less than 0.5. Also, it is interesting to note that similar to the finite element results; generally, in the experimental results the high elastic modulus material (such as the steel) resulted in the negative head-area slope *m*.

Figure 5-3 that follows shows graphically how the N1 varies with the elastic modulus at the two pressures (20m and 100m) for the three holes (See Table 5-2).

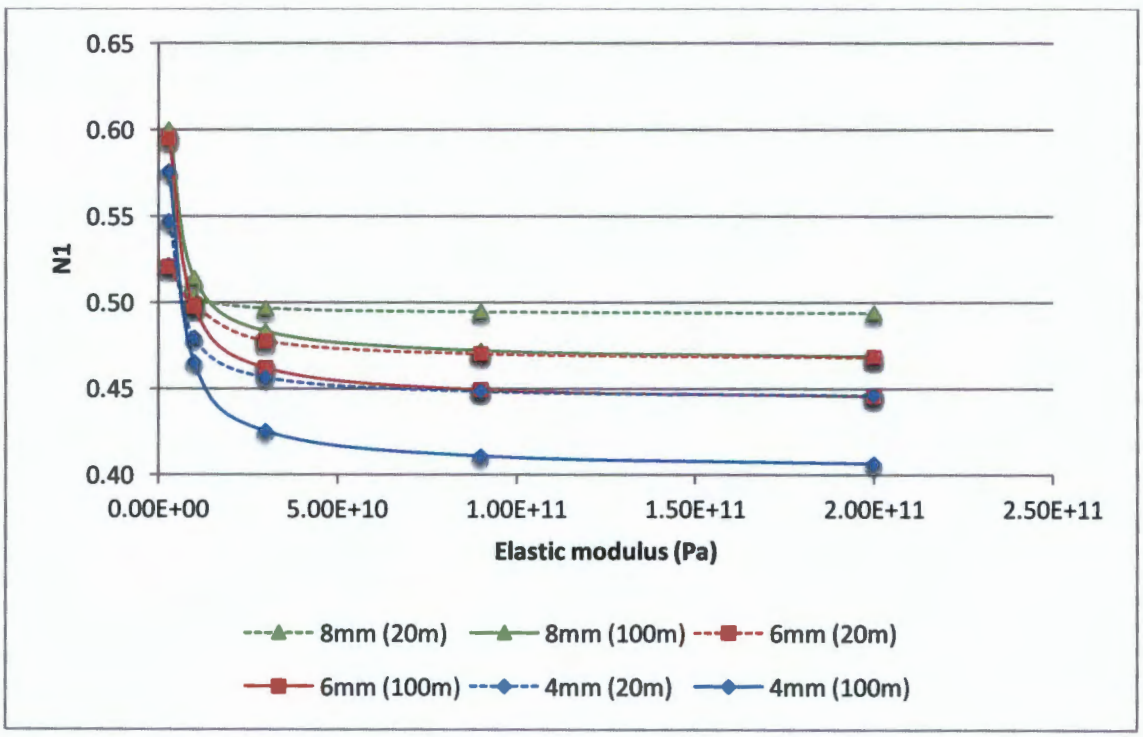

Figure 5-3: Relationship Betweent Leakage Exponent and the Elastic Modulus for Various Pressures

Figure 5-3 shows that for round holes, the leakage number also has an inversely proportional relationship to the elastic modulus. The leakage exponent N1 is very sensitive at Lower E's (i.e. for plastic pipes). For higher elastic moduli (e.g. steel) the N1 remains fairly constant. The difference between the leakage exponents at the two pressures is not particularly significant, implying that lower ranges of N1 are expected, depending on the systems pressure. Once again, it is shown that leakage exponents of less than 0.5 were found, and this was for the cases where the head-area slopes *m* was negative.

5.2 Effect of Poisson's Ratio on the Head-Area Slope *m*

The Poisson's ratio is also a property of the pipe material and is defined as the lateral strain divided by the axial strain. The analysis carried out here will be similar to that of the elastic modulus, but with the Poisson's ratio being the parameter that changes. The longitudinal stress was set at 5.2 MPa, the wall thickness at 3 mm, the internal diameter at 110 mm, and the elastic modulus was set at 3 GPa.

The values of the Poisson's ratio varied from 0.17, 0.21, 0.29, 0.4, 0.45, and 0.495. Again, this range of Poisson's ratio covers some Poisson's ratios of pipe materials used in industry (Cassa, 2011). For example, Cast Iron has a Poisson's ratio of 0.21, Steel has a Poisson's ratio of 0.3, uPVC has a Poisson's ratio of 0.4 and the other values that are used are the limits that the Poisson ratio can reach, with the maximum limit of 0.495, which would imply a nearly perfectly incompressible material.

For each Poisson ratio an *area vs pressure head* graph was plotted. A trend line was fitted through the FEA data points of the *area vs pressure head* graph as was done previously. In order to determine the head-area slope *m* for each Poisson's ratio, the slope of the *area vs pressure head* graph was calculated by simply computing the gradient (i.e. **$\Delta A/\Delta h$**)

Table 5-4 shows the results of the head-area slopes *m* and how the head-area slope varied with the Poisson's ratio for the three holes.

Table 5-4: Areas of Holes at Varying Poisson Ratio

Hole Diameter (mm)	Poisson Ratio x 10^{-1}	Area in m^2 x10^{-5}	Head-Area Slope *m*(m) x10^{-8}
8	1.70	5.39	5.94
8	2.10	5.39	5.88
8	2.90	5.38	5.77
8	4.00	5.37	5.62
8	4.50	5.37	5.56
8	4.95	5.36	5.51
6	1.70	3.02	3.08
6	2.10	3.01	3.06
6	2.90	3.01	3.03
6	4.00	3.01	2.98
6	4.50	3.01	2.96
6	4.95	3.01	2.95
4	1.70	1.32	1.04

4	2.10	1.32	1.04
4	2.90	1.32	1.04
4	4.00	1.32	1.04
4	4.50	1.32	1.04
4	4.95	1.32	1.04

Figure 5-4 that follows, shows graphically the relationship between the head-area slope *m* and the Poisson ratio for the 4 mm, 6 mm and 8 mm hole pipes.

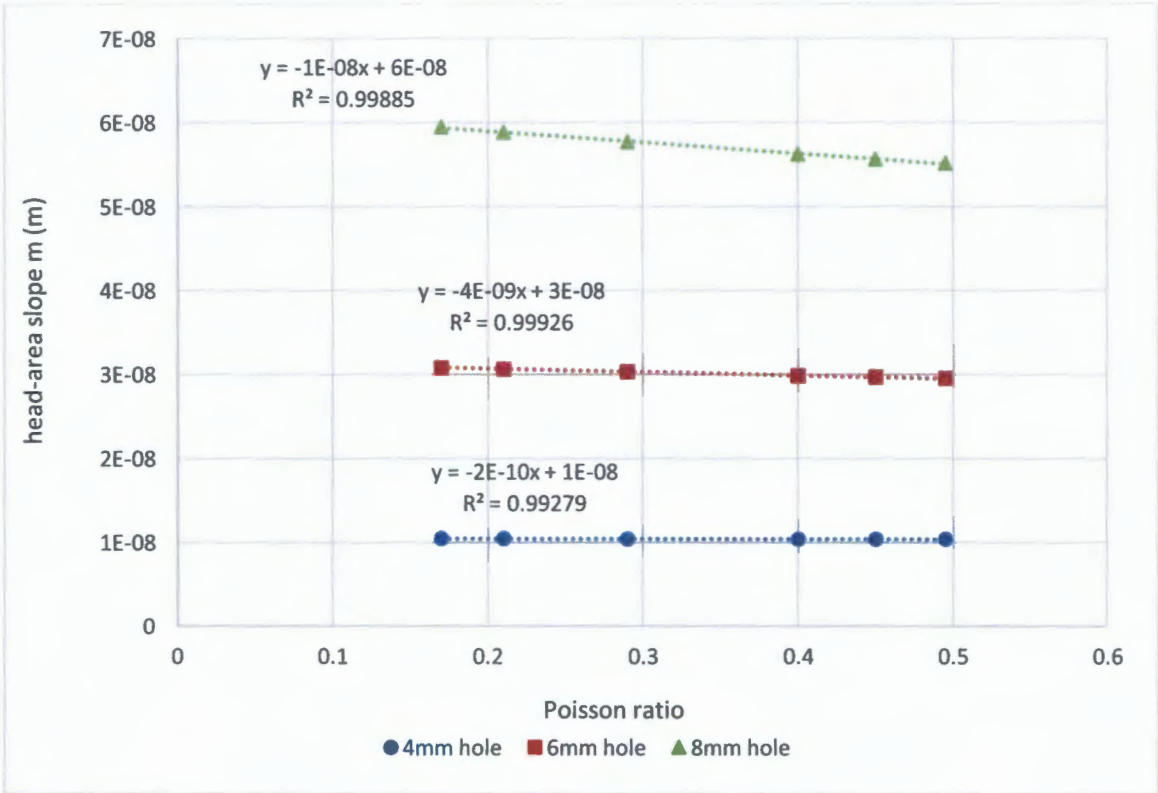

Figure 5-4: Pressure-Area Slope *m* for a Change in Poisson Ratio for Different Holes

In order to investigate the relationship between the Poisson's ratio and the head-area slope, a linear trend line was fitted to the data points, as can be seen in Figure 5-4. It can be seen from Figure 5-4 that the Poisson's ratio has very little effect on the head-area slope *m*. This is also justified by the linear trend lines having small gradients of negative $2x10^{-10}$, negative $4x10^{-9}$ and negative $1x10^{-8}$ for the 4 mm hole, 6 mm hole and 8 mm hole, respectively. However, the variation of the linear trend line slopes (i.e. increasing slope as the hole diameter increases) indicates that the relationship between the head-area slope *m* and the Poisson's ratio differs, depending on the hole diameter. In other words, the larger the hole diameter, the more significant the Poisson's ratio effect becomes.

Once more, these were related to the conventionally used leakage exponent N1. A similar method that was used in the previous section is adopted here. First the leakage number was calculated at two pressure heads (20 m and 100 m) and, thereafter, the leakage exponent was

determined from the leakage numbers. Table 5-5 shows the results of the calculated Leakage number (L_N) and the Leakage Exponent (N1) for the two pressures. Before illustrating the table, a sample calculation of the first row of Table 5-5 is shown. The first row calculates the L_N and N1 for the pipe model with an 8mm hole (A_0=50.27x10^{-6}m^2) and a Poisson's ratio of 0.17, and a head-area slope *m* of 5.94 x10^{-8}m.

Leakage number (L_N) and the Leakage Exponent (N1) at 20 m head:

$$L_N = \frac{mh}{A_0} = \frac{5.94\times10^{-8}(20)}{50.27\times10^{-6}} = 2.36\times10^{-2}$$

$$N1 = \frac{(1.5\,L_N+0.5)}{(1+L_N)} = \frac{(1.5\,(2.36\times10^{-2})+0.5)}{(1+2.36\times10^{-2})} = 5.23\times10^{-1}$$

Leakage number (L_N) and the Leakage Exponent (N1) at 100 m head:

$$L_N = \frac{mh}{A_0} = \frac{5.94\times10^{-8}(100)}{50.27\times10^{-6}} = 1.18\times10^{-1}$$

$$N1 = \frac{(1.5\,L_N+0.5)}{(1+L_N)} = \frac{(1.5\,(1.18\times10^{-1})+0.5)}{(1+1.18\times10^{-1})} = 6.06\times10^{-1}$$

The results of all the calculations done are presented in Table 5-5.

Table 5-5: Illustrating Leakage Number and Leakage Exponent Results

				20m		100m	
Hole Diameter (mm)	Poisson Ratio	Area in m^2 x10^{-5}	Head-Area Slope *m* (m) x10^{-8}	L_n x 10^{-2}	N1x10^{-1}	L_nx10^{-2}	N1x10^{-1}
8	0.17	5.39	5.94	2.36	0.52	0.12	0.61
8	0.21	5.39	5.88	2.34	0.52	0.12	0.6
8	0.29	5.38	5.77	2.29	0.52	0.11	0.6
8	0.4	5.37	5.62	2.23	0.52	0.11	0.6
8	0.45	5.37	5.56	2.21	0.52	0.11	0.599
8	0.495	5.36	5.51	2.19	0.52	0.109	0.598
6	0.17	3.02	3.08	2.17	0.52	0.109	0.598
6	0.21	3.01	3.06	2.17	0.52	0.108	0.598
6	0.29	3.01	3.03	2.14	0.52	0.107	0.597
6	0.4	3.01	2.98	2.11	0.52	0.105	0.595
6	0.45	3.01	2.96	2.1	0.52	0.104	0.595
6	0.495	3.01	2.95	2.09	0.52	0.104	0.594
4	0.17	1.32	1.04	1.66	0.516	0.0829	0.577
4	0.21	1.32	1.041	1.66	0.516	0.0828	0.576
4	0.29	1.32	1.039	1.65	0.516	0.0827	0.576
4	0.4	1.32	1.037	1.65	0.516	0.0825	0.576
4	0.45	1.32	1.037	1.65	0.516	0.0825	0.576
4	0.495	1.32	1.036	1.65	0.516	0.0825	0.576

Figure 5-5 shows, graphically, how the N1 varies with Poisson's ratio. It can be seen that irrespective of the material of the pipe, the system will generally experience substantially high ranges of leakage exponents N1.

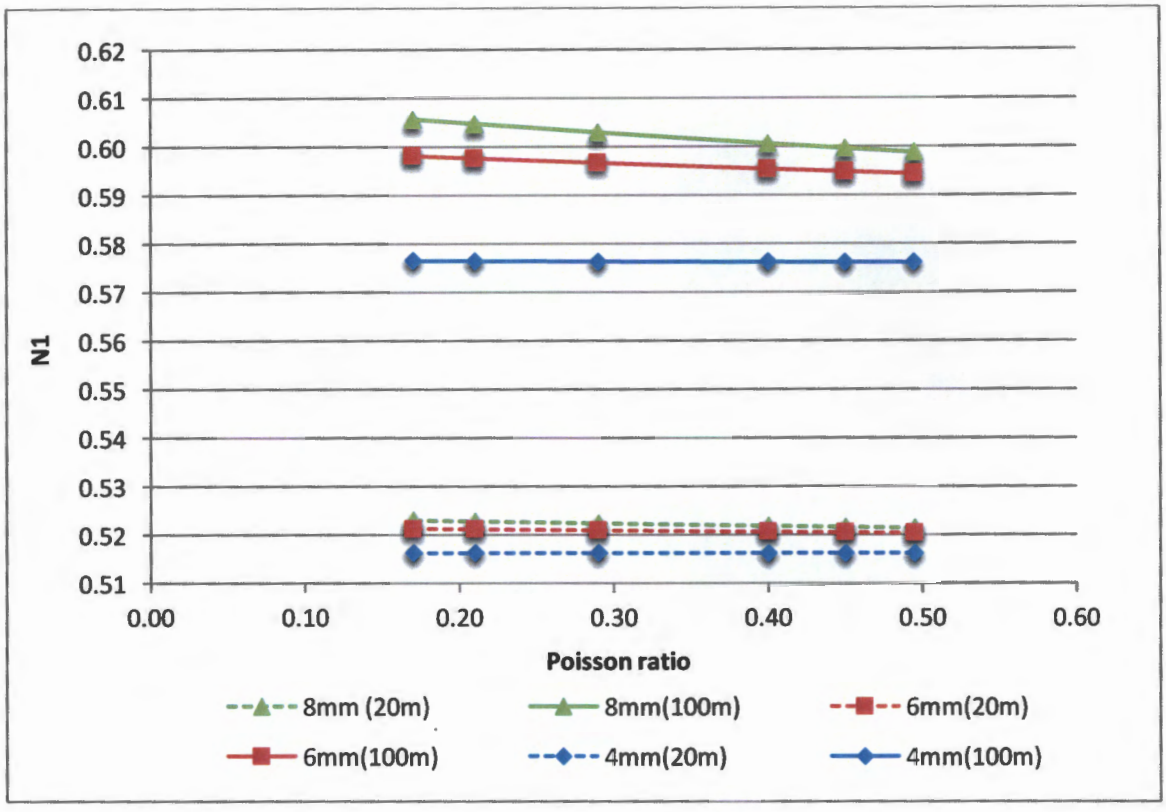

Figure 5-5: Relationship Between the Leakage Exponent and the Poisson Ratio for Various Pressures

5.3 Effect of Internal Diameter on the Head-Area Slope *m*

The geometric properties of the pipe can also have an effect on the head-area slope. This section looks at the effect of the pipe's internal diameter D to the head-area slopes. The analysis carried out here was similar to that of the previous analyses, but with the internal diameter being the parameter that changes. The longitudinal stress was set at 5.2 MPa, the wall thickness at 3 mm, the Poisson's ratio at 0.4, and the elastic modulus was set at 3 GPa.

Unlike the elastic modulus and the Poisson's ratio, the internal diameter is a geometric property and, therefore, a sensitivity analyses must be done for each pipe diameter change in order for the optimum element size to be determined. The sensitivity analyses for the different internal diameters appear in Appendix B. Regardless of the hole size, the internal diameters varied from 54, 84, 104 (base model), 144, 214 and 244 mm.

For each internal diameter an *area vs pressure head* graph was plotted and a trend line was fit through the data points. In order to determine the head-area slope m for each internal diameter, the slope of the *area vs pressure head* trend line was calculated.

Table 5-6 shows the results of the head-area slopes m and how the head-area slope varied with the internal diameters for the three holes.

Table 5-6: Areas of Holes at Varying Internal Diameters for the Three Holes

Hole Diameter(mm)	Internal Diameter (m) x 10^{-3}	Area (m^2) x 10^{-6}	Head-Area Slope *m*(m) x 10^{-9}
8	54	51.43	19.00
8	84	52.79	41.30
8	104	53.70	56.20
8	144	55.41	84.00
8	214	57.31	115.00
8	244	58.93	142.00
6	54	28.83	9.00
6	84	29.68	23.00
6	104	30.22	31.80
6	144	31.23	48.30
6	214	32.35	66.70
6	244	33.32	82.60
4	54	12.95	6.35
4	84	13.00	7.06
4	104	13.03	7.52
4	144	13.08	8.45
4	214	13.15	9.59
4	244	13.22	10.70

Figure 5-6 shows, graphically, the effect the internal diameter D has on the head-area slope *m* in a pipe with different hole diameters.

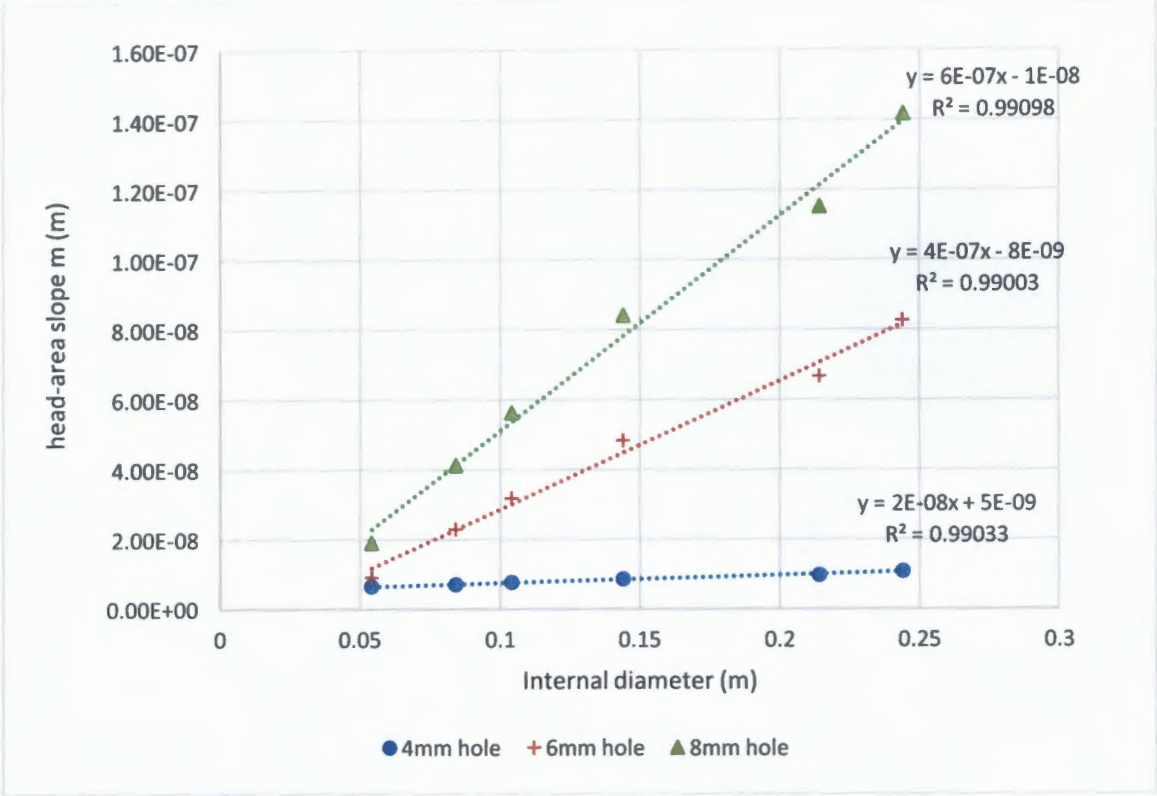

Figure 5-6: Pressure-Area Slope m for a Change in Internal Diameter for Different Holes

From Figure 5-6 it can be seen that a trend line has been fitted to the data points in order to determine the relationship between the internal diameter and the head-area slope *m* of the three holes. It was found that a linear trend line best fits the data of the three holes. From Figure 5-6 it can be seen that the 4mm hole has the smallest slope, followed by the 6 mm hole, and the 8 mm hole has the highest slope. This, therefore, means that for small holes, the internal diameter has an insignificant effect, and as the hole size increases the hole becomes increasingly sensitive to the effect the internal diameter has on the head-area slope. Also, the ratio of the hole size to the internal diameter is also important because this determines whether the curvature of the pipe starts to play a role in the round hole behaviour. In this study all hole sizes were much smaller compared to the internal diameter and, therefore, the curvature of the pipe does not play a role.

These results were also related to the conventionally used leakage exponent N1. Once again, the leakage numbers were calculated at two pressure heads (20 m and 100 m) and, thereafter, the leakage exponents were determined from the leakage numbers. Table 5-7shows the results of the calculated Leakage number (L_N) and the Leakage Exponent (N1) for the two pressures. Before illustrating the table, a sample calculation of the first row of Table 5-7 is shown. The first row calculates the L_N and N1 for the pipe model with an 8mm hole (A_0=50.27x10^{-6}m^2) and an internal diameter of 54 mm, and a head-area slope *m* of 1.90 x10^{-8}m.

Leakage number (L_N) and Leakage exponent (N1) at 20 m:

$$L_N = \frac{mh}{A_0} = \frac{1.90\times10^{-8}(20)}{50.27\times10^{-6}} = 7.56\times10^{-2}$$

$$N1 = \frac{(1.5\ L_N+0.5)}{(1+L_N)} = \frac{(1.5\ (7.56\times10^{-2})+0.5)}{(1+7.56\times10^{-2})} = 5.08\times10^{-1}$$

Leakage number (L_N) and Leakage exponent (N1) at 100 m:

$$L_N = \frac{mh}{A_0} = \frac{1.90\times10^{-8}(100)}{50.27\times10^{-6}} = 3.79\times10^{-2}$$

$$N1 = \frac{(1.5\ L_N+0.5)}{(1+L_N)} = \frac{(1.5\ (3.79\times10^{-2})+0.5)}{(1+3.79\times10^{-2})} = 5.37\times10^{-1}$$

The results of all the calculations done are presented in Table 5-7.

Table 5-7: Illustrating Leakage Number and Leakage Exponent Results

				20m		100m	
hole diameter(mm)	Internal Diameter (m) x 10^{-3}	Area (m^2) x 10^{-6}	Head-Area Slope *m* (m)	Ln	N1	Ln	N1
8	54	51.43	19.00	0.008	0.508	0.038	0.537
8	84	52.79	41.30	0.016	0.516	0.082	0.576
8	104	53.70	56.20	0.022	0.522	0.112	0.601
8	144	55.41	84.00	0.033	0.532	0.167	0.643
8	214	57.31	115.00	0.046	0.544	0.229	0.686
8	244	58.93	142.00	0.056	0.553	0.282	0.720
6	54	28.83	9.00	0.006	0.506	0.032	0.531
6	84	29.68	23.00	0.016	0.516	0.081	0.575
6	104	30.22	31.80	0.022	0.522	0.112	0.601
6	144	31.23	48.30	0.034	0.533	0.171	0.646
6	214	32.35	66.70	0.047	0.545	0.236	0.691
6	244	33.32	82.60	0.058	0.555	0.292	0.726
4	54	12.95	6.35	0.010	0.510	0.051	0.548
4	84	13.00	7.06	0.011	0.511	0.056	0.553
4	104	13.03	7.52	0.012	0.512	0.060	0.556
4	144	13.08	8.45	0.013	0.513	0.067	0.563
4	214	13.15	9.59	0.015	0.515	0.076	0.571
4	244	13.22	10.70	0.017	0.517	0.085	0.579

Figure 5-7 shows, graphically, the relationship of the internal diameter to the conventional leakage exponent *N1*.

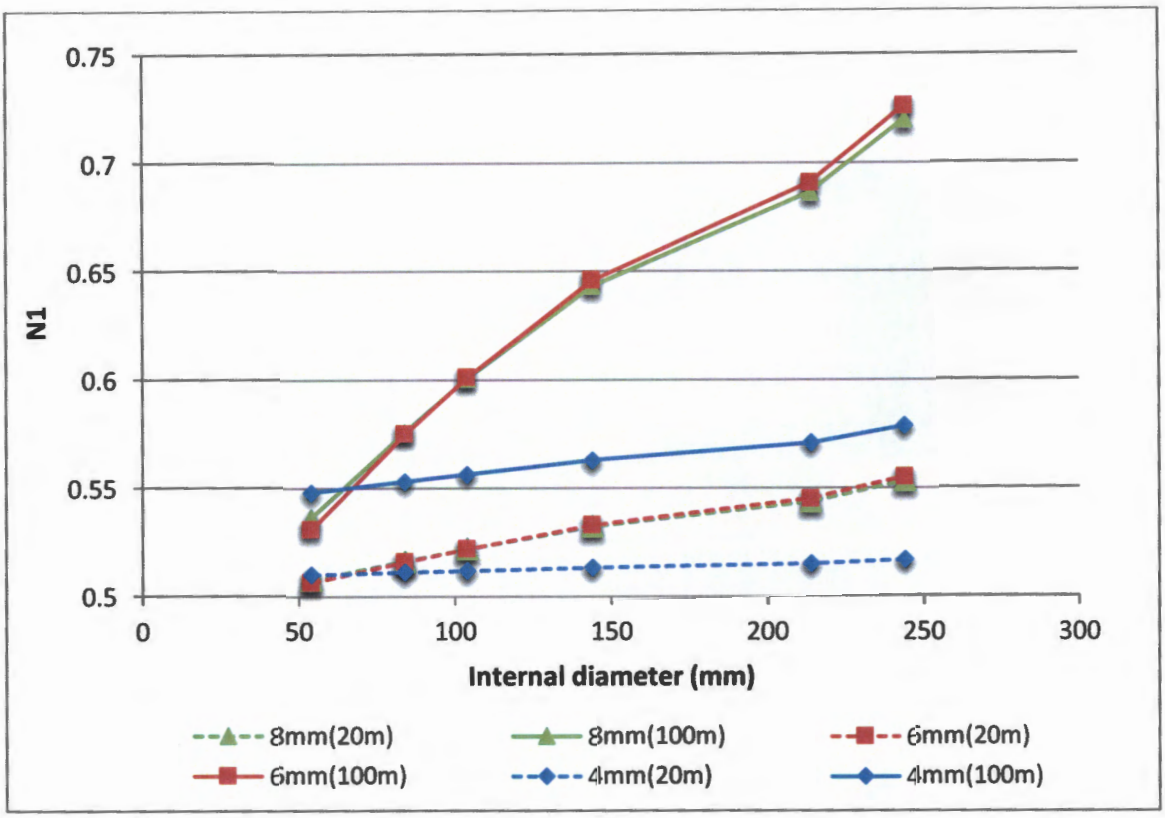

Figure 5-7: Relationship Between the Leakage Exponent and the Internal Diameter for Various Pressures

From Figure 5-7 it can be seen that the variance in *N1* between the different pressures, at which the leakage exponent is calculated, increases with increasing internal diameter. Also, it is interesting to note that at 20m pressure head, the leakage number's *N1* for the 6mm hole is very close to the leakage numbers *N1* for the 8mm hole.

5.4 Effect of Longitudinal Stress

In order to investigate the effect of longitudinal stress, the longitudinal stress was applied in the longitudinal direction of the pipe acting around the thickness of the pipe. The analysis, thereafter, was much the same as for the other previous parameters. In this case, the simulation was set up such that the elastic modulus was set at 3 GPa, the Poisson's ratio at 0.4, the wall thickness at 3 mm, the internal diameter at 110 mm, and the longitudinal stress was varied.

Five models were run with the longitudinal stress ranging from 0, 5.2, 10.4, 15.6, 20.8 MPa. A value of zero stress was used to indicate the uniaxial stress state. Previous work by Cassa (2006) did indicate that the longitudinal stress is not always present. This stress state occurs when the longitudinal stress is absorbed by joints in the water reticulation system (Cassa (2006)).

For each longitudinal stress applied, the area vs pressure head graph was plotted and a trend line was fitted through the data points. In order to determine the head-area slope *m* for each longitudinal stress applied, the slope of the *area vs pressure head* graph was calculated. Table

5-8 shows the results of the head-area slopes *m* and how the head-area slope varied with the internal diameters for the three holes.

Table 5-8: Areas of Holes at Varying Longitudinal Stress for the Three Holes

Hole Diameter (mm)	Longitudinal Stress (MPa)	Area m^2 x 10^{-5}	Head-Area Slope *m* (m)
8	0	5.34	5.11E-08
8	5.2	5.35	5.21E-08
8	10.4	5.35	5.30E-08
8	15.6	5.36	5.39E-08
8	20.8	5.36	5.49E-08
6	0	2.997	2.77E-08
6	5.2	3	2.82E-08
6	10.4	3.003	2.87E-08
6	15.6	3.006	2.92E-08
6	20.8	3.009	2.97E-08
4	0	1.314	9.44E-09
4	5.2	1.316	9.66E-09
4	10.4	1.317	9.88E-09
4	15.6	1.318	1.01E-08
4	20.8	1.32	1.03E-08

It can be seen from Table 5-8 that as the longitudinal stress increases, the area of the hole increases ever so slightly. Table 5-8 that follows shows, graphically, the relationship between the head-area slope *m* and the longitudinal stress.

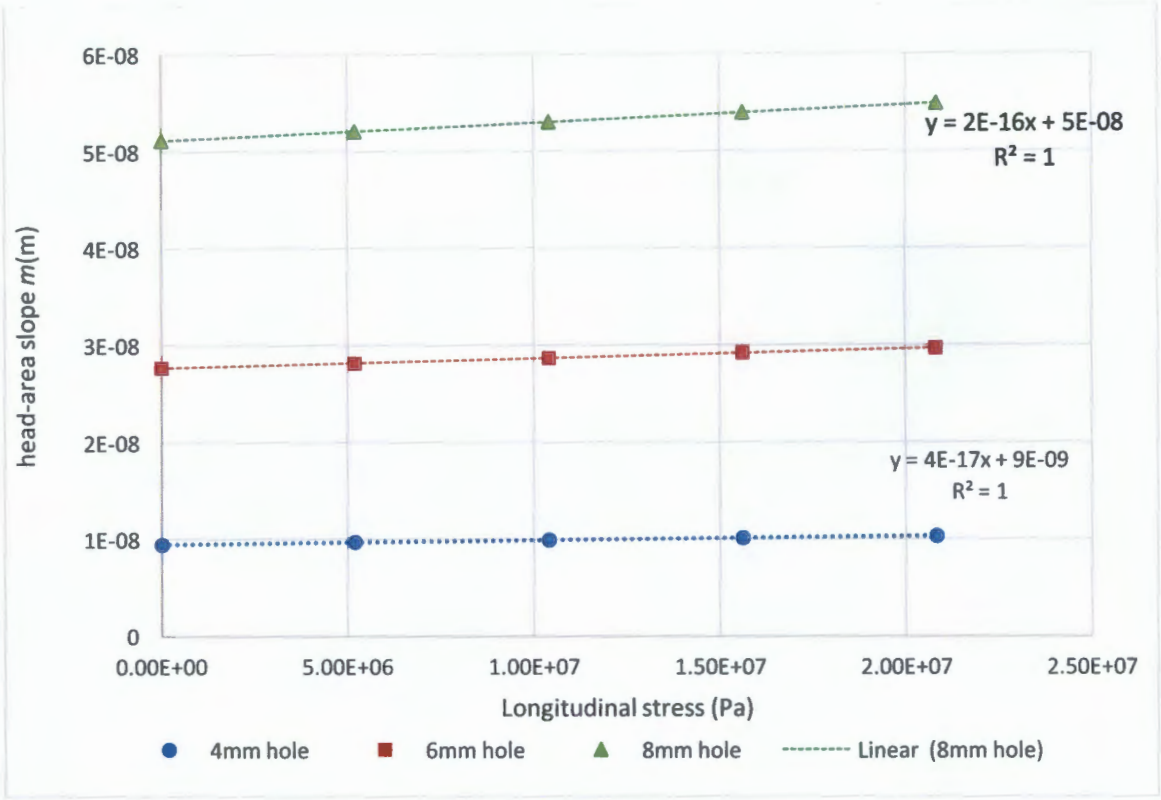

Figure 5-8: Head-Area Slope m for a Change in Longitudinal Stress for Different Holes

As can be seen from Figure 5-8, a linear trend line can be fitted to the data to determine the relationship between the longitudinal stress and the head-area slope. All three holes exhibit the same behaviour; as the longitudinal stress increases, the head-area slope increases as well. These increases, however, are very small, with gradients of $4x10^{-17}$, $1x10^{-16}$ and $2x10^{-16}$ for the 4 mm, 6 mm and 8 mm holes, respectively. The small increases could be attributed to the natural stability of the round hole as Cassa and van Zyl (2011) suggested. It can also be seen that the effect of longitudinal stress increases with increasing hole size. This is based on the increasing gradient of the trend lines.

These results were related to the conventionally used leakage exponent N1. Once again, the leakage numbers were calculated at two pressure heads (20 m and 100 m) and, thereafter, the leakage exponents were determined from the leakage numbers.

Leakage number (L_N) and Leakage exponent (N1) at 20 m:

$$L_N = \frac{mh}{A_0} = \frac{5.11\times10^{-8}(20)}{50.27\times10^{-6}} = 2.03\times10^{-2}$$

$$N1 = \frac{(1.5\,L_N+0.5)}{(1+L_N)} = \frac{(1.5\,(2.03\times10^{-2})+0.5)}{(1+2.03\times10^{-2})} = 5.19\times10^{-1}$$

Leakage number (L_N) and Leakage exponent (N1) at 100 m:

$$L_N = \frac{mh}{A_0} = \frac{5.11\times10^{-8}(100)}{50.27\times10^{-6}} = 1.02 \times 10^{-1}$$

$$N1 = \frac{(1.5\,L_N+0.5)}{(1+L_N)} = \frac{(1.5\,(1.02\times10^{-1})+0.5)}{(1+1.02\times10^{-1})} = 5.92\times10^{-1}$$

Table 5-9 shows the results of the head-area slopes *m* and how the head-area slope varied with the longitudinal stress for the three holes.

Table 5-9: Illustrating Leakage Number and Leakage Exponent Results

			20m		100m	
Hole diameter (mm)	Longitudinal stress Mpa	Head-Area slope *m* (m)	Ln	N1	Ln	N1
8	0	5.11E-08	2.03E-02	5.20E-01	1.02E-01	5.92E-01
8	5.2	5.21E-08	2.07E-02	5.20E-01	1.04E-01	5.94E-01
8	10.4	5.30E-08	2.11E-02	5.21E-01	1.05E-01	5.95E-01
8	15.6	5.39E-08	2.15E-02	5.21E-01	1.07E-01	5.97E-01
8	20.8	5.49E-08	2.18E-02	5.21E-01	1.09E-01	5.98E-01
6	0	2.77E-08	1.96E-02	5.19E-01	9.78E-02	5.89E-01
6	5.2	2.82E-08	1.99E-02	5.20E-01	9.96E-02	5.91E-01
6	10.4	2.87E-08	2.03E-02	5.20E-01	1.01E-01	5.92E-01
6	15.6	2.92E-08	2.06E-02	5.20E-01	1.03E-01	5.94E-01
6	20.8	2.97E-08	2.10E-02	5.21E-01	1.05E-01	5.95E-01
4	0	9.44E-09	1.44E-02	5.14E-01	7.51E-02	5.70E-01
4	5.2	9.66E-09	1.47E-02	5.14E-01	7.69E-02	5.71E-01
4	10.4	9.88E-09	1.50E-02	5.15E-01	7.86E-02	5.73E-01
4	15.6	1.01E-08	1.53E-02	5.15E-01	8.04E-02	5.74E-01
4	20.8	1.03E-08	1.56E-02	5.15E-01	8.21E-02	5.76E-01

Figure 5-9 shows, graphically, the relationship between the longitudinal stress and the conventional leakage exponent N1.

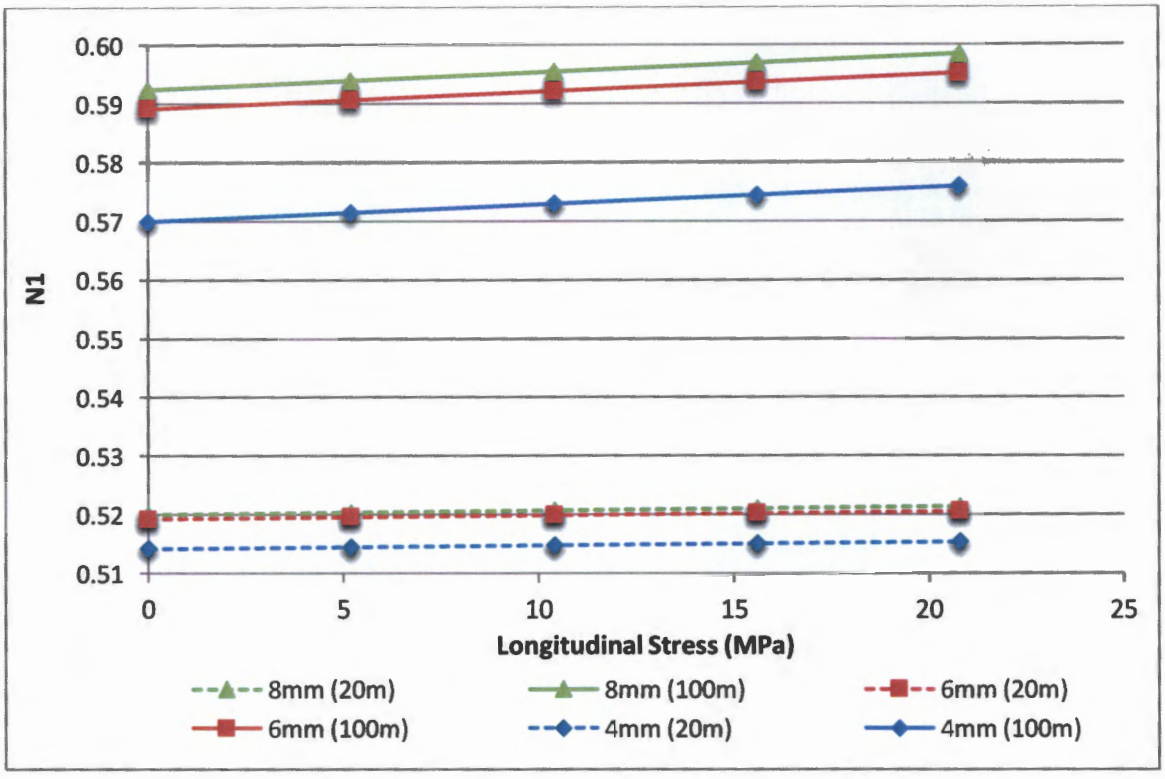

Figure 5-9: Relationship Between the Leakage Exponent and the Longitudinal Stress for Various Pressures

From Figure 5-9 it can be seen that the range of *N1* values range significantly with increasing pressure, with the 4 mm hole having an average *N1* of 0.515 at 20 m head and having an average *N1* of 0.573 at a head of 100 m. The 6 mm had an average *N1* of 0.52 at 20 m head and, eventually, reaching an average *N1* of 0.592 at 100 m. Finally, for the 8 mm hole, the average *N1* at 20 m was 0.521, reaching an average *N1* of 0.595 at 100 m.

5.5 Effect of Wall Thickness on the Head-Area Slope *m*

The pipe wall thickness of the pipe is the second geometric property of the pipe that can affect the head-area slope. As was the case for the internal diameter, a sensitivity analysis had to be undertaken in order to determine the optimum element size for the various pipe wall thicknesses. The sensitivity analyses done can be found in Appendix B. As a result of the similarity of the leaks, i.e. all being round hole leaks, the sensitivity analysis was done only for the largest hole, which was the 8 mm hole, and the results were used for the other smaller holes. The effect of the pipe wall thickness was simulated by keeping all other parameters constant and varying the wall thickness.

The wall thicknesses varied from 2 mm, 2.5 mm, 3 mm, 4 mm and 5 mm, for all three holes investigated. This range of wall thicknesses is particularly favourable because it represents the spread of pipe wall thicknesses for pipes that are commonly used in water distribution systems (Cassa, 2011).

For each pipe wall thickness an *area vs pressure head* graph was plotted and a trend line was fitted through the data points. In order to determine the head-area slope *m* for each longitudinal stress applied, the slope of the *area vs pressure head* graph was calculated. Table 5-10 shows the results of the head-area slope *m* and how the head-area slope varied with the wall thickness for the three holes.

Table 5-10: Areas of Holes at 600 kPa Varying Wall Thickness

Hole Diameter (mm)	Wall Thickness (m) $x10^{-3}$	Area (m^2) $x10^{-5}$	Head-Area Slope *m*(m) $x10^{-8}$
8	2	5.46	7.15
8	2.5	5.40	6.03
8	3	5.33	4.97
8	4	5.26	3.74
8	5	5.19	2.59
6	2	3.11	4.54
6	2.5	3.06	3.81
6	3	3.01	2.98
6	4	2.96	2.23
6	5	2.92	1.56
4	2	1.37	1.85E-08
4	2.5	1.34	1.39E-08
4	3	1.32	1.04E-08
4	4	1.29	5.45E-09
4	5	1.27	2.22E-09

From Table 5-10 it can be seen that as the wall thickness increases the hole area decreases. Figure 5-10 that follows shows the relationship between the wall thickness and the head area slope *m*.

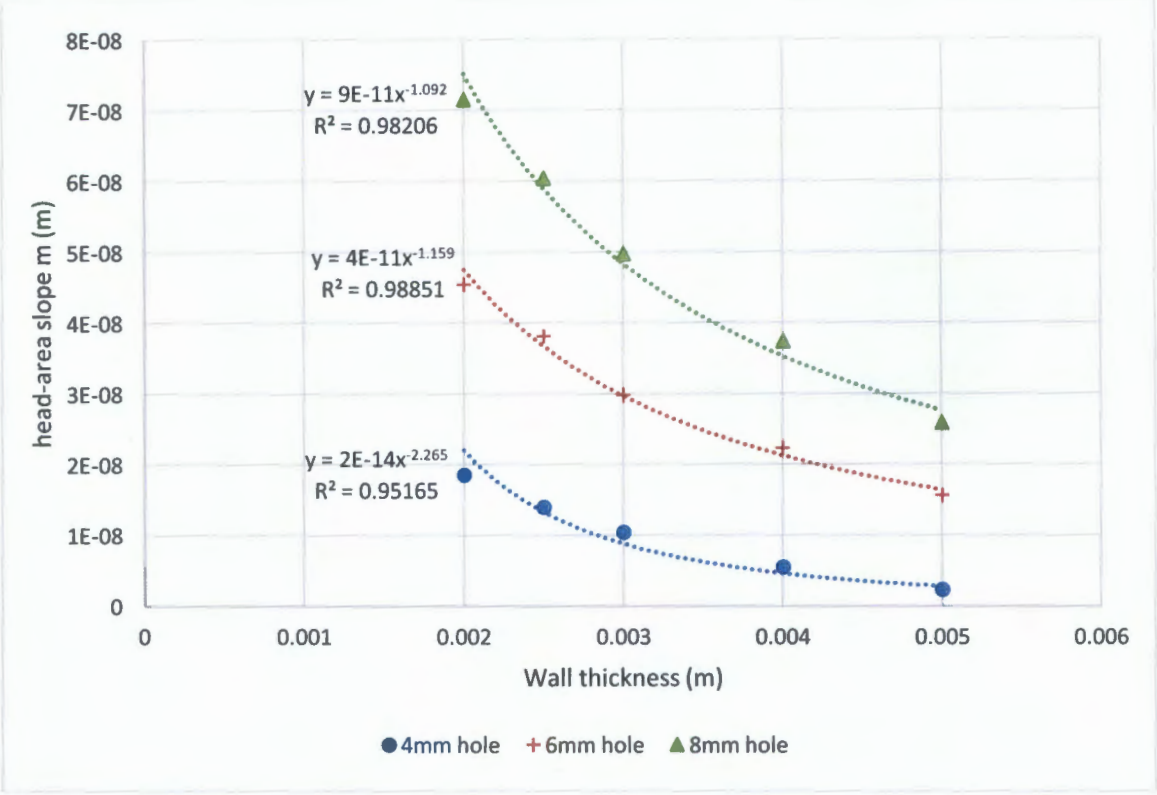

Figure 5-10: Head-Area Slope m for a Change in Wall Thickness for Different Holes

From Figure 5-10 it can be seen that the three holes showed similar behaviour. A power trend line was fitted through all the data points for the three holes, each hole having an inversely proportional relationship to the wall thickness, essentially, illustrating that as the wall thickness increases the head-area slopes *m* of the holes decreases. For the 4mm hole it was found that the head-area slope is inversely proportional to the wall thickness that is raised to the power 2.265. The 6mm hole was found to have a head-area slope that is inversely proportional to the wall thickness that is raised to the power 1.159. Finally, the 8 mm hole had a head-area slope that is inversely proportional to the wall thickness that is raised to the power 1.092.

These results were related to the conventionally used leakage exponent *N1*. Once again, the leakage numbers were calculated at two pressure heads (20 m and 100 m) and, thereafter, the leakage exponents were determined from the leakage numbers. Table 5-11 shows the results of the calculated Leakage number (L_N) and the Leakage Exponent (*N1*) for the two pressures. Before illustrating the table, a sample calculation of the first row of Table 5-11 is shown. The first row calculates the L_N and *N1* for the pipe model with an 8 mm hole (A_0=50.27x10^{-6}m^2) and the wall thickness of 2 mm, and a head-area slope *m* of 7.15 x10^{-8}m.

Leakage number (L_N) and Leakage exponent (N1) at 20 m:

$$L_N = \frac{mh}{A_0} = \frac{7.15\times10^{-8}(20)}{50.27\times10^{-6}} = 2.84\times10^{-2}$$

$$N1 = \frac{(1.5\,L_N+0.5)}{(1+L_N)} = \frac{(1.5\,(2.84\times10^{-2})+0.5)}{(1+2.84\times10^{-2})} = 5.28\times10^{-1}$$

Leakage number (L_N) and Leakage exponent (N1) at 100 m:

$$L_N = \frac{mh}{A_0} = \frac{7.15\times10^{-8}(100)}{50.27\times10^{-6}} = 1.42\times10^{-1}$$

$$N1 = \frac{(1.5\,L_N+0.5)}{(1+L_N)} = \frac{(1.5\,(1.42\times10^{-1})+0.5)}{(1+1.42\times10^{-1})} = 6.24\times10^{-1}$$

The results of all the calculations done are presented in Table 5-11.

Table 5-11: Illustrating the Leakage Number and Leakage Exponent Results

				20m		100m	
Hole diameter (mm)	Wall thickness (m)x10^{-3}	Area (m^2)x10^{-5}	Head-Area Slope *m* (m)	Ln	N1	Ln	N1
8	2	5.46	7.15E-08	0.028	0.528	0.142	0.624
8	2.5	5.40	6.03E-08	0.024	0.523	0.120	0.607
8	3	5.33	4.97E-08	0.020	0.519	0.099	0.590
8	4	5.26	3.74E-08	0.015	0.515	0.074	0.569
8	5	5.19	2.59E-08	0.010	0.510	0.052	0.549
6	2	3.11	4.54E-08	0.032	0.531	0.161	0.638
6	2.5	3.06	3.81E-08	0.027	0.526	0.135	0.619
6	3	3.01	2.98E-08	0.021	0.521	0.106	0.595
6	4	2.96	2.23E-08	0.016	0.516	0.079	0.573
6	5	2.92	1.56E-08	0.011	0.511	0.055	0.552
4	2	1.37	1.85E-08	0.029	0.529	0.147	0.628
4	2.5	1.34	1.39E-08	0.022	0.522	0.110	0.599
4	3	1.32	1.04E-08	0.017	0.516	0.083	0.576
4	4	1.29	5.45E-09	0.009	0.509	0.043	0.542
4	5	1.27	2.22E-09	0.004	0.504	0.018	0.517

Figure 5-11 shows, graphically, the relationship between the wall thickness and the conventional leakage exponent *N1*.

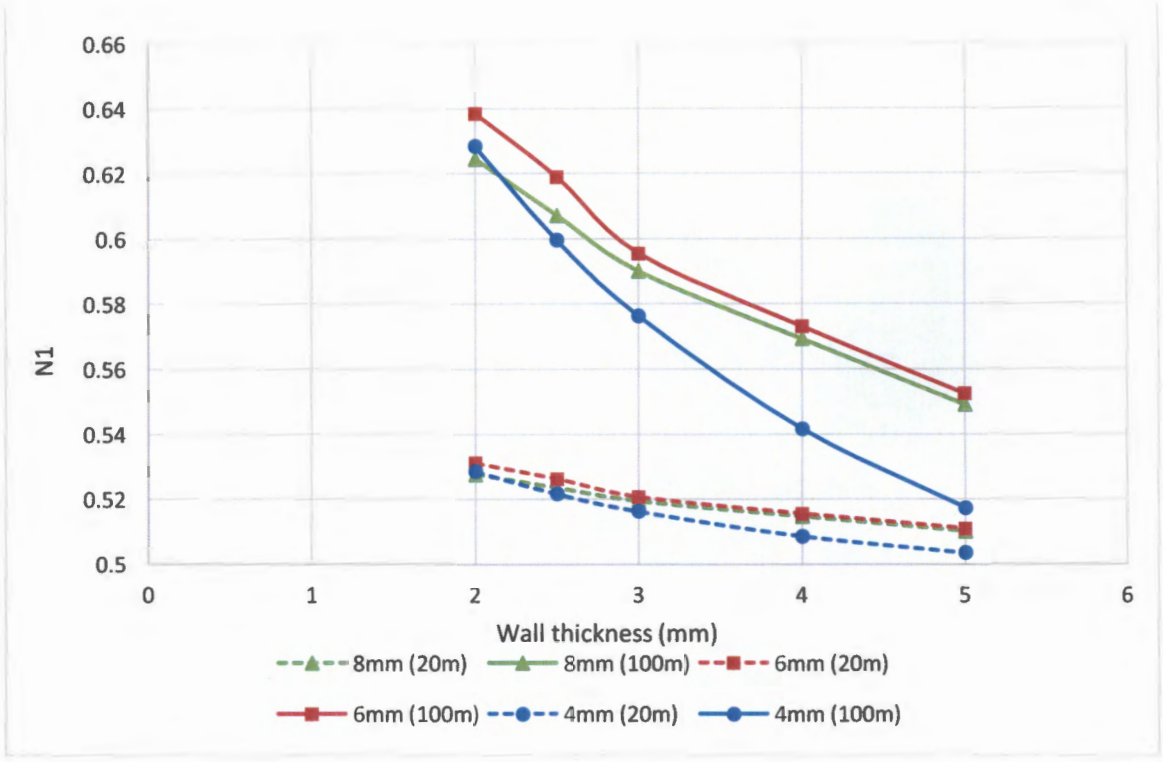

Figure 5-11: Relationship Between the Leakage Exponent and the Wall Thickness for Various Pressures

Figure 5-11 shows how the leakage exponent varies for the three holes when subjected to a pressure head of 20 m and 100 m. It can be seen that, as the wall thickness gets larger, the variation of the *N1* gets smaller and smaller, for example, when the 8 mm hole has a 2 mm wall thickness the *N1* will be 0.53 at 20 m and at 100 m the *N1* will be 0.64, making the *N1* difference between the two pressures 0.11. However, when the 8 mm hole has a wall thickness of 5 mm, the *N1* is 0.51 at 20 m and 0.55 at 100 m, having a difference of only 0.04 which is much reduced when compared to the *N1* difference of 0.11 that is found for the smaller wall thicknesses.

5.6 Comparison of Parameters

The parameters were compared, using a bar graph, in order to investigate which parameter has the largest effect on the head–area slope *m*. In order to do this it was important to check how the head-area *m* changes over each parameter investigated. Figure 5-12 shows the bar graph that was plotted. From this the parameters that contributed the most to the change in head-area slope can be seen.

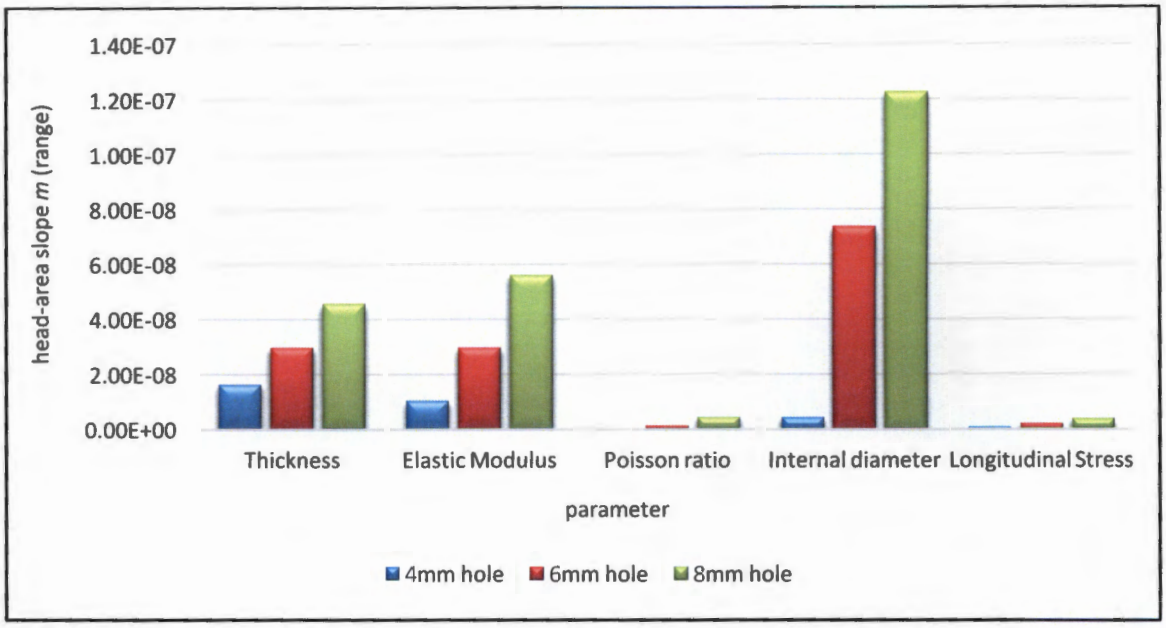

Figure 5-12: Bar Graph Showing Head-Area Slope Range for Each Parameter

It can be seen, from Figure 5-12, that the internal diameter plays the most significant role, followed by the elastic modulus and then the wall thickness of the pipe. The Poisson ratio and the longitudinal stress play an insignificant role with regards to the head-area slopes for round holes. With this information it is now possible to start formulating an equation that describes the leakage through a crack based on the investigated parameters.

5.7 Discussion of Head-Area Slope m for Different Holes

It can be concluded that for round holes they are three parameters that have a significant effect on the head–area slope *m.* These are: wall thickness, elastic modulus and pipe internal diameter.

The head-area slopes *m* were all very small and it was found that the head-area slope *m,* in turn, has an effect on the leakage exponent N1 for round holes. The N1 values found ranged from 0.4-0.65, which contrasts to the original orifice equation. In most cases it was shown that the larger the hole size, the higher the head-area slope *m,* and, consequently, the higher the leakage exponent.

The leakage exponent N1 for the elastic modulus parameter was less than 0.5 as the elastic modulus increased. This was the case because the head-area slopes, in this instance, were found to be negative. The negative *m* occurs when$\Delta A = A_{deformed} - A_0 < 0$, i.e.

$$A_0 > A_{deformed}$$

$$\frac{\pi d_0^2}{4} > \frac{\pi d_c d_l}{4}$$

$$d_0^2 > d_c d_l$$

Therefore, from this formulation, it can be seen that when the product of the initial leak hole diameter is greater than the product of the diameter in the longitudinal (d_l) and circumferential direction (d_c), then the head-area slope will become negative. The reason why this may happen is because of the Poisson's ratio effect which, essentially, reduces the dimensions when a load is applied and, thus, the overall area can be reduced if the material has a relatively high Poisson ratio coefficient (for the elastic modulus simulation the Poisson's ratio was set at 0.4). Another possibility is the local deformation that occurs around the round hole. The increased local stresses could cause local strains that tend to reduce the hole area, especially in the inner lip of the hole.

These results re-confirm the need to reconsider the orifice equation, by expanding it to include other parameters, as they have an effect on the leakage exponent N1 and the generic behaviour of round hole leaks.

6 Developing an Equation to Predict the Head-Area Slope *m* for Round Holes

Based on the FEA data obtained in Chapter 5, Chapter 6 aims to use the data and attempt to predict an equation for the behaviour of round holes in pipes under pressure. The aim of the equation is to predict the head-area slope *m* for round hole leaks of different geometric and material pipe parameters. This head-area slope *m* was found to exist as a result of the leak area expanding linearly with pressure, and the gradient of this linear relationship is what is denoted as the head-area slope. Chapter 5 went on to better understand this head-area slope *m* by looking at geometric and material parameters of the pipe. It went on to show that, by holding all the other parameters constant at the base values, one parameter can be varied to show how that specific parameter changes the head-area slope *m*. From this information for round holes, it was shown that the *N1* value for round holes can exceed the theoretical 0.5 and, for the cases where the head-area slope is negative, N1 can be less than 0.5. This is another indication that the original orifice equation needs to be re-examined and updated so that it includes more parameters, and thus these differences can be highlighted.

This chapter, therefore, attempts to formulate an empirical equation that better suits leakage in distribution systems, as compared to the current conventional orifice equation. Two processing techniques are explored in this chapter: dimensionless analysis and the regression analysis. The dimensionless analysis is used to obtain dimensionless relationships between the parameters/variables, and the regression analysis is a statistical method used to describe the relationship between parameters or variables. The process carried out is shown in this chapter.

6.1 Dimensional Analysis

Dimensional analysis is the first method used in determining an equation that relates the variables of the round holes. Dimensional analysis is a mathematical method of considerable value to problems found in the field of science and engineering, especially in physics and fluid mechanics.

All quantities that are physical can be expressed in terms of three primary quantities, which are: Length (L), Mass (M) and Time (T).

e.g. Force = Mass x Acceleration

$$= \text{Mass x Length/Time}^2 = ML T^{-2}$$

The homogeneity of dimension is a principal that can be used to do a number of useful analyses. Firstly, this principal can be used to check whether an equation has been formed correctly, i.e. the left hand side of the equation, as well as the right hand side, are compatible. Secondly, the principal can be used to relate a number of variables, and establishing the form of the equation with these variables. Finally, this principal can assist in the analysis of data.

There are many methods that are available for dimensional analysis; however, the Buckingham π theorem will be used. This is the most common method used for dimensional

analysis and is the basis for the matrix and other methods. This method requires some knowledge on all the variables relevant to the problem. The variables are then joined into π-groups, or dimensionless groups, that are independent (Hughes & Brighton, 1999). A dimensionless group, according to Shames (1992), is a group of variables that, when multiplied together, they yield a dimensional representation of unity.

According to the Buckingham π theorem, if n variables exist in a problem and these variables contain r primary dimensions (e.g. M, L and T), the resulting equation that relates the variables will contain n-r dimensional groups or π groups. Buckingham described these dimensionless groups as $\pi_1, \pi_2, \pi_3, \ldots, \pi_{n-m}$.

The Buckingham π theorem can be applied using a systematic approach adopted from Cassa (2011), using the following approach:

- Count the number of variables of variables (*n*)
- Count the number of dimensions (*r*) that appear in the variables
- Calculate the number of π- groups (*n-r*)
- Pick (*r*) common variables that construct the general form of the (*n-r*) π-groups
- Solve each of the (*n-r*) π-groups
- Establish a relationship.

Some variables may appear in more than one π-group, and these variables are known as common variables. It is, therefore, possible to formulate different combinations of common variables for any one physical phenomenon. This, then, leads to many different solutions depending on the choice of common variables. Thus, there is not only one solution to a problem when using dimensional analysis.

6.1.1 Dimensional Analysis for Round Holes

In this section dimensional analysis is performed for the parameters used in the analysis of the round holes, in order to find the possible formulation of the dimensionless group, as it was described above, in order to predict an equation relating the parameters to each other. Since the parameters currently being investigated are very similar, two new parameters will be included to help with the analysis. The parameters are fluid properties of the fluid that flows in the pipe: the density, ρ, and the dynamic viscosity, μ. The first step, after establishing all the parameters, that will play a role is writing them down in their simplest form, i.e. in terms of the three fundamental units described earlier; mass, time and length. Table 6-1 that follows lists all the parameters looked at for the round hole, with their units and their break down, in terms of their fundamental units.

Table 6-1 Variables to be Used in the Dimensional Analysis for the Round Holes

Variable	Unit	Fundamental Unit	Variable	Unit	Fundamental Unit
ρ	Kg/m^3	$M.L^{-3}$	D	m	L
M	Pa.s	M.L	T	m	L
E	Pa	$M.L^{-1}.T^{-2}$	d	m	L
A	m^2	L^2	v		
σ	Pa	$M.L^{-1}.T^{-2}$	P	Pa	$M.L^{-1}.T^{-2}$

It is important to note that the variables that have no dimensions (i.e. dimensionless) e.g. the Poisson's ratio are not included in the dimensional analysis. In order to conduct the dimensional analysis the Buckingham π theorem is used, as outlined in section 6.1.

The number of variables, n, that the analysis has is 9. The number of common variables, r, assigned to the analysis, is 3. This results in the number of π-groups, n-r, and being 9-3=6 π groups. The choice of common variables, or repeaters, is generally chosen to be arbitrary, and the analysis usually contains more than one set of possible common variables. For this reason, all possibilities must be explored. The first choice of common variables is ρ, E, t whilst the other variables remain separated. A check must be done to ensure that there is no possibility for dimensionless groups from the chosen common variables. The π-groups formulation can now be written as follows:

Π-groups:

$$\pi_1 = \rho^x.E^y.t^z.\mu \qquad \pi_4 = \rho^x.E^y.t^z.D$$

$$\pi_2 = \rho^x.E^y.t^z.A \qquad \pi_5 = \rho^x.E^y.t^z.d$$

$$\pi_3 = \rho^x.E^y.t^z.\sigma \qquad \pi_6 = \rho^x.E^y.t^z.P$$

The exponents x, y, z have to be calculated for each π-groups. Thereafter, the π-groups can be combined in order to describe an expression for a pipe with a round hole defect in it. Since the common variables appear in each π-group, a common calculation can be done and carried through. This calculation is as follows:

$$\rho^x.E^y.t^z = (M.L^{-3})^x.(M.L^{-1}.T^{-2})^y.(L)^z$$

$$= M^x.L^{3x}.M^y.L^{-y}.T^{-2y}.L^z$$

$$= M^{x+y}.L^{-3x-y+z}.T^{-2y}$$

π-groups calculations:

$\pi_1 = \rho^x.E^y.t^z.\mu$

$$M^0.L^0.T^0 = M^{x+y}.L^{-3x-y+z}.T^{-2y}.M.L^{-1}.T^{-1}$$

$T: 0 = -2y - 1$

$2y = -1$

$\therefore y = -1/2$

$M: 0 = x + y + 1$

$0 = x + (-1/2) + 1$

$\therefore x = -1/2$

$L: 0 = -3x - y + z - 1$

$0 = -3(-1/2) - (-1/2) + z - 1$

$\therefore z = -1$

$$\pi_1 = \rho^{-1/2}.E^{-1/2}.t^{-1}.\mu$$

$$\pi_1 = \frac{\mu}{t\sqrt{\rho E}}$$

$\pi_2 = \rho^x.E^y.t^z.A$

$$M^0.L^0.T^0 = M^{x+y}.L^{-3x-y+z}.T^{-2y}.L^2$$

$T: 0 = -2y$

$\therefore y = 0$

$M: 0 = x + y$

$0 = x + (0)$

$\therefore x = 0$

$L: 0 = -3x - y + z + 2$

$0 = -3(0) - (0) + z + 1$

$\therefore z = -1$

$$\pi_2 = \rho^0.E^0.t^{-2}.A$$

$$\pi_2 = \frac{A}{t^2}$$

$\pi_3 = \rho^x.E^y.t^z.\sigma$

$$M^0.L^0.T^0 = M^{x+y}.L^{-3x-y+z}.T^{-2y}.M.L^{-1}.T^{-2}$$

$T: 0 = -2y - 2$

$2y = -2$

$\therefore y = -1$

$M: 0 = x + y + 1$

$0 = x + (-1) + 1$

$x = 0$

$L: 0 = -3x - y + z - 1$

$0 = -3(0) - (-1) + z - 1$

$\therefore z = 0$

$$\pi_3 = \rho^0.E^{-1}.t^0.\sigma$$

$$\pi_3 = \frac{\sigma}{E}$$

$\pi_4 = \rho^x.E^y.t^z.D$

$$M^0.L^0.T^0 = M^{x+y}.L^{-3x-y+z}.T^{-2y}.L$$

$M: 0 = x + y$ $\quad L: 0 = -3x - y + z + 1$

$T: 0 = -2y$ $\quad 0 = x + (0)$ $\quad 0 = -3(0) - (0) + z + 1$

$\therefore y = 0$ $\quad x = 0$ $\quad \therefore z = -1$

$$\pi_4 = \rho^0 . E^0 . t^{-1} . D$$

$$\pi_4 = \frac{D}{t}$$

$\pi_5 = \rho^x . E^y . t^z . d$

$$M^0 . L^0 . T^0 = M^{x+y} . L^{-3x-y+z} . T^{-2y} . L$$

$M: 0 = x + y$ $\quad L: 0 = -3x - y + z + 1$

$T: 0 = -2y$ $\quad 0 = x + (0)$ $\quad 0 = -3(0) - (0) + z + 1$

$\therefore y = 0$ $\quad x = 0$ $\quad \therefore z = -1$

$$\pi_4 = \rho^0 . E^0 . t^{-1} . d$$

$$\pi_5 = \frac{d}{t}$$

$\pi_6 = \rho^x . E^y . t^z . P$

$$M^0 . L^0 . T^0 = M^{x+y} . L^{-3x-y+z} . T^{-2y} . M . L^{-1} . T^{-2}$$

$T: 0 = -2y - 2$ $\quad M: 0 = x + y + 1$ $\quad L: 0 = -3x - y + z - 1$

$2y = -2$ $\quad 0 = x + (-1) + 1$ $\quad 0 = -3(0) - (-1) + z - 1$

$\therefore y = -1$ $\quad x = 0$ $\quad \therefore z = 0$

$$\pi_3 = \rho^0 . E^{-1} . t^0 . P$$

$$\pi_6 = \frac{P}{E}$$

Summary of analysis:

With the common variable ρ, E, t

$$\pi_1 = \frac{\mu}{t\sqrt{\rho E}} \qquad \pi_2 = \frac{A}{t^2} \qquad \pi_3 = \frac{\sigma}{E} \qquad \pi_4 = \frac{D}{t} \qquad \pi_5 = \frac{d}{t} \qquad \pi_6 = \frac{P}{E}$$

After determining all the π-groups, they can now be used to find other relationships of the variables for a pipe with a round hole in it. The area of the leak is the variable expected to play the most significant role in the leakage equation. For this reason, the π-group containing the area variable was made the subject of the formula. Thus, the expressions are in the form $\pi_3 = \phi(\pi_1, \pi_2, \pi_4, \pi_5, \pi_6)$ to give the following equation set:

$$\frac{A}{t^2}=\phi\left(\frac{\mu}{t\sqrt{\rho E}};\frac{\sigma}{E};\frac{D}{t};\frac{d}{t};\frac{P}{E}\right)$$

Equation 6-1

These π-groups can also be interchanged because some variables have the same units. For example σ, E, P have the same units and, therefore, can be interchanged; also D, d, t have the same units and can be interchanged amongst each other.

There is another possible set of common variables that can be looked at for the round holes and these are μ, σ_l, D, while the other variables remain separated. It is always important to check that there is no possible dimensionless group from the common variables chosen. The formulation of π-groups for this set of common variables is as follows:

π-groups:

$$\pi_1=\mu^x\sigma_l^y D^z\rho \qquad \pi_4=\mu^x\sigma_l^y D^z t$$
$$\pi_2=\mu^x\sigma_l^y D^z E \qquad \pi_5=\mu^x\sigma_l^y D^z d$$
$$\pi_3=\mu^x\sigma_l^y D^z A \qquad \pi_6=\mu^x\sigma_l^y D^z P$$

The exponents for x, y, z can be calculated for all the π-groups. As was done in the previous analysis, the common variables can be calculated and carried through for the rest of the analysis. Their common calculation is carried out as follows:

Common calculation:

$$\mu^x.\sigma_l^y.D^z=\left(M.L^{-1}.T^{-1}\right)^x.\left(M.L^{-1}.T^{-2}\right)^y.(L)^z$$

$$M^0.L^0.T^0=M^x.L^{-x}.T^{-x}.M^y.L^{-y}.T^{-2y}.L^z$$

$$\mu^x.\sigma_l^y.D^z=M^{x+y}.L^{-x-y+z}.T^{-x-2y}$$

π-group calculations:

$\pi_1=\mu^x\sigma_l^y D^z\rho$

$$M^0.L^0.T^0=M^{x+y}.L^{-x-y+z}.T^{-x-2y}.M.L^{-3}$$

$M:0=x+y+1$

$x=-y-1$

$x=-1-1$

$\therefore x=-2$

$T:0=-x-2y$

$0=-(-y-1)-2y$

$\therefore y=1$

$L:0=-x-y+z-3$

$0=-(-2)-(1)+z-3$

$\therefore z=2$

$$\pi_1=\mu^{-2}\sigma_l^1 D^2\rho$$

$$\pi_1 = \frac{\rho \sigma_l D^2}{\mu^2}$$

$\pi_2 = \mu^x \sigma_l^y D^z E$

$$M^0.L^0.T^0 = M^{x+y}.L^{-x-y+z}.T^{-x-2y}.M.L^{-1}.T^{-2}$$

$M: 0 = x + y + 1$

$x = -y - 1$

$T: 0 = -x - 2y - 2$

$0 = -(-y-1) - 2y - 2$

$\therefore y = -1$

$L: 0 = -x - y + z - 1$

$0 = -(0) - (-1) + z - 1$

$\therefore z = 0$

$x = -(-1) - 1$

$\therefore x = 0$

$$\pi_2 = \mu^0 \sigma_l^{-1} D^0 E$$

$$\pi_2 = \frac{E}{\sigma_l}$$

$\pi_3 = \mu^x \sigma_l^y D^z A$

$$M^0.L^0.T^0 = M^{x+y}.L^{-x-y+z}.T^{-x-2y}.L^2$$

$M: 0 = x + y$

$x = -y$

$T: 0 = -a - 2b$

$0 = -(-y) - 2y$

$\therefore y = 0$

$L: 0 = -x - y + z + 2$

$0 = -(0) - (0) + z + 2$

$\therefore z = -2$

$\therefore x = 0$

$$\pi_3 = \mu^0 . \sigma_l^0 . D^{-2} . A$$

$$\pi_3 = \frac{A}{D^2}$$

$\pi_4 = \mu^x \sigma_l^y D^z t$

$$M^0.L^0.T^0 = M^{x+y}.L^{-x-y+z}.T^{-x-2y}.L$$

$M: 0 = x + y$

$x = -y$

$T: 0 = -x - 2y$

$0 = -(-y) - 2y$

$\therefore y = 0$

$L: 0 = -x - y + z + 1$

$0 = -(0) - (0) + z + 1$

$\therefore z = -1$

$\therefore x = 0$

$$\pi_4 = \mu^0 . \sigma_l^0 . D^{-1} . t$$

$$\pi_4 = \frac{t}{D}$$

$\pi_5 = \mu^x \sigma_l^y D^z d$

$$M^0.L^0.T^0 = M^{x+y}.L^{-x-y+z}.T^{-x-2y}.L$$

$M: 0 = x + y$

$x = -y$

$\therefore x = 0$

$T: 0 = -x - 2y$

$0 = -(-y) - 2y$

$\therefore y = 0$

$L: 0 = -x - y + z + 1$

$0 = -(0) - (0) + z + 1$

$\therefore z = -1$

$$\pi_5 = \mu^0.\sigma_l^0.D^{-1}.d$$

$$\pi_5 = \frac{d}{D}$$

$\pi_6 = \mu^x \sigma_l^y D^z P$

$$M^0.L^0.T^0 = M^{x+y}.L^{-x-y+z}.T^{-x-2y}.M.L^{-1}.T^{-2}$$

$M: 0 = x + y + 1$

$x = -y - 1$

$x = -(-1) - 1$

$\therefore x = 0$

$T: 0 = -x - 2y - 2$

$0 = -(-y - 1) - 2y - 2$

$\therefore y = -1$

$L: 0 = -x - y + z - 1$

$0 = -(0) - (-1) + z - 1$

$\therefore z = 0$

$$\pi_6 = \mu^0 \sigma_l^{-1} D^0 P$$

$$\pi_6 = \frac{P}{\sigma_l}$$

Summary of analysis:

With the common variables: μ, σ_l, D:

$$\pi_1 = \frac{\rho \sigma_l D^2}{\mu^2} \quad \pi_2 = \frac{E}{\sigma_l} \quad \pi_3 = \frac{A}{D^2} \quad \pi_4 = \frac{t}{D} \quad \pi_5 = \frac{d}{D} \quad \pi_6 = \frac{P}{\sigma_l}$$

After determining all the π-groups, they can now be used to find other relationships of the variables for a pipe with a round hole in it. The area of the leak is the variable expected to play the most significant role in the leakage equation. For this reason, the π-group containing the area variable was made the subject of the formula. Thus, the expressions are in the form $\pi_3 = \phi(\pi_1, \pi_2, \pi_4, \pi_5, \pi_6)$ to give the following equation set:

$$\frac{A}{D^2} = \phi\left(\frac{\rho\sigma_1 D^2}{\mu^2}; \frac{E}{\sigma_1}; \frac{t}{D}; \frac{d}{D}; \frac{P}{\sigma_1}\right)$$

Equation 6-2

These π-groups can also be interchanged because some variables have the same units. For example, σ, E, P have the same units and, therefore, can be interchanged; also D, d, t have the same units and can be interchanged amongst each other.

6.1.2 Dimension Analysis Discussion

The dimension analysis is carried out to provide various sets of equations that can be formulated; also various dimensionless groups are derived that relate the parameters of round holes. It is important to note that the above analysis does not provide a final solution to the problem, but it can only give insight into what possible formulations can, perhaps, be considered. The underlying problem is far more complex than dimensional analysis can resolve. Some parameters, such as the Poisson's ratio, are dimensionless and, therefore, this parameter will have no bearing in the equation sets, however, this does not mean that the parameter can be ignored as it may, or may not, play a vital role in the behaviour of the leak. The dimensionless parameter can be interchanged and be a part of any dimensionless group because it has no effect on the dimension of the equation. The role the parameters play can be justified through extensive data analysis.

6.2 Regression

The next step in this process was to conduct a regression analysis. The regression analysis is a statistical process for estimating the relationships amongst variables. For this particular case, the regression analysis will assist in seeking to ascertain the casual effect of the variables upon another. In other words, the regression analysis will help with quantifying the structural relationship between the variables. Understanding these relationships can help to develop equations that can assist in predicting the unknown values of certain variables, given that other related variables are known (Sykes, 1993).

Whilst regression analysis can show the form of the relationship of one independent variable with one dependant variable, there is another statistical analysis, called the correlation analysis, which measures the closeness (link) of the relationship between two or many variables without knowing the functional relationships.

There are two main models of regression that are investigated in this section: the additive regression model (linear regression) and the multiplicative (exponential regression). There are other regression models available; however, they are not explored in this study due to the nature of the data collected for this study. The two mentioned will suffice. The following sections will explain how the two models work and the methodology used to conduct the analysis for each model.

6.2.1 Linear Regression Model

The linear regression model is usually used for measuring a responsive variable (dependant) "*y*" at different values for a controlling variable (independent) "*x*"; linear regression is the procedure of fitting a straight line at each '*x*' with the value of '*y*' (Sykes, 1993).

This study used Microsoft Excel to perform a regression analysis on the data that was obtained from the FEA results. The function used to perform this analysis uses the method of "least squares" to calculate a line that best fits the obtained data. This function then returns an array that describes what the straight line relationship is. This function is called the *LINEST* function on Excel and it is, typically, entered as an array formula. (Microsoft Excel Guide, 2011). The equation for a straight line is given by:

$$y = ax + b \qquad \text{Equation 6-3}$$

This expression is for simple linear regression that consists of only one independent variable. However, if more than one independent variable describes the dependent variable, then the expression can be written as follows:

$$y = a_1x_1 + a_2x_2 + a_3x_3 + \ldots a_nx_n + b \qquad \text{Equation 6-4}$$

It can be seen that for both these equations the dependant y-value is a function of the independent x values. The values labelled ***a*** in the equations are co-efficient that correspond to each x-value, and b is the constant. The *LINEST* function, once inserted in Excel, returns an array of information providing various regression statistic that describe the straight line relationship between all the variables. The following syntax is used in Excel to call up the *LINEST* function regression stats:

$$=LINEST\ (known\_y's,\ know\_\ x's,\ const,\ stat) \qquad \text{Equation 6-5}$$

Equation 6-5 also returns additional regression statistics given in:

Table 6-2: Showing Additional Regression Statistics

	A	B	C	D	E	F
1	a_n	a_{n-1}	....	a_2	a_1	b
2	S_{en}	S_{en-1}	....	S_{e2}	S_{e1}	S_{eb}
3	R^2	S_{ey}				
4	F	df				
5	SS_{reg}	SS_{resid}				

From Table 6-2 the $a_1, a_2, \ldots, a_n$ are the coefficients shown in Equation 5-4, the $S_{e1}, S_{e2}, \ldots, S_{en}$ values are the standard error values, S_{eb} being the standard error for the constant b, and S_{ey} the standard error for the y-estimate. The R^2 is the coefficient of determination which helps to determine how good the relationship is in predicting y. This is done by comparing the estimated y-values against the actual y-values. The R^2 coefficient ranges from 0 to 1, where 0 shows a poor correlation and, thus, the regression equation is not helpful in predicting the y-value, and 1 show that the regression equation is a perfect correlation. F is known as the F-statistic or F-observed value. This is commonly the test done to test whether the relationship between the x and y variable occurs by chance. To determine the confidence level of the regression model the *df's*, which are the degrees of freedom, are used to help find the F-critical values to compare with the F-statistic. Finally, the SS_{reg} is the regression sum of squares where the SS_{resid} is the residual sum of squares.

6.2.2 Multiplicative Regression Model

For the multiplicative regression model the dependant variable is affected multiplicatively by the independent variables. The appropriate model for this case, according to Nau, (2015) is:

$$y = b \cdot x_1^{a_1} \cdot x_2^{a} \qquad \text{Equation 6-6}$$

In this case y (the dependant variable) is proportional to the product of x_1 and x_2 (both independent variables); each of them raised to some power here denoted as a_1 and a_2, respectively. The powers a_1 and a_2 are referred to as the elasticity's of y with respect to x_1 and x_2, respectively.

In the case where either of the independent variables is equal to 1, then the elasticity is unitary, meaning the response of y to that variable is unitary. In the case where either of the independent variables is less than 1, then the response is said to be inelastic. Sometimes it is possible to have the elasticity of y with respect to the independent variables x_1 and x_2 constant (Nau, 2015).

Equation 6-6 cannot be fitted using linear regression techniques, because of the form it is in. In order to use this form in a linear regression it must be transformed into an equivalent linear model. This transformation can be done using logarithm transformation. The logarithm function then transforms products into sums e.g. log (xy) = log (x) + log (y). This, therefore, implies, for any positive x and y, the logarithm of their product is the sum of the separate logarithms (Nau, 2015). Another benefit of the logarithm transformation is that it can convert powers into multipliers i.e. log (x^b) = b log (x). If the transformation rules, explained above, are applied to Equation 5-6 the multiplicative regression model then becomes:

$$\log(y) = \log\left(b \cdot x_1^{a_1} \cdot x_2^{a_2}\right) = \log(b) + a_1 \log(x_1) + a_2 \log(x_2) \qquad \text{Equation 6-7}$$

Equation 6-7 now shows that log(y), the dependant variable, is a linear function of log(x_1) and log(x_2), which are now the new independent variables.

With these two linear regressions it is now possible to proceed with the intended analysis.

6.3 Additive Regression Models for Round Holes

This section will show the linear regression analysis performed for a pipe with round holes. As Cassa (2011) points out, when it comes to regression analysis, it is not always known how the parameters are grouped together and, hence, the importance of the dimensional analysis carried out in Section 6.1. The dimensional analysis gives a possible starting point of the regression models. The regression model is then set up in the form described by Equation 6-3, where the independent variable (x) and dependant variable (y) are replaced by the respective dependant and independent variables that must be regressed. Four regression models were investigated for each of the three holes; 4mm, 6mm and 8mm, respectively. The process is explained in detail for the 4mm hole and this same process is followed for the 6mm and 8mm hole and, therefore, was not repeated when showing the results of these holes. The full regression analyses for the three holes, including the tables, are shown in Appendix A

6.3.1 Additive Regression Model Analysis for the 4mm Hole

The first equation to be analysed comes from the first set of dimensional analysis done, given by Equation 6-1 and 6-2, and repeated here:

$$\frac{A}{t^2} = \phi\left(\frac{\mu}{t\sqrt{\rho E}}; \frac{\sigma}{E}; \frac{D}{t}; \frac{d}{t}; \frac{P}{E}\right)$$

$$\frac{A}{D^2} = \phi\left(\frac{\rho\sigma_1 D^2}{\mu^2}; \frac{E}{\sigma_1}; \frac{t}{D}; \frac{d}{D}; \frac{P}{\sigma_1}\right)$$

The first guesses connected these parameters additively, giving the following form of the equations:

$$\frac{A}{t^2} = a_1\frac{\mu}{t\sqrt{\rho E}} + a_2\frac{\sigma_1}{E} + a_3\frac{D}{t} + a_4\frac{d}{t} + a_5\frac{P}{E} + b \qquad \text{Equation 6-8}$$

Where a_1 to a_5 are the independent variables and b is the constant. In order to begin the regression analysis the dependant and independent variables were setup in columns that correspond to the original data and the data obtained from the finite element analysis. Table 6-3 below shows the calculated data points required to do the regression statistic.

Table 6-3 Inputs for Independent and Dependent Variables

x1	x2	x3	x4	x5	y
$\mu/t(\rho E)^{0.5}$	σ/E	D/t	d/t	P/E	A/t^2
2.19E-07	0.00E+00	3.57E+01	1.33E+00	0.00E+00	1.32E+00
2.19E-07	2.97E-04	3.57E+01	1.33E+00	3.40E-09	1.32E+00
2.19E-07	5.94E-04	3.57E+01	1.33E+00	6.80E-09	1.33E+00
2.19E-07	8.92E-04	3.57E+01	1.33E+00	1.02E-08	1.33E+00
2.19E-07	1.19E-03	3.57E+01	1.33E+00	1.36E-08	1.33E+00
2.19E-07	1.49E-03	3.57E+01	1.33E+00	1.70E-08	1.33E+00
2.19E-07	1.78E-03	3.57E+01	1.33E+00	2.04E-08	1.34E+00
2.19E-07	2.08E-03	3.57E+01	1.33E+00	2.38E-08	1.34E+00
2.19E-07	2.38E-03	3.57E+01	1.33E+00	2.72E-08	1.34E+00
2.19E-07	2.68E-03	3.57E+01	1.33E+00	3.06E-08	1.34E+00
2.19E-07	2.97E-03	3.57E+01	1.33E+00	3.40E-08	1.35E+00
2.19E-07	1.73E-03	3.57E+01	1.33E+00	2.04E-08	1.47E+00
1.20E-07	5.20E-04	3.57E+01	1.33E+00	6.12E-09	1.37E+00
6.94E-08	1.73E-04	3.57E+01	1.33E+00	2.04E-09	1.34E+00
4.01E-08	5.78E-05	3.57E+01	1.33E+00	6.80E-10	1.33E+00
2.69E-08	2.60E-05	3.57E+01	1.33E+00	3.06E-10	1.32E+00
2.19E-07	1.73E-03	3.57E+01	1.33E+00	2.04E-08	1.47E+00
2.19E-07	1.73E-03	3.57E+01	1.33E+00	2.04E-08	1.47E+00
2.19E-07	1.73E-03	3.57E+01	1.33E+00	2.04E-08	1.47E+00
2.19E-07	1.73E-03	3.57E+01	1.33E+00	2.04E-08	1.47E+00
2.19E-07	1.73E-03	3.57E+01	1.33E+00	2.04E-08	1.47E+00
2.19E-07	1.73E-03	3.57E+01	1.33E+00	2.04E-08	1.47E+00
3.29E-07	2.65E-03	5.35E+01	2.00E+00	2.04E-08	3.42E+00
2.63E-07	2.10E-03	4.28E+01	1.60E+00	2.04E-08	2.15E+00
2.19E-07	1.73E-03	3.57E+01	1.33E+00	2.04E-08	1.47E+00
1.65E-07	1.28E-03	2.68E+01	1.00E+00	2.04E-08	8.06E-01
1.32E-07	1.00E-03	2.14E+01	8.00E-01	2.04E-08	5.08E-01
2.19E-07	9.00E-04	1.90E+01	1.33E+00	2.04E-08	1.44E+00
2.19E-07	1.40E-03	2.90E+01	1.33E+00	2.04E-08	1.44E+00
2.19E-07	1.73E-03	3.57E+01	1.33E+00	2.04E-08	1.45E+00
2.19E-07	2.40E-03	4.90E+01	1.33E+00	2.04E-08	1.45E+00
2.19E-07	3.57E-03	7.13E+01	1.33E+00	2.04E-08	1.46E+00
2.19E-07	4.07E-03	8.23E+01	1.33E+00	2.04E-08	1.47E+00
2.19E-07	1.78E-03	3.57E+01	1.33E+00	2.04E-08	1.34E+00
2.19E-07	1.78E-03	3.57E+01	2.00E+00	2.04E-08	3.34E+00
2.19E-07	1.78E-03	3.57E+01	2.67E+00	2.04E-08	5.97E+00
2.19E-07	0.00E+00	3.57E+01	1.33E+00	2.04E-08	1.46E+00
2.19E-07	3.47E-04	3.57E+01	1.33E+00	2.04E-08	1.46E+00
2.19E-07	6.93E-04	3.57E+01	1.33E+00	2.04E-08	1.46E+00
2.19E-07	1.04E-03	3.57E+01	1.33E+00	2.04E-08	1.46E+00
2.19E-07	1.73E-03	3.57E+01	1.33E+00	2.04E-08	1.47E+00

Once all the data points have been calculated the *LINEST* syntax function, that is described by Equation 6-5, is used to create the array described by Table 6-4.

Table 6-4 Regression Statistics for Equation 6-8

10902807.62	3.10026755	-0.00125021	-20.71766507	-989153.6872	-2.60976
6774416.534	0.098194206	0.00422385	65.26098127	622626.2888	0.203018
0.969369293	0.159462384	#N/A	#N/A	#N/A	#N/A
221.5288408	35	#N/A	#N/A	#N/A	#N/A
28.16545581	0.889988816	#N/A	#N/A	#N/A	#N/A

From the array shown in Table 6-4, the following equation can be deduced to:

$$\frac{A}{t^2} = -989153.69\frac{\mu}{t\sqrt{\rho E}} - 20.718\frac{\sigma_1}{E} - 0.00125\frac{D}{t} + 3.1002\frac{d}{t} + 10902807\frac{P}{E} - 2.609$$

The important factors to look at in Table 6-4 are the coefficient of R^2 which is 0.969, indicating a 96.9% fit, the degrees of freedom (*df*), which in this case are 35, and the F-statistic which is 221.53. This F-statistic and the *df* can be used to determine the confidence level of the regression model. This is done by assessing the likelihood of a higher F-statistic value occurring by chance. The *FDIST* function is used to calculate the probability of a larger F value occurring by chance. The F distribution tests whether two observed samples have the same variance and, thus, requires two degrees of freedom: s_1 and s_2 to be determined. According to Stinson and Dodge (2003), cited by Cassa (2011), if there is n number of data points and "constants= TRUE", then s_1=*n-df-1* and s_2=*df*. In this case the *FDIST* was $1.882\text{x}10^{-25}$ which shows that the relationship, given in Table 6-4, did not occur by chance because this number is very small.

Other possibilities were also explored and regressed, and these are shown in Table 6-5. Note that numerous other regression models exist, but for purposes of illustrating the process, only a few regression models were analysed.

Table 6-5: Further Regression Analysis for the 4mm Hole

$$\frac{A}{t^2} = a_1\frac{t\sqrt{\rho E}}{\mu} + a_2\frac{P}{E} + a_3\frac{t}{d} + a_4\frac{t}{D} + a_5\frac{\sigma_1}{E} + b \qquad \text{Equation 6-9}$$

$$\frac{A}{t^2} = 1.18995\times10^{-9}\frac{t\sqrt{\rho E}}{\mu} - 2866496\frac{P}{E} - 6.36997\frac{t}{d} + 37.972\frac{t}{D} + 157.297\frac{\sigma_1}{E} + 5.0686$$

R^2=69.5 d*f*=35 FDIST=$2.702\text{x}10^{-8}$

$$\frac{A}{D^2} = a_1\frac{\rho\sigma_1 D^2}{\mu^2} + a_2\frac{\sigma_1}{E} + a_3\frac{t}{D} + a_4\frac{d}{D} + a_5\frac{P}{E} + b \qquad \text{Equation 6-10}$$

$$\frac{A}{D^2} = 2.291\times10^{-18}\frac{\rho\sigma_l D^2}{\mu^2} - 0.0684\frac{\sigma_l}{E} - 0.0058\frac{t}{D} + 0.0912\frac{d}{D} + 6205.072\frac{P}{E} - 0.00224$$

R^2= 98.84% df=35 F*DIST*=7.660x10^{-33}

$$\frac{A}{d^2} = a_1\frac{\rho\sigma_l D^2}{\mu^2} + a_2\frac{\sigma_l}{E} + a_3\frac{D}{t} + a_4\frac{D}{d} + a_5\frac{P}{E} + b \qquad \text{Equation 6-11}$$

$$\frac{A}{d^2} = 1.1541\frac{\rho\sigma_l D^2}{\mu^2} - 27.6313\frac{\sigma_l}{E} + 0.00348\frac{D}{t} - 0.003496\frac{D}{d} + 4177581.282\frac{P}{E} + 0.721$$

R^2 = 91.66 df=29 F*DIST*=0.00236

From the possible equations that are regressed, it is clear that the regression model given by Equation 6-10 is the best additive model, just based on the R^2 and F*DIST* results. It is now possible to show, graphically, how good this regression model is. This is done by comparing the model to the FEA data values for the 4mm round hole. Figure 6-1 shows the correlation between the regression model and the FEA data values, using the 4mm hole FEA data.

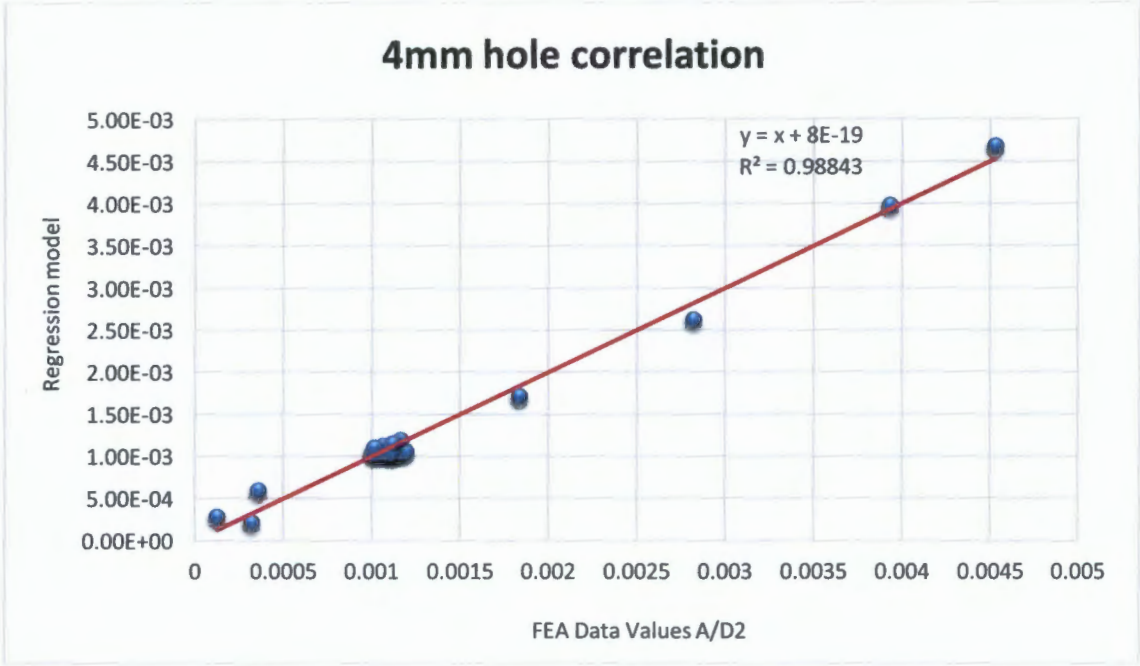

Figure 6-1: Correlation Between the Regression Model and the FEA data Values

From Figure 6-1 it can be seen that the regression model predicts the FEA data model relatively well, because the FEA data points are relatively close to the straight 45 degree line (red line) representing the best fit line. Figure 6-2, which follows, shows graphically how each parameter was predicted.

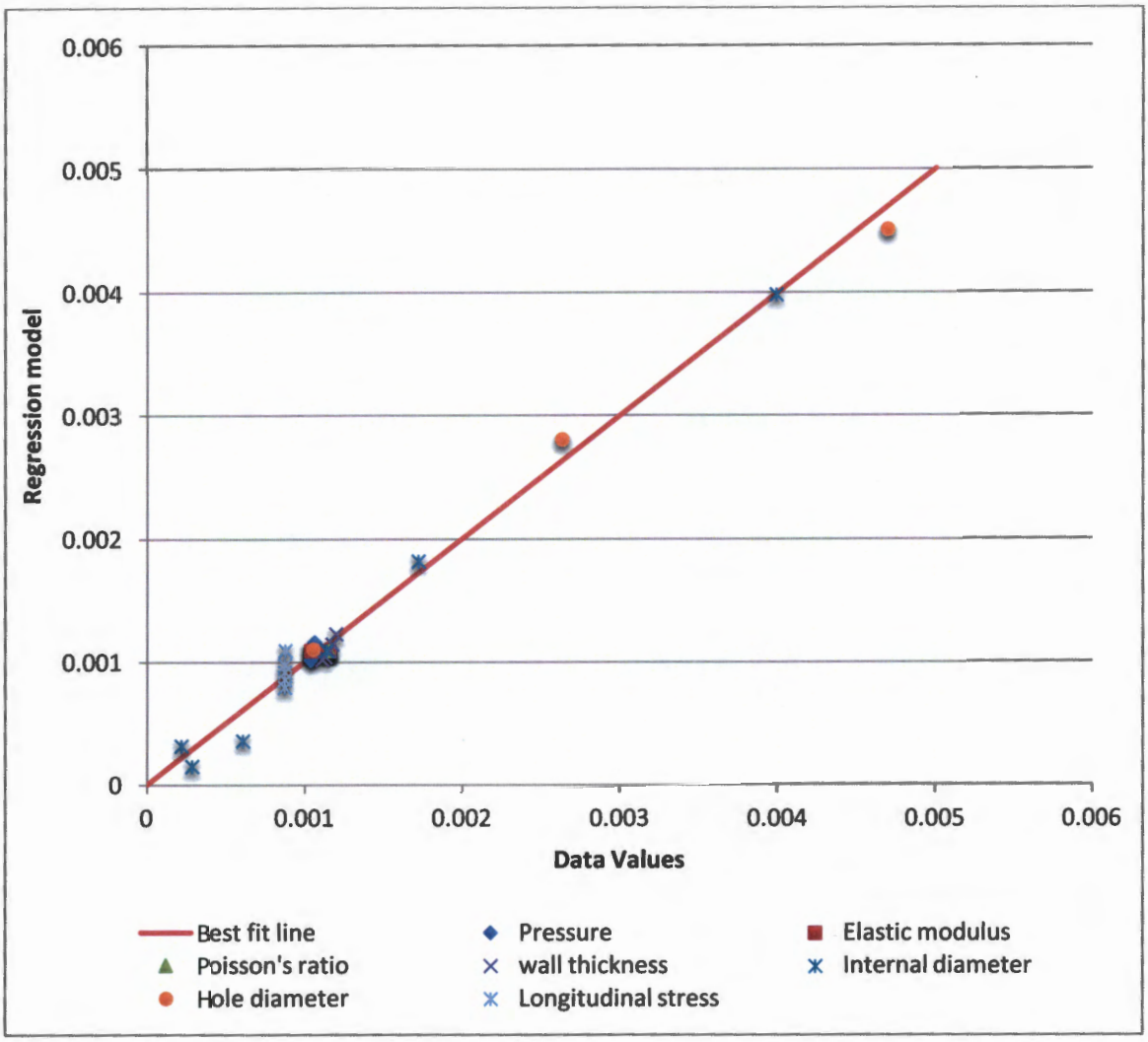

Figure 6-2: Showing the Correlation Between the Regression Model and the FEA data Values for Each Parameter

From Figure 6-2 it can be seen that, although the regression model shown by Equation 5-10 is a relatively good fit, some clear outliers exist, mainly with the longitudinal stress. It is possible to actually connect the parameters multiplicatively and explore other regression models. Thus, the next section will explore multiplicative regression models. Perhaps better models will be obtained that can predict the FEA data values much better.

6.3.2 Additive Regression Model Analysis for the 6mm Hole

The same regression models used for the 4mm hole were used for the 6mm hole. The results of the regression analysis are shown in Table 6-6, along with their statistics.

Table 6-6 Regression Analysis for the 6mm Hole

$$\frac{A}{t^2} = a_1\frac{\mu}{t\sqrt{\rho E}} + a_2\frac{\sigma_l}{E} + a_3\frac{D}{t} + a_4\frac{d}{t} + a_5\frac{P}{E} + b \qquad \text{Equation 6-8}$$

$$\frac{A}{t^2} = 410661.2987\frac{\mu}{t\sqrt{\rho E}} + 62.163\frac{\sigma_l}{E} + 0.00313\frac{D}{t} + 3.4984\frac{d}{t} + 10493850.13\frac{P}{E} - 4.098$$

R^2=96.89% df=35 FDIST=2.442×10^{-25}

$$\frac{A}{t^2} = a_1\frac{t\sqrt{\rho E}}{\mu} + a_2\frac{P}{E} + a_3\frac{t}{d} + a_4\frac{t}{D} + a_5\frac{\sigma_l}{E} + b \qquad \text{Equation 6-9}$$

$$\frac{A}{t^2} = -3.872\times10^{-9}\frac{t\sqrt{\rho E}}{\mu} + 1530039.037\frac{P}{E} - 10.734\frac{t}{d} + 7.626\frac{t}{D} + 225.222\frac{\sigma_l}{E} + 8.2979$$

R^2=76.29% df=35 *FDIST*=4.803×10^{-10}

$$\frac{A}{D^2} = a_1\frac{\rho\sigma_l D^2}{\mu^2} + a_2\frac{\sigma_l}{E} + a_3\frac{t}{D} + a_4\frac{d}{D} + a_5\frac{P}{E} + b \qquad \text{Equation 6-10}$$

$$\frac{A}{D^2} = 3.524\times10^{-18}\frac{\rho\sigma_l D^2}{\mu^2} - 0.0128\frac{\sigma_l}{E} + 0.00930\frac{t}{D} + 0.115\frac{d}{D} + 9778.948\frac{P}{E} - 0.004373$$

R^2= 98.35% df=35 F*DIST*=3.788×10^{-30}

$$\frac{A}{d^2} = a_1\frac{\rho\sigma_l D^2}{\mu^2} + a_2\frac{\sigma_l}{E} + a_3\frac{D}{t} + a_4\frac{D}{d} + a_5\frac{P}{E} + b \qquad \text{Equation 6-11}$$

$$\frac{A}{d^2} = 1.713\times10^{-16}\frac{\rho\sigma_l D^2}{\mu^2} - 5.527\frac{\sigma_l}{E} + 0.00261\frac{D}{t} - 0.004375\frac{D}{d} + 3738901.28\frac{P}{E} + 0.743$$

R^2 = 92.69% df=35 F*DIST*=7.0924×10^{-19}

Based on the above, additive regression models for the 6mm hole, once again the best fit regression model, was that presented by Equation 6-10. It is possible to see how good this relationship actually is by comparing the regression model to the FEA data values for the 6mm hole. Simply plotting the model against the dependent variable's values does this. Figure 6-3 shows the correlation between the regression model and the FEA data values for the 6mm hole.

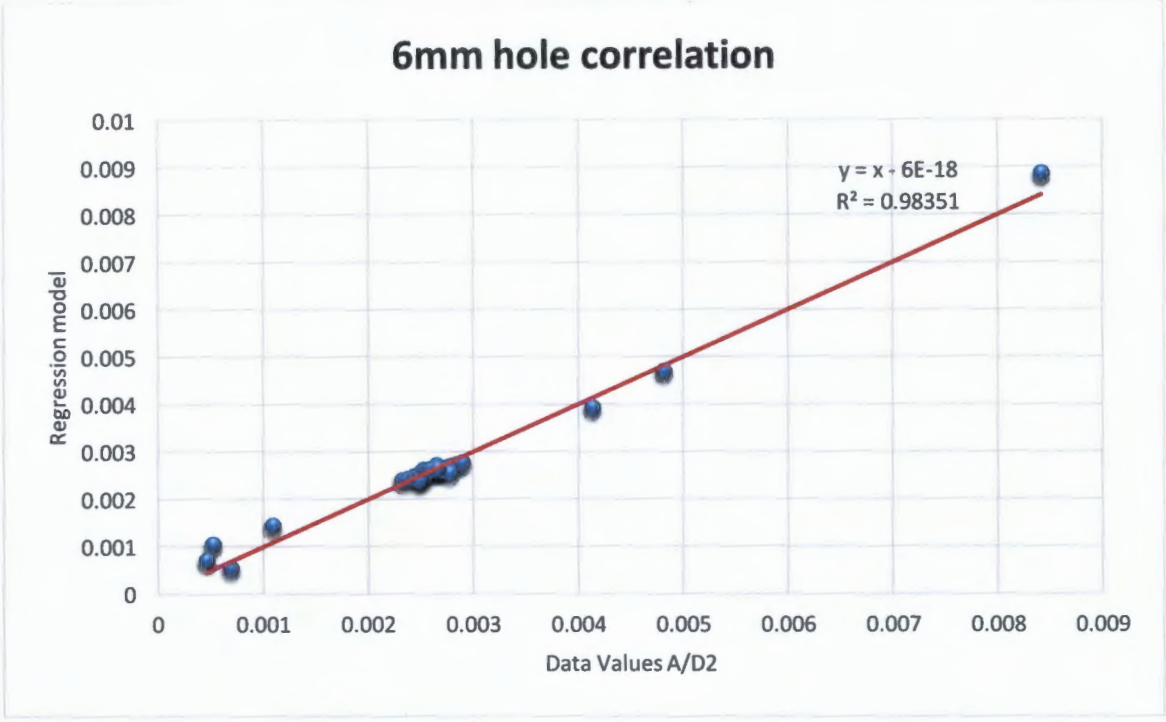

Figure 6-3 Showing Correlation Between the Regression Model of Equation 2-10 and the FEA data Values for the 6mm Hole

6.3.3 Additive Regression Model Analysis for the 8mm Hole

The same regression models used for the 4mm and 6mm hole, were used for the 8mm hole. The results of the regression analysis are shown in Table 6-7, along with their statistics.

Table 6-7 Regression Analysis for the 8mm Hole

$\frac{A}{t^2} = a_1 \frac{\mu}{t\sqrt{\rho E}} + a_2 \frac{\sigma_l}{E} + a_3 \frac{D}{t} + a_4 \frac{d}{t} + a_5 \frac{P}{E} + b$ **Equation 6-8** $\frac{A}{t^2} = 2358314.44 \frac{\mu}{t\sqrt{\rho E}} + 109.54 \frac{\sigma_l}{E} + 0.00816 \frac{D}{t} + 4.1598 \frac{d}{t} + 8213805.65 \frac{P}{E} - 6.168$ R^2=96.32% df=35 FDIST=4.642×10^{-24}
$\frac{A}{t^2} = a_1 \frac{t\sqrt{\rho E}}{\mu} + a_2 \frac{P}{E} + a_3 \frac{t}{d} + a_4 \frac{t}{D} + a_5 \frac{\sigma_l}{E} + b$ **Equation 6-9** $\frac{A}{t^2} = -1.19842 \times 10^{-8} \frac{t\sqrt{\rho E}}{\mu} + 4255743.01 \frac{P}{E} - 17.157 \frac{t}{d} - 28.897 \frac{t}{D} + 267.69 \frac{\sigma_l}{E} + 12.969$ R^2=73.84% df=35 *FDIST*=2.6264×10^{-9}
$\frac{A}{D^2} = a_1 \frac{\rho \sigma_l D^2}{\mu^2} + a_2 \frac{\sigma_l}{E} + a_3 \frac{t}{D} + a_4 \frac{d}{D} + a_5 \frac{P}{E} + b$ **Equation 6-10** $\frac{A}{D^2} = 5.1651 \times 10^{-18} \frac{\rho \sigma_l D^2}{\mu^2} + 0.05809 \frac{\sigma_l}{E} + 0.04020 \frac{t}{D} + 0.1381 \frac{d}{D} + 10831.86 \frac{P}{E} - 0.007222$ R^2= 96.75% df=35 F*DIST*=5.335×10^{-25}

$$\frac{A}{d^2} = a_1 \frac{\rho \sigma_l D^2}{\mu^2} + a_2 \frac{\sigma_l}{E} + a_3 \frac{D}{t} + a_4 \frac{D}{d} + a_5 \frac{P}{E} + b$$

Equation 6-11

$$\frac{A}{d^2} = 1.3710 \times 10^{-16} \frac{\rho \sigma_l D^2}{\mu^2} - 3.4951 \frac{\sigma_l}{E} + 0.00221 \frac{D}{t} - 0.00455 \frac{D}{d} + 3179140.17 \frac{P}{E} + 0.7526$$

$R^2 = 93.84\%$ $df=35$ $FDIST=3.662 \times 10^{-20}$

Based on the above, additive regression models that were analysed for the 8mm hole, were once again the best fit regression model that was presented by Equation 6-10. It is possible to see how good this relationship actually is by comparing the regression model to the FEA data values for the 8mm hole. Simply plotting the model against the dependent variable's values does this. Figure 6-4 shows the correlation between the regression model and the FEA data values for the 8mm hole.

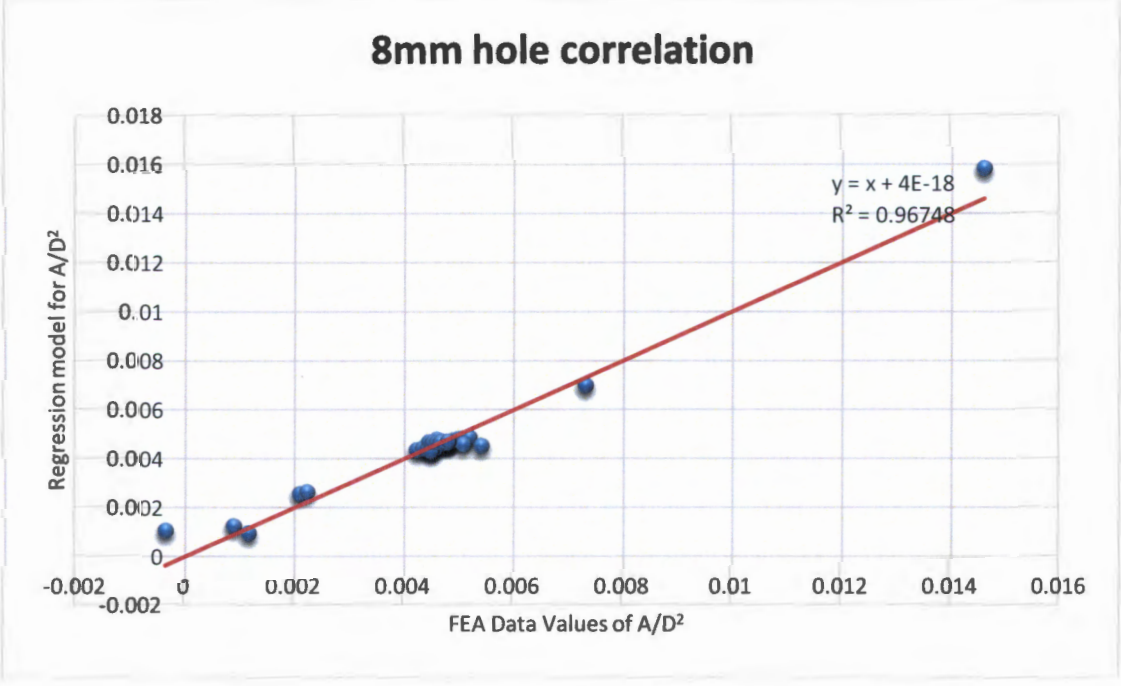

Figure 6-4: Showing Correlation Between the Regression Model of Equation 2-10 and the FEA data Values for the 8mm Hole

6.3.4 Discussion of Additive Regression Models for the Round Holes

The coefficient of determination of the regression models, shown for the three holes, show good fits for the model given by Equation 6-10, which is shown again here:

$$\frac{A}{D^2} = a_1 \frac{\rho \sigma_l D^2}{\mu^2} + a_2 \frac{\sigma_l}{E} + a_3 \frac{t}{D} + a_4 \frac{d}{D} + a_5 \frac{P}{E} + b$$

Once the regression analyses have been performed, it was found that the relationships differ significantly. All three holes showed different coefficient values for the same model. Another

possibility to assess is the possibility that the parameters are meant to be connected multiplicatively, since some of the properties of the pipe are closely linked to each other.

6.4 Multiplicative Regression Models

This section will show how linear regression can be performed when the dependent variable is affected multiplicatively by the independent variables. Conducting a logarithmic transformation will help set the regression models and, thereafter, the regression analysis process will follow. For illustration purposes, the full regression procedure is shown only for the 4mm hole. Due to the similar nature of the procedure undertaken for all three holes, only a summary of the regression statistics are given for the 6mm hole and the 8mm hole. The full procedures and the regression analyses for the three holes, including all the tables and regression statistics are shown in Appendix B.

The analysis begins with the collection of FEA data for each parameter (geometric and material). The new deformed round hole areas, resulting from varying the parameters, are recorded and the original area of the hole is also captured in the FEA data collection. The next step is to select the dependent variables, which will be a function of the independent variables. For the multiplicative regression models the selected dependent variable was the change in area, i.e. ΔA. The primary reason for selecting the change in area, as the dependent variable, is due to the fact that the relationship between the areas of the leak area in a pipe is known to be linearly proportional to the pressure which, subsequently, leads to the familiar linear equation, expressed as follows:

$$A = A_0 + m'P$$

If this equation is rearranged to show the change in Area, the equation becomes:

$$A - A_0 = m'P$$

$$\Delta A = m'P \qquad \text{Equation 6-12}$$

Equation 6-12 can be used in the multiplicative regression analysis. The m' in Equation 6-12 is the head-area slope and is assumed (for the purposes of this study) that it is influenced by other variables (pipe material and geometric properties). However, before the regression analysis is done, the elasticity of the variables influencing the head-area slope is checked. According to Lindert and Pugel (1996) an "elastic" variable is one which is very sensitive to small changes, i.e. responds significantly to small changes in other parameters. An "inelastic" variable is one which is not very sensitive to changes in other parameters. Using the base model pipe as a baseline, and investigating the changes in the area over the range of each parameter, the elasticity's of the dependent variable, with respect to the independent variables, are checked. The elasticity is simply found by dividing the change by the baseline. The results of this sensitivity will be shown in the following tables presented for the varying leak hole areas. ΔA is the change in Area, P is the Pressure, E is the elastic modulus, $\blacklozenge$ is the Poisson's ratio, t is the thickness, d is the hole diameter, and D is the internal pipe diameter.

Table 6-8 Analysis of Pipe With a 4mm Hole Defect

4mm hole					
Parameter	Minimum ΔA	Baseline ΔA	Maximum ΔA	Change ΔA	Elasticity (%)
P	2.70E-08		2.40E-07	2.13E-07	145.89
E	2.48E-08		1.32E-06	1.30E-06	887.12
v	1.32E-06		1.32E-06	3.00E-09	2.05
t	8.22E-07	1.46E-07	1.82E-06	9.98E-07	683.56
d	1.07E-06		1.34E-06	2.70E-07	184.93
D	1.46E-07		4.00E-06	3.85E-06	2639.73
σ_l	1.86E-06		1.88E-06	2.00E-08	13.70

From Table 6-8 it can be seen that most of the parameters are elastic (elasticity well above 100%), with the exception of the Poisson's ratio and the longitudinal stress, which are inelastic, due to their low elasticity's. This could mean that the Poisson's ratio and the longitudinal stress play an insignificant role in the overall analysis and, possibly, can be left out during the analysis. The finite element analysis, done in Chapter 6, will investigate this further. Finally, according to Table 6-8, the internal diameter of the pipe, *D*, has the highest elasticity.

Table 6-9 Analysis of Pipe With a 6mm Hole Defect

6mm hole					
Parameter	Minimum ΔA	Baseline ΔA	Maximum ΔA	Change ΔA	Elasticity (%)
P	3.14E-07		4.08E-06	3.77E-06	145.94
E	8.88E-08		2.58E-06	2.49E-06	96.54
v	2.56E-06		2.64E-06	8.00E-08	3.10
t	1.71E-06	2.58E-06	3.53E-06	1.82E-06	70.53
d	1.46E-07		4.00E-06	3.85E-06	149.35
D	1.31E-06		5.81E-06	4.50E-06	174.38
σ_l	2.45E-06		2.46E-06	1.00E-08	0.39

From Table 6-9 it can be seen, similar to the 4mm round hole, that for the 6mm round hole all the parameters are elastic, except the Poisson's ratio and the longitudinal stress. Once again, the internal diameter of the pipe, *D*, has the highest elasticity.

Table 6-10 Analysis of Pipe With a 8mm Hole Defect

8mm hole					
Parameter	Minimum ΔA	Baseline ΔA	Maximum ΔA	Change ΔA	Elasticity (%)
P	6.62E-07		6.15E-06	5.49E-06	137.74
E	2.77E-08		3.98E-06	3.95E-06	99.19
v	3.92E-06		4.18E-06	2.60E-07	6.53
t	2.13E-06	3.98E-06	4.92E-06	2.79E-06	70.02
d	1.46E-07		4.00E-06	3.85E-06	96.73
D	1.71E-06		9.21E-06	7.50E-06	188.20
σ_l	3.67E-06		3.77E-06	1.00E-07	2.51

From Table 6-10 it can be seen that, similar to the 4mm and the 6mm hole, for the 8mm hole all parameters are elastic with the exception of the Poisson's ratio and the longitudinal stress, which can be assumed inelastic due to their poor sensitivity. Once again, this could be indicative that these two parameters could be left out of the analysis. It can also be noted that, for all three holes, the internal diameter is the parameter with the highest elasticity.

6.4.1 Multiplicative Regression Models for the 4mm Hole

Based on the elasticity analyses shown above, regression models can now be developed. The first regression model contains all the parameters, except the longitudinal stress. σ_l is dropped here because σ_l contains a data point of 0 MPa (the uniaxial stress state condition) which becomes undefined once the logarithmic transformation is applied and, thus, the model to be regressed will have the form:

$$\Delta A = b \cdot P^{a_1} \cdot E^{a_2} \cdot \upsilon^{a_3} \cdot t^{a_4} \cdot d^{a_5} \cdot D^{a_6} \qquad \text{Equation 6-13}$$

ΔA is the change in Area, P is the Pressure, E is the elastic modulus, v is the Poisson's ratio, t is the thickness, d is the hole diameter, D is the internal pipe diameter, and σ_l is the longitudinal stress. The subscripts a_1, a_2, a_3, a_4, a_5, a_6 and a_7 are the coefficients to be determined by the regression analysis that will be performed. After the log transformation equation 6-13 becomes:

$$\log \Delta A = \log b + a_1 \log P + a_2 \log E + a_3 \log \upsilon + a_4 \log t + a_5 \log d + a_6 \log D$$

As was done in the additive regression model, a table is set up containing all the dependant and independent variables. The input FEA data for the regression analysis of the 4mm hole is shown in Table 6-11.

Table 6-11 Input FEA data for the Regression Analysis of the 4mm Hole Multiplicative Regression

Pressure	E(Gpa)	v	t(m)	D(m)	d0	Longitudinal stress	A	ΔA	
0	3.00E+09	0.4	0.003	0.107	4.00E-03	0.00E+00	1.19E-05	0.00E+00	Change in Pressure
10.19367992	3.00E+09	0.4	0.003	0.107	4.00E-03	8.92E+05	1.19E-05	2.90E-08	
20.38735984	3.00E+09	0.4	0.003	0.107	4.00E-03	1.78E+06	1.19311E-05	5.11E-08	
30.58103976	3.00E+09	0.4	0.003	0.107	4.00E-03	2.68E+06	1.19543E-05	7.43E-08	
40.77471967	3.00E+09	0.4	0.003	0.107	4.00E-03	3.57E+06	1.19789E-05	9.89E-08	
50.96839959	3.00E+09	0.4	0.003	0.107	4.00E-03	4.46E+06	1.20027E-05	1.23E-07	
61.16207951	3.00E+09	0.4	0.003	0.107	4.00E-03	5.35E+06	1.20264E-05	1.46E-07	
71.35575943	3.00E+09	0.4	0.003	0.107	4.00E-03	6.24E+06	1.205E-05	1.70E-07	
81.54943935	3.00E+09	0.4	0.003	0.107	4.00E-03	7.13E+06	1.20735E-05	1.94E-07	
91.74311927	3.00E+09	0.4	0.003	0.107	4.00E-03	8.03E+06	1.2097E-05	2.17E-07	
101.9367992	3.00E+09	0.4	0.003	0.107	4.00E-03	8.92E+06	1.21204E-05	2.40E-07	
61.16207951	3.00E+09	0.4	0.003	0.107	4.00E-03	5.20E+06	1.32008E-05	1.32E-06	Change in Elastic Modulus
61.16207951	1.00E+10	0.4	0.003	0.107	4.00E-03	5.20E+06	1.23052E-05	4.25E-07	
61.16207951	3.00E+10	0.4	0.003	0.107	4.00E-03	5.20E+06	1.20264E-05	1.46E-07	
61.16207951	9.00E+10	0.4	0.003	0.107	4.00E-03	5.20E+06	1.19311E-05	5.11E-08	
61.16207951	2.00E+11	0.4	0.003	0.107	4.00E-03	5.20E+06	1.19048E-05	2.48E-08	
61.16207951	3.00E+09	0.17	0.003	0.107	4.00E-03	5.20E+06	1.32033E-05	1.32E-06	Change in poisson ratio
61.16207951	3.00E+09	0.21	0.003	0.107	4.00E-03	5.20E+06	1.32028E-05	1.32E-06	
61.16207951	3.00E+09	0.29	0.003	0.107	4.00E-03	5.20E+06	1.32019E-05	1.32E-06	
61.16207951	3.00E+09	0.4	0.003	0.107	4.00E-03	5.20E+06	1.32008E-05	1.32E-06	
61.16207951	3.00E+09	0.45	0.003	0.107	4.00E-03	5.20E+06	1.32004E-05	1.32E-06	
61.16207951	3.00E+09	0.495	0.003	0.107	4.00E-03	5.20E+06	1.32001E-05	1.32E-06	
61.16207951	3.00E+09	0.4	0.002	0.107	4.00E-03	7.95E+06	1.36975E-05	1.82E-06	Change in thickness
61.16207951	3.00E+09	0.4	0.0025	0.107	4.00E-03	6.30E+06	1.34156E-05	1.54E-06	
61.16207951	3.00E+09	0.4	0.003	0.107	4.00E-03	5.20E+06	1.32007E-05	1.32E-06	
61.16207951	3.00E+09	0.4	0.004	0.107	4.00E-03	3.83E+06	1.28996E-05	1.02E-06	
61.16207951	3.00E+09	0.4	0.005	0.107	4.00E-03	3.00E+06	1.27019E-05	8.22E-07	
61.16207951	3.00E+09	0.4	0.003	0.057	4.00E-03	2.70E+06	1.29548E-05	1.07E-06	Change in Internal diameter
61.16207951	3.00E+09	0.4	0.003	0.087	4.00E-03	4.20E+06	1.29979E-05	1.12E-06	
61.16207951	3.00E+09	0.4	0.003	0.107	4.00E-03	5.20E+06	1.30264E-05	1.15E-06	
61.16207951	3.00E+09	0.4	0.003	0.147	4.00E-03	7.20E+06	1.30829E-05	1.20E-06	
61.16207951	3.00E+09	0.4	0.003	0.214	4.00E-03	1.07E+07	1.3153E-05	1.27E-06	
61.16207951	3.00E+09	0.4	0.003	0.247	4.00E-03	1.22E+07	1.32221E-05	1.34E-06	
61.16207951	3.00E+09	0.4	0.003	0.107	4.00E-03	5.35E+06	1.20264E-05	1.46E-07	Change in hole diameter
61.16207951	3.00E+09	0.4	0.003	0.107	6.00E-03	5.35E+06	3.00989E-05	1.82E-05	
61.16207951	3.00E+09	0.4	0.003	0.107	8.00E-03	5.35E+06	5.37044E-05	4.18E-05	
61.16207951	3.00E+09	0.4	0.003	0.107	4.00E-03	0.00E+00	1.31442E-05	1.26E-06	Change in longitudinal stress
61.16207951	3.00E+09	0.4	0.003	0.107	4.00E-03	1.04E+06	1.31576E-05	1.28E-06	
61.16207951	3.00E+09	0.4	0.003	0.107	4.00E-03	2.08E+06	1.31709E-05	1.29E-06	
61.16207951	3.00E+09	0.4	0.003	0.107	4.00E-03	3.12E+06	1.31843E-05	1.30E-06	
61.16207951	3.00E+09	0.4	0.003	0.107	4.00E-03	5.20E+06	1.31977E-05	1.32E-06	

Table 6-12 now shows the setup that contains all the dependent and independent variables.

Table 6-12 Showing the Regression Table for the 4mm Round Holes

x1	x2	x3	x4	x5	x6	y
log P	log E	log v	log t	log d	log D	log ΔA
1.008330993	9.477121255	-0.397940009	-2.522878745	-2.397940009	-0.970616222	-7.537602002
1.309360988	9.477121255	-0.397940009	-2.522878745	-2.397940009	-0.970616222	-7.291239276
1.485452247	9.477121255	-0.397940009	-2.522878745	-2.397940009	-0.970616222	-7.129011186
1.610390984	9.477121255	-0.397940009	-2.522878745	-2.397940009	-0.970616222	-7.004856407
1.707300997	9.477121255	-0.397940009	-2.522878745	-2.397940009	-0.970616222	-6.911272256
1.786482243	9.477121255	-0.397940009	-2.522878745	-2.397940009	-0.970616222	-6.834602525
1.853429033	9.477121255	-0.397940009	-2.522878745	-2.397940009	-0.970616222	-6.76962006
1.91142098	9.477121255	-0.397940009	-2.522878745	-2.397940009	-0.970616222	-6.713228276
1.962573502	9.477121255	-0.397940009	-2.522878745	-2.397940009	-0.970616222	-6.66348023
2.008330993	9.477121255	-0.397940009	-2.522878745	-2.397940009	-0.970616222	-6.618980637
1.786482243	9.477121255	-0.397940009	-2.522878745	-2.397940009	-0.970616222	-5.879172804
1.786482243	10	-0.397940009	-2.522878745	-2.397940009	-0.970616222	-6.371422065
1.786482243	10.47712125	-0.397940009	-2.522878745	-2.397940009	-0.970616222	-6.834602434
1.786482243	10.95424251	-0.397940009	-2.522878745	-2.397940009	-0.970616222	-7.291290233
1.786482243	11.30103	-0.397940009	-2.522878745	-2.397940009	-0.970616222	-7.605898698
1.786482243	9.477121255	-0.769551079	-2.522878745	-2.397940009	-0.970616222	-5.878329971
1.786482243	9.477121255	-0.677780705	-2.522878745	-2.397940009	-0.970616222	-5.878490153
1.786482243	9.477121255	-0.537602002	-2.522878745	-2.397940009	-0.970616222	-5.878797225
1.786482243	9.477121255	-0.397940009	-2.522878745	-2.397940009	-0.970616222	-5.879172804
1.786482243	9.477121255	-0.346787486	-2.522878745	-2.397940009	-0.970616222	-5.879304352
1.786482243	9.477121255	-0.305394801	-2.522878745	-2.397940009	-0.970616222	-5.879393169
1.786482243	9.477121255	-0.397940009	-2.698970004	-2.397940009	-0.970616222	-5.74052558
1.786482243	9.477121255	-0.397940009	-2.602059991	-2.397940009	-0.970616222	-5.813721897
1.786482243	9.477121255	-0.397940009	-2.522878745	-2.397940009	-0.970616222	-5.879195822
1.786482243	9.477121255	-0.397940009	-2.397940009	-2.397940009	-0.970616222	-5.991561654
1.786482243	9.477121255	-0.397940009	-2.301029996	-2.397940009	-0.970616222	-6.085204376
1.786482243	9.477121255	-0.397940009	-2.522878745	-2.397940009	-1.244125144	-5.968672342
1.786482243	9.477121255	-0.397940009	-2.522878745	-2.397940009	-1.060480747	-5.951608699
1.786482243	9.477121255	-0.397940009	-2.522878745	-2.397940009	-0.970616222	-5.940663823
1.786482243	9.477121255	-0.397940009	-2.522878745	-2.397940009	-0.832682665	-5.919770475
1.786482243	9.477121255	-0.397940009	-2.522878745	-2.397940009	-0.669586227	-5.895185243
1.786482243	9.477121255	-0.397940009	-2.522878745	-2.397940009	-0.607303047	-5.87220218
1.786482243	9.477121255	-0.397940009	-2.522878745	-2.397940009	-0.970616222	-6.834602525
1.786482243	9.477121255	-0.397940009	-2.522878745	-2.22184875	-0.970616222	-4.739476894
1.786482243	9.477121255	-0.397940009	-2.522878745	-2.096910013	-0.970616222	-4.378570769
1.786482243	9.477121255	-0.397940009	-2.522878745	-2.397940009	-0.970616222	-5.898185588
1.786482243	9.477121255	-0.397940009	-2.522878745	-2.397940009	-0.970616222	-5.893622094
1.786482243	9.477121255	-0.397940009	-2.522878745	-2.397940009	-0.970616222	-5.88909226
1.786482243	9.477121255	-0.397940009	-2.522878745	-2.397940009	-0.970616222	-5.884617178
1.786482243	9.477121255	-0.397940009	-2.522878745	-2.397940009	-0.970616222	-5.880196638

Table 6-13 that follows shows the regression statistic associated with the regression model:

Table 6-13 Regression Statistics for 4mm Round Hole

0.485210884	6.564963822	-0.600670599	-0.804467239	-0.733025526	1.67739767	12.14282147
0.75026783	1.250136372	1.32667174	0.874739798	0.171350561	0.420179	4.839529777
0.67106834	0.423360479	#N/A	#N/A	#N/A	#N/A	#N/A
11.22079847	33	#N/A	#N/A	#N/A	#N/A	#N/A
12.06689796	5.914725134	#N/A	#N/A	#N/A	#N/A	#N/A

From Table 6-13 the R^2 is 67.10%, which is not a good fit. They are 33 degrees of freedom (*df*) and have a F*DIST* of 3.54 x10^{-7} which shows that the results of this model might not be the most reliable. The above regression statistics, lead to the following equation.

$$\Delta A = 1.38 \times 10^{12,14} \cdot P^{1.677} \cdot E^{-0.733} \cdot \upsilon^{-0.8045} \cdot t^{-0.60067} \cdot d^{6.565} \cdot D^{0.4852}$$

One observation that can be made is that the exponents of the pressure and the elastic modulus are inverse of each other. The thickness can also be an inverse of either the hole size d, or the internal diameter D. Making use of some of the additive models, these can also be related multiplicatively and, thus, the next form of equation to be regressed has the following form:

$$\Delta A = b \cdot \left(\frac{\mu}{t\sqrt{\rho E}} \right)^{a_1} \cdot \left(\frac{D}{t} \right)^{a_2} \cdot \left(\frac{d}{t} \right)^{a_3} \cdot \left(\frac{P}{E} \right)^{a_4} \qquad \text{Equation 6-14}$$

This can be logged and will become:

$$\log \Delta A = \log b + a_1 \log\left(\frac{\mu}{t\sqrt{\rho E}} \right) + a_2 \log\left(\frac{D}{t} \right) + a_3 \log\left(\frac{d}{t} \right) + a_4 \log\left(\frac{P}{E} \right)$$

Table 6-14 shows the set up that contains all dependent and independent variables.

Table 6-14 Input Regression Table for the 4mm Hole

x1	x3	x4	x5	x5
log(μ/t(ρE)0.5)	log(D/t)	log(d/t)	log(P/E)	log ΔA
-6.658777031	1.552262523	0.124938737	-8.468790262	-7.537602002
-6.658777031	1.552262523	0.124938737	-8.167760266	-7.291239276
-6.658777031	1.552262523	0.124938737	-7.991669007	-7.129011186
-6.658777031	1.552262523	0.124938737	-7.866730271	-7.004856407
-6.658777031	1.552262523	0.124938737	-7.769820258	-6.911272256
-6.658777031	1.552262523	0.124938737	-7.690639012	-6.834602525
-6.658777031	1.552262523	0.124938737	-7.623692222	-6.76962006
-6.658777031	1.552262523	0.124938737	-7.565700275	-6.713228276
-6.658777031	1.552262523	0.124938737	-7.514547753	-6.66348023
-6.658777031	1.552262523	0.124938737	-7.468790262	-6.618980637
-6.658777031	1.552262523	0.124938737	-7.690639012	-5.879172804
-6.920216403	1.552262523	0.124938737	-8.213517757	-6.371422065
-7.158777031	1.552262523	0.124938737	-8.690639012	-6.834602434
-7.397337658	1.552262523	0.124938737	-9.167760266	-7.291290233
-7.570731401	1.552262523	0.124938737	-9.514547753	-7.605898698
-6.658777031	1.552262523	0.124938737	-7.690639012	-5.878329971
-6.658777031	1.552262523	0.124938737	-7.690639012	-5.878490153
-6.658777031	1.552262523	0.124938737	-7.690639012	-5.878797225
-6.658777031	1.552262523	0.124938737	-7.690639012	-5.879172804
-6.658777031	1.552262523	0.124938737	-7.690639012	-5.879304352
-6.658777031	1.552262523	0.124938737	-7.690639012	-5.879393169
-6.482685772	1.728353782	0.301029996	-7.690639012	-5.74052558
-6.579595785	1.631443769	0.204119983	-7.690639012	-5.813721897
-6.658777031	1.552262523	0.124938737	-7.690639012	-5.879195822
-6.783715767	1.427323786	0	-7.690639012	-5.991561654
-6.88062578	1.330413773	-0.096910013	-7.690639012	-6.085204376
-6.658777031	1.278753601	0.124938737	-7.690639012	-5.968672342
-6.658777031	1.462397998	0.124938737	-7.690639012	-5.951608699
-6.658777031	1.552262523	0.124938737	-7.690639012	-5.940663823
-6.658777031	1.69019608	0.124938737	-7.690639012	-5.919770475
-6.658777031	1.853292519	0.124938737	-7.690639012	-5.895185243
-6.658777031	1.915575699	0.124938737	-7.690639012	-5.87220218
-6.658777031	1.552262523	0.124938737	-7.690639012	-6.834602525
-6.658777031	1.552262523	0.301029996	-7.690639012	-4.739476894
-6.658777031	1.552262523	0.425968732	-7.690639012	-4.378570769
-6.658777031	1.552262523	0.124938737	-7.690639012	-5.898185588
-6.658777031	1.552262523	0.124938737	-7.690639012	-5.893622094
-6.658777031	1.552262523	0.124938737	-7.690639012	-5.88909226
-6.658777031	1.552262523	0.124938737	-7.690639012	-5.884617178

Table 6-15 shows the regression statistics solutions for the 4mm hole regression model.

Table 6-15 Regression Statistics

2.042725864	5.019402324	-0.08885582	-2.65519456	-8.600914307
0.401624472	1.057518655	0.733387066	0.846177165	3.531180969
0.622907311	0.445021651	#N/A	#N/A	#N/A
14.04087722	34	#N/A	#N/A	#N/A
11.12286111	6.733505174	#N/A	#N/A	#N/A

From Table 6-15 the R^2 is 62.29%, which is a worse fit than the previous model. They are 34 degrees of freedom (*df*) and have a *FDIST* of $5.699\text{x}10^{-8}$ which shows that the results of this model might not be the most reliable. The above regression statistics from Table 6-15 lead to the following equation:

$$\Delta A = 2.5\times10^{-9}\cdot\left(\frac{\mu}{t\sqrt{\rho E}}\right)^{-2.6552}\cdot\left(\frac{D}{t}\right)^{-0.0889}\cdot\left(\frac{d}{t}\right)^{5.0194}\cdot\left(\frac{P}{E}\right)^{2.04272}$$

Another possibility is also explored and is shown along with its statistics.

Table 6-16 Other Possibilities to be Regressed

$\Delta A = b\cdot\left(\frac{t\sqrt{\rho E}}{\mu}\right)^{a_1}\cdot\left(\frac{P}{E}\right)^{a_2}\cdot\left(\frac{t}{d}\right)^{a_3}\cdot\left(\frac{t}{D}\right)^{a_4}$	Equation 6-15
$\Delta A = 2.511\times10^{-9}\cdot\left(\frac{t\sqrt{\rho E}}{\mu}\right)^{2.655}\cdot\left(\frac{P}{E}\right)^{2.043}\cdot\left(\frac{t}{d}\right)^{-5.019}\cdot\left(\frac{t}{D}\right)^{0.088}$	
$R^2 = 62.29\%$ df=34 *FDIST*=$5.70\text{x}10^{-8}$	

From the possible equations that are regressed multiplicatively, it is clear that the regression model, given by equation 6-13, is the best multiplicative model, just based on the R^2 and *FDIST* results. However, this model is far less accurate when compared to the results that were found for the 4mm additive models (See Table 6-5). This, therefore, implies that the 4mm round hole is probably best represented additively and the additive model presented by Equation 6-10 can be adopted.

6.4.2 Multiplicative Regression Models for the 6mm Hole

The same multiplicative regression models that are used for the 4mm hole are used for the 6mm hole, as well. The results of the regression analysis are shown in Table 6-17.

Table 6-17 Regression Analyses and Their Statistics for the 6mm Hole

$\Delta A = b\cdot P^{a_1}\cdot E^{a_2}\cdot\upsilon^{a_3}\cdot t^{a_4}\cdot d^{a_5}\cdot D^{a_6}$	equation 6-13
$\Delta A = 0.3684\cdot P^{1.155}\cdot E^{-0.925}\cdot\upsilon^{0.0792}\cdot t^{-0.824}\cdot d^{-0.1989}\cdot D^{0.9298}$	
R^2=77.53% df=33 *FDIST*=$6.837\text{x}10^{-10}$	
$\Delta A = b\cdot\left(\frac{\mu}{t\sqrt{\rho E}}\right)^{a_1}\cdot\left(\frac{D}{t}\right)^{a_2}\cdot\left(\frac{d}{t}\right)^{a_3}\cdot\left(\frac{P}{E}\right)^{a_4}$	equation 6-14
$\Delta A = 0.0847\cdot\left(\frac{\mu}{t\sqrt{\rho E}}\right)^{-0.397}\cdot\left(\frac{D}{t}\right)^{0.975}\cdot\left(\frac{d}{t}\right)^{0.106}\cdot\left(\frac{P}{E}\right)^{1.127}$	
R^2=77.42% df=34 FDIST=$4.844\text{x}10^{-12}$	

$$\Delta A = b \cdot \left(\frac{t\sqrt{\rho E}}{\mu}\right)^{a_1} \cdot \left(\frac{P}{E}\right)^{a_2} \cdot \left(\frac{t}{d}\right)^{a_3} \cdot \left(\frac{t}{D}\right)^{a_4}$$

equation 6-15

$$\Delta A = 0.08465 \cdot \left(\frac{t\sqrt{\rho E}}{\mu}\right)^{0.397} \cdot \left(\frac{P}{E}\right)^{1.127} \cdot \left(\frac{t}{d}\right)^{-0.106} \cdot \left(\frac{t}{D}\right)^{-0.975}$$

R^2= 77.42% df=34 $FDIST$=4.844x10^{-12}

From the above equations that are regressed multiplicatively for the 6mm hole, it is clear that the regression model, given by equation 6-13, is the best multiplicative model, just based on the R^2 and F$DIST$ results. However, these models are less accurate when compared to the results that were found for the 6mm additive models (See Table 6-6). This, therefore, implies that the 6mm round hole is probably best represented additively and the additive model presented by Equation 6-10 can be adopted.

6.4.3 Multiplicative Regression Model for the 8mm Hole

The same multiplicative regression models that are used for the 4mm hole and the 6mm hole are used for the 8mm hole, as well. The results of the regression analyses are shown in Table 6-18, along with their statistics.

Table 6-18 Regression Analyses and Their Statistics for the 8mm Hole

$$\Delta A = b \cdot P^{a_1} \cdot E^{a_2} \cdot \upsilon^{a_3} \cdot t^{a_4} \cdot d^{a_5} \cdot D^{a_6}$$

equation 6-13

$$\Delta A = 128.16 \times 10^{6} \cdot P^{0.9976} \cdot E^{-0.8318} \cdot \upsilon^{-0.1498} \cdot t^{-0.9133} \cdot d^{4.159} \cdot D^{1.1147}$$

R^2=81.38% df=33 $FDIST$ = 3.103x10^{-11}

$$\Delta A = b \cdot \left(\frac{\mu}{t\sqrt{\rho E}}\right)^{a_1} \cdot \left(\frac{D}{t}\right)^{a_2} \cdot \left(\frac{d}{t}\right)^{a_3} \cdot \left(\frac{P}{E}\right)^{a_4}$$

equation 6-14

$$\Delta A = 4.509 \times 10^{-5} \cdot \left(\frac{\mu}{t\sqrt{\rho E}}\right)^{-0.989} \cdot \left(\frac{D}{t}\right)^{0.652} \cdot \left(\frac{d}{t}\right)^{2.73} \cdot \left(\frac{P}{E}\right)^{1.280}$$

R^2=74.16% df=34 FDIST=5.5397x10^{-11}

$$\Delta A = b \cdot \left(\frac{t\sqrt{\rho E}}{\mu}\right)^{a_1} \cdot \left(\frac{P}{E}\right)^{a_2} \cdot \left(\frac{t}{d}\right)^{a_3} \cdot \left(\frac{t}{D}\right)^{a_4}$$

equation 6-15

$$\Delta A = 4.509 \times 10^{-5} \cdot \left(\frac{t\sqrt{\rho E}}{\mu}\right)^{0.989} \cdot \left(\frac{P}{E}\right)^{1.280} \cdot \left(\frac{t}{d}\right)^{-2.729} \cdot \left(\frac{t}{D}\right)^{-0.652}$$

R^2= 74.16% df=34 $FDIST$=5.5397x10^{-11}

From the above equations presented in Table 6-18, that are regressed multiplicatively for the 8mm hole, it is clear that the regression model, given by Equation 6-13, is the best multiplicative model, just based on the R^2 and F$DIST$ results. However, this model is less

accurate when compared to the results that were found for the 8mm additive models (See Table 6-7). Similar to the 4mm and the 6mm hole, this, therefore implies that the 8mm round hole is probably best represented additively and the additive model presented by Equation 6-10 can be adopted.

6.4.4 Discussion of the Multiplicative Regression Models

It was found that for the multiplicative regression models, based on the R^2 and the *FDIST,* the best models of each hole analysis varied significantly. The R^2 seemed to increase as the hole area increased, for a given regression model. Despite this, in general, the multiplicative models did not possess a very good R^2. It is important to note that there are numerous other multiplicative regression model possibilities that can be tried. Based on the models chosen to be regressed in this study, the results suggest that the relationship between the independent and the dependent variables is not multiplicative.

6.5 Developing the Head-Area Slope from the Regression Analysis

There are two main models of regression that were looked at in this section, namely, the additive regression model (linear regression) and the multiplicative regression model (the exponential regression).

The dimensional analysis was a useful technique adopted to have a good starting point of possible groupings of parameters for the regression models. It is important to note that the dimensional analysis, alone, does not provide a final solution to the problem, but it can only give insight into what possible formulations can, perhaps, be considered. The regression analysis is then conducted in order to obtain a class of statistical models that can describe or predict relationships among dependent variables and independent variables. In this case, there was only one dependent variable set and several independent variables.

Generally, it was found that the multiplicative regression models were all less accurate when compared to the additive regression models. Unlike the additive models, the multiplicative models did not have a consistent regression model that was the best fit for all three holes. In other words, each hole had a different regression model that was the most accurate. All these factors suggest the possibility that, perhaps, the parameters are not meant to be connected multiplicatively and are actually only best connected additively, as the additive regression models gave reasonably good results.

From the additive analyses it was found that, although the same regression model was always lead to the best fit, the form of the equations differed with respect to the coefficients. This meant that each round hole had a unique equation from the analysis.

For the 4mm hole the resulting equation was:

$$\frac{A}{D^2} = 2.291\times10^{-18}\frac{\rho\sigma_l D^2}{\mu^2} - 0.0684\frac{\sigma_l}{E} - 0.0058\frac{t}{D} + 0.0912\frac{d}{D} + 6205.072\frac{P}{E} - 0.00224$$

For the 6mm hole the resulting equation was:

$$\frac{A}{D^2} = 3.524\times10^{-18}\frac{\rho\sigma_l D^2}{\mu^2} - 0.0128\frac{\sigma_l}{E} + 0.00930\frac{t}{D} + 0.115\frac{d}{D} + 9778.948\frac{P}{E} - 0.004373$$

For the 8mm hole the resulting equation was:

$$\frac{A}{D^2} = 5.1651\times10^{-18}\frac{\rho\sigma_l D^2}{\mu^2} + 0.05809\frac{\sigma_l}{E} + 0.04020\frac{t}{D} + 0.1381\frac{d}{D} + 10831.86\frac{P}{E} - 0.007222$$

As can be seen, all three holes had different equations defining the dependent variables. This meant that the head-area slope can be calculated for the individual round hole. The head-area slope for each hole was then derived as follows:

For the 4mm hole:

$$A = 2.291\times10^{-18}\frac{\rho\sigma_l D^4}{\mu^2} - 0.0684\frac{D^2\sigma_l}{E} - 0.0058Dt + 0.0912Dd + 6205.072\frac{D^2P}{E} - 0.00224D^2$$

$$A_0 + mh = 2.291\times10^{-18}\frac{\rho\sigma_l D^4}{\mu^2} - 0.0684\frac{D^2\sigma_l}{E} - 0.0058Dt + 0.0912Dd + 6205.072\frac{D^2P}{E} - 0.00224D^2$$

$$m = 2.291\times10^{-18}\frac{\rho\sigma_l D^4}{\mu^2 h} - 0.0684\frac{D^2\sigma_l}{hE} - 0.0058\frac{Dt}{h} + 0.0912\frac{Dd}{h} + 6205.072\frac{D^2\rho gh}{hE} - 0.00224\frac{D^2}{h} - \frac{A_0}{h}$$

For the 6mm hole:

$$A = 3.524\times10^{-18}\frac{\rho\sigma_l D^4}{\mu^2} - 0.0128\frac{D^2\sigma_l}{E} + 0.00930Dt + 0.115Dd + 9778.948\frac{D^2P}{E} - 0.004373D^2$$

$$A_0 + mh = 3.524\times10^{-18}\frac{\rho\sigma_l D^4}{\mu^2} - 0.0128\frac{D^2\sigma_l}{E} + 0.00930Dt + 0.115Dd + 9778.948\frac{D^2P}{E} - 0.004373D^2$$

$$m = 3.524\times10^{-18}\frac{\rho\sigma_l D^4}{h\mu^2} - 0.0128\frac{D^2\sigma_l}{hE} + 0.00930\frac{Dt}{h} + 0.115\frac{Dd}{h} + 9778.948\frac{D^2\rho gh}{hE} - 0.004373D^2 - \frac{A_0}{h}$$

For the 8mm hole:

$$A = 5.1651\times10^{-18}\frac{\rho\sigma_l D^4}{\mu^2} + 0.05809\frac{D^2\sigma_l}{E} + 0.04020Dt + 0.1381Dd + 10831.86\frac{D^2P}{E} - 0.0072D^2$$

$$A_0 + mh = 5.1651\times10^{-18}\frac{\rho\sigma_l D^4}{\mu^2} + 0.05809\frac{D^2\sigma_l}{E} + 0.04020Dt + 0.1381Dd + 10831.86\frac{D^2P}{E} - 0.0072D^2$$

$$m = 5.1651\times10^{-18}\frac{\rho\sigma_l D^4}{h\mu^2} - 0.05809\frac{D^2\sigma_l}{hE} + 0.04020\frac{Dt}{h} + 0.1381\frac{Dd}{h} + 10831.86\frac{D^2\rho gh}{hE} - 0.007222D^2 - \frac{A_0}{h}$$

The head-area slope equations have been developed for the three holes this study investigates. It is now clear that the following methodology used develops equations for individual round holes only, in this case for the 4mm, 6mm and 8mm round hole only. Thus the applicability of the model is limited because in practice it is not always the case that only one type of round hole leak exists in a distribution system. In most cases, numerous holes of various sizes tend to occur in a real distribution system and, therefore, the following equations are only useful if one is investigating an individual leak of known size. The aim of this research goes beyond just the individual leak and seeks to develop a generic umbrella equation that can be used for all sorts of round hole sizes, and is not limited to the three holes investigated here.

In order to do this, a new approach will be used, and this approach will be based on solid mechanics and other fundamental scientific principles. A scientific derivation will be developed and the next chapter will go through this derivation. The new equation will be explored in more detail and the results obtained from this will be compared to the results given by the finite element analysis. This is done to check whether or not the finite element analysis FEA data results can be predicted using the proposed scientific model that will be developed.

7 Theoretical Derivation of the Head-Area Slope Equation

This chapter looks at the theoretical derivation of the head-area slope equation for round holes in different pipes and materials. An equation is derived using solid mechanics elastic theory and other scientific principles. The derivation will be based on Buckley's (2007) derivation discussed in the literature review.

7.1 Solid Mechanics Theory

In this section some solid mechanics principles are used to derive an equation for the head-area slope *m* that can be used to predict the *m* for round hole leaks in different pipe materials and geometry.

7.1.1 Biaxial Stress Conditions

In a biaxial stress state the following stress conditions occur in the circumferential and longitudinal direction:

$$\sigma_c = \frac{K\mathrm{Pr}}{t} = \frac{K\rho ghr}{t} \qquad \text{Equation 7-1}$$

$$\sigma_l = \alpha\sigma_c = \frac{\alpha K\rho ghr}{t} \qquad \text{Equation 7-2}$$

Where:
σ_c= Circumferential stress
σ_l= Longitudinal stress
α= The ratio of longitudinal stress to circumferential stress
K= Stress concentration factor
ρ= Density
g= Gravitational acceleration
h= Pressure head
r= Pipe radius
t= Pipe thickness

Literature on pressurised cylinders/pipes suggests that the circumferential stress in a cylindrical vessel is always equal to twice that of the longitudinal stress. This is true for the case where the pipe is not surrounded by soil, and the pipe/cylinder has closed ends. For the case when the pipes are buried in the ground, other loads need to be taken into account. In this analysis, some coefficient "α" is introduced to take into account other external factors that play a role in the behaviour of the pipe.

Various loadings induce different stresses and strains. For the case of buried pipes the loadings can be categorised into two categories: internal pressure or external loads. The internal pressure comprises of the hydrostatic pressure and the surge pressure. The external loads, on the other hand, are made up of external soil pressure and/or surface (live) loads. Other external loadings to be considered are differential settlements, longitudinal bending and shear loadings, as well as temperature induced stresses, that could be caused by either internal or external effects (Mosner & Folkman, 2008) as cited by Cassa (2011). In order to allow the

incorporation all the above mentioned factors when appropriate this study will introduce the term "α" and this term will be denoted as the ratio of longitudinal stress to circumferential stress, as shown below, which would vary for buried pipes.

$$\alpha = \frac{\sigma_l}{\sigma_c}$$

Equation 7-3

For unburied pipes "α" will always be equal to a half, as is shown in most literature. Also, for the uniaxial stress states where the longitudinal stress (σ_l) does not exist, "α" would be equal to 0, because σ_l is set to 0.

7.1.2 Circumferential Strain

The derivation then follows by looking at the resulting strains in both directions. Hooke's law was used to determine the relationship of stress and strain. First the circumferential strain will be explored. For the biaxial stress state both the circumferential and longitudinal stresses play a part in the overall circumferential strain and, thus, the strain is given by:

$$\varepsilon_c = \frac{\sigma_c}{E} - \frac{\nu\sigma_l}{E}$$

Equation 7-4

From Equation (7-2) σ_l in Equation (7-4) can be rewritten as follows:

$$\varepsilon_c = \frac{\sigma_c}{E} - \frac{\nu(\alpha\sigma_c)}{E}$$

Equation 7-5

$$\varepsilon_c = \frac{\sigma_c}{E}(1 - \nu\alpha)$$

Equation 7-6

From Equation (7-1) σ_c in Equation (7-6) can be rewritten as follows:

$$\varepsilon_c = \frac{\mathrm{Pr}}{tE}(1 - \nu\alpha)$$

Equation 7-7

Strain in the circumferential direction is a function of the change in diametrical length (Δd_c) over the original diametrical length (d_0) in the circumferential direction, equating this to Equation (7) the strain can be expressed as follows:

$$\varepsilon_c = \frac{\Delta d_c}{d_0} = \frac{K\,\mathrm{Pr}}{tE}(1 - \nu\alpha)$$

Equation 7-8

Thus the new diametrical length in the circumferential direction is given by:

$$d_c = d_0 + \Delta d_c = d_0 + \frac{d_0 \Pr}{tE}(1 - \nu\alpha) = d_0\left[1 + \frac{K\Pr}{tE}(1 - \nu\alpha)\right]$$

Equation 7-9

7.1.3 Longitudinal Strain

Similar to the circumferential strain, for the overall longitudinal strain, both the circumferential and longitudinal stress play a part and, thus, according to Hooke's law, the strain can be expressed as follows:

$$\varepsilon_l = \frac{\sigma_l}{E} - \frac{\nu\sigma_c}{E}$$

Equation 7-10

From Equation (2-2) σ_l in Equation (2-10) can be rewritten as follows:

$$\varepsilon_l = \frac{\alpha\sigma_c}{E} - \frac{\nu\sigma_c}{E}$$

Equation 7-11

$$\varepsilon_l = \frac{\sigma_c}{E}(\alpha - \nu)$$

Equation 7-12

From Equation (2-1) σ_c in Equation (2-12) can be rewritten as follows:

$$\varepsilon_l = \frac{K\Pr}{tE}(\alpha - \nu)$$

Equation 7-13

The longitudinal strain, expressed as a function of the change in longitudinal diameter length (Δd_l) over the original longitudinal diameter length (d_0) is given as:

$$\varepsilon_l = \frac{\Delta d_l}{d_0} = \frac{K\Pr}{tE}(\alpha - \nu)$$

Equation 7-14

Thus the new longitudinal diameter length is given by:

$$d_l = d_0 + \Delta d_l = d_0 + \frac{d_0 \Pr}{tE}(\alpha - \nu) = d_0\left[1 + \frac{K\Pr}{tE}(\alpha - \nu)\right]$$

Equation 7-15

The area of an ellipse is calculated using Eq (2-16) which is given as:

$$A = \frac{\pi}{4} d_c d_l$$

Equation 7-16

Substituting d_c and d_l from Equation (2-9) and Equation (2-15) respectively, into Equation (2-16) derives:

$$A=\frac{\pi}{4}d_0^2\left[1+\frac{KPr}{tE}(1-v\alpha)\right]\left[1+\frac{KPr}{tE}(\alpha-v)\right]$$

Equation 7-17

By multiplying the brackets, and simplifying the expression, the round hole leak area, as a function of material properties and geometric properties, is obtained. The simplification steps are shown by the following equation:

$$A=\frac{\pi}{4}d_0^2\left[1+\frac{KPr}{tE}(\alpha-v)+\frac{KPr}{tE}(1-v\alpha)+\left(\frac{KPr}{tE}\right)^2(1-v\alpha)(\alpha-v)\right]$$

Therefore, the round hole leak area, subjected to biaxial stress state, can be expressed as Equation (2-18):

$$A=\frac{\pi}{4}d_0^2\left[1+\frac{KPr}{tE}(a-v+1-va)+\left(\frac{KPr}{tE}\right)^2(1-va)(a-v)\right]$$

Equation 7-18

Where d_0 is the hole diameter, K is the stress concentration factor, P is the internal pressure, r is the pipe internal radius, t is the pipe wall thickness, E is the pipe elastic modulus, v is the Poisson's ratio and α is the ratio of longitudinal stress and circumferential stress. Cassa, et al., (2010) showed that although the stress concentration factor for a circular hole is normally 3, the stress concentration factor can vary linearly with hole size. In this study K is taken as 3.

7.1.4 Head-Area Slope Derivation

Van Zyl and Cassa (2005) showed that the area of a round hole expands linearly with increasing pressure. They derived the following expression:

$$A=A_0+mh$$

Equation 7-19

This equation shows the fixed or initial leak area, A_0 and the variable leak area, mh which varies with pressure. Equation (7-18) and Equation (7-19) are, essentially, calculating a leak area for an elastically deforming hole. Hence, technically speaking, it is possible to equate them in the following manner.

$$A_0+mh=\frac{\pi}{4}d_0^2\left[1+\frac{KPr}{tE}(a-v+1-va)+\left(\frac{KPr}{tE}\right)^2(1-va)(a-v)\right]$$

Equation 7-20

From Equation (2-20) the head-area slope m can be made the subject of the equation. This is illustrated by following some simple mathematical manipulation carried out next:

$$A_0+mh=\left[\frac{\pi}{4}d_0^2+\left(\frac{\pi}{4}d_0^2\right)\left(\frac{KPr}{tE}\right)\left((a-v+1-va)+\left(\frac{KPr}{tE}\right)(1-va)(a-v)\right)\right]$$

$$A_0+mh=\left[A_0+A_0\left(\frac{KPr}{tE}\right)\left((a-v+1-va)+\left(\frac{KPr}{tE}\right)(1-va)(a-v)\right)\right]$$

$$mh = A_0\left(\frac{K\mathrm{Pr}}{tE}\right)\left[(\alpha-\nu+1-\nu\alpha)+\left(\frac{K\mathrm{Pr}}{tE}\right)(1-\nu\alpha)(\alpha-\nu)\right]$$

$$mh = A_0\left(\frac{K\rho gh\mathrm{r}}{tE}\right)\left[(\alpha-\nu+1-\nu\alpha)+\left(\frac{K\rho gh\mathrm{r}}{tE}\right)(1-\nu\alpha)(\alpha-\nu)\right]$$

Finally, cancelling out the pressure head h, which is a common factor on both the left hand side and right hand side of the equation, the head-area slope m is given as:

$$m = A_0\left(\frac{K\rho g\mathrm{r}}{tE}\right)\left[(\alpha-\nu+1-\nu\alpha)+\left(\frac{K\rho gh\mathrm{r}}{tE}\right)(1-\nu\alpha)(\alpha-\nu)\right] \quad \text{Equation 7-21}$$

If α is = ½ then m becomes:

$$m = A_0\left(\frac{K\rho g\mathrm{r}}{tE}\right)\left[\frac{3}{2}(1-\nu)+\left(\frac{K\rho gh\mathrm{r}}{2tE}\right)(2-\nu)(1-2\nu)\right]$$

This m equation matches the m that would be obtained from Buckley's (2007) work, where α was always equal to a half.

7.2 Further Analysis of Derived Equation

This section investigates, in detail, the derived equation 7-21 in order to understand what it means, and the type of results to expect from it. Firstly, the derived equation is assessed by checking how well the equation predicts the FEA results obtained. This is done by comparing the head-area slopes of the FEA results and the head-area slopes obtained by the equation.

7.2.1 Head-Area Slope Equation Assessment 1

The head-area slopes obtained from using Equation 7-21 are calculated for the various parameters (See Appendix C). Figure 7-1 shows how the results of the FEA head-area slope m compared to those of Equation 7-21.

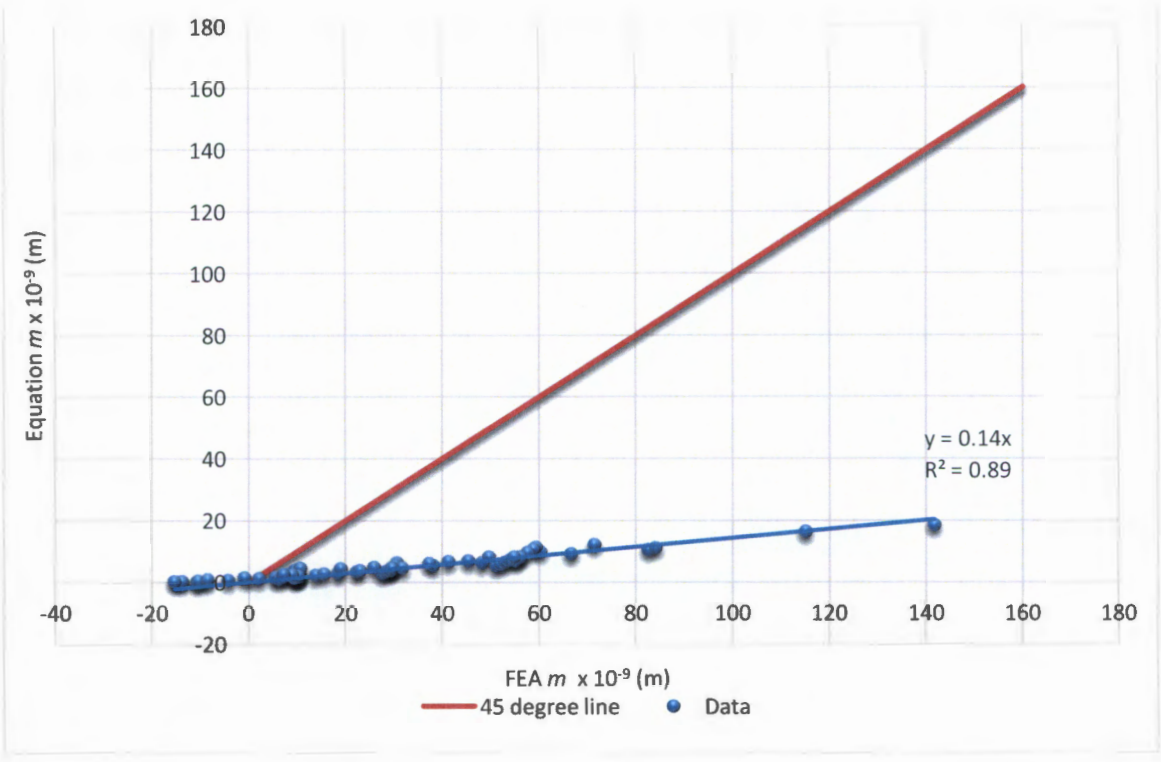

Figure 7-1: Head-Area Slope Equation vs Head-Area Slope FEA

From Figure 7-1 it can be seen that the equation does not predict the FEA results very well. The red line is a 45 degree line that represents the perfect fit, this is where the data points should ideally plot, if the equation predicts the FEA head-area slopes accurately. However, it can be seen that from the linear trend line of the equation and FEA data points, this is not necessarily the case and, therefore, the equation needs to be improved further. The second assessment described in section 7.2.2 will look at the structure of equation 7-21.

7.2.2 Head-Area Slope Equation Assessment 2

Further analysis of the equation suggested that Equation 7-21 can be split into two parts, as follows.

$$m = m_1 + m_2 \qquad \text{Equation 7-22}$$

Where:

$$m_1 = A_0\left(\frac{K\rho g r}{tE}\right)\left[(-\nu+1-\nu\alpha)\right]$$

$$m_2 = A_0\left(\frac{K\rho g r}{tE}\right)\left[\left(\frac{K\rho g h r}{tE}\right)(1-\nu\alpha)(\alpha-\nu)\right]$$

The sum of m_1 and m_2 gives the derived Equation 7-21 for the head-area slope. The next step is to check which of the two m's play a significant role. After the value of m_1 and m_2 are calculated, a comparison is done by working out the percentage contribution each m makes to the original m equation. Table 7-1 shows how m_1 contributed, compared to m_2 for all three round holes.

Table 7-1: Percentage Contribution to m Equation for the Three Holes

	Percentage Contribution to m					
	4 mm		6 mm		8 mm	
Parameter	m1	m2	m1	m2	m1	m2
Wall thickness	99.90%	0.10%	99.90%	0.10%	99.90%	0.10%
Elastic modulus	99.97%	0.03%	99.97%	0.03%	99.97%	0.03%
Poisson ratio	99.86%	0.14%	99.86%	0.14%	99.86%	0.14%
Internal diameter	99.87%	0.13%	99.87%	0.13%	99.87%	0.13%
Longitudinal stress	99.96%	0.04%	99.96%	0.04%	99.96%	0.04%

From Table 7-1 it can be seen that m_1 contributes more to m when compared to m_2. In fact, m_2 is insignificant for all parameters, and this can be explained by the structure of the equations. From the structure of the m_2 equation, it can be seen that when the Poisson ratio (which is always less than 0.5) is multiplied out, it becomes squared and, therefore, results in m_2 being smaller. Also, the elastic modulus is squared when multiplied out and becomes a big number, and because it is inversely proportional to m_2, this causes m_2 to become smaller.

Based on this analysis, m_2 can be eliminated and the new head-area slope m equation now only contains m_1:

$$m_1 = \left[\left(\frac{A_0 K \rho g r}{tE}\right)(\alpha - \upsilon + 1 - \upsilon\alpha)\right] \qquad \text{Equation 7-23}$$

However, this only changes the structure of the head-area slope equation because m_2 is eliminated. Figure 7-2 shows, graphically, how the m_1 equation predicts the FEA head-area slope m.

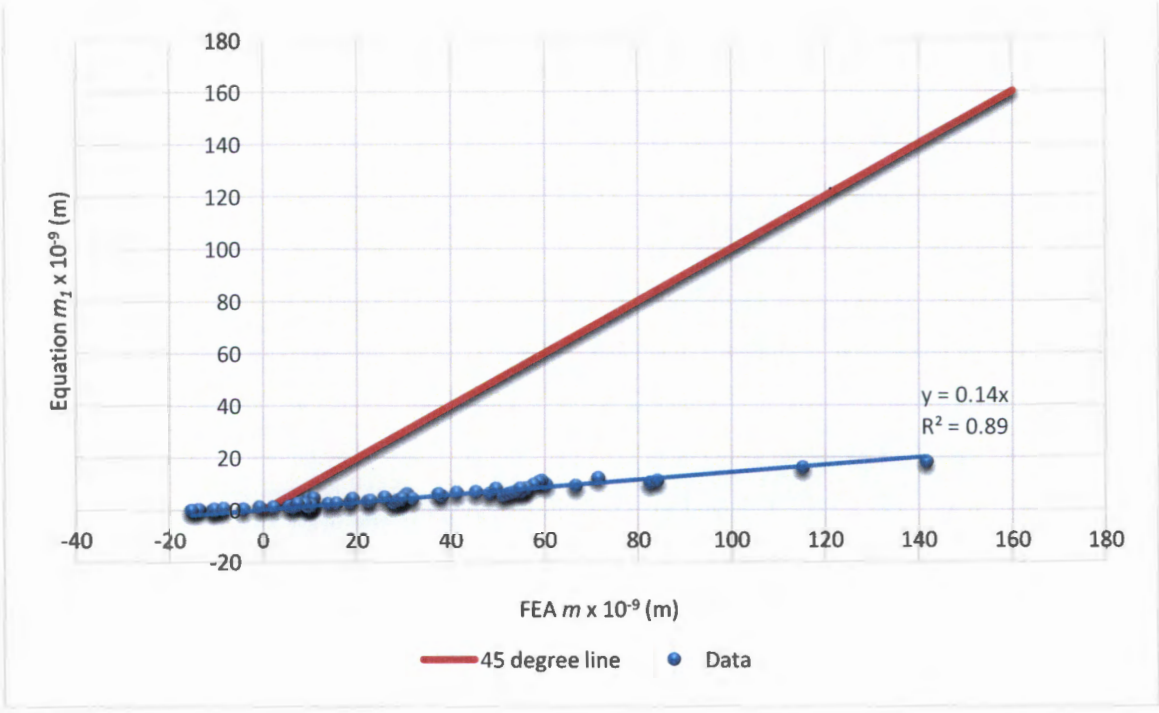

Figure 7-2: Showing How m_1 Predicted the FEA Head-Area Slope

As expected, it can be seen from Figure 7-2 that the m_1 equation presents a very similar graph to that presented by Figure 7-1. This is due to the dominance of m_1 in the original head-area slope equation given by Equation 7-22. The benefit of modifying equation 7-22 to Eqaution 7-23, m_1, is that it provides a simpler form of the head-area slope equation, however further modification has to be done in order to improve how well the equation predicts the FEA results. The final assessment described in section 7.2.3, considered including constants in order to achieve a better prediction model.

7.2.3 Head-Area Slope Equation Assessment 3

Even though the slope of the line in Figure 7-2 was different from the perfect fit line, it was still a linear relationship. Therefore, in order to make the line of the FEA data coincide with the best fit line (45^0 in Figure 7-2); two constants are introduced, to Equation 7-23, β and φ. The constants β and φ are introduced in order to adjust the slope and the intercept, respectively. The introduction of these constants changes the form of Equation 7-23 to the following:

$$m_{eq} = \beta\left[\left(\frac{A_0 K\rho g r}{tE}\right)(\alpha - \upsilon + 1 - \upsilon\alpha)\right] + \varphi$$

This can also be written in vector form as:

$$m_{eq}(\beta,\varphi) = \beta\bar{x} + \varphi$$

The constants β and φ, representing the gradient and intercept of the line, can be solved using a regression analysis called the method of least squares. Mathematically, the least squares

method stipulates that the sum of the vertical differences between the head-area slope of the equation m_{eq} and the head-area slope for the FEA m_{FEA} should be a minimum.

As was shown in Figure 7-1, in general, there are n pairs of observations (m_{FEA}, m_{eq}). These points do not all lie on the perfect fit line (i.e. the 45 degree line) again, as was shown in Figure 7-1. Letting $f(x_i, \beta, \varphi)$ to be the vertical difference between the m_{eq} and the associated m_{FEA} value, it can be expressed as follows:

$$f(x_i,\beta,\varphi)=\left(m_{FEM}(x_i)-m_{eq}(\beta,\varphi)\right)$$

Thus, the sum of squares can be denoted by θ as follows:

$$\theta=\sum f(x_i,\beta,\varphi)^2=\sum_{i=0}^{n}\left(m_{FEM}(x_i)-m_{eq}(\beta,\varphi)\right)^2$$

$$\theta=\sum_{i=0}^{n}\left(m_{FEM}(x_i)-\beta\bar{x}-\varphi\right)^2$$

The objective here is to find values for β and φ which minimises the sum of squares θ. The mathematical procedure followed to do this was to differentiate θ firstly, with respect to β and, secondly, to differentiate θ with respect to φ. Each of the derivatives is then set to zero. This gives two equations in two "unknowns", β and φ, which can be solved. Technically, the derivatives are known as **partial derivatives,** because this is a derivative of a function of two variables, and will be derived with respect to one variable, while the other is treated as a constant. The mathematical notation for partial derivatives is adopted here as:

$$\frac{\partial\theta}{\partial\beta}=-2\sum_{i=0}^{n}\bar{x}\left(m_{FEM}(x_i)-\beta\bar{x}-\varphi\right)^2=0$$

$$\frac{\partial\theta}{\partial\varphi}=-2\sum_{i=0}^{n}\left(m_{FEM}(x_i)-\beta\bar{x}-\varphi\right)^2=0$$

These partial derivatives can be solved by setting them equal to zero.

It is possible to calculate $\sum_{i=1}^{n}\bar{x}$, $\sum_{i=1}^{n}\bar{x}^2$, $\sum_{i=1}^{n}\bar{x}m_{fem}$ using the FEA data, with n being the number of sample points. The only unknowns are, therefore, the coefficients β and φ. The constants β and φ can be solved:

$$\beta = \frac{\sum x\bar{m}_{fem} - \frac{\sum \bar{x} \sum m_{fem}}{n}}{\sum \left(\bar{x}\right)^2 - \frac{\sum \left(\bar{x}\right)^2}{n}}$$

$$\varphi = \frac{\sum m_{fem} - \beta \sum x}{n}$$

The values of β and φ were calculated to be ***8.00*** and ***-8.00x10^{-9}*** respectively. This meant that the equation for the head-area slope could now be written as follows:

$$m_{eq} = 8.00\left[\left(\frac{A_0 K \rho g r}{tE}\right)(\alpha - \upsilon + 1 - \upsilon\alpha)\right] - 8\times10^{-9} \qquad \text{Equation 7-24}$$

Where m_{eq} is the head-area slope, A_0 is the initial hole area, K is the stress concentration factor normally 3, ρ is the fluid density, g is the acceleration due to gravity, r is the internal pipe radius, t is the pipe wall thickness, E is the elastic modulus, α is the ratio of the longitudinal stress and the circumferential stress, which can vary.

7.3 Plotting the Head-Area Slope *m* for the Equation Against the FEA *m*

The new head area slope given by Equation 7-24 m_{eq} can now be plotted against the head-area slope for the FEA results m_{FEA}. Figure 7-3 shows, graphically, how the results of the FEA *m* compared to the results obtained using Equation 7-24.

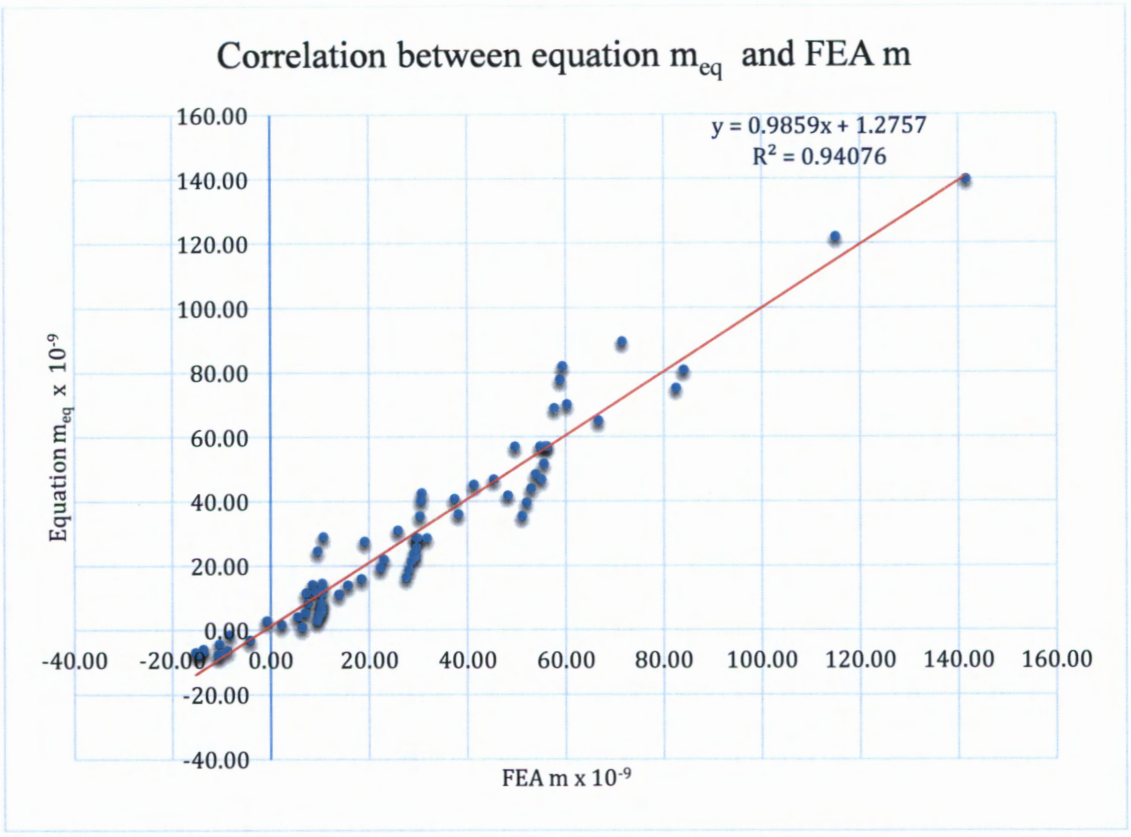

Figure 7-3: Head-Area Slope Equation vs Head-Area Slope FEA

From Figure 7-3 it can be seen that the head area slope equation now predicts the FEA results much better than before. The trend line fitted through the data points is now very close to the best fit line (45 degree line). In order to show the variation in the different parameters for each hole, the data plots are plotted in different colours and shown in Figure 7-4.

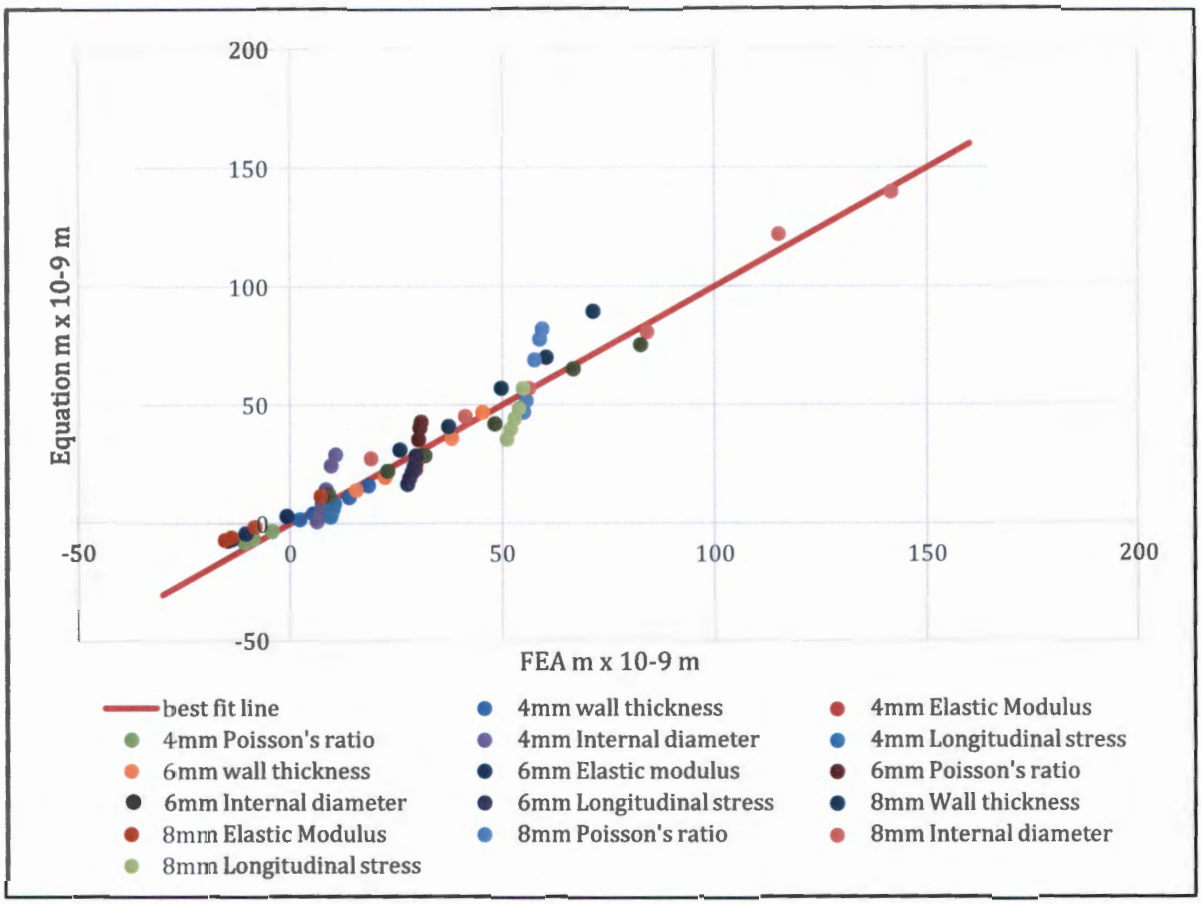

Figure 7-4: Showing the Variation of the Different Parameters

Figure 7-4 shows a graphical presentation of how the different parameters for each hole varied. It can be seen that the parameters predicted least accurately are the Poisson's ratio and the longitudinal stress - all other parameters are predicted reasonably well. Table 7-2 shows a summary of the FEA head-area slopes and the calculated head-area slopes for the 8 mm hole. As mentioned previously, the calculated head-area slope was calculated using Equation 7-24:

$$m_{eq} = 8.00\left[\left(\frac{A_0 K\rho g r}{tE}\right)(\alpha - \upsilon + 1 - \upsilon\alpha)\right] - 8\times10^{-9}$$

The last column labelled as "m_{eq} x 10^{9}" in Table 7-2 can be recalculated using Equation 7-24 above.

Table 7-2: Showing the FEA Head-Area Slope and the Equation m

Parameter change	t (m)	E (Pa)	v	Internal Diameter (m)	α	K	A_0 (m^2)	m_{FEM} x10^9 (m)	m_{eq} x 10^9 (m)
change in thickness	2.00E-03	3.00E+09	4.00E-01	1.06E-01	5.00E-01	3.00E+00	5.03E-05	7.15E+01	8.95E+01
	2.50E-03	3.00E+09	4.00E-01	1.05E-01	5.00E-01	3.00E+00	5.03E-05	6.03E+01	7.00E+01
	3.00E-03	3.00E+09	4.00E-01	1.04E-01	5.00E-01	3.00E+00	5.03E-05	4.97E+01	5.70E+01
	4.00E-03	3.00E+09	4.00E-01	1.02E-01	5.00E-01	3.00E+00	5.03E-05	3.74E+01	4.08E+01
	5.00E-03	3.00E+09	4.00E-01	1.00E-01	5.00E-01	3.00E+00	5.03E-05	2.59E+01	3.10E+01
Change in elastic modulus	3.00E-03	3.00E+09	4.00E-01	1.04E-01	5.00E-01	3.00E+00	5.03E-05	5.58E+01	5.70E+01
	3.00E-03	1.00E+10	4.00E-01	1.04E-01	5.00E-01	3.00E+00	5.03E-05	7.23E+00	1.15E+01
	3.00E-03	3.00E+10	4.00E-01	1.04E-01	5.00E-01	3.00E+00	5.03E-05	-8.41E+00	-1.50E+00
	3.00E-03	9.00E+10	4.00E-01	1.04E-01	5.00E-01	3.00E+00	5.03E-05	-1.38E+01	-5.83E+00
	3.00E-03	2.00E+11	4.00E-01	1.04E-01	5.00E-01	3.00E+00	5.03E-05	-1.53E+01	-7.02E+00
Change in poisson ratio	3.00E-03	3.00E+09	1.70E-01	1.04E-01	5.00E-01	3.00E+00	5.03E-05	5.94E+01	8.19E+01
	3.00E-03	3.00E+09	2.10E-01	1.04E-01	5.00E-01	3.00E+00	5.03E-05	5.88E+01	7.76E+01
	3.00E-03	3.00E+09	2.90E-01	1.04E-01	5.00E-01	3.00E+00	5.03E-05	5.77E+01	6.89E+01
	3.00E-03	3.00E+09	4.00E-01	1.04E-01	5.00E-01	3.00E+00	5.03E-05	5.62E+01	5.70E+01
	3.00E-03	3.00E+09	4.50E-01	1.04E-01	5.00E-01	3.00E+00	5.03E-05	5.56E+01	5.16E+01
	3.00E-03	3.00E+09	4.95E-01	1.04E-01	5.00E-01	3.00E+00	5.03E-05	5.51E+01	4.67E+01
Change in internal diameter	3.00E-03	3.00E+09	4.00E-01	5.40E-02	5.00E-01	3.00E+00	5.03E-05	1.90E+01	2.75E+01
	3.00E-03	3.00E+09	4.00E-01	8.40E-02	5.00E-01	3.00E+00	5.03E-05	4.13E+01	4.52E+01
	3.00E-03	3.00E+09	4.00E-01	1.04E-01	5.00E-01	3.00E+00	5.03E-05	5.62E+01	5.70E+01
	3.00E-03	3.00E+09	4.00E-01	1.44E-01	5.00E-01	3.00E+00	5.03E-05	8.40E+01	8.07E+01
	3.00E-03	3.00E+09	4.00E-01	2.14E-01	5.00E-01	3.00E+00	5.03E-05	1.15E+02	1.22E+02
	3.00E-03	3.00E+09	4.00E-01	2.44E-01	5.00E-01	3.00E+00	5.03E-05	1.42E+02	1.40E+02
Change in longitudinal stress	3.00E-03	3.00E+09	4.00E-01	1.04E-01	0.00E+00	3.00E+00	5.03E-05	5.11E+01	3.53E+01
	3.00E-03	3.00E+09	4.00E-01	1.04E-01	1.00E-01	3.00E+00	5.03E-05	5.21E+01	3.97E+01
	3.00E-03	3.00E+09	4.00E-01	1.04E-01	2.00E-01	3.00E+00	5.03E-05	5.30E+01	4.40E+01
	3.00E-03	3.00E+09	4.00E-01	1.04E-01	3.00E-01	3.00E+00	5.03E-05	5.39E+01	4.84E+01
	3.00E-03	3.00E+09	4.00E-01	1.04E-01	5.00E-01	3.00E+00	5.03E-05	5.49E+01	5.70E+01

7.4 Verification of Head-Area slope Equation

Malde (2015) experimentally determined the head-area slopes of 12 mm diameter round holes in 110 mm uPVC, HDPE and steel pipes. His experimental setup used a magnetic flow meter and calibrated pressure transducer to measure the flow rate at different pressures, from which the hole area at these pressures could be determined.

A linear function was fitted to the plot of the leak area against the pressure head. Since the initial leak area was known, precise values for the discharge coefficient and head-area slope could be determined. A statistical analysis of the data was done to determine the 95 % confidence intervals for the head-area slope in each experiment. Malde's results are summarised in Table 7-4.

Equation 7-24 was now used to predict the head-area slopes of the leaks tested by Malde, assuming typical values for the material properties. Malde's results of the head-area slopes for the 12mm diameter hole were calculated for the various materials. The head-area slopes of these leaks were also determined using FEA. Table 7-3 shows all the values used in the calculation. α was assumed 0.5 implying that the longitudinal stress was half the circumferential stress. The predicted head-area slopes and FEA results are summarised in Table 7-4

Table 7-3: Values used in the calculation of m

Material	Wall Thickness (mm)	Pipe Length (mm)	Elastic Modulus (MPa)	Poisson ratio	K	ρg (N/m^3)	α
uPVC	4.54	500	3000	0.4	3	9810	0.5
Steel	4.92	500	200000	0.3	3	9810	0.5
HDPE	6.38	500	1035	0.425	3	9810	0.5

Table 7-4: Comparison of the head-area slope

	uPVC	Steel	HDPE
min *m* (lower limit)	-3.20E-06	-7.70E-06	1.00E-07
m_{FEA}	7.00E-08	1.00E-09	1.00E-07
m_{exp}	-1.40E-06	-4.90E-06	2.80E-06
m_{eq}	8.88E-08	-6.44E-09	1.83E-07
max *m* (upper limit)	4.00E-07	-2.00E-06	5.50E-06

Figure 7-5 compares the equation and FEA results with Malde's experimental findings. The figure shows close correlation between the results of equation (17) and FEA for all three pipes. This shows some robustness in the equation since the holes tested are larger than the range of holes used to calibrate the equation.

When compared to the experimental results, the FEA and equation consistently have smaller absolute slopes. For uPVC and HDPE the values predicted by the equation falls within the 95 % confidence interval of the experimental results, while for steel it falls outside this range.

It is not immediately clear why the experimental study generally found larger absolute slopes than the equation. Several factors may contribute to this difference, including errors in the assumed material property values and localised viscoelastic or plastic deformation in the experimental pipes due to stress concentrations.

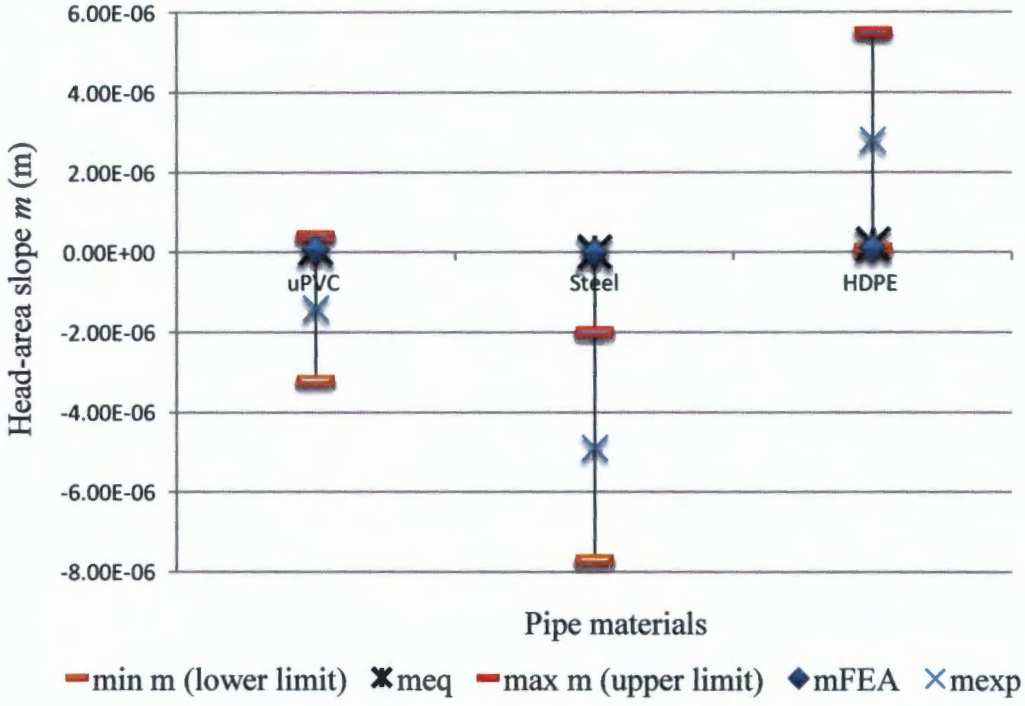

Figure 7-5: Showing the confidence interval and where the various head-area slope lie

8 Further Comparison of the Overall Results

In order to understand how well each parameter was predicted by the equation, a comparison was made of the results obtained using the calculated *m* and the head-area slope obtained from FEA for each parameter. Microsoft Excel was used to compare all the results. The spreadsheet had columns labelled: trial number; elasticity modulus; wall thickness; hole diameter; Poisson's ratio; longitudinal stress, internal diameter, m FEA and m calculated (See Appendix C.).

The FEA *m* was obtained from the results of the finite element analysis. The calculated *m* was obtained from inputting the various parameters in the derived Equation 7-24. A graph of each variable (E, *v*, D, t, and σ_l.) was plotted showing both the FEA *m* and the calculated *m* against the parameter for all three holes. The FEA data was plotted as data points and the calculated data was plotted as a line. This chapter looks at how the head-area slopes plot against each parameter for the three holes.

8.1 Wall Thickness

The calculated head-area slope *m* and the FEA *m* results correlated well, when varied against the wall thickness of the pipe. As can be seen from Figure 8-1, the calculated head-area slope, obtained from the equation, exhibits similar behaviour to the head-area slope obtained from FEA results. There is some sort of convergence between the equation and FEA as the wall thickness increases, i.e. the vertical distance between the FEA and the equation gets smaller as the wall thickness increased.

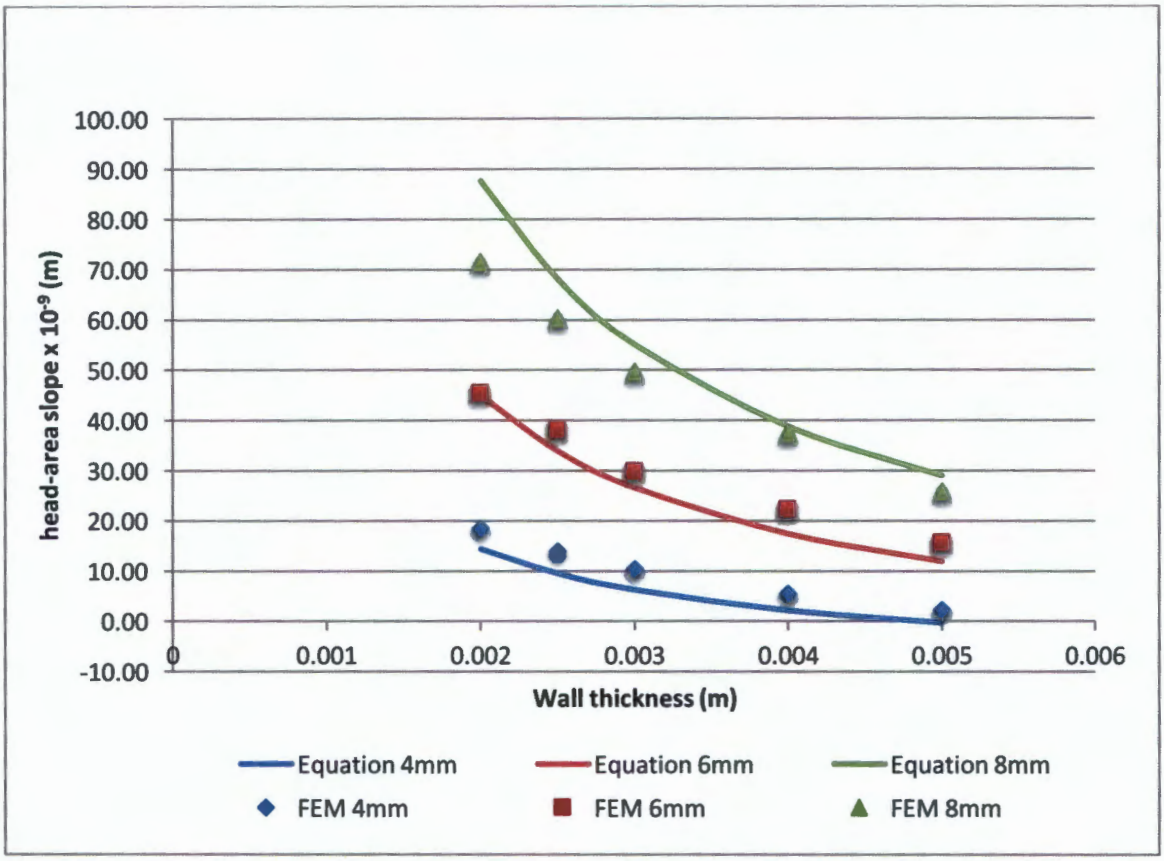

Figure 8-1: Equation m and FEA m Against Wall Thickness

From Figure 8-1 it can be seen that the head-area slope has an inversely proportional relationship to the wall thickness, so as the pipe wall thickness increases the head-area slope reduces. Larger holes (8 mm in this case) show a greater differential in the head–area slope, with respect to a change in wall thickness, when compared to the smaller holes (4 mm in this case). Also, it can be seen that the equation over-estimates the head-area slope *m* for the 8 mm hole, but slightly under-estimates the 6 mm and 4 mm hole. The commonly used pipes in distribution systems have a nominal wall thickness of about 3 mm. From Figure 8-1, one can see how the head-area slope would vary for the three different holes (i.e. 4 mm, 6 mm and 8 mm).

8.2 Elastic Modulus

Once again, it was found that the head-area slope, obtained from FEA and the equation, exhibit similar behaviour. From Figure 8-2 it can be seen that the inversely proportional relationship between the head-area slope and the elastic modulus was maintained, as Equation 7-24 suggests (E is a denominator in the equation).

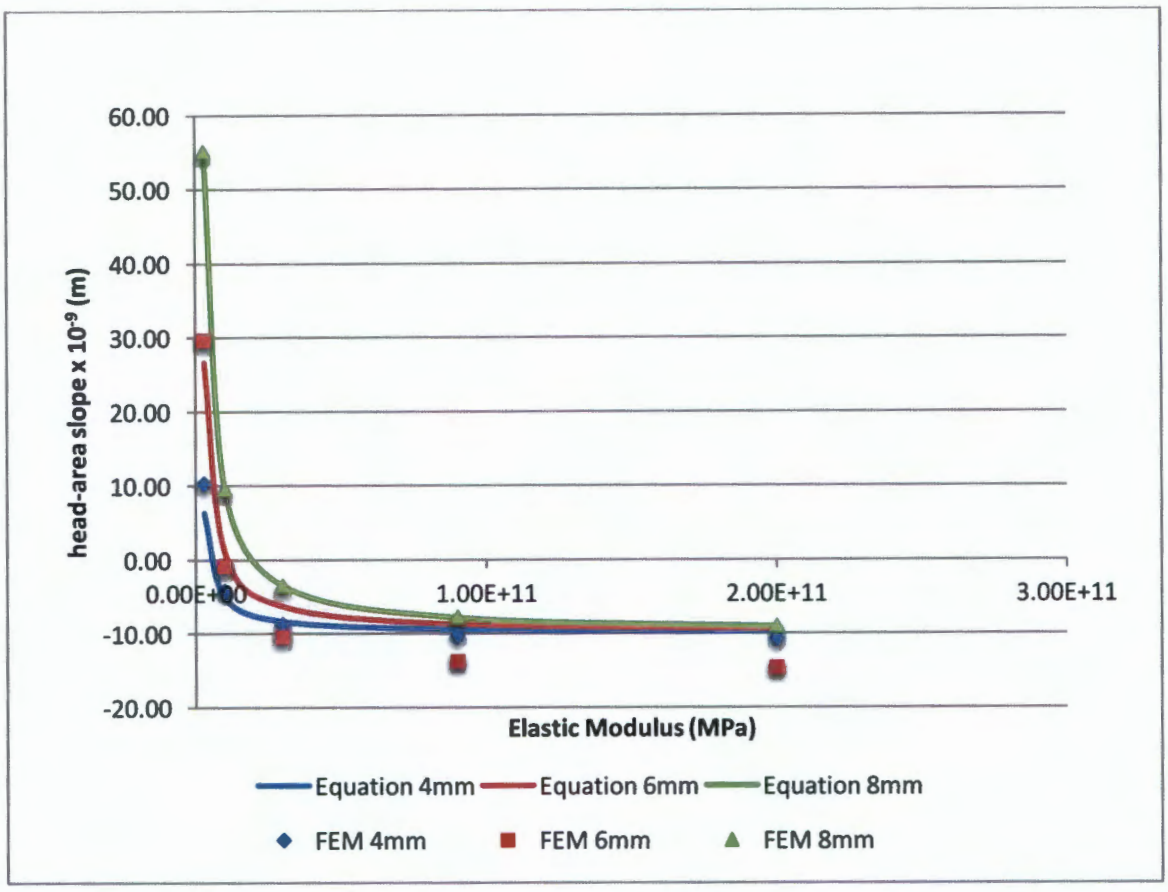

Figure 8-2: Equation m and FEA m Against Elastic Modulus

Figure 8-2 shows that the head-area slopes become negative with increasing elastic modulus. Materials with high elastic modulus are generally rigid, implying high stiffness and, therefore, for any induced stress there is a relatively small strain that results. This shows that the rigidity/stiffness of the material plays a role with round holes. What was found with the FEA results was that, assuming elastic deformation, for a fixed pressure head, the hole area decreased as the elastic modulus increased for a given round hole. This is shown in Table 8-1 below. This results in a negative head-area slope. The implication of negative head-area slopes is that the corresponding leakage exponents *N1* are less than 0.5.

Table 8-1: Variation of Hole Leak Area with Increasing Elastic Modulus

Hole Diameter (mm)	Elastic Modulus (Pa) $x10^9$	Area (m^2) $x\ 10^{-5}$
8	3	5.37
8	10	5.07
8	30	4.97
8	90	4.94
8	200	4.93

6	3	3.01
6	10	2.82
6	30	2.76
6	90	2.74
6	200	2.74
4	3	1.32
4	10	1.23
4	30	1.20
4	90	1.19
4	200	1.19

8.3 Internal Diameter

The equation results and the FEA results show similar behaviour with regards to the relationships between the head-area slope *m* and the internal pipe diameter. The internal pipe diameter D is the outer diameter subtracted by the wall thickness. Figure 8-3 shows how the equation and FEA models predicted each other. It can be seen that the larger holes were predicted much more accurately compared to the smaller hole.

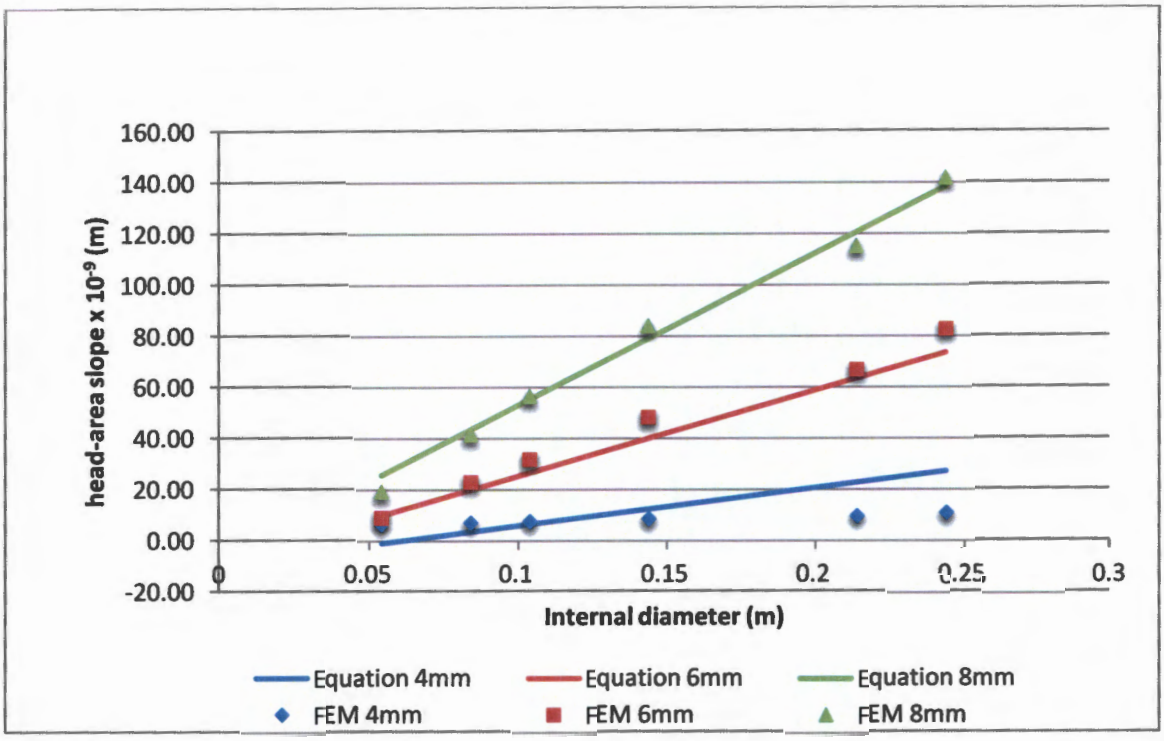

Figure 8-3: Equation *m* and FEA *m* Against Internal Diameter

From Figure 8-3 it can be seen that, as the internal diameter (D) increases, the head-area slope increases proportionally. This implies that there is some sort of linear relationship between the head-area slope and the internal diameter. This is also shown from the equation, which shows that m is related to D linearly and, thus, this is expected. The sensitivity of m head-area slope to the internal diameter D increases as the hole leak area increases. This is justified by the increasing gradients of the relationships shown in Figure 8-3.

8.4 Poisson's Ratio

Figure 8-4 shows how the calculated head-area slope m and the FEA head-area slope m results relate to the Poisson's ratio.

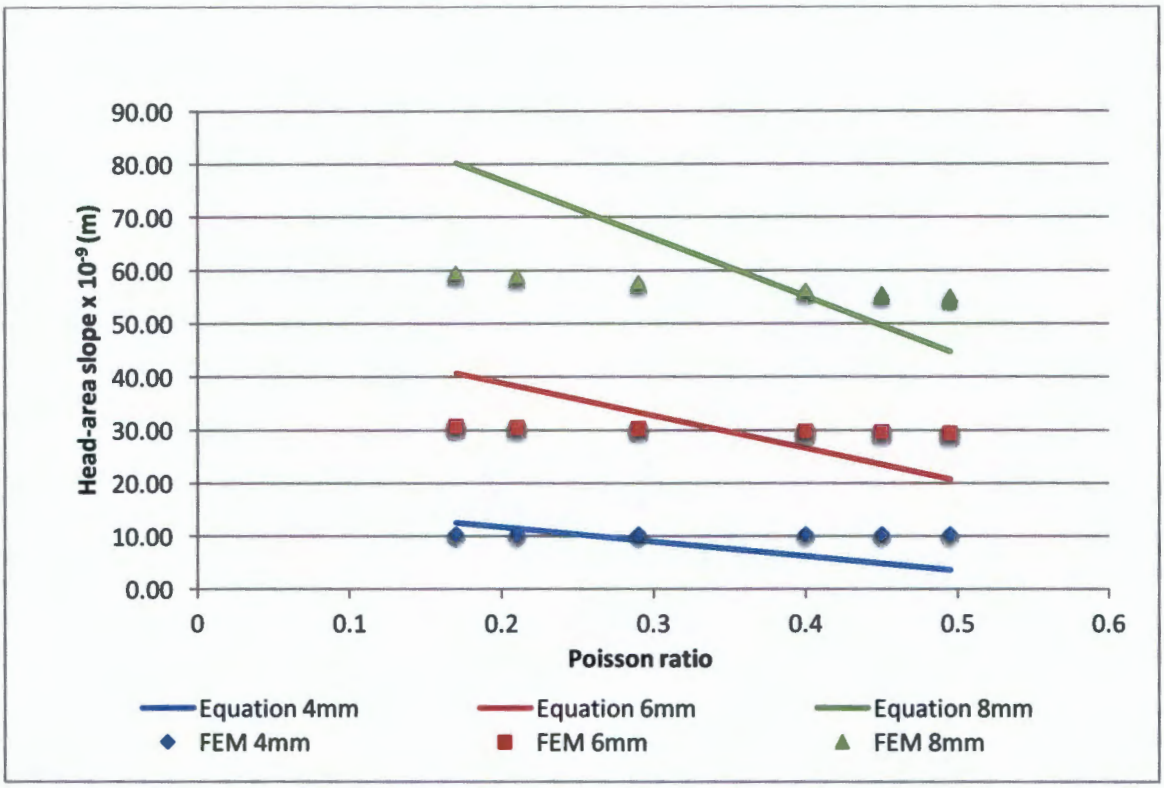

Figure 8-4: Equation *m* and FEA *m* Against Poisson Ratio

From Figure 8-4 it can be seen that, based on the FEA results, it is clear that the Poisson ratio plays an insignificant role when it comes to the effect it has on the head-area slope. This was shown in Section 5.2. However, the equation shows that the Poisson ratio plays a slightly more significant role in the effect it has on the head-area slope. This discrepancy can be due to the fact that, in the derived equation, the Poisson ratio is linearly related to the head-area slope. The derived equation, Equation 2-24, is shown below, and it can be seen that the Poisson ratio, ν, is related to the head-area slope *m* linearly, with a negative slope. Hence, the calculated head-area slope in Figure 8-4 is negatively sloping.

$$m_{eq} = 8.00\left[\left(\frac{A_0 K\rho g r}{tE}\right)(\alpha - \upsilon + 1 - \upsilon\alpha)\right] - 8\times10^{-9} \qquad \text{Equation 2-24}$$

Although the calculated *m* and the FEA *m* seems to not fit each other well in Figure 8-4, the variations between them are very small. In other words, the error margin between the calculated *m* and the FEA *m* is insignificant.

8.5 Longitudinal Stress

Figure 8-5 shows how the calculated head–area slope *m* and the FEA *m* varied with longitudinal stress. The longitudinal stress was assumed to be some factor, α , multiplied by the circumferential stress, as it was given in Equation 7-3, recited here as:

$$\alpha = \frac{\sigma_l}{\sigma_c}$$

α was always assumed to be less than one, because the longitudinal stress σ_l is assumed to be less than the circumferential stress σ_c. In this study, all cases investigated were such that σ_c was greater than σ_l.

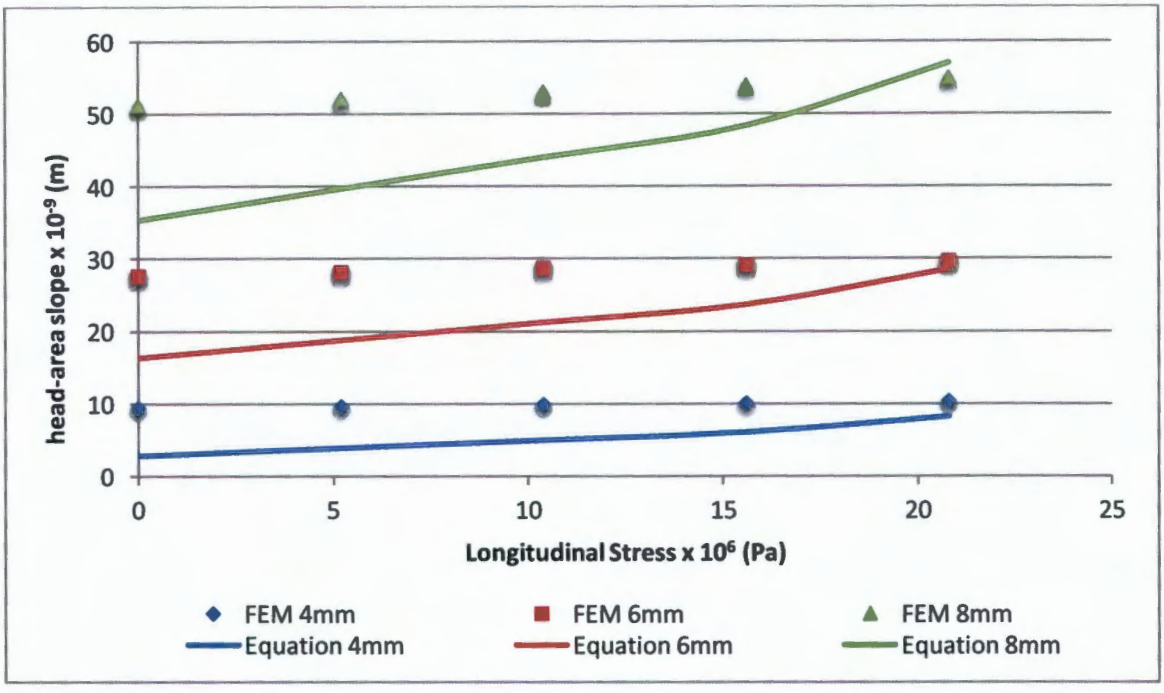

Figure 8-5: Equation m and FEA m Against Longitudinal Stress

From Figure 8-5 it can be seen that the longitudinal stress plays an insignificant role with the FEA head-area slope *m*. However, the calculated *m* shows some variation as the longitudinal stress increases. Again, this could be attributed to the fact that in the derived Equation 7-24 that is used to calculate the head-area slope, the constant α is linearly proportional to head-area slope. What is common between the relationships of the calculated *m* and the FEA *m* to the longitudinal stress, is that longitudinal stress has a larger effect as the leak hole increases.

8.6 Comparison of Variation in Parameters

In order to understand how well the FEA *m* and the equation *m* compared for each parameter, some bar graphs are shown. The bar graphs are a good indicator to show how the calculated *m* and the FEA *m* compared for the various parameters looked at. The bar graphs show the range between the head-area slopes for the calculated case and the FEA case.

Figure 8-6 shows how the range of the head-area slopes varied for the calculated *m* and FEA *m* for the 4 mm hole. It can be seen that the range of FEA *m* and the equation *m* varied for all parameters, particularly for the internal diameter and the Poisson's ratio which has large differences for the 4 mm hole.

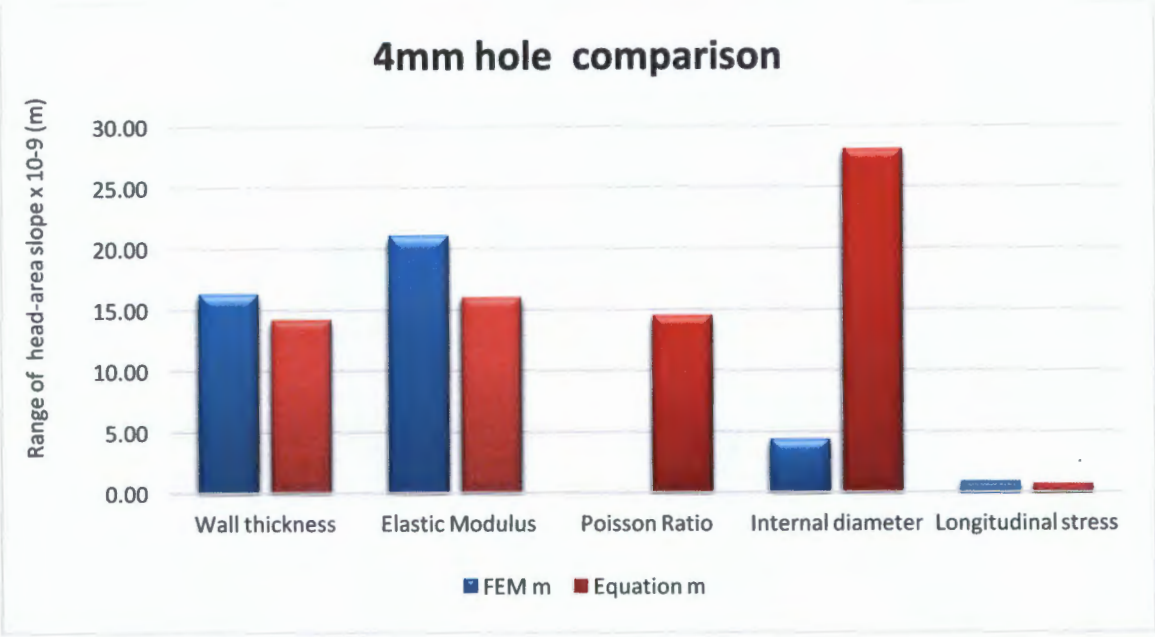

Figure 8-6: Parameter Comparison of the Range of Equation *m* and FEA *m* for the 4 mm Hole

Figure 8-7 now shows how the 6 mm hole compared for the various parameters. It can be seen that this was a much better comparison, when compared to the 4 mm hole, particularly for the internal diameter. It can be seen that, unlike the 4 mm hole, which showed a significant range of the equation *m* compared to the FEA *m*, for the internal diameter, this is not the case for the 6 mm hole. As can be seen in Figure 8-7, the equation *m* has a smaller range compared to the FEA *m* range. It can also be noted that the three parameters that were found to play the most significant role in affecting the head-area slope (i.e. wall thickness, elastic modulus and internal diameter) have compared relatively well for the 6 mm hole.

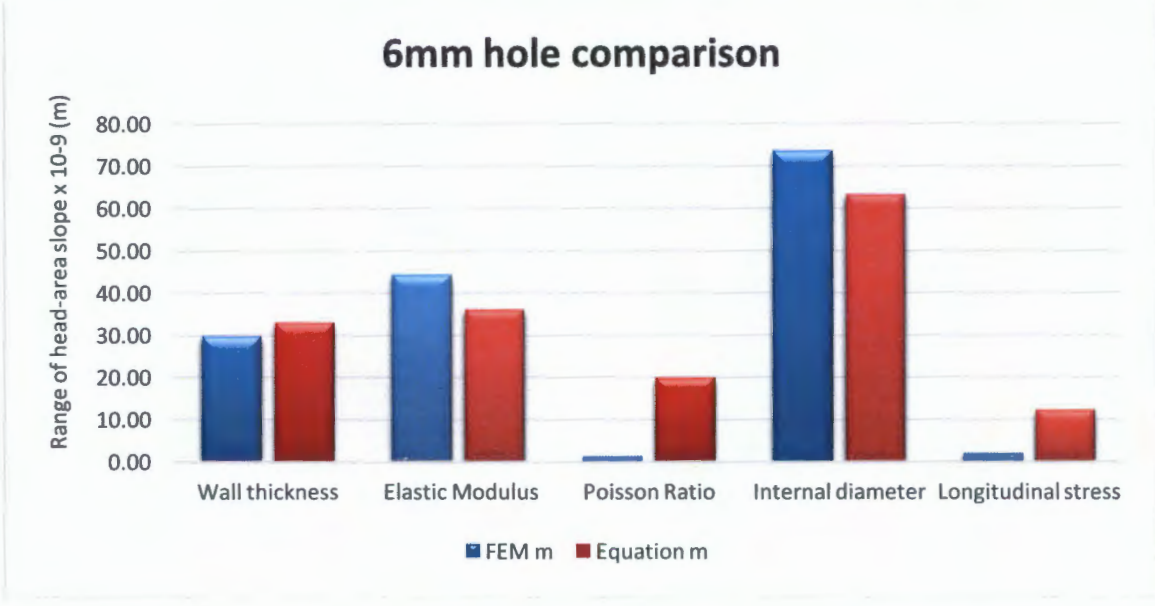

Figure 8-7: Parameter Comparison of Range of Equation *m* and FEA *m* for the 6 mm Hole

Finally, Figure 8-8 below shows how the 8 mm hole FEA *m* range compared to the equation *m* range for the different parameters. Once again, the three parameters that play a significant

role to the head-area slope (i.e. wall thickness, elastic modulus and internal diameter) compared relatively well. When comparing the range it can be seen that the equation has a higher range for the wall thickness, but a lower range for the elastic modulus and internal diameter only slightly.

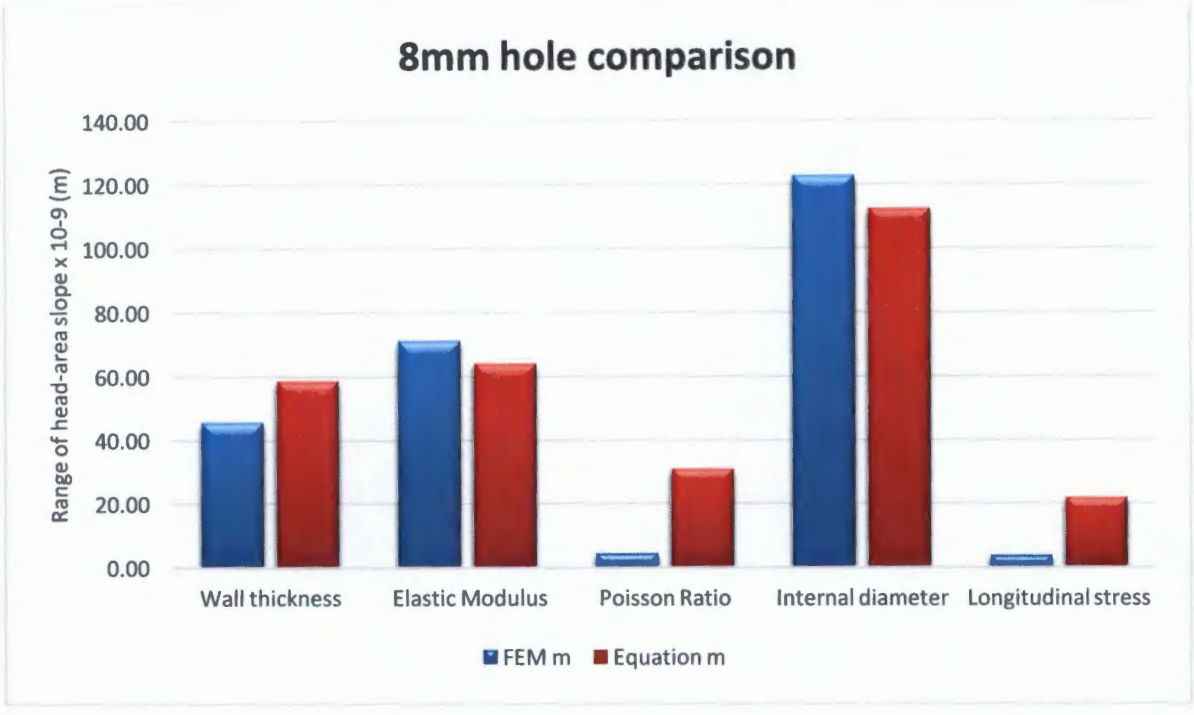

Figure 8-8: Parameter Comparison of Range of the Equation *m* and FEA *m* for the 8 mm Hole

8.7 Discussion

While this study allows the head-area slope of round holes to be predicted by Equation 7-24, the study also shows that round holes show very little variation in area (i.e. very small head-area slopes) compared to other cracks.

Equation 7-24, used to calculate the head-area slope *m,* predicted the FEA *m* reasonably well for the 6 mm hole and the 8 mm hole. This could be due to the fact that very small holes are considered stable holes, and the theoretical elastic theory is not as apparent as it would be for larger holes. Therefore, the equation that is derived from solid mechanics elastic theory may not predict the exact behaviour of very small holes well, and must be used with caution when dealing with very small hole leaks (i.e. holes less than 6 mm in diameter). Generally it was found that larger hole diameters displayed larger absolute head-area slopes for all cases.

Once again, the three parameters that were found to make the most significant influence on the head-area slope for round holes were the internal diameter, wall thickness and the elastic modulus. Based on this finding, it is safe to presume that the head-area slope, *m,* depends on variables describing both pipe geometry and material properties. The Torricelli equation that is still commonly used in practice, does not account for the pipes deformation and geometric factors and yet they are clearly fundamental in influencing the deformability of a leak hole in a pressurised pipe.

This head-area slope expression can be combined with Cassa & van Zyl's (2010) linear relationship of leak area and head and the Torricelli equstion to formulate a new relationship for leakage through round holes.

$$A = A_o + mh \text{ (Cassa \& Van Zyl's 2010 linear relationship equation)}$$

$$Q = C_d A\sqrt{2gh} \text{ (Torricelli equation)}$$

Substituting the above mentioned equation derives the FAVAD equation:

$$Q = C_d\sqrt{2g}\left(A_0 h^{0.5} + mh^{1.5}\right)$$

Finally, substituting the head-area slope equation presented by Equation 7-4 derives the new equation for leakage through a round hole

$$Q = C_d\sqrt{2g}\left(A_0 h^{0.5} + \frac{8A_0 K\rho gr(\alpha - \upsilon + 1 - \upsilon\alpha) - 8\times10^{-9}(tE)}{tE}h^{1.5}\right) \qquad \text{Equation 8-1}$$

Where:

C_d= The discharge coefficient

g = Acceleration due to gravity

A_0 = Initial hole area

h = Pressure head

K = Stress concentration factor

ρ= The fluid density

t = Pipe wall thickness

E = Elastic Modulus of pipe material

α= Ratio of longitudinal stress to circumferential stress

υ= Poisson's ratio

Q= Leakage Flow Rate

Equation 8-1 therefore presents a new equation that can be used for predicting leakage through round hole leaks where both pipe geometry and pipe material properties, which influence the leak are also taken into account.

9 Conclusions and Recommendations

This study focussed on the behaviour of round holes in pressurised pipes. Using finite element analysis the relationship between pressure and leak area was investigated in different pipes with holes of diameters of 4 mm, 6 mm and 8 mm.

Previous literature consistently assumed that round holes in pressurised pipes deform into an ellipse. In this study a validation model was developed to test whether round holes really do deform into elliptical shapes. A mathematical model was developed to calculate the deformed leak area, using Riemann sums, and compared the results of the model to the equivalent ellipse area. It was found that, indeed, a round hole leak does deform into an ellipse.

After investigating the relationship between pressure and leak area, it was found that for materials limited to elastic deformation, the hole areas increase linearly with pressure, as expected. The slope or gradient of this linear relationship, also referred to as the head-area slope m, depends on various parameters: the loading condition, geometric properties and material properties. It is not yet well understood which parameters influence this head-area slope m. In order to investigate which parameters influenced this head-area slope a parametric study was done. The parameters investigated were: elastic modulus, Poisson's ratio, longitudinal stress, wall thickness and pipe internal diameter. The head-area slope obtained from FEA results was plotted against the above mentioned parameters to understand how these parameters affect the head-area slope, and also how the head-area slope behaves when these parameters are varied.

In addition to investigating how the head-area slope m varied with various geometric and material properties, the link between the leakage exponent and the head-area slope was further investigated. Generally, it was found that the leakage exponent for the same leak can vary significantly, depending on the pressure at which it is determined.

Various attempts were then made to find a theoretical expression that describes the head-area slope as a function of these parameters. First an empirical approach, similar to Cassa (2011) was taken, where dimensional analysis and regression models were used to develop an equation. This approach, however, developed different equations for each hole size, and did not generate an equation that could be used for any round hole leak. A second attempt was made to derive a more generic equation that could be used for all round holes. This attempt made use of a more theoretical approach that used elastic solid mechanics theories and other fundamental scientific theories in order to develop the equation. With this new equation the head-area slope can be predicted for different round holes, pipe material conditions and different geometries. This expression is applicable to round holes only.

Finally, the head-area slope that was calculated from the derived equation was compared to the FEA head-area slope, in order to validate the equation.

9.1 Conclusions

If a pipe with a round hole leak is pressurised, the round hole leak becomes elliptical with increasing pressure. This can be attributed to the fact that the circumferential stresses are greater than the longitudinal stresses, and also the effect of the Poisson's ratio on the pipe material.

A new constant α was introduced, as the ratio between the longitudinal stress and the circumferential stress. For the case of buried pipes, the loadings can be categorised into two categories: internal pressure or external loads. The internal pressure comprises of the hydrostatic pressure and the surge pressure. The external loads, on the other hand, are made up of external soil pressure and/or surface (live) loads. Other external loadings to be considered are differential settlements, longitudinal bending and shear loadings. Also, temperature induced stresses, which could be caused by either internal or external effects. In order to incorporate all the above mentioned factors, this study introduced the term '↦'and this term will be denoted as the ratio of longitudinal stress to circumferential stress, as shown below, and can be varied for buried pipes.

$$\alpha = \frac{\sigma_l}{\sigma_c}$$

α ranged from 0, 0.1, 0.2, 0.3 and 0.5; where α=0 is the uniaxial stress state and α=0.5 is the biaxial state stress, where no external factors affect the behaviour of the pipe. Values of greater than 0.5 were not tested because the internal water pressure was found to always be greater than the external loadings and, thus, the possibility of the longitudinal stress increasing more than half the circumferential stress is unlikely, given the normal operational pressures of distribution systems.

In the relationship between pressure and leak area, the results showed that there was a linear expansion in the hole area due to an increase in pressure, regardless of the hole size. However, the slope of the linear lines differed, with larger hole sizes having greater slopes, compared to the smaller holes. This slope was called the head-area slope and was investigated further.

A parametric study was carried out on the head-area slope, to determine which parameters influence the head-area slope most significantly. The parameters included material properties of the pipe (Elastic modulus, Poisson's ratio and longitudinal stress) and geometric properties of the pipe (internal diameters and wall thickness). It was shown how the head-area slope m changed as each individual parameter changed. This was done by varying one parameter at a time, while fixing all the other parameters. In order to determine a suitable range of values to be varied, typical values used in practice for the specific parameter were used.

The parameters that played the most significant role in influencing the head-area slope were the elastic modulus, the internal diameter and the wall thickness. The Poisson's ratio and the longitudinal stress had little effect on the head-area slope *m,* for all three hole sizes investigated.

All three round holes showed similar trend lines, in terms of how the head-area slope behaved with each varied parameter. However, as the hole size increased, the effect of each parameter became more significant. The elastic modulus and wall thickness were inversely proportional to the head-area slope, whilst the longitudinal stress and internal diameter were positively linearly proportional to the head-area slope and, finally, the Poisson's ratio which was negatively linearly proportional to the head-area slope.

The elastic modulus was the only parameter that resulted in some negative head-area slopes. These negative head area slopes occurred for materials with high elastic modulus' (e.g. steel). An experimental study by Malde (2015) also found this to be true. The negative m occurs when $\Delta A = A_{deformed} - A_0 < 0$, i.e.

$$A_0 > A_{deformed}$$
$$\frac{\pi d_0^2}{4} > \frac{\pi d_c d_l}{4}$$
$$d_0^2 > d_c d_l$$

Therefore, from this formulation, it can be seen that when the product of the initial leak hole diameter is greater than the product of the diameter in the longitudinal direction (d_l) and circumferential direction (d_c), then the head-area slope will become negative. The reason why this may happen is because of the Poisson's ratio effect. As a result of the Poisson's ratio effect, the diametric dimensions are reduced when a load is applied and, thus, the overall area reduces. This is especially true for the case where the material has a relatively high Poisson ratio coefficient. Other reasons could be due to local deformation that occurs as a result of the inner material forces which concentrate around the hole. These forces create stress concentrators that tend to magnify the stress levels around the hole area. These stresses are usually higher in the surrounding hole area than they are in surrounding regions of the pipe, causing local deformation of the inside lip of the hole. These deformations cause the inside edge of the hole to rotate and, depending on the material strength, can sometimes result in the hole area contracting. This contraction, therefore, causes the overall leak area to reduce. Finally, local hydraulics can also have an effect, and this effect should not differ from pipe to pipe.

Using the leakage number formula, the leakage number (L_N) can be determined from the head-area slopes and, thereafter, the leakage exponent $N1$ can be obtained. It is important to note, however, that the head-area slopes, found in this study, were all very small. Also, it was noted that for all negative head-area slopes, the corresponding leakage exponent was less than the theoretical 0.5. For all other cases, where the head area slope was positive, the leakage exponent $N1$ was greater than 0.5. Although these $N1$ values varied they were all in the range of 0.4-0.6. Also, it was found that for most of the parameters when the leakage exponent $N1$ was plotted against the parameter, it followed a similar trend to the trend of the head – area slope against the parameter.

Various techniques were then used to obtain the expression for the head-area slopes for round holes. Using solid mechanics theory, a formulation was developed for the expression of the head-area slope. This derivation followed closely to Buckley's (2007) analytical derivation for the theoretical behaviour of round holes. In addition to the analytical procedure, some regression analysis techniques were adopted to improve the results of the derived equation. After using the method of least squares, this study has presented a semi- empirical analytical formula for a reliable evaluation of the behaviour of the head—area slope of round holes, and is given as:

$$m_{eq} = 8.00\left[\left(\frac{A_0 K\rho g r}{tE}\right)(\alpha - \upsilon + 1 - \upsilon\alpha)\right] - 8\times10^{-9}$$

This proposed expression has been calibrated and validated through a comparison with the finite element analysis results. Essentially, the head-area slope calculated using the proposed equation was compared to the head-area slope of the finite element models.

The results of the FEA and equation were compared with experimental values determined by Malde (2015). The results showed that for the equation results were within or close to the 95 % confidence intervals of the experimental study

The head-area slopes of round holes are generally much smaller than those of longitudinal cracks, and practically speaking these slopes may generally be assumed as zero. An exception may be corrosion holes in metal pipes where the wall thickness surrounding the hole has been reduced substantially ((Greyvenstein & Van Zyl, 2007). In most cases, assuming a head-area slope of zero for round holes would be reasonable.

This proposed equation does not predict small holes very well. However, for this case, the 4 mm, 6 mm and 8 mm holes were predicted reasonably well. The new equation for flow through round holes can now be expressed as follows:

$$Q = C_d\sqrt{2g}\left(A_0 h^{0.5} + \frac{8A_0 K\rho g r(\alpha - \upsilon + 1 - \upsilon\alpha) - 8\times10^{-9}(tE)}{tE}h^{1.5}\right)$$

This equation presents a new expression that can be used for predicting leakage through round hole leaks where both pipe geometry and pipe material properties, which influence the leak area, are also taken into account.

9.2 Recommendations

The following recommendations are made for future studies:

- Other forms of failure beyond elastic should be simulated to see how the head-area slope is affected.

- The simulation of actual failed pipes in the field can be run in order to compare how well the equation can predict the actual behaviour of real systems. This study was limited to finite element analysis.
- This equation is valid only for individual leaks, and should be tested for multiple leaks in one system to see how well it models for larger system leakages.

LIST OF REFERENCES

Almeida, B., & Ramos, H. (2010). Water supply operation: diagnosis and reliability analysis in a Lisbon pumping system. *Journal of Water Supply, 59*(1), 66-78.

Ashton, C., & Hope, V. (2001). Environmental valuation and the economic level of leakage . *Urban Water Journal, 3*(4), 261-270.

Bartlett, L. (2004). *Pressure Dependant Demands in Student Town Phase 3.* B.Eng Thesis, University of Johannesburg, Department of Civil Engineering, Johannesburg.

Benham, P., Crawford, P., & Armstrong, C. (1996). *Mechanics of Engineering materials* (2nd edition ed.). Prentice Hall.

Brater, E., & King, H. (1976). *Problems, Handbook of Hydraulics for the solution of Hydraulic Engineering.* University of Michigan. McGraw-Hill.

Buckley. (2007). *pipes., Theoretical Investigation and experimentation into the expansion of round holes and cracks within pressurised.* University of Johannesburg, Department of Civil Engineering.

Buckley, R. (2007). *pipes., Theoretical Investigation and experimentation into the expansion of round holes and cracks within pressurised.* University of Johannesburg, Department of Civil Engineering.

Cassa, A., & Van Zyl, J. (2011). Predicting the head-area slopes and leakage exponents of cracks in pipes. *CCWI.* University of Exeter.

Cassa, A., van Zyl, J., & Laubscher, R. (2010, February 12). A numerical investigation into the effect of pressure on holes and cracks in water supply pipes. *Urban water journal*, 1-12.

Davis, P. (2007). A physical probabilistic model to predict failure rates in buried PVC pipelines. *Reliability Engineering and System Safety*(92), 1258-1266.

Fagan, M. J. (1992). *Finite Element Analysis Theory and Practice* . Malaysia: Pearson Education Limited.

Farshad. (2006). *Plastic pipe systems.* London: Elsevier.

Ferrante, M., Massari, C., Brunone, B., & Meniconi, S. (2011). Experimental evidence of hysteresis in the head-dischargerelationship for a leak in a polyethylene pipe. *Journal of Hydraulic Engineering*, 775-780.

Franchini, M., & Lanza, L. (2013, December 20). Leakages in pipes: generalizing Torricelli's equation to deal with different elastic materials, diameters and orifice shape and dimensions . *Urban Water Journal.*

gcsescience. (2015). *GCSESCIENCE.* Retrieved April 2015, from http://www.gcsescience.com/o58.htm

Gere, J. (2001). *Mechanics of materials* (6th Edition ed.). Thomson Learning Inc.

Greyvenstein, B., & Van Zyl, J. (2007). An experimental investigation into the pressure–leakage relationship of some failed water pipes. *ournal of Water Supply: Research and Technology* .

Greyvenstein, M., & Van Zyl, J. (2007). An experimental investigation into the pressure leakage relationship of some failed water pipes. *Journal of water supply: Research and Technology*, 117-124.

Hibbeler, R. C. (2008). *Mechanics of Material* (7th Edition ed.). Singapore: Prentice Hall.

Hibbit, K. S. (2004). *ABAQUS: Superior Finite Element Analysis Solutions* . USA: Copyright ABAQUS .

Hu, & Hubble. (2007). Factors contributing to the failure of asbestos cement water mains. *Canadian Journal of Civil Engineering*(34), 608-621.

Hughes, F. W., & Brighton, A. J. (1999). *Schaum's Outline of Theory and Problems of Fluid Dynamics.* New York: Mac-Graw-Hill.

Jesus, M.-R., Xitlali, D.-G., Helena, R., & Lopez-Jimenez. (2013). An overview of leaks and intrusion for different pipe materials and failures. *Urban water journal.*

JM. Rodriguez, X. G. (2012). An overview of leaks and intrusion for different pipe materials and failures. *Urban Water Journal*, 47-41.

K. Valravamoorthy, J. L. (1998). Leakage Reduction in Water Distribution Systems: Optimal Valve Controll. *Journal of Hydraulic Engineering, 124.*

Lambert, A. (2001). What do we know about pressure: Leakage relationships in distribution systems? *International Water Data Comparison.*

Lea, F. (1908). Hydraulics. New York: E. Arnold.

Lower, S. (2009). *States of matter: Polymers and plastics*. Retrieved August 26, 2014, from http://www.chem1.com/acad/webtext/states/polymers.html

Makar, M. (2007). Mechanical Behavior of Spun-Cast Gray Iron Pipe. *Journal of Materials in Civil Engineering*, 826-833.

Malde , R., & Van Zyl, J. (2015). *An experimental study of the hydraulic behaviour of leaks with pressure.* Masters Thesis, University of Cape Town, Civil Engineering.

May, J. (1994). Leakage, Pressure and Control BICS., (p. International Conference on leakage control Investigation in underground Assets). London.

Mckenzie, R., Siqalaba, Z., & Wegelin, W. (2012). *The State of Non-Revenue Water in South Africa (2012).* Water Research commission. Water Research Commission.

Microsoft Excel Guide. (2011).

Midstate Steel. (2015). *Midstate Corporation.* Retrieved 2015, from Mids Websitetate: http://midstate-steel.com/how-pipe-is-manufactured.html

Molnar, K., Finno, R., & Rossow, E. (2005, October). *Analysis of effects of deep braced excavations on adjacent buried utilities.* Retrieved from http://www.iti.northewestern.edu/publications: http://www.iti.northewestern.edu/publications

Mosner, A., & Folkman, S. (2008). *Buried Pipe Design* (3rd Edition ed.). USA: MacGraw-Hill.

Nau, R. (2015). *Fuqua School of Business, Duke University.* Retrieved September 2015, from Fuqua School of Business, Duke University: http://people.duke.edu/~rnau/411home.htm

Nsanzubuhoro, R. M., & van Zyl, K. (2013). *Investigating the impact of linear viscoelasticity on the pressure leakage relationship.* Cape Town: University of Cape Town.

Ogura. (1979). *Japan Waterworks*, 38-45.

Olivier de Weck, & IL Yong Kim. (2004, January 12). Finite Element Method.

Peng, L.-C. (1978, May). Stress analysis methods for underground pipelines. *Pipe Line Industry*. Houston.

Prevost, R., & Kienow, K. (1994, July/August). Basics of Flexible Pipe Structural Design. *ASCE J. of Transportation Eng, 120*(4), 652-671.

R. Puust, Z. K. (2010). A review on methods for leakage management in pipe networks. *Urban Water*(7:1), 25-45.

Rahman, S. (2010, November). An objective Understanding of Pipe-Soil interaction, Design and Instalation. *Rigid and Flexible Pipes*.

Rajani, B., & Kleiner, Y. (2001). Comprehensive review of structural deterioration of water mains: physically based models. *Urban water journal, 3*(3), 151-154.

Reynold K, W., & Loren R, A. (1999). *Structural Mechanics of Buried Pipes.* CRC Press.

Roylance, D. (2001, August 23). Stress-Strain Curves. *Massachusetts Institute of Technology*. Cambridge, United States of America.

Schwaller, J. (2012). *Modelling the effects of a large number of leaks in a water distribution network using the FAVAD equation.* University of Applied Sciences Karlsruhe, Civil Engineering.

scu.edu. (n.d.). *Material properties for part design.* Retrieved August 09, 2014, from edu website: http://www.dc.engr.scu.edu/cmdoc/dg_doc/develop/material/property/a2200002.htm

Shames, H. I. (1992). *Mechanics Of Fluids* (3rd Edition ed.). New York: McGraw-Hill.

SHARMA, S. C. (2015). *Department of Mechanical & Industrial Engineering.* Retrieved from Indian Institute of Technology Roorkee: http://nptel.ac.in/courses/Webcourse-contents/IIT-ROORKEE/strength%20of%20materials/lects%20&%20picts/image/lect11/lecture11.htm

Shingo Adachi, S. T. (2014). Estimating area leakage in water networks bades on hydraulic model and asset information. *WDSA.* Yokohama: Elsevier Ltd.

Staff, M. (2011, January 18). *The nature of polyethylene pipe failure.* Retrieved from Plastics Today : http://www.plasticstoday.com/nature-polyethylene-pipe-failure/12289981915310

Stewart, B., & al, e. (1999). Pipe leakage – future challenges and solutions. *In: Pipes Wagga Wagga Conference*, (pp. 1-18). Australia.

Sykes, A. O. (1993). An Introduction to Regression Analysis. Chicago.

Thornton, J. (2003, October). Managing leakage by managing pressure: a practical approach.

Urquhart, W. (1977). Hydraulics. In *Hydraulics.*

van Zyl, J. E. (2014). Theoretical modeling of pressure and leakage in water distribution systems. *16th Conference on Water Distribution System Analysis, WDSA 2014.*

van Zyl, J., & Cassa, A. (2014). Modeling Elastically Deforming Leaks in Water Distribution Pipes. *American Society of Civil Enginners.*

Van Zyl, J., & Clayton, C. (2005). *The effect of pressure on leakage in water distribtion systems.* Institution of Civil Engineers. UK: ICE.

Van Zyl, J., Haarhoff, J., & Husselmann, M. (2003). Potential application of end-use demand modelling in South Africa. . *Journal of the South African Institute of Civil Engineering , 45*(2), 9-19.

Vermersh, M., & Rizzo, A. (2008). *Designing an Action Plan to Control Non-Revenue Water.*

Walski, T., Whitman, B., Baron, M., & Gerloff, F. (2009). *Pressure vs . Flow Relationship for Pipe Leaks. In World Environmental and Water Resources Congress.* Kansas City, Missouri: American Society of Civil Engineers.

Ward, I. (1971). *Mechanical Properties of Solid Polymers.* London, UK: John Wiley & Sons Ltd.

Widas, P. (1997, August 04). *Introduction to Finite Element Analysis.* Retrieved June 10, 2015, from Virginia Tech Material Science and Engineering: http://www.sv.vt.edu/classes/MSE2094_NoteBook/97ClassProj/num/widas/history.html

WISA. (2009). *WISA Newsletter.* Water Institute of Southern Africa.

APPENDICES

A. Regression analyses for pipes with different round holes

A.1 Regression analysis for the 4mm hole

This section contains the full regression analyses of regression models carried out for the 4m hole. It illustrates all the tables that are needed to set up each model. The regression models along with their results and statistics appear after each regression. Both the additive and multiplicative regression models are carried out for the 4mm hole. The values of ρ and μ are 1000kg/m^3 and 0.00114kg/m.s respectively.

A.1.1 Additive Regression models for the 4mm hole

Table 0-1 shows the input values to be used for the additive models.

Table 0-1: Input values to be used for the 4mm hole multiplicative models

Pressure	E(Gpa)	v	t(m)	D(m)	d0	Longitudinal stress	A	
0.00	3.00E+09	0.4	0.003	0.107	0.004	0.00E+00	1.19E-05	Change in Pressure
10.19	3.00E+09	0.4	0.003	0.107	0.004	8.92E+05	1.19E-05	
20.39	3.00E+09	0.4	0.003	0.107	0.004	1.78E+06	1.19311E-05	
30.58	3.00E+09	0.4	0.003	0.107	0.004	2.68E+06	1.19543E-05	
40.77	3.00E+09	0.4	0.003	0.107	0.004	3.57E+06	1.19789E-05	
50.97	3.00E+09	0.4	0.003	0.107	0.004	4.46E+06	1.20027E-05	
61.16	3.00E+09	0.4	0.003	0.107	0.004	5.35E+06	1.20264E-05	
71.36	3.00E+09	0.4	0.003	0.107	0.004	6.24E+06	1.205E-05	
81.55	3.00E+09	0.4	0.003	0.107	0.004	7.13E+06	1.20735E-05	
91.74	3.00E+09	0.4	0.003	0.107	0.004	8.03E+06	1.2097E-05	
101.94	3.00E+09	0.4	0.003	0.107	0.004	8.92E+06	1.21204E-05	
61.16	3.00E+09	0.4	0.003	0.107	0.004	5.20E+06	1.32008E-05	Change in Elastic Modulus
61.16	1.00E+10	0.4	0.003	0.107	0.004	5.20E+06	1.23052E-05	
61.16	3.00E+10	0.4	0.003	0.107	0.004	5.20E+06	1.20264E-05	
61.16	9.00E+10	0.4	0.003	0.107	0.004	5.20E+06	1.19311E-05	
61.16	2.00E+11	0.4	0.003	0.107	0.004	5.20E+06	1.19048E-05	
61.16	3.00E+09	0.17	0.003	0.107	0.004	5.20E+06	1.32033E-05	Change in poisson ratio
61.16	3.00E+09	0.21	0.003	0.107	0.004	5.20E+06	1.32028E-05	
61.16	3.00E+09	0.29	0.003	0.107	0.004	5.20E+06	1.32019E-05	
61.16	3.00E+09	0.4	0.003	0.107	0.004	5.20E+06	1.32008E-05	
61.16	3.00E+09	0.45	0.003	0.107	0.004	5.20E+06	1.32004E-05	
61.16	3.00E+09	0.495	0.003	0.107	0.004	5.20E+06	1.32001E-05	
61.16	3.00E+09	0.4	0.002	0.107	0.004	7.95E+06	1.36975E-05	Change in thickness
61.16	3.00E+09	0.4	0.0025	0.107	0.004	6.30E+06	1.34156E-05	
61.16	3.00E+09	0.4	0.003	0.107	0.004	5.20E+06	1.32007E-05	
61.16	3.00E+09	0.4	0.004	0.107	0.004	3.83E+06	1.28996E-05	
61.16	3.00E+09	0.4	0.005	0.107	0.004	3.00E+06	1.27019E-05	
61.16	3.00E+09	0.4	0.003	0.057	0.004	2.70E+06	1.29548E-05	Change in Internal diameter
61.16	3.00E+09	0.4	0.003	0.087	0.004	4.20E+06	1.29979E-05	
61.16	3.00E+09	0.4	0.003	0.107	0.004	5.20E+06	1.30264E-05	
61.16	3.00E+09	0.4	0.003	0.147	0.004	7.20E+06	1.30829E-05	
61.16	3.00E+09	0.4	0.003	0.214	0.004	1.07E+07	1.3153E-05	
61.16	3.00E+09	0.4	0.003	0.247	0.004	1.22E+07	1.32221E-05	
61.16	3.00E+09	0.4	0.003	0.107	0.004	5.35E+06	1.20264E-05	Change in hole diameter
61.16	3.00E+09	0.4	0.003	0.107	0.006	5.35E+06	3.00989E-05	
61.16	3.00E+09	0.4	0.003	0.107	0.008	5.35E+06	5.37044E-05	
61.16	3.00E+09	0.4	0.003	0.107	0.004	0.00E+00	1.31442E-05	Change in longitudinal stress
61.16	3.00E+09	0.4	0.003	0.107	0.004	1.04E+06	1.31576E-05	
61.16	3.00E+09	0.4	0.003	0.107	0.004	2.08E+06	1.31709E-05	
61.16	3.00E+09	0.4	0.003	0.107	0.004	3.12E+06	1.31843E-05	
61.16	3.00E+09	0.4	0.003	0.107	0.004	5.20E+06	1.31977E-05	

The first regression model to be assessed was taken from the dimensional analysis set shown in chapter 4. The form of the model is:

$$\frac{A}{t^2} = a_1 \frac{\mu}{t\sqrt{\rho E}} + a_2 \frac{\sigma_l}{E} + a_3 \frac{D}{t} + a_4 \frac{d}{t} + a_5 \frac{P}{E} + b \qquad \textbf{Equation i}$$

Table 0-2 that follows shows how the independent and the dependent variables were setup for each data point.

Table 0-2: Input dada for of equation i regression analysis for the 4mm hole

x1	x2	x3	x4	x5	y
$\mu/t(\rho E)^{0.5}$	σ/E	D/t	d/t	P/E	A/t^2
2.19E-07	0.00E+00	3.57E+01	1.33E+00	0.00E+00	1.32E+00
2.19E-07	2.97E-04	3.57E+01	1.33E+00	3.40E-09	1.32E+00
2.19E-07	5.94E-04	3.57E+01	1.33E+00	6.80E-09	1.33E+00
2.19E-07	8.92E-04	3.57E+01	1.33E+00	1.02E-08	1.33E+00
2.19E-07	1.19E-03	3.57E+01	1.33E+00	1.36E-08	1.33E+00
2.19E-07	1.49E-03	3.57E+01	1.33E+00	1.70E-08	1.33E+00
2.19E-07	1.78E-03	3.57E+01	1.33E+00	2.04E-08	1.34E+00
2.19E-07	2.08E-03	3.57E+01	1.33E+00	2.38E-08	1.34E+00
2.19E-07	2.38E-03	3.57E+01	1.33E+00	2.72E-08	1.34E+00
2.19E-07	2.68E-03	3.57E+01	1.33E+00	3.06E-08	1.34E+00
2.19E-07	2.97E-03	3.57E+01	1.33E+00	3.40E-08	1.35E+00
2.19E-07	1.73E-03	3.57E+01	1.33E+00	2.04E-08	1.47E+00
1.20E-07	5.20E-04	3.57E+01	1.33E+00	6.12E-09	1.37E+00
6.94E-08	1.73E-04	3.57E+01	1.33E+00	2.04E-09	1.34E+00
4.01E-08	5.78E-05	3.57E+01	1.33E+00	6.80E-10	1.33E+00
2.69E-08	2.60E-05	3.57E+01	1.33E+00	3.06E-10	1.32E+00
2.19E-07	1.73E-03	3.57E+01	1.33E+00	2.04E-08	1.47E+00
2.19E-07	1.73E-03	3.57E+01	1.33E+00	2.04E-08	1.47E+00
2.19E-07	1.73E-03	3.57E+01	1.33E+00	2.04E-08	1.47E+00
2.19E-07	1.73E-03	3.57E+01	1.33E+00	2.04E-08	1.47E+00
2.19E-07	1.73E-03	3.57E+01	1.33E+00	2.04E-08	1.47E+00
2.19E-07	1.73E-03	3.57E+01	1.33E+00	2.04E-08	1.47E+00
3.29E-07	2.65E-03	5.35E+01	2.00E+00	2.04E-08	3.42E+00
2.63E-07	2.10E-03	4.28E+01	1.60E+00	2.04E-08	2.15E+00
2.19E-07	1.73E-03	3.57E+01	1.33E+00	2.04E-08	1.47E+00
1.65E-07	1.28E-03	2.68E+01	1.00E+00	2.04E-08	8.06E-01
1.32E-07	1.00E-03	2.14E+01	8.00E-01	2.04E-08	5.08E-01
2.19E-07	9.00E-04	1.90E+01	1.33E+00	2.04E-08	1.44E+00
2.19E-07	1.40E-03	2.90E+01	1.33E+00	2.04E-08	1.44E+00
2.19E-07	1.73E-03	3.57E+01	1.33E+00	2.04E-08	1.45E+00
2.19E-07	2.40E-03	4.90E+01	1.33E+00	2.04E-08	1.45E+00
2.19E-07	3.57E-03	7.13E+01	1.33E+00	2.04E-08	1.46E+00
2.19E-07	4.07E-03	8.23E+01	1.33E+00	2.04E-08	1.47E+00
2.19E-07	1.78E-03	3.57E+01	1.33E+00	2.04E-08	1.34E+00
2.19E-07	1.78E-03	3.57E+01	2.00E+00	2.04E-08	3.34E+00
2.19E-07	1.78E-03	3.57E+01	2.67E+00	2.04E-08	5.97E+00
2.19E-07	0.00E+00	3.57E+01	1.33E+00	2.04E-08	1.46E+00
2.19E-07	3.47E-04	3.57E+01	1.33E+00	2.04E-08	1.46E+00
2.19E-07	6.93E-04	3.57E+01	1.33E+00	2.04E-08	1.46E+00
2.19E-07	1.04E-03	3.57E+01	1.33E+00	2.04E-08	1.46E+00
2.19E-07	1.73E-03	3.57E+01	1.33E+00	2.04E-08	1.47E+00

Table 0-3 shows the regression statistics for the additive regression model described above.

Table 0-3: Regression statistics for equation i

10902807.62	3.10026755	-0.00125021	-20.71766507	-989153.6872	-2.60976
6774416.534	0.098194206	0.00422385	65.26098127	622626.2888	0.203018
0.969369293	0.159462384	#N/A	#N/A	#N/A	#N/A
221.5288408	35	#N/A	#N/A	#N/A	#N/A
28.16545581	0.889988816	#N/A	#N/A	#N/A	#N/A

R^2=96.93%	df=35	FDIST=1.8821×10^{-25}

From Table 0-3 it can be seen that the R^2= 96.9% which is a decent fit, the df= 35 and the FDIST= 1.8821×10^{-25}

$$\frac{A}{t^2} = -989153.69\frac{\mu}{t\sqrt{\rho E}} - 20.718\frac{\sigma_1}{E} - 0.00125\frac{D}{t} + 3.1002\frac{d}{t} + 10902807\frac{P}{E} - 2.609$$

The next model is also a set from the dimensionless analysis conducted in Chapter 4. The equation has the basic form:

$$\frac{A}{t^2} = a_1\frac{t\sqrt{\rho E}}{\mu} + a_2\frac{P}{E} + a_3\frac{t}{d} + a_4\frac{t}{D} + a_5\frac{\sigma_1}{E} + b \qquad \textbf{Equation ii}$$

Table 0-4 shows the dependent and the independent variables set up for each FEA data point.

Table 0-4: Input FEA data for equation ii regression analysis for the 4mm hole

x1	x2	x3	x4	x5	y
$t(\rho E)^{0.5}/\mu$	P/E	t/d	t/D	σ/E	A/t^2
4.56E+06	0.00E+00	7.50E-01	0.028037383	0.00E+00	1.32E+00
4.56E+06	3.40E-09	7.50E-01	0.028037383	2.97E-04	1.32E+00
4.56E+06	6.80E-09	7.50E-01	0.028037383	5.94E-04	1.33E+00
4.56E+06	1.02E-08	7.50E-01	0.028037383	8.92E-04	1.33E+00
4.56E+06	1.36E-08	7.50E-01	0.028037383	1.19E-03	1.33E+00
4.56E+06	1.70E-08	7.50E-01	0.028037383	1.49E-03	1.33E+00
4.56E+06	2.04E-08	7.50E-01	0.028037383	1.78E-03	1.34E+00
4.56E+06	2.38E-08	7.50E-01	0.028037383	2.08E-03	1.34E+00
4.56E+06	2.72E-08	7.50E-01	0.028037383	2.38E-03	1.34E+00
4.56E+06	3.06E-08	7.50E-01	0.028037383	2.68E-03	1.34E+00
4.56E+06	3.40E-08	7.50E-01	0.028037383	2.97E-03	1.35E+00
4.56E+06	2.04E-08	7.50E-01	0.028037383	1.73E-03	1.47E+00
8.32E+06	6.12E-09	7.50E-01	0.028037383	5.20E-04	1.37E+00
1.44E+07	2.04E-09	7.50E-01	0.028037383	1.73E-04	1.34E+00
2.50E+07	6.80E-10	7.50E-01	0.028037383	5.78E-05	1.33E+00
3.72E+07	3.06E-10	7.50E-01	0.028037383	2.60E-05	1.32E+00
4.56E+06	2.04E-08	7.50E-01	0.028037383	1.73E-03	1.47E+00
4.56E+06	2.04E-08	7.50E-01	0.028037383	1.73E-03	1.47E+00
4.56E+06	2.04E-08	7.50E-01	0.028037383	1.73E-03	1.47E+00
4.56E+06	2.04E-08	7.50E-01	0.028037383	1.73E-03	1.47E+00
4.56E+06	2.04E-08	7.50E-01	0.028037383	1.73E-03	1.47E+00
4.56E+06	2.04E-08	7.50E-01	0.028037383	1.73E-03	1.47E+00
3.04E+06	2.04E-08	5.00E-01	0.018691589	2.65E-03	3.42E+00
3.80E+06	2.04E-08	6.25E-01	0.023364486	2.10E-03	2.15E+00
4.56E+06	2.04E-08	7.50E-01	0.028037383	1.73E-03	1.47E+00
6.08E+06	2.04E-08	1.00E+00	0.037383178	1.28E-03	8.06E-01
7.60E+06	2.04E-08	1.25E+00	0.046728972	1.00E-03	5.08E-01
4.56E+06	2.04E-08	7.50E-01	0.052631579	9.00E-04	1.44E+00
4.56E+06	2.04E-08	7.50E-01	0.034482759	1.40E-03	1.44E+00
4.56E+06	2.04E-08	7.50E-01	0.028037383	1.73E-03	1.45E+00
4.56E+06	2.04E-08	7.50E-01	0.020408163	2.40E-03	1.45E+00
4.56E+06	2.04E-08	7.50E-01	0.014018692	3.57E-03	1.46E+00
4.56E+06	2.04E-08	7.50E-01	0.012145749	4.07E-03	1.47E+00
4.56E+06	2.04E-08	7.50E-01	0.028037383	1.78E-03	1.34E+00
4.56E+06	2.04E-08	5.00E-01	0.028037383	1.78E-03	3.34E+00
4.56E+06	2.04E-08	3.75E-01	0.028037383	1.78E-03	5.97E+00
4.56E+06	2.04E-08	7.50E-01	0.028037383	0.00E+00	1.46E+00
4.56E+06	2.04E-08	7.50E-01	0.028037383	3.47E-04	1.46E+00
4.56E+06	2.04E-08	7.50E-01	0.028037383	6.93E-04	1.46E+00
4.56E+06	2.04E-08	7.50E-01	0.028037383	1.04E-03	1.46E+00
4.56E+06	2.04E-08	7.50E-01	0.028037383	1.73E-03	1.47E+00

Table 0-5 shows the additional regression statistics for the above model

Table 0-5: Regression Statistics for equation ii for the 4mm hole

157.29798	37.97162377	-6.369973967	-2866496.744	1.18995E-09	5.068614137
158.9017101	18.0595584	0.7386921	18552613.86	1.59744E-08	0.627161297
0.699503909	0.499458207	#N/A	#N/A	#N/A	#N/A
16.29481219	35	#N/A	#N/A	#N/A	#N/A
20.3243971	8.731047526	#N/A	#N/A	#N/A	#N/A

R^2=69.95%	df=35	FDIST=2.702×10^{-8}

The regression statistics shown in Table 0-5 for the model leads to the following equation:

$$\frac{A}{t^2} = 1.18995\times10^{-9}\frac{t\sqrt{\rho E}}{\mu} - 2866496\frac{P}{E} - 6.36997\frac{t}{d} + 37.972\frac{t}{D} + 157.297\frac{\sigma_l}{E} + 5.0686$$

The next additive model shown is based on the dimensionless analysis, the parameters are interchanged such that the unit dimensions are still maintained. The following equation was developed:

$$\frac{A}{D^2} = a_1\frac{\rho\sigma_l D^2}{\mu^2} + a_2\frac{\sigma_l}{E} + a_3\frac{t}{D} + a_4\frac{d}{D} + a_5\frac{P}{E} + b \qquad \textbf{Equation iii}$$

Table 0-6: Input FEA data for equation iii regression analysis of the 4mm hole

x1	x2	x3	x4	x5	y
$\rho\sigma_l D^2/\mu^2$	σ_l / E	t/D	d/D	P/E	A/D^2
0.00E+00	0.00E+00	2.80E-02	3.74E-02	0.00E+00	1.04E-03
7.86E+12	2.97E-04	2.80E-02	3.74E-02	3.40E-09	1.04E-03
1.57E+13	5.94E-04	2.80E-02	3.74E-02	6.80E-09	1.04E-03
2.36E+13	8.92E-04	2.80E-02	3.74E-02	1.02E-08	1.04E-03
3.14E+13	1.19E-03	2.80E-02	3.74E-02	1.36E-08	1.05E-03
3.93E+13	1.49E-03	2.80E-02	3.74E-02	1.70E-08	1.05E-03
4.71E+13	1.78E-03	2.80E-02	3.74E-02	2.04E-08	1.05E-03
5.50E+13	2.08E-03	2.80E-02	3.74E-02	2.38E-08	1.05E-03
6.28E+13	2.38E-03	2.80E-02	3.74E-02	2.72E-08	1.05E-03
7.07E+13	2.68E-03	2.80E-02	3.74E-02	3.06E-08	1.06E-03
7.86E+13	2.97E-03	2.80E-02	3.74E-02	3.40E-08	1.06E-03
4.58E+13	1.73E-03	2.80E-02	3.74E-02	2.04E-08	1.15E-03
4.58E+13	5.20E-04	2.80E-02	3.74E-02	6.12E-09	1.07E-03
4.58E+13	1.73E-04	2.80E-02	3.74E-02	2.04E-09	1.05E-03
4.58E+13	5.78E-05	2.80E-02	3.74E-02	6.80E-10	1.04E-03
4.58E+13	2.60E-05	2.80E-02	3.74E-02	3.06E-10	1.04E-03
4.58E+13	1.73E-03	2.80E-02	3.74E-02	2.04E-08	1.15E-03
4.58E+13	1.73E-03	2.80E-02	3.74E-02	2.04E-08	1.15E-03
4.58E+13	1.73E-03	2.80E-02	3.74E-02	2.04E-08	1.15E-03
4.58E+13	1.73E-03	2.80E-02	3.74E-02	2.04E-08	1.15E-03
4.58E+13	1.73E-03	2.80E-02	3.74E-02	2.04E-08	1.15E-03
4.58E+13	1.73E-03	2.80E-02	3.74E-02	2.04E-08	1.15E-03
7.00E+13	2.65E-03	1.87E-02	3.74E-02	2.04E-08	1.20E-03
5.55E+13	2.10E-03	2.34E-02	3.74E-02	2.04E-08	1.17E-03
4.58E+13	1.73E-03	2.80E-02	3.74E-02	2.04E-08	1.15E-03
3.37E+13	1.28E-03	3.74E-02	3.74E-02	2.04E-08	1.13E-03
2.64E+13	1.00E-03	4.67E-02	3.74E-02	2.04E-08	1.11E-03
6.75E+12	9.00E-04	5.26E-02	7.02E-02	2.04E-08	3.99E-03
2.45E+13	1.40E-03	3.45E-02	4.60E-02	2.04E-08	1.72E-03
4.58E+13	1.73E-03	2.80E-02	3.74E-02	2.04E-08	1.14E-03
1.20E+14	2.40E-03	2.04E-02	2.72E-02	2.04E-08	6.05E-04
3.77E+14	3.57E-03	1.40E-02	1.87E-02	2.04E-08	2.87E-04
5.73E+14	4.07E-03	1.21E-02	1.62E-02	2.04E-08	2.17E-04
4.71E+13	1.78E-03	2.80E-02	3.74E-02	2.04E-08	1.05E-03
4.71E+13	1.78E-03	2.80E-02	5.61E-02	2.04E-08	2.63E-03
4.71E+13	1.78E-03	2.80E-02	7.48E-02	2.04E-08	4.69E-03
0.00E+00	0.00E+00	2.80E-02	3.74E-02	2.04E-08	1.15E-03
9.16E+12	3.47E-04	2.80E-02	3.74E-02	2.04E-08	1.15E-03
1.83E+13	6.93E-04	2.80E-02	3.74E-02	2.04E-08	1.15E-03
2.75E+13	1.04E-03	2.80E-02	3.74E-02	2.04E-08	1.15E-03
4.58E+13	1.73E-03	2.80E-02	3.74E-02	2.04E-08	1.15E-03

Table 0-7 shows the additional regression statistic for the model shown by equation A-3.

Table 0-7: Regression Statistics for equation iii for the 4mm hole

6205.071733	0.091213931	-0.00579217	-0.068363188	2.29052E-18	-0.002242906
3537.477976	0.001958958	0.003341471	0.039649338	2.63565E-19	9.83998E-05
0.988434094	9.03174E-05	#N/A	#N/A	#N/A	#N/A
598.2271417	35	#N/A	#N/A	#N/A	#N/A
2.43994E-05	2.85503E-07	#N/A	#N/A	#N/A	#N/A

R^2=98.84%	df=35	FDIST=7.66031×10^{-33}

The information from Table 0-7 leads to the following equation.

$$\frac{A}{D^2} = 2.291\times10^{-18}\frac{\rho\sigma_l D^2}{\mu^2} - 0.0684\frac{\sigma_l}{E} - 0.0058\frac{t}{D} + 0.0912\frac{d}{D} + 6205.072\frac{P}{E} - 0.00224$$

The final additive regression model was also based on the dimensional analysis results. The parameters are interchanged and the unit dimension is maintained. This model was of the form:

$$\frac{A}{d^2} = a_1\frac{\rho\sigma_l D^2}{\mu^2} + a_2\frac{\sigma_l}{E} + a_3\frac{D}{t} + a_4\frac{D}{d} + a_5\frac{P}{E} + b \qquad \textbf{Equation iv}$$

Table 0-8 is the set up that contains all dependent and independent input variables.

Table 0-8: Input FEA data for equation iv regression analysis for the 4mm hole

x1	x2	x3	x4	x5	y
$\rho\sigma_l D^2/\mu^2$	σ_l/E	D/t	D/d	P/E	A/d^2
0.00E+00	0.00E+00	35.66666667	2.68E+01	0.00E+00	7.43E-01
7.86E+12	2.97E-04	35.66666667	2.68E+01	3.40E-09	7.44E-01
1.57E+13	5.94E-04	35.66666667	2.68E+01	6.80E-09	7.46E-01
2.36E+13	8.92E-04	35.66666667	2.68E+01	1.02E-08	7.47E-01
3.14E+13	1.19E-03	35.66666667	2.68E+01	1.36E-08	7.49E-01
3.93E+13	1.49E-03	35.66666667	2.68E+01	1.70E-08	7.50E-01
4.71E+13	1.78E-03	35.66666667	2.68E+01	2.04E-08	7.52E-01
5.50E+13	2.08E-03	35.66666667	2.68E+01	2.38E-08	7.53E-01
6.28E+13	2.38E-03	35.66666667	2.68E+01	2.72E-08	7.55E-01
7.07E+13	2.68E-03	35.66666667	2.68E+01	3.06E-08	7.56E-01
7.86E+13	2.97E-03	35.66666667	2.68E+01	3.40E-08	7.58E-01
4.58E+13	1.73E-03	35.66666667	2.68E+01	2.04E-08	8.25E-01
4.58E+13	5.20E-04	35.66666667	2.68E+01	6.12E-09	7.69E-01
4.58E+13	1.73E-04	35.66666667	2.68E+01	2.04E-09	7.52E-01
4.58E+13	5.78E-05	35.66666667	2.68E+01	6.80E-10	7.46E-01
4.58E+13	2.60E-05	35.66666667	2.68E+01	3.06E-10	7.44E-01
4.58E+13	1.73E-03	35.66666667	2.68E+01	2.04E-08	8.25E-01
4.58E+13	1.73E-03	35.66666667	2.68E+01	2.04E-08	8.25E-01
4.58E+13	1.73E-03	35.66666667	2.68E+01	2.04E-08	8.25E-01
4.58E+13	1.73E-03	35.66666667	2.68E+01	2.04E-08	8.25E-01
4.58E+13	1.73E-03	35.66666667	2.68E+01	2.04E-08	8.25E-01
4.58E+13	1.73E-03	35.66666667	2.68E+01	2.04E-08	8.25E-01
7.00E+13	2.65E-03	53.5	2.68E+01	2.04E-08	8.56E-01
5.55E+13	2.10E-03	42.8	2.68E+01	2.04E-08	8.38E-01
4.58E+13	1.73E-03	35.66666667	2.68E+01	2.04E-08	8.25E-01
3.37E+13	1.28E-03	26.75	2.68E+01	2.04E-08	8.06E-01
2.64E+13	1.00E-03	21.4	2.68E+01	2.04E-08	7.94E-01
6.75E+12	9.00E-04	19	1.43E+01	2.04E-08	8.10E-01
2.45E+13	1.40E-03	29	2.18E+01	2.04E-08	8.12E-01
4.58E+13	1.73E-03	35.66666667	2.68E+01	2.04E-08	8.14E-01
1.20E+14	2.40E-03	49	3.68E+01	2.04E-08	8.18E-01
3.77E+14	3.57E-03	71.33333333	5.35E+01	2.04E-08	8.22E-01
5.73E+14	4.07E-03	82.33333333	6.18E+01	2.04E-08	8.26E-01
4.71E+13	1.78E-03	35.66666667	2.68E+01	2.04E-08	7.52E-01
4.71E+13	1.78E-03	35.66666667	1.78E+01	2.04E-08	8.36E-01
4.71E+13	1.78E-03	35.66666667	1.34E+01	2.04E-08	8.39E-01
0.00E+00	0.00E+00	35.66666667	2.68E+01	2.04E-08	8.22E-01
9.16E+12	3.47E-04	35.66666667	2.68E+01	2.04E-08	8.22E-01
1.83E+13	6.93E-04	35.66666667	2.68E+01	2.04E-08	8.23E-01
2.75E+13	1.04E-03	35.66666667	2.68E+01	2.04E-08	8.24E-01
4.58E+13	1.73E-03	35.66666667	2.68E+01	2.04E-08	8.25E-01

Table 0-9 shows the regression statistics solutions for the model above.

Table 0-9: Regression statistics for equation iv for the 4mm hole

4177581.282	-0.003496146	0.003481614	-27.63132125	1.15415E-16	0.721051849
1212772.008	0.001624152	0.001249246	13.66434768	1.50671E-16	0.047280254
0.398573531	0.030899682	#N/A	#N/A	#N/A	#N/A
4.63899555	35	#N/A	#N/A	#N/A	#N/A
0.022146341	0.033417662	#N/A	#N/A	#N/A	#N/A
R^2=39.86%	df=35	FDIST=0.00236			

The regression statistics lead to the following equation:

$$\frac{A}{d^2} = 1.1541\frac{\rho\sigma_l D^2}{\mu^2} - 27.6313\frac{\sigma_l}{E} + 0.00348\frac{D}{t} - 0.003496\frac{D}{d} + 4177581.282\frac{P}{E} + 0.721$$

A.1.2 Multiplicative Regression models for the 4mm hole

The following section will show the full regression analyses of the multiplicative regression models that appear for the 4mm round holes. It will include the tables of all the models that were set up for each multiplicative model. The final equations modelled along with the results after each regression are also illustrated.

Table 0-10: Input values to be used for the 4mm hole multiplicative models.

Pressure	E(Gpa)	v	t(m)	D(m)	d0	Longitudinal stress	A	ΔA	
0.00	3.00E+09	0.4	0.003	0.107	0.004	0.00E+00	1.19E-05	0.00E+00	Change in Pressure
10.19	3.00E+09	0.4	0.003	0.107	0.004	8.92E+05	1.19E-05	2.90E-08	
20.39	3.00E+09	0.4	0.003	0.107	0.004	1.78E+06	1.19311E-05	5.11E-08	
30.58	3.00E+09	0.4	0.003	0.107	0.004	2.68E+06	1.19543E-05	7.43E-08	
40.77	3.00E+09	0.4	0.003	0.107	0.004	3.57E+06	1.19789E-05	9.89E-08	
50.97	3.00E+09	0.4	0.003	0.107	0.004	4.46E+06	1.20027E-05	1.23E-07	
61.16	3.00E+09	0.4	0.003	0.107	0.004	5.35E+06	1.20264E-05	1.46E-07	
71.36	3.00E+09	0.4	0.003	0.107	0.004	6.24E+06	1.205E-05	1.70E-07	
81.55	3.00E+09	0.4	0.003	0.107	0.004	7.13E+06	1.20735E-05	1.94E-07	
91.74	3.00E+09	0.4	0.003	0.107	0.004	8.03E+06	1.2097E-05	2.17E-07	
101.94	3.00E+09	0.4	0.003	0.107	0.004	8.92E+06	1.21204E-05	2.40E-07	
61.16	3.00E+09	0.4	0.003	0.107	0.004	5.20E+06	1.32008E-05	1.32E-06	Change in Elastic Modulus
61.16	1.00E+10	0.4	0.003	0.107	0.004	5.20E+06	1.23052E-05	4.25E-07	
61.16	3.00E+10	0.4	0.003	0.107	0.004	5.20E+06	1.20264E-05	1.46E-07	
61.16	9.00E+10	0.4	0.003	0.107	0.004	5.20E+06	1.19311E-05	5.11E-08	
61.16	2.00E+11	0.4	0.003	0.107	0.004	5.20E+06	1.19048E-05	2.48E-08	
61.16	3.00E+09	0.17	0.003	0.107	0.004	5.20E+06	1.32033E-05	1.32E-06	Change in poisson ratio
61.16	3.00E+09	0.21	0.003	0.107	0.004	5.20E+06	1.32028E-05	1.32E-06	
61.16	3.00E+09	0.29	0.003	0.107	0.004	5.20E+06	1.32019E-05	1.32E-06	
61.16	3.00E+09	0.4	0.003	0.107	0.004	5.20E+06	1.32008E-05	1.32E-06	
61.16	3.00E+09	0.45	0.003	0.107	0.004	5.20E+06	1.32004E-05	1.32E-06	
61.16	3.00E+09	0.495	0.003	0.107	0.004	5.20E+06	1.32001E-05	1.32E-06	
61.16	3.00E+09	0.4	0.002	0.107	0.004	7.95E+06	1.36975E-05	1.82E-06	Change in thickness
61.16	3.00E+09	0.4	0.0025	0.107	0.004	6.30E+06	1.34156E-05	1.54E-06	
61.16	3.00E+09	0.4	0.003	0.107	0.004	5.20E+06	1.32007E-05	1.32E-06	
61.16	3.00E+09	0.4	0.004	0.107	0.004	3.83E+06	1.28996E-05	1.02E-06	
61.16	3.00E+09	0.4	0.005	0.107	0.004	3.00E+06	1.27019E-05	8.22E-07	
61.16	3.00E+09	0.4	0.003	0.057	0.004	2.70E+06	1.29548E-05	1.07E-06	Change in Internal diameter
61.16	3.00E+09	0.4	0.003	0.087	0.004	4.20E+06	1.29979E-05	1.12E-06	
61.16	3.00E+09	0.4	0.003	0.107	0.004	5.20E+06	1.30264E-05	1.15E-06	
61.16	3.00E+09	0.4	0.003	0.147	0.004	7.20E+06	1.30829E-05	1.20E-06	
61.16	3.00E+09	0.4	0.003	0.214	0.004	1.07E+07	1.3153E-05	1.27E-06	
61.16	3.00E+09	0.4	0.003	0.247	0.004	1.22E+07	1.32221E-05	1.34E-06	
61.16	3.00E+09	0.4	0.003	0.107	0.004	5.35E+06	1.20264E-05	1.46E-07	Change in hole diameter
61.16	3.00E+09	0.4	0.003	0.107	0.006	5.35E+06	3.00989E-05	1.82E-05	
61.16	3.00E+09	0.4	0.003	0.107	0.008	5.35E+06	5.37044E-05	4.18E-05	
61.16	3.00E+09	0.4	0.003	0.107	0.004	0.00E+00	1.31442E-05	1.26E-06	Change in longitudinal stress
61.16	3.00E+09	0.4	0.003	0.107	0.004	1.04E+06	1.31576E-05	1.28E-06	
61.16	3.00E+09	0.4	0.003	0.107	0.004	2.08E+06	1.31709E-05	1.29E-06	
61.16	3.00E+09	0.4	0.003	0.107	0.004	3.12E+06	1.31843E-05	1.30E-06	
61.16	3.00E+09	0.4	0.003	0.107	0.004	5.20E+06	1.31977E-05	1.32E-06	

The first multiplicative regression that was performed had all the parameters except the longitudinal stress because the longitudinal stress has a data point with 0MPa, which is undefined when the logarithmic transformation is applied. The basic form of the first model was therefore:

$$\Delta A = b \cdot P^{a_1} \cdot E^{a_2} \cdot \upsilon^{a_3} \cdot t^{a_4} \cdot d^{a_5} \cdot D^{a_6} \qquad \textbf{Equation v}$$

Table 0-11 shows the set up that contains all dependent and independent variables

Table 0-11: Input FEA data for equation v for the regression analysis of the 4mm hole

x1	x2	x3	x4	x5	x6	y
log P	log E	log v	log t	log d	log D	log ΔA
1.008330993	9.477121255	-0.397940009	-2.522878745	-2.397940009	-0.970616222	-7.537602002
1.309360988	9.477121255	-0.397940009	-2.522878745	-2.397940009	-0.970616222	-7.291239276
1.485452247	9.477121255	-0.397940009	-2.522878745	-2.397940009	-0.970616222	-7.129011186
1.610390984	9.477121255	-0.397940009	-2.522878745	-2.397940009	-0.970616222	-7.004856407
1.707300997	9.477121255	-0.397940009	-2.522878745	-2.397940009	-0.970616222	-6.911272256
1.786482243	9.477121255	-0.397940009	-2.522878745	-2.397940009	-0.970616222	-6.834602525
1.853429033	9.477121255	-0.397940009	-2.522878745	-2.397940009	-0.970616222	-6.76962006
1.91142098	9.477121255	-0.397940009	-2.522878745	-2.397940009	-0.970616222	-6.713228276
1.962573502	9.477121255	-0.397940009	-2.522878745	-2.397940009	-0.970616222	-6.66348023
2.008330993	9.477121255	-0.397940009	-2.522878745	-2.397940009	-0.970616222	-6.618980637
1.786482243	9.477121255	-0.397940009	-2.522878745	-2.397940009	-0.970616222	-5.879172804
1.786482243	10	-0.397940009	-2.522878745	-2.397940009	-0.970616222	-6.371422065
1.786482243	10.47712125	-0.397940009	-2.522878745	-2.397940009	-0.970616222	-6.834602434
1.786482243	10.95424251	-0.397940009	-2.522878745	-2.397940009	-0.970616222	-7.291290233
1.786482243	11.30103	-0.397940009	-2.522878745	-2.397940009	-0.970616222	-7.605898698
1.786482243	9.477121255	-0.769551079	-2.522878745	-2.397940009	-0.970616222	-5.878329971
1.786482243	9.477121255	-0.677780705	-2.522878745	-2.397940009	-0.970616222	-5.878490153
1.786482243	9.477121255	-0.537602002	-2.522878745	-2.397940009	-0.970616222	-5.878797225
1.786482243	9.477121255	-0.397940009	-2.522878745	-2.397940009	-0.970616222	-5.879172804
1.786482243	9.477121255	-0.346787486	-2.522878745	-2.397940009	-0.970616222	-5.879304352
1.786482243	9.477121255	-0.305394801	-2.522878745	-2.397940009	-0.970616222	-5.879393169
1.786482243	9.477121255	-0.397940009	-2.698970004	-2.397940009	-0.970616222	-5.74052558
1.786482243	9.477121255	-0.397940009	-2.602059991	-2.397940009	-0.970616222	-5.813721897
1.786482243	9.477121255	-0.397940009	-2.522878745	-2.397940009	-0.970616222	-5.879195822
1.786482243	9.477121255	-0.397940009	-2.397940009	-2.397940009	-0.970616222	-5.991561654
1.786482243	9.477121255	-0.397940009	-2.301029996	-2.397940009	-0.970616222	-6.085204376
1.786482243	9.477121255	-0.397940009	-2.522878745	-2.397940009	-1.244125144	-5.968672342
1.786482243	9.477121255	-0.397940009	-2.522878745	-2.397940009	-1.060480747	-5.951608699
1.786482243	9.477121255	-0.397940009	-2.522878745	-2.397940009	-0.970616222	-5.940663823
1.786482243	9.477121255	-0.397940009	-2.522878745	-2.397940009	-0.832682665	-5.919770475
1.786482243	9.477121255	-0.397940009	-2.522878745	-2.397940009	-0.669586227	-5.895185243
1.786482243	9.477121255	-0.397940009	-2.522878745	-2.397940009	-0.607303047	-5.87220218
1.786482243	9.477121255	-0.397940009	-2.522878745	-2.397940009	-0.970616222	-6.834602525
1.786482243	9.477121255	-0.397940009	-2.522878745	-2.22184875	-0.970616222	-4.739476894
1.786482243	9.477121255	-0.397940009	-2.522878745	-2.096910013	-0.970616222	-4.378570769
1.786482243	9.477121255	-0.397940009	-2.522878745	-2.397940009	-0.970616222	-5.898185588
1.786482243	9.477121255	-0.397940009	-2.522878745	-2.397940009	-0.970616222	-5.893622094
1.786482243	9.477121255	-0.397940009	-2.522878745	-2.397940009	-0.970616222	-5.88909226
1.786482243	9.477121255	-0.397940009	-2.522878745	-2.397940009	-0.970616222	-5.884617178
1.786482243	9.477121255	-0.397940009	-2.522878745	-2.397940009	-0.970616222	-5.880196638

Table 0-12 that follows shows the regression statistics solutions for equation v

Table 0-12: Regression statistics for equation v of s the 4mm hole.

0.485210884	6.564963822	-0.600670599	-0.804467239	-0.733025526	1.67739767	12.14282147
0.75026783	1.250136372	1.32667174	0.874739798	0.171350561	0.420179	4.839529777
0.67106834	0.423360479	#N/A	#N/A	#N/A	#N/A	#N/A
11.22079847	33	#N/A	#N/A	#N/A	#N/A	#N/A
12.06689796	5.914725134	#N/A	#N/A	#N/A	#N/A	#N/A

R^2=67.10%	df=33	FDIST=3.54x10-7

The above regression statistics in Table 0-12 lead to the following equation:

$$\Delta A = 1.38\times10^{12.14}\cdot P^{1.677}\cdot E^{-0.733}\cdot \upsilon^{-0.8045}\cdot t^{-0.60067}\cdot d^{6.565}\cdot D^{0.4852}$$

One observation that can be made from the equation above is that the pressure and the elastic modulus are inverse of each other and this observation leads to the next form of equation to be regressed which had the parameters inverse of each other. The equation thus had the form:

$$\Delta A = b\cdot\left(\frac{\mu}{t\sqrt{\rho E}}\right)^{a_1}\cdot\left(\frac{D}{t}\right)^{a_2}\cdot\left(\frac{d}{t}\right)^{a_3}\cdot\left(\frac{P}{E}\right)^{a_4} \qquad \textbf{Equation vi}$$

Table 0-13 shows the set up that contains all dependent and independent variables.

Table 0-13: Input FEA data for equation vi for the regression analysis of the 4mm hole

x1	x3	x4	x5	x5
log(μ/t(ρE)0.5)	log(D/t)	log(d/t)	log(P/E)	log ΔA
-6.658777031	1.552262523	0.124938737	-8.468790262	-7.537602002
-6.658777031	1.552262523	0.124938737	-8.167760266	-7.291239276
-6.658777031	1.552262523	0.124938737	-7.991669007	-7.129011186
-6.658777031	1.552262523	0.124938737	-7.866730271	-7.004856407
-6.658777031	1.552262523	0.124938737	-7.769820258	-6.911272256
-6.658777031	1.552262523	0.124938737	-7.690639012	-6.834602525
-6.658777031	1.552262523	0.124938737	-7.623692222	-6.76962006
-6.658777031	1.552262523	0.124938737	-7.565700275	-6.713228276
-6.658777031	1.552262523	0.124938737	-7.514547753	-6.66348023
-6.658777031	1.552262523	0.124938737	-7.468790262	-6.618980637
-6.658777031	1.552262523	0.124938737	-7.690639012	-5.879172804
-6.920216403	1.552262523	0.124938737	-8.213517757	-6.371422065
-7.158777031	1.552262523	0.124938737	-8.690639012	-6.834602434
-7.397337658	1.552262523	0.124938737	-9.167760266	-7.291290233
-7.570731401	1.552262523	0.124938737	-9.514547753	-7.605898698
-6.658777031	1.552262523	0.124938737	-7.690639012	-5.878329971
-6.658777031	1.552262523	0.124938737	-7.690639012	-5.878490153
-6.658777031	1.552262523	0.124938737	-7.690639012	-5.878797225
-6.658777031	1.552262523	0.124938737	-7.690639012	-5.879172804
-6.658777031	1.552262523	0.124938737	-7.690639012	-5.879304352
-6.658777031	1.552262523	0.124938737	-7.690639012	-5.879393169
-6.482685772	1.728353782	0.301029996	-7.690639012	-5.74052558
-6.579595785	1.631443769	0.204119983	-7.690639012	-5.813721897
-6.658777031	1.552262523	0.124938737	-7.690639012	-5.879195822
-6.783715767	1.427323786	0	-7.690639012	-5.991561654
-6.88062578	1.330413773	-0.096910013	-7.690639012	-6.085204376
-6.658777031	1.278753601	0.124938737	-7.690639012	-5.968672342
-6.658777031	1.462397998	0.124938737	-7.690639012	-5.951608699
-6.658777031	1.552262523	0.124938737	-7.690639012	-5.940663823
-6.658777031	1.69019608	0.124938737	-7.690639012	-5.919770475
-6.658777031	1.853292519	0.124938737	-7.690639012	-5.895185243
-6.658777031	1.915575699	0.124938737	-7.690639012	-5.87220218
-6.658777031	1.552262523	0.124938737	-7.690639012	-6.834602525
-6.658777031	1.552262523	0.301029996	-7.690639012	-4.739476894
-6.658777031	1.552262523	0.425968732	-7.690639012	-4.378570769
-6.658777031	1.552262523	0.124938737	-7.690639012	-5.898185588
-6.658777031	1.552262523	0.124938737	-7.690639012	-5.893622094
-6.658777031	1.552262523	0.124938737	-7.690639012	-5.88909226
-6.658777031	1.552262523	0.124938737	-7.690639012	-5.884617178

Table 0-14 shows the regression statistics solutions for equation vi

Table 0-14: Regression statistics for equation vi for the 4mm hole

2.042725864	5.019402324	-0.08885582	-2.65519456	-8.600914307
0.401624472	1.057518655	0.733387066	0.846177165	3.531180969
0.622907311	0.445021651	#N/A	#N/A	#N/A
14.04087722	34	#N/A	#N/A	#N/A
11.12286111	6.733505174	#N/A	#N/A	#N/A

R^2=62.29%	df=34	FDIST=5.6988×10^{-8}

The above regression statistics in Table 0-14 leads to the following equation:

$$\Delta A = 2.5\times10^{-9}\cdot\left(\frac{\mu}{t\sqrt{\rho E}}\right)^{-2.6552}\cdot\left(\frac{D}{t}\right)^{-0.0889}\cdot\left(\frac{d}{t}\right)^{5.0194}\cdot\left(\frac{P}{E}\right)^{2.04272}$$

With only an R^2 of 62.29% from equation A-6 another multiplicative model was investigated. This model also had the parameters inverse of each other, and followed a similar trend to the relationships forund in the dimensionless analysis, except it was setup in a multiplicative way. This equation had the following form.

$$\Delta A = b\cdot\left(\frac{t\sqrt{\rho E}}{\mu}\right)^{a_1}\cdot\left(\frac{P}{E}\right)^{a_2}\cdot\left(\frac{t}{d}\right)^{a_3}\cdot\left(\frac{t}{D}\right)^{a_4} \qquad \textbf{Equation vi}$$

Table 0-15 shows the set up that contains all dependent and independent variables of equation vii

Table 0-15: Input FEA data for equation vii for the regression analysis of the 4mm hole

x1	x2	x3	x4	x5
log(t(ρE)0.5/μ)	log(P/E)	log(t/d)	log(t/D)	log ΔA
6.658777031	-8.468790262	-0.124938737	-1.552262523	-7.537602002
6.658777031	-8.167760266	-0.124938737	-1.552262523	-7.291239276
6.658777031	-7.991669007	-0.124938737	-1.552262523	-7.129011186
6.658777031	-7.866730271	-0.124938737	-1.552262523	-7.004856407
6.658777031	-7.769820258	-0.124938737	-1.552262523	-6.911272256
6.658777031	-7.690639012	-0.124938737	-1.552262523	-6.834602525
6.658777031	-7.623692222	-0.124938737	-1.552262523	-6.76962006
6.658777031	-7.565700275	-0.124938737	-1.552262523	-6.713228276
6.658777031	-7.514547753	-0.124938737	-1.552262523	-6.66348023
6.658777031	-7.468790262	-0.124938737	-1.552262523	-6.618980637
6.658777031	-7.690639012	-0.124938737	-1.552262523	-5.879172804
6.920216403	-8.213517757	-0.124938737	-1.552262523	-6.371422065
7.158777031	-8.690639012	-0.124938737	-1.552262523	-6.834602434
7.397337658	-9.167760266	-0.124938737	-1.552262523	-7.291290233
7.570731401	-9.514547753	-0.124938737	-1.552262523	-7.605898698
6.658777031	-7.690639012	-0.124938737	-1.552262523	-5.878329971
6.658777031	-7.690639012	-0.124938737	-1.552262523	-5.878490153
6.658777031	-7.690639012	-0.124938737	-1.552262523	-5.878797225
6.658777031	-7.690639012	-0.124938737	-1.552262523	-5.879172804
6.658777031	-7.690639012	-0.124938737	-1.552262523	-5.879304352
6.658777031	-7.690639012	-0.124938737	-1.552262523	-5.879393169
6.482685772	-7.690639012	-0.301029996	-1.728353782	-5.74052558
6.579595785	-7.690639012	-0.204119983	-1.631443769	-5.813721897
6.658777031	-7.690639012	-0.124938737	-1.552262523	-5.879195822
6.783715767	-7.690639012	0	-1.427323786	-5.991561654
6.88062578	-7.690639012	0.096910013	-1.330413773	-6.085204376
6.658777031	-7.690639012	-0.124938737	-1.278753601	-5.968672342
6.658777031	-7.690639012	-0.124938737	-1.462397998	-5.951608699
6.658777031	-7.690639012	-0.124938737	-1.552262523	-5.940663823
6.658777031	-7.690639012	-0.124938737	-1.69019608	-5.919770475
6.658777031	-7.690639012	-0.124938737	-1.853292519	-5.895185243
6.658777031	-7.690639012	-0.124938737	-1.915575699	-5.87220218
6.658777031	-7.690639012	-0.124938737	-1.552262523	-6.834602525
6.658777031	-7.690639012	-0.301029996	-1.552262523	-4.739476894
6.658777031	-7.690639012	-0.425968732	-1.552262523	-4.378570769
6.658777031	-7.690639012	-0.124938737	-1.552262523	-5.898185588
6.658777031	-7.690639012	-0.124938737	-1.552262523	-5.893622094
6.658777031	-7.690639012	-0.124938737	-1.552262523	-5.88909226
6.658777031	-7.690639012	-0.124938737	-1.552262523	-5.884617178

Table 0-16 shows the regression statistics solutions for equation vii

Table 0-16: Regression statistics for equation vii

0.08885582	-5.019402324	2.042725864	2.65519456	-8.600914307
0.733387066	1.057518655	0.401624472	0.846177165	3.531180969
0.622907311	0.445021651	#N/A	#N/A	#N/A
14.04087722	34	#N/A	#N/A	#N/A
11.12286111	6.733505174	#N/A	#N/A	#N/A
#N/A	#N/A	#N/A	#N/A	#N/A

R^2=62.29%	df=34	FDIST=5.70x10^{-8}

The above regression statistics in Table 0-16 leads to the following equation:

$$\Delta A = 2.511\times10^{-9}\cdot\left(\frac{t\sqrt{\rho E}}{\mu}\right)^{2.655}\cdot\left(\frac{P}{E}\right)^{2.043}\cdot\left(\frac{t}{d}\right)^{-5.019}\cdot\left(\frac{t}{D}\right)^{0.088}$$

A.1.3 Discussion on the 4mm hole regression models

Based on the above additive and multiplicative regression models, the best fit model was that presented by equation iii. It is possible to see how good this relationship actually is by comparing the regression model of equation iii to the FEA data values. Simply plotting the model against the dependent variable's values does this. Figure 0-1 shows the correlation between the regression model and the FEA data values of equation iii.

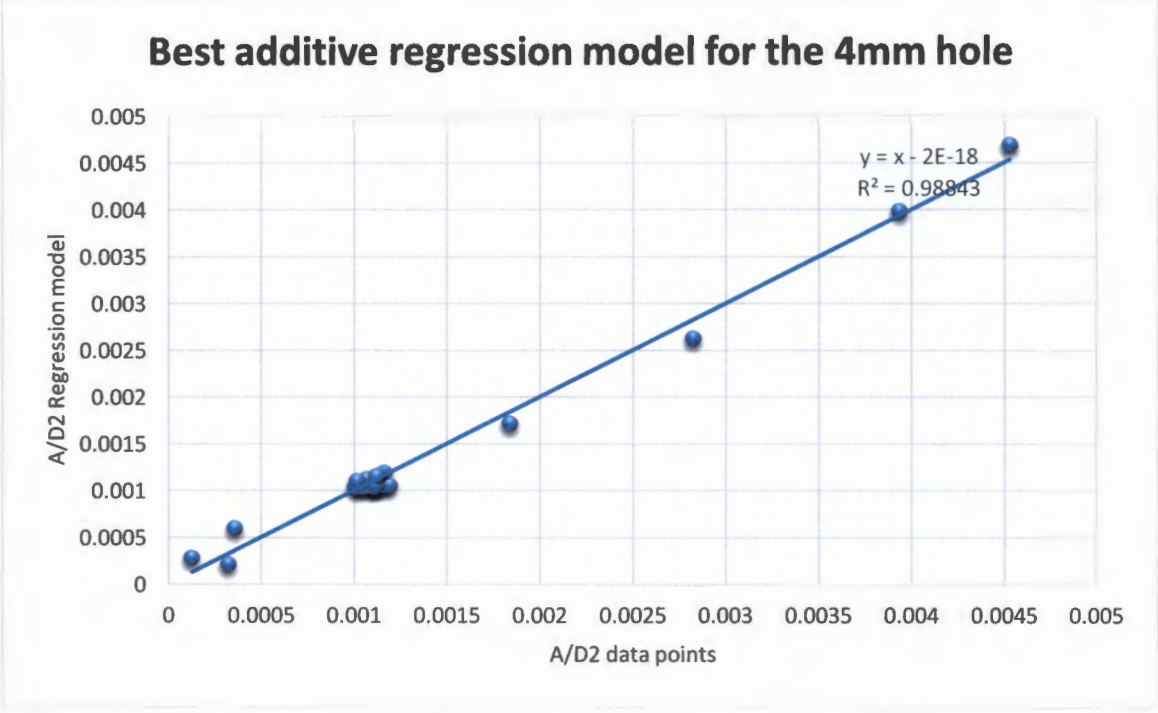

Figure 0-1: Correlation between regression model of equation iii and the date values.

A.2 Regression analysis for the 6mm hole

The same additive and multiplicative regression models that were used for the 4mm holes were also used for the 6mm hole. This section contains the full regression analyses of regression models used for the 6mm hole. Also, other tables that are needed to set up each model are shown. The equations that have been modeled along with their results and additional statistics appear after each regression. Both the additive and multiplicative regression models are carried out. The values of ρ and μ are 1000kg/m^3 and 0.00114kg/m.s respectively.

A.2.1 Additive Regression models for the 6mm hole

This section starts with Table 0-7 that shows the input values to be used for the additive models of the 6mm hole.

Table 0-17: Input values to be used for the 6mm hole additive models.

Pressure	E(Gpa)	v	t(m)	D(m)	d0	Longitudinal stress	A	
0	3.00E+09	0.4	0.003	0.107	0.006	0.00E+00	2.75E-05	Change in Pressure
10.19367992	3.00E+09	0.4	0.003	0.107	0.006	8.92E+05	2.78E-05	
20.38735984	3.00E+09	0.4	0.003	0.107	0.006	1.78E+06	2.83207E-05	
30.58103976	3.00E+09	0.4	0.003	0.107	0.006	2.68E+06	2.87913E-05	
40.77471967	3.00E+09	0.4	0.003	0.107	0.006	3.57E+06	2.92439E-05	
50.96839959	3.00E+09	0.4	0.003	0.107	0.006	4.46E+06	2.96805E-05	
61.16207951	3.00E+09	0.4	0.003	0.107	0.006	5.35E+06	3.00989E-05	
71.35575943	3.00E+09	0.4	0.003	0.107	0.006	6.24E+06	3.05E-05	
81.54943935	3.00E+09	0.4	0.003	0.107	0.006	7.13E+06	3.08837E-05	
91.74311927	3.00E+09	0.4	0.003	0.107	0.006	8.03E+06	0.00003125	
101.9367992	3.00E+09	0.4	0.003	0.107	0.006	8.92E+06	3.15988E-05	
61.16207951	3.00E+09	0.4	0.003	0.107	0.006	5.20E+06	3.00989E-05	Change in Elastic Modulus
61.16207951	1.00E+10	0.4	0.003	0.107	0.006	5.20E+06	2.82244E-05	
61.16207951	3.00E+10	0.4	0.003	0.107	0.006	5.20E+06	2.76325E-05	
61.16207951	9.00E+10	0.4	0.003	0.107	0.006	5.20E+06	2.74296E-05	
61.16207951	2.00E+11	0.4	0.003	0.107	0.006	5.20E+06	2.73734E-05	
61.16207951	3.00E+09	0.17	0.003	0.107	0.006	5.20E+06	3.01569E-05	Change in poisson ratio
61.16207951	3.00E+09	0.21	0.003	0.107	0.006	5.20E+06	3.01464E-05	
61.16207951	3.00E+09	0.29	0.003	0.107	0.006	5.20E+06	3.01258E-05	
61.16207951	3.00E+09	0.4	0.003	0.107	0.006	5.20E+06	3.00989E-05	
61.16207951	3.00E+09	0.45	0.003	0.107	0.006	5.20E+06	3.00875E-05	
61.16207951	3.00E+09	0.495	0.003	0.107	0.006	5.20E+06	3.00778E-05	
61.16207951	3.00E+09	0.4	0.002	0.107	0.006	7.95E+06	3.10503E-05	Change in thickness
61.16207951	3.00E+09	0.4	0.0025	0.107	0.006	6.30E+06	3.06072E-05	
61.16207951	3.00E+09	0.4	0.003	0.107	0.006	5.20E+06	3.00989E-05	
61.16207951	3.00E+09	0.4	0.004	0.107	0.006	3.83E+06	2.96383E-05	
61.16207951	3.00E+09	0.4	0.005	0.107	0.006	3.00E+06	2.92303E-05	
61.16207951	3.00E+09	0.4	0.003	0.057	0.006	2.70E+06	0.000028825	Change in Internal diameter
61.16207951	3.00E+09	0.4	0.003	0.087	0.006	4.20E+06	2.96792E-05	
61.16207951	3.00E+09	0.4	0.003	0.107	0.006	5.20E+06	3.02196E-05	
61.16207951	3.00E+09	0.4	0.003	0.147	0.006	7.20E+06	3.12266E-05	
61.16207951	3.00E+09	0.4	0.003	0.214	0.006	1.07E+07	3.23524E-05	
61.16207951	3.00E+09	0.4	0.003	0.247	0.006	1.22E+07	3.3324E-05	
61.16207951	3.00E+09	0.4	0.003	0.107	0.004	5.35E+06	1.20264E-05	Change in hole diameter
61.16207951	3.00E+09	0.4	0.003	0.107	0.006	5.35E+06	3.00989E-05	
61.16207951	3.00E+09	0.4	0.003	0.107	0.008	5.35E+06	5.37044E-05	
61.16207951	3.00E+09	0.4	0.003	0.107	0.006	0.00E+00	2.99667E-05	Change in longitudinal stress
61.16207951	3.00E+09	0.4	0.003	0.107	0.006	1.04E+06	0.000029998	
61.16207951	3.00E+09	0.4	0.003	0.107	0.006	2.08E+06	3.00293E-05	
61.16207951	3.00E+09	0.4	0.003	0.107	0.006	3.12E+06	3.00605E-05	
61.16207951	3.00E+09	0.4	0.003	0.107	0.006	5.20E+06	3.00918E-05	

The first regression model was taken from the dimensional analysis and the form of the model is:

$$\frac{A}{t^2} = a_1 \frac{\mu}{t\sqrt{\rho E}} + a_2 \frac{\sigma_l}{E} + a_3 \frac{D}{t} + a_4 \frac{d}{t} + a_5 \frac{P}{E} + b \qquad \textbf{equation i}$$

Table 0-18 that follows shows how the independent and the dependent variables were set up in Excel.

Table 0-18: Input FEA data for equation i for the regression analysis of the 6mm hole

x1	x2	x3	x4	x5	y
μ/(ρE)0.5	σ/E	D/t	d/t	P/E	A/t2
2.19E-07	0.00E+00	3.57E+01	2.00E+00	0.00E+00	3.06E+00
2.19E-07	2.97E-04	3.57E+01	2.00E+00	3.40E-09	3.09E+00
2.19E-07	5.94E-04	3.57E+01	2.00E+00	6.80E-09	3.15E+00
2.19E-07	8.92E-04	3.57E+01	2.00E+00	1.02E-08	3.20E+00
2.19E-07	1.19E-03	3.57E+01	2.00E+00	1.36E-08	3.25E+00
2.19E-07	1.49E-03	3.57E+01	2.00E+00	1.70E-08	3.30E+00
2.19E-07	1.78E-03	3.57E+01	2.00E+00	2.04E-08	3.34E+00
2.19E-07	2.08E-03	3.57E+01	2.00E+00	2.38E-08	3.39E+00
2.19E-07	2.38E-03	3.57E+01	2.00E+00	2.72E-08	3.43E+00
2.19E-07	2.68E-03	3.57E+01	2.00E+00	3.06E-08	3.47E+00
2.19E-07	2.97E-03	3.57E+01	2.00E+00	3.40E-08	3.51E+00
2.19E-07	1.73E-03	3.57E+01	2.00E+00	2.04E-08	3.34E+00
1.20E-07	5.20E-04	3.57E+01	2.00E+00	6.12E-09	3.14E+00
6.94E-08	1.73E-04	3.57E+01	2.00E+00	2.04E-09	3.07E+00
4.01E-08	5.78E-05	3.57E+01	2.00E+00	6.80E-10	3.05E+00
2.69E-08	2.60E-05	3.57E+01	2.00E+00	3.06E-10	3.04E+00
2.19E-07	1.73E-03	3.57E+01	2.00E+00	2.04E-08	3.35E+00
2.19E-07	1.73E-03	3.57E+01	2.00E+00	2.04E-08	3.35E+00
2.19E-07	1.73E-03	3.57E+01	2.00E+00	2.04E-08	3.35E+00
2.19E-07	1.73E-03	3.57E+01	2.00E+00	2.04E-08	3.34E+00
2.19E-07	1.73E-03	3.57E+01	2.00E+00	2.04E-08	3.34E+00
2.19E-07	1.73E-03	3.57E+01	2.00E+00	2.04E-08	3.34E+00
3.29E-07	2.65E-03	5.35E+01	3.00E+00	2.04E-08	7.76E+00
2.63E-07	2.10E-03	4.28E+01	2.40E+00	2.04E-08	4.90E+00
2.19E-07	1.73E-03	3.57E+01	2.00E+00	2.04E-08	3.34E+00
1.65E-07	1.28E-03	2.68E+01	1.50E+00	2.04E-08	1.85E+00
1.32E-07	1.00E-03	2.14E+01	1.20E+00	2.04E-08	1.17E+00
2.19E-07	9.00E-04	1.90E+01	2.00E+00	2.04E-08	3.20E+00
2.19E-07	1.40E-03	2.90E+01	2.00E+00	2.04E-08	3.30E+00
2.19E-07	1.73E-03	3.57E+01	2.00E+00	2.04E-08	3.36E+00
2.19E-07	2.40E-03	4.90E+01	2.00E+00	2.04E-08	3.47E+00
2.19E-07	3.57E-03	7.13E+01	2.00E+00	2.04E-08	3.59E+00
2.19E-07	4.07E-03	8.23E+01	2.00E+00	2.04E-08	3.70E+00
2.19E-07	1.78E-03	3.57E+01	1.33E+00	2.04E-08	1.34E+00
2.19E-07	1.78E-03	3.57E+01	2.00E+00	2.04E-08	3.34E+00
2.19E-07	1.78E-03	3.57E+01	2.67E+00	2.04E-08	5.97E+00
2.19E-07	0.00E+00	3.57E+01	2.00E+00	2.04E-08	3.33E+00
2.19E-07	3.47E-04	3.57E+01	2.00E+00	2.04E-08	3.33E+00
2.19E-07	6.93E-04	3.57E+01	2.00E+00	2.04E-08	3.34E+00
2.19E-07	1.04E-03	3.57E+01	2.00E+00	2.04E-08	3.34E+00
2.19E-07	1.73E-03	3.57E+01	2.00E+00	2.04E-08	3.34E+00

Table 0-19 shows the regression statistics for the additive regression model

Table 0-19: Regression statistics of equation i for the 6mm hole

10493850.13	3.498385557	0.003127655	62.16312644	410661.2987	-4.097648
8103180.448	0.129620747	0.005070687	77.32091248	783291.0728	0.278598
0.968907877	0.189731323	#N/A	#N/A	#N/A	#N/A
218.1374058	35	#N/A	#N/A	#N/A	#N/A
39.26252434	1.259929123	#N/A	#N/A	#N/A	#N/A

R^2=96.89%	df=35	FDIST=2.442×10^{-25}

The regression statistics shown in Table 0-19 leads to the following equation:

$$\frac{A}{t^2} = 410661.2987\frac{\mu}{t\sqrt{\rho E}} + 62.163\frac{\sigma_l}{E} + 0.00313\frac{D}{t} + 3.4984\frac{d}{t} + 10493850.13\frac{P}{E} - 4.098$$

The next model is also a set from the dimensionless analysis conducted in Chapter 4. The next equation investigated has the basic form:

$$\frac{A}{t^2} = a_1\frac{t\sqrt{\rho E}}{\mu} + a_2\frac{P}{E} + a_3\frac{t}{d} + a_4\frac{t}{D} + a_5\frac{\sigma_l}{E} + b$$

equation ii

Table 0-20 shows the dependent and the independent variables set up on Excel for each FEA data point.

Table 0-20: Input FEA data of equation ii for the regression analysis of the 6mm hole

x1	x2	x3	x4	x5	y
t(ρE)0.5/μ	P/E	t/d	t/D	σ/E	A/t2
4.56E+06	0.00E+00	5.00E-01	0.028037383	0.00E+00	3.06E+00
4.56E+06	3.40E-09	5.00E-01	0.028037383	2.97E-04	3.09E+00
4.56E+06	6.80E-09	5.00E-01	0.028037383	5.94E-04	3.15E+00
4.56E+06	1.02E-08	5.00E-01	0.028037383	8.92E-04	3.20E+00
4.56E+06	1.36E-08	5.00E-01	0.028037383	1.19E-03	3.25E+00
4.56E+06	1.70E-08	5.00E-01	0.028037383	1.49E-03	3.30E+00
4.56E+06	2.04E-08	5.00E-01	0.028037383	1.78E-03	3.34E+00
4.56E+06	2.38E-08	5.00E-01	0.028037383	2.08E-03	3.39E+00
4.56E+06	2.72E-08	5.00E-01	0.028037383	2.38E-03	3.43E+00
4.56E+06	3.06E-08	5.00E-01	0.028037383	2.68E-03	3.47E+00
4.56E+06	3.40E-08	5.00E-01	0.028037383	2.97E-03	3.51E+00
4.56E+06	2.04E-08	5.00E-01	0.028037383	1.73E-03	3.34E+00
8.32E+06	6.12E-09	5.00E-01	0.028037383	5.20E-04	3.14E+00
1.44E+07	2.04E-09	5.00E-01	0.028037383	1.73E-04	3.07E+00
2.50E+07	6.80E-10	5.00E-01	0.028037383	5.78E-05	3.05E+00
3.72E+07	3.06E-10	5.00E-01	0.028037383	2.60E-05	3.04E+00
4.56E+06	2.04E-08	5.00E-01	0.028037383	1.73E-03	3.35E+00
4.56E+06	2.04E-08	5.00E-01	0.028037383	1.73E-03	3.35E+00
4.56E+06	2.04E-08	5.00E-01	0.028037383	1.73E-03	3.35E+00
4.56E+06	2.04E-08	5.00E-01	0.028037383	1.73E-03	3.34E+00
4.56E+06	2.04E-08	5.00E-01	0.028037383	1.73E-03	3.34E+00
4.56E+06	2.04E-08	5.00E-01	0.028037383	1.73E-03	3.34E+00
3.04E+06	2.04E-08	3.33E-01	0.018691589	2.65E-03	7.76E+00
3.80E+06	2.04E-08	4.17E-01	0.023364486	2.10E-03	4.90E+00
4.56E+06	2.04E-08	5.00E-01	0.028037383	1.73E-03	3.34E+00
6.08E+06	2.04E-08	6.67E-01	0.037383178	1.28E-03	1.85E+00
7.60E+06	2.04E-08	8.33E-01	0.046728972	1.00E-03	1.17E+00
4.56E+06	2.04E-08	5.00E-01	0.052631579	9.00E-04	3.20E+00
4.56E+06	2.04E-08	5.00E-01	0.034482759	1.40E-03	3.30E+00
4.56E+06	2.04E-08	5.00E-01	0.028037383	1.73E-03	3.36E+00
4.56E+06	2.04E-08	5.00E-01	0.020408163	2.40E-03	3.47E+00
4.56E+06	2.04E-08	5.00E-01	0.014018692	3.57E-03	3.59E+00
4.56E+06	2.04E-08	5.00E-01	0.012145749	4.07E-03	3.70E+00
4.56E+06	2.04E-08	7.50E-01	0.028037383	1.78E-03	1.34E+00
4.56E+06	2.04E-08	5.00E-01	0.028037383	1.78E-03	3.34E+00
4.56E+06	2.04E-08	3.75E-01	0.028037383	1.78E-03	5.97E+00
4.56E+06	2.04E-08	5.00E-01	0.028037383	0.00E+00	3.33E+00
4.56E+06	2.04E-08	5.00E-01	0.028037383	3.47E-04	3.33E+00
4.56E+06	2.04E-08	5.00E-01	0.028037383	6.93E-04	3.34E+00
4.56E+06	2.04E-08	5.00E-01	0.028037383	1.04E-03	3.34E+00
4.56E+06	2.04E-08	5.00E-01	0.028037383	1.73E-03	3.34E+00

Table 0-21 shows the regression statistics for the additive regression model

Table 0-21: Regression statistics of equation ii for the 6m hole

225.2216239	7.625761126	-10.73351916	1530039.037	-3.87236E-09	8.297907598
167.1398249	19.13557228	1.205570912	19447469.57	1.67385E-08	0.666271765
0.762903623	0.523933663	#N/A	#N/A	#N/A	#N/A
22.52385899	35	#N/A	#N/A	#N/A	#N/A
30.91472656	9.6077269	#N/A	#N/A	#N/A	#N/A

R^2=76.29%	df=35	FDIST=4.80344x10^{-10}

The regression statistics shown in Table 0-21 leads to the following equation:

$$\frac{A}{t^2} = -3.872\times10^{-9}\frac{t\sqrt{\rho E}}{\mu} + 1530039.037\frac{P}{E} - 10.734\frac{t}{d} + 7.626\frac{t}{D} + 225.222\frac{\sigma_l}{E} + 8.2979$$

The next additive model shown is also based on the dimensionless analysis, the parameters of the dependent and independent variables are interchanged such that the unitless dimensions are still maintained. The following equation was thus developed:

$$\frac{A}{D^2} = a_1\frac{\rho\sigma_l D^2}{\mu^2} + a_2\frac{\sigma_l}{E} + a_3\frac{t}{D} + a_4\frac{d}{D} + a_5\frac{P}{E} + b \qquad \textbf{equation iii}$$

Table 0-22 that follows shows how the independent and the dependent variables were set up in Excel.

Table 0-22: Input FEA data of equation iii for the regression analysis of the 6mm hole

x1	x2	x3	x4	x5	y
$\rho\sigma_l D^2/\mu^2$	σ_l/E	t/D	d/D	P/E	A/D2
0.00E+00	0.00E+00	2.80E-02	5.61E-02	0.00E+00	2.40E-03
7.86E+12	2.97E-04	2.80E-02	5.61E-02	3.40E-09	2.43E-03
1.57E+13	5.94E-04	2.80E-02	5.61E-02	6.80E-09	2.47E-03
2.36E+13	8.92E-04	2.80E-02	5.61E-02	1.02E-08	2.51E-03
3.14E+13	1.19E-03	2.80E-02	5.61E-02	1.36E-08	2.55E-03
3.93E+13	1.49E-03	2.80E-02	5.61E-02	1.70E-08	2.59E-03
4.71E+13	1.78E-03	2.80E-02	5.61E-02	2.04E-08	2.63E-03
5.50E+13	2.08E-03	2.80E-02	5.61E-02	2.38E-08	2.66E-03
6.28E+13	2.38E-03	2.80E-02	5.61E-02	2.72E-08	2.70E-03
7.07E+13	2.68E-03	2.80E-02	5.61E-02	3.06E-08	2.73E-03
7.86E+13	2.97E-03	2.80E-02	5.61E-02	3.40E-08	2.76E-03
4.58E+13	1.73E-03	2.80E-02	5.61E-02	2.04E-08	2.63E-03
4.58E+13	5.20E-04	2.80E-02	5.61E-02	6.12E-09	2.47E-03
4.58E+13	1.73E-04	2.80E-02	5.61E-02	2.04E-09	2.41E-03
4.58E+13	5.78E-05	2.80E-02	5.61E-02	6.80E-10	2.40E-03
4.58E+13	2.60E-05	2.80E-02	5.61E-02	3.06E-10	2.39E-03
4.58E+13	1.73E-03	2.80E-02	5.61E-02	2.04E-08	2.63E-03
4.58E+13	1.73E-03	2.80E-02	5.61E-02	2.04E-08	2.63E-03
4.58E+13	1.73E-03	2.80E-02	5.61E-02	2.04E-08	2.63E-03
4.58E+13	1.73E-03	2.80E-02	5.61E-02	2.04E-08	2.63E-03
4.58E+13	1.73E-03	2.80E-02	5.61E-02	2.04E-08	2.63E-03
4.58E+13	1.73E-03	2.80E-02	5.61E-02	2.04E-08	2.63E-03
7.00E+13	2.65E-03	1.87E-02	5.61E-02	2.04E-08	2.71E-03
5.55E+13	2.10E-03	2.34E-02	5.61E-02	2.04E-08	2.67E-03
4.58E+13	1.73E-03	2.80E-02	5.61E-02	2.04E-08	2.63E-03
3.37E+13	1.28E-03	3.74E-02	5.61E-02	2.04E-08	2.59E-03
2.64E+13	1.00E-03	4.67E-02	5.61E-02	2.04E-08	2.55E-03
6.75E+12	9.00E-04	5.26E-02	1.05E-01	2.04E-08	8.87E-03
2.45E+13	1.40E-03	3.45E-02	6.90E-02	2.04E-08	3.92E-03
4.58E+13	1.73E-03	2.80E-02	5.61E-02	2.04E-08	2.64E-03
1.20E+14	2.40E-03	2.04E-02	4.08E-02	2.04E-08	1.45E-03
3.77E+14	3.57E-03	1.40E-02	2.80E-02	2.04E-08	7.06E-04
5.73E+14	4.07E-03	1.21E-02	2.43E-02	2.04E-08	5.46E-04
4.71E+13	1.78E-03	2.80E-02	3.74E-02	2.04E-08	1.05E-03
4.71E+13	1.78E-03	2.80E-02	5.61E-02	2.04E-08	2.63E-03
4.71E+13	1.78E-03	2.80E-02	7.48E-02	2.04E-08	4.69E-03
0.00E+00	0.00E+00	2.80E-02	5.61E-02	2.04E-08	2.62E-03
9.16E+12	3.47E-04	2.80E-02	5.61E-02	2.04E-08	2.62E-03
1.83E+13	6.93E-04	2.80E-02	5.61E-02	2.04E-08	2.62E-03
2.75E+13	1.04E-03	2.80E-02	5.61E-02	2.04E-08	2.63E-03
4.58E+13	1.73E-03	2.80E-02	5.61E-02	2.04E-08	2.63E-03

Table 0-23 shows the regression statistics for the additive regression model

Table 0-23: Regression statistics for the additive model of equation iii

9778.948088	0.114822277	0.009302735	-0.012765392	3.52422E-18	-0.004372789
6434.149033	0.003792871	0.006965406	0.071791977	4.85588E-19	0.000192555
0.983506768	0.000164086	#N/A	#N/A	#N/A	#N/A
417.4165003	35	#N/A	#N/A	#N/A	#N/A
5.61932E-05	9.42349E-07	#N/A	#N/A	#N/A	#N/A

R2=98.35%	df=35	FDIST=3.7877×10^{-30}

The regression statistics shown in Table 0-23 leads to the following equation:

$$\frac{A}{D^2} = 3.524\times10^{-18}\frac{\rho\sigma_l D^2}{\mu^2} - 0.0128\frac{\sigma_l}{E} + 0.00930\frac{t}{D} + 0.115\frac{d}{D} + 9778.948\frac{P}{E} - 0.004373$$

The final additive regression model was also based on the dimensional analysis results. The parameters are interchanged and the unit dimension is maintained. This model was of the form:

$$\frac{A}{d^2} = a_1 \frac{\rho \sigma_l D^2}{\mu^2} + a_2 \frac{\sigma_l}{E} + a_3 \frac{D}{t} + a_4 \frac{D}{d} + a_5 \frac{P}{E} + b \qquad \textbf{equation iv}$$

Table 0-24 is the set up that contains all dependent and independent variables.

Table 0-24: Input FEA data values for equation iv for regression analysis for the 6mm hole

x1	x2	x3	x4	x5	y
$\rho\sigma_l D^2/\mu^2$	σ_l /E	D/t	D/d	P/E	A/d^2
0.00E+00	0.00E+00	35.666667	1.78E+01	0.00E+00	7.64E-01
7.86E+12	2.97E-04	35.666667	1.78E+01	3.40E-09	7.73E-01
1.57E+13	5.94E-04	35.666667	1.78E+01	6.80E-09	7.87E-01
2.36E+13	8.92E-04	35.666667	1.78E+01	1.02E-08	8.00E-01
3.14E+13	1.19E-03	35.666667	1.78E+01	1.36E-08	8.12E-01
3.93E+13	1.49E-03	35.666667	1.78E+01	1.70E-08	8.24E-01
4.71E+13	1.78E-03	35.666667	1.78E+01	2.04E-08	8.36E-01
5.50E+13	2.08E-03	35.666667	1.78E+01	2.38E-08	8.47E-01
6.28E+13	2.38E-03	35.666667	1.78E+01	2.72E-08	8.58E-01
7.07E+13	2.68E-03	35.666667	1.78E+01	3.06E-08	8.68E-01
7.86E+13	2.97E-03	35.666667	1.78E+01	3.40E-08	8.78E-01
4.58E+13	1.73E-03	35.666667	1.78E+01	2.04E-08	8.36E-01
4.58E+13	5.20E-04	35.666667	1.78E+01	6.12E-09	7.84E-01
4.58E+13	1.73E-04	35.666667	1.78E+01	2.04E-09	7.68E-01
4.58E+13	5.78E-05	35.666667	1.78E+01	6.80E-10	7.62E-01
4.58E+13	2.60E-05	35.666667	1.78E+01	3.06E-10	7.60E-01
4.58E+13	1.73E-03	35.666667	1.78E+01	2.04E-08	8.38E-01
4.58E+13	1.73E-03	35.666667	1.78E+01	2.04E-08	8.37E-01
4.58E+13	1.73E-03	35.666667	1.78E+01	2.04E-08	8.37E-01
4.58E+13	1.73E-03	35.666667	1.78E+01	2.04E-08	8.36E-01
4.58E+13	1.73E-03	35.666667	1.78E+01	2.04E-08	8.36E-01
4.58E+13	1.73E-03	35.666667	1.78E+01	2.04E-08	8.35E-01
7.00E+13	2.65E-03	53.500000	1.78E+01	2.04E-08	8.63E-01
5.55E+13	2.10E-03	42.800000	1.78E+01	2.04E-08	8.50E-01
4.58E+13	1.73E-03	35.666667	1.78E+01	2.04E-08	8.36E-01
3.37E+13	1.28E-03	26.750000	1.78E+01	2.04E-08	8.23E-01
2.64E+13	1.00E-03	21.400000	1.78E+01	2.04E-08	8.12E-01
6.75E+12	9.00E-04	19.000000	9.50E+00	2.04E-08	8.01E-01
2.45E+13	1.40E-03	29.000000	1.45E+01	2.04E-08	8.24E-01
4.58E+13	1.73E-03	35.666667	1.78E+01	2.04E-08	8.39E-01
1.20E+14	2.40E-03	49.000000	2.45E+01	2.04E-08	8.67E-01
3.77E+14	3.57E-03	71.333333	3.57E+01	2.04E-08	8.99E-01
5.73E+14	4.07E-03	82.333333	4.12E+01	2.04E-08	9.26E-01
4.71E+13	1.78E-03	35.666667	2.68E+01	2.04E-08	7.52E-01
4.71E+13	1.78E-03	35.666667	1.78E+01	2.04E-08	8.36E-01
4.71E+13	1.78E-03	35.666667	1.34E+01	2.04E-08	8.39E-01
0.00E+00	0.00E+00	35.666667	1.78E+01	2.04E-08	8.32E-01
9.16E+12	3.47E-04	35.666667	1.78E+01	2.04E-08	8.33E-01
1.83E+13	6.93E-04	35.666667	1.78E+01	2.04E-08	8.34E-01
2.75E+13	1.04E-03	35.666667	1.78E+01	2.04E-08	8.35E-01
4.58E+13	1.73E-03	35.666667	1.78E+01	2.04E-08	8.36E-01

Table 0-25 shows the regression statistics for the additive regression model

Table 0-25: Regression statistics for equation iv for the 6mm hole

3738901.238	-0.004374773	0.002611124	-5.526993824	1.71308E-16	0.743056163
420099.5337	0.000852072	0.000428946	4.640580463	5.12196E-17	0.016856095
0.926966304	0.010756258	#N/A	#N/A	#N/A	#N/A
88.84616931	35	#N/A	#N/A	#N/A	#N/A
0.051396212	0.004049398	#N/A	#N/A	#N/A	#N/A

R^2=92.70%	df=35	FDIST=7.0924x10^{-19}

The regression statistics shown in Table 0-25 leads to the following equation:

$$\frac{A}{d^2} = 1.713\times10^{-16}\frac{\rho\sigma_l D^2}{\mu^2} - 5.527\frac{\sigma_l}{E} + 0.00261\frac{D}{t} - 0.004375\frac{D}{d} + 3738901.28\frac{P}{E} + 0.743$$

A.2.2 Multiplicative Regression models for the 6mm hole

The following section will show the full regression analyses of the multiplicative regression models that appear for the 6mm round holes. The final equations modelled along with the results after each regression are also illustrated. Table 0-26 shows the input values to be used for the multiplicative models for the 6mm hole.

Table 0-26: : Input values to be used for the 6mm hole multiplicative regression models.

Pressure	E(Gpa)	v	t(m)	D(m)	d0	Longitudinal stress	A	ΔA	
0	3.00E+09	0.4	0.003	0.107	0.006	0.00E+00	2.75E-05	0.00E+00	Change in Pressure
10.19367992	3.00E+09	0.4	0.003	0.107	0.006	8.92E+05	2.78E-05	3.13E-07	
20.38735984	3.00E+09	0.4	0.003	0.107	0.006	1.78E+06	2.83207E-05	8.01E-07	
30.58103976	3.00E+09	0.4	0.003	0.107	0.006	2.68E+06	2.87913E-05	1.27E-06	
40.77471967	3.00E+09	0.4	0.003	0.107	0.006	3.57E+06	2.92439E-05	1.72E-06	
50.96839959	3.00E+09	0.4	0.003	0.107	0.006	4.46E+06	2.96805E-05	2.16E-06	
61.16207951	3.00E+09	0.4	0.003	0.107	0.006	5.35E+06	3.00989E-05	2.58E-06	
71.35575943	3.00E+09	0.4	0.003	0.107	0.006	6.24E+06	3.05E-05	2.98E-06	
81.54943935	3.00E+09	0.4	0.003	0.107	0.006	7.13E+06	3.08837E-05	3.36E-06	
91.74311927	3.00E+09	0.4	0.003	0.107	0.006	8.03E+06	0.00003125	3.73E-06	
101.9367992	3.00E+09	0.4	0.003	0.107	0.006	8.92E+06	3.15988E-05	4.08E-06	
61.16207951	3.00E+09	0.4	0.003	0.107	0.006	5.20E+06	3.00989E-05	2.58E-06	Change in Elastic Modulus
61.16207951	1.00E+10	0.4	0.003	0.107	0.006	5.20E+06	2.82244E-05	7.04E-07	
61.16207951	3.00E+10	0.4	0.003	0.107	0.006	5.20E+06	2.76325E-05	1.13E-07	
61.16207951	9.00E+10	0.4	0.003	0.107	0.006	5.20E+06	2.74296E-05	-9.04E-08	
61.16207951	2.00E+11	0.4	0.003	0.107	0.006	5.20E+06	2.73734E-05	-1.47E-07	
61.16207951	3.00E+09	0.17	0.003	0.107	0.006	5.20E+06	3.01569E-05	2.64E-06	Change in poisson ratio
61.16207951	3.00E+09	0.21	0.003	0.107	0.006	5.20E+06	3.01464E-05	2.63E-06	
61.16207951	3.00E+09	0.29	0.003	0.107	0.006	5.20E+06	3.01258E-05	2.61E-06	
61.16207951	3.00E+09	0.4	0.003	0.107	0.006	5.20E+06	3.00989E-05	2.58E-06	
61.16207951	3.00E+09	0.45	0.003	0.107	0.006	5.20E+06	3.00875E-05	2.57E-06	
61.16207951	3.00E+09	0.495	0.003	0.107	0.006	5.20E+06	3.00778E-05	2.56E-06	
61.16207951	3.00E+09	0.4	0.002	0.107	0.006	7.95E+06	3.10503E-05	3.53E-06	Change in thickness
61.16207951	3.00E+09	0.4	0.0025	0.107	0.006	6.30E+06	3.06072E-05	3.09E-06	
61.16207951	3.00E+09	0.4	0.003	0.107	0.006	5.20E+06	3.00989E-05	2.58E-06	
61.16207951	3.00E+09	0.4	0.004	0.107	0.006	3.83E+06	2.96383E-05	2.12E-06	
61.16207951	3.00E+09	0.4	0.005	0.107	0.006	3.00E+06	2.92303E-05	1.71E-06	
61.16207951	3.00E+09	0.4	0.003	0.057	0.006	2.70E+06	0.000028825	1.31E-06	Change in Internal diameter
61.16207951	3.00E+09	0.4	0.003	0.087	0.006	4.20E+06	2.96792E-05	2.16E-06	
61.16207951	3.00E+09	0.4	0.003	0.107	0.006	5.20E+06	3.02196E-05	2.70E-06	
61.16207951	3.00E+09	0.4	0.003	0.147	0.006	7.20E+06	3.12266E-05	3.71E-06	
61.16207951	3.00E+09	0.4	0.003	0.214	0.006	1.07E+07	3.23524E-05	4.83E-06	
61.16207951	3.00E+09	0.4	0.003	0.247	0.006	1.22E+07	3.3324E-05	5.80E-06	
61.16207951	3.00E+09	0.4	0.003	0.107	0.004	5.35E+06	1.20264E-05	-1.55E-05	Change in hole diameter
61.16207951	3.00E+09	0.4	0.003	0.107	0.006	5.35E+06	3.00989E-05	2.58E-06	
61.16207951	3.00E+09	0.4	0.003	0.107	0.008	5.35E+06	5.37044E-05	2.62E-05	
61.16207951	3.00E+09	0.4	0.003	0.107	0.006	0.00E+00	2.99667E-05	2.45E-06	Change in longitudinal stress
61.16207951	3.00E+09	0.4	0.003	0.107	0.006	1.04E+06	0.000029998	2.48E-06	
61.16207951	3.00E+09	0.4	0.003	0.107	0.006	2.08E+06	3.00293E-05	2.51E-06	
61.16207951	3.00E+09	0.4	0.003	0.107	0.006	3.12E+06	3.00605E-05	2.54E-06	
61.16207951	3.00E+09	0.4	0.003	0.107	0.006	5.20E+06	3.00918E-05	2.57E-06	

The first multiplicative regression that was performed had all the parameters except the longitudinal stress because the longitudinal stress has a FEA data point with 0MPa which is undefined when the logarithmic transformation is applied. The basic form of the first model was:

$$\Delta A = b \cdot P^{a_1} \cdot E^{a_2} \cdot \upsilon^{a_3} \cdot t^{a_4} \cdot d^{a_5} \cdot D^{a_6} \qquad \textbf{equation v}$$

Table 0-27 shows the set up that contains all dependent and independent variables.

Table 0-27: Input FEA data values of equation v regression analysis for the 6mm hole

x1	x2	x3	x4	x5	x6	y
log P	log E	log v	log t	log d	log D	log ΔA
1.008330993	9.477121255	-0.397940009	-2.522878745	-2.22184875	-0.970616222	-6.505147755
1.309360988	9.477121255	-0.397940009	-2.522878745	-2.22184875	-0.970616222	-6.096508476
1.485452247	9.477121255	-0.397940009	-2.522878745	-2.22184875	-0.970616222	-5.895738289
1.610390984	9.477121255	-0.397940009	-2.522878745	-2.22184875	-0.970616222	-5.763500527
1.707300997	9.477121255	-0.397940009	-2.522878745	-2.22184875	-0.970616222	-5.665443719
1.786482243	9.477121255	-0.397940009	-2.522878745	-2.22184875	-0.970616222	-5.588558762
1.853429033	9.477121255	-0.397940009	-2.522878745	-2.22184875	-0.970616222	-5.525788545
1.91142098	9.477121255	-0.397940009	-2.522878745	-2.22184875	-0.970616222	-5.473182745
1.962573502	9.477121255	-0.397940009	-2.522878745	-2.22184875	-0.970616222	-5.428291168
2.008330993	9.477121255	-0.397940009	-2.522878745	-2.22184875	-0.970616222	-5.389470858
1.786482243	9.477121255	-0.397940009	-2.522878745	-2.22184875	-0.970616222	-5.588565498
1.786482243	10	-0.397940009	-2.522878745	-2.22184875	-0.970616222	-6.152159074
1.786482243	10.47712125	-0.397940009	-2.522878745	-2.22184875	-0.970616222	-6.948843617
1.786482243	10.95424251	-0.397940009	-2.522878745	-2.22184875	-0.970616222	-7.043826765
1.786482243	11.30103	-0.397940009	-2.522878745	-2.22184875	-0.970616222	-6.833723856
1.786482243	9.477121255	-0.769551079	-2.522878745	-2.22184875	-0.970616222	-5.578914575
1.786482243	9.477121255	-0.677780705	-2.522878745	-2.22184875	-0.970616222	-5.580640321
1.786482243	9.477121255	-0.537602002	-2.522878745	-2.22184875	-0.970616222	-5.584059254
1.786482243	9.477121255	-0.397940009	-2.522878745	-2.22184875	-0.970616222	-5.588565498
1.786482243	9.477121255	-0.346787486	-2.522878745	-2.22184875	-0.970616222	-5.590487687
1.786482243	9.477121255	-0.305394801	-2.522878745	-2.22184875	-0.970616222	-5.592128119
1.786482243	9.477121255	-0.397940009	-2.698970004	-2.22184875	-0.970616222	-5.452193308
1.786482243	9.477121255	-0.397940009	-2.602059991	-2.22184875	-0.970616222	-5.510435234
1.786482243	9.477121255	-0.397940009	-2.522878745	-2.22184875	-0.970616222	-5.588565498
1.786482243	9.477121255	-0.397940009	-2.397940009	-2.22184875	-0.970616222	-5.674003308
1.786482243	9.477121255	-0.397940009	-2.301029996	-2.22184875	-0.970616222	-5.766935322
1.786482243	9.477121255	-0.397940009	-2.522878745	-2.22184875	-1.244125144	-5.884389488
1.786482243	9.477121255	-0.397940009	-2.522878745	-2.22184875	-1.060480747	-5.665707128
1.786482243	9.477121255	-0.397940009	-2.522878745	-2.22184875	-0.970616222	-5.568700581
1.786482243	9.477121255	-0.397940009	-2.522878745	-2.22184875	-0.832682665	-5.431024279
1.786482243	9.477121255	-0.397940009	-2.522878745	-2.22184875	-0.669586227	-5.315837124
1.786482243	9.477121255	-0.397940009	-2.522878745	-2.22184875	-0.607303047	-5.236269603
1.786482243	9.477121255	-0.397940009	-2.522878745	-2.397940009	-0.970616222	-4.809846304
1.786482243	9.477121255	-0.397940009	-2.522878745	-2.22184875	-0.970616222	-5.588558762
1.786482243	9.477121255	-0.397940009	-2.522878745	-2.096910013	-0.970616222	-4.581958153
1.786482243	9.477121255	-0.397940009	-2.522878745	-2.22184875	-0.970616222	-5.611419278
1.786482243	9.477121255	-0.397940009	-2.522878745	-2.22184875	-0.970616222	-5.605898698
1.786482243	9.477121255	-0.397940009	-2.522878745	-2.22184875	-0.970616222	-5.600443952
1.786482243	9.477121255	-0.397940009	-2.522878745	-2.22184875	-0.970616222	-5.595073963
1.786482243	9.477121255	-0.397940009	-2.522878745	-2.22184875	-0.970616222	-5.589767874

Table 0-28 shows the regression statistics for the additive regression model

Table 0-28: Regression statistics for equation v for the 6mm hole

0.929810836	-0.198912154	-0.824475558	0.07921029	-0.924895755	1.154955781	-0.433688722
0.432553668	1.132027574	0.765212869	0.503851145	0.098566611	0.242080827	3.357153589
0.775336044	0.244208608	#N/A	#N/A	#N/A	#N/A	#N/A
18.98100748	33	#N/A	#N/A	#N/A	#N/A	#N/A
6.79191821	1.968048861	#N/A	#N/A	#N/A	#N/A	#N/A

R^2=77.53%	df=33	FDIST=6.837×10^{-10}

The regression statistics shown in Table 0-28 leads to the following equation:

$$\Delta A = 0.3684 \cdot P^{1.155} \cdot E^{-0.925} \cdot \upsilon^{0.0792} \cdot t^{-0.824} \cdot d^{-0.1989} \cdot D^{0.9298}$$

Once again an observation that can be made from the equation above is that the pressure and the elastic modulus are inverse of each, thus the next form of equation to be regressed has the following form:

$$\Delta A = b \cdot \left(\frac{\mu}{t\sqrt{\rho E}}\right)^{a_1} \cdot \left(\frac{D}{t}\right)^{a_2} \cdot \left(\frac{d}{t}\right)^{a_3} \cdot \left(\frac{P}{E}\right)^{a_4} \qquad \textbf{equation vi}$$

Table 0-29 shows the set up that contains all dependent and independent variables.

Table 0-29: Input FEA data value for equation vi regression analysis for the 6mm hole

x1	x3	x4	x5	x5
$\log(\mu/t(\rho E)^{0.5})$	log(D/t)	log(d/t)	log(P/E)	log ΔA
-6.658777031	1.552262523	0.301029996	-8.468790262	-6.505147755
-6.658777031	1.552262523	0.301029996	-8.167760266	-6.096508476
-6.658777031	1.552262523	0.301029996	-7.991669007	-5.895738289
-6.658777031	1.552262523	0.301029996	-7.866730271	-5.763500527
-6.658777031	1.552262523	0.301029996	-7.769820258	-5.665443719
-6.658777031	1.552262523	0.301029996	-7.690639012	-5.588558762
-6.658777031	1.552262523	0.301029996	-7.623692222	-5.525788545
-6.658777031	1.552262523	0.301029996	-7.565700275	-5.473182745
-6.658777031	1.552262523	0.301029996	-7.514547753	-5.428291168
-6.658777031	1.552262523	0.301029996	-7.468790262	-5.389470858
-6.658777031	1.552262523	0.301029996	-7.690639012	-5.588565498
-6.920216403	1.552262523	0.301029996	-8.213517757	-6.152159074
-7.158777031	1.552262523	0.301029996	-8.690639012	-6.948843617
-7.397337658	1.552262523	0.301029996	-9.167760266	-7.043826765
-7.570731401	1.552262523	0.301029996	-9.514547753	-6.833723856
-6.658777031	1.552262523	0.301029996	-7.690639012	-5.578914575
-6.658777031	1.552262523	0.301029996	-7.690639012	-5.580640321
-6.658777031	1.552262523	0.301029996	-7.690639012	-5.584059254
-6.658777031	1.552262523	0.301029996	-7.690639012	-5.588565498
-6.658777031	1.552262523	0.301029996	-7.690639012	-5.590487687
-6.658777031	1.552262523	0.301029996	-7.690639012	-5.592128119
-6.482685772	1.728353782	0.477121255	-7.690639012	-5.452193308
-6.579595785	1.631443769	0.380211242	-7.690639012	-5.510435234
-6.658777031	1.552262523	0.301029996	-7.690639012	-5.588565498
-6.783715767	1.427323786	0.176091259	-7.690639012	-5.674003308
-6.88062578	1.330413773	0.079181246	-7.690639012	-5.766935322
-6.658777031	1.278753601	0.301029996	-7.690639012	-5.884389488
-6.658777031	1.462397998	0.301029996	-7.690639012	-5.665707128
-6.658777031	1.552262523	0.301029996	-7.690639012	-5.568700581
-6.658777031	1.69019608	0.301029996	-7.690639012	-5.431024279
-6.658777031	1.853292519	0.301029996	-7.690639012	-5.315837124
-6.658777031	1.915575699	0.301029996	-7.690639012	-5.236269603
-6.658777031	1.552262523	0.124938737	-7.690639012	-4.809846304
-6.658777031	1.552262523	0.301029996	-7.690639012	-5.588558762
-6.658777031	1.552262523	0.425968732	-7.690639012	-4.581958153
-6.658777031	1.552262523	0.301029996	-7.690639012	-5.611419278
-6.658777031	1.552262523	0.301029996	-7.690639012	-5.605898698
-6.658777031	1.552262523	0.301029996	-7.690639012	-5.600443952
-6.658777031	1.552262523	0.301029996	-7.690639012	-5.595073963

Table 0-30 shows the regression statistics for the additive regression model

Table 0-30: Regression statistics of equation vi for the 6m hole

1.126782901	0.105576038	0.975275985	-0.396993308	-1.072353722
0.226568715	0.750915765	0.408966138	0.474834089	1.960187401
0.77420976	0.241058559	#N/A	#N/A	#N/A
29.14555984	34	#N/A	#N/A	#N/A
6.774504005	1.975713775	#N/A	#N/A	#N/A

R2=77.42%	df=34	FDIST=4.844x10-12

The regression statistics shown in Table 0-28 leads to the following equation:

$$\Delta A = 0.0847 \cdot \left(\frac{\mu}{t\sqrt{\rho E}}\right)^{-0.397} \cdot \left(\frac{D}{t}\right)^{0.975} \cdot \left(\frac{d}{t}\right)^{0.106} \cdot \left(\frac{P}{E}\right)^{1.127}$$

The final multiplicative model that was investigated had the following form:

$$\Delta A = b \cdot \left(\frac{t\sqrt{\rho E}}{\mu}\right)^{a_1} \cdot \left(\frac{P}{E}\right)^{a_2} \cdot \left(\frac{t}{d}\right)^{a_3} \cdot \left(\frac{t}{D}\right)^{a_4} \qquad \textbf{equation vii}$$

Table 31 shows the set up that contains all the dependent and independent variables.

Table 0-31: Input FEA data values of equation vii regression analysis for the 6mm hole

6.658777031	-8.468790262	-0.301029996	-1.552262523	-6.505147755
6.658777031	-8.167760266	-0.301029996	-1.552262523	-6.096508476
6.658777031	-7.991669007	-0.301029996	-1.552262523	-5.895738289
6.658777031	-7.866730271	-0.301029996	-1.552262523	-5.763500527
6.658777031	-7.769820258	-0.301029996	-1.552262523	-5.665443719
6.658777031	-7.690639012	-0.301029996	-1.552262523	-5.588558762
6.658777031	-7.623692222	-0.301029996	-1.552262523	-5.525788545
6.658777031	-7.565700275	-0.301029996	-1.552262523	-5.473182745
6.658777031	-7.514547753	-0.301029996	-1.552262523	-5.428291168
6.658777031	-7.468790262	-0.301029996	-1.552262523	-5.389470858
6.658777031	-7.690639012	-0.301029996	-1.552262523	-5.588565498
6.920216403	-8.213517757	-0.301029996	-1.552262523	-6.152159074
7.158777031	-8.690639012	-0.301029996	-1.552262523	-6.948843617
7.397337658	-9.167760266	-0.301029996	-1.552262523	-7.043826765
7.570731401	-9.514547753	-0.301029996	-1.552262523	-6.833723856
6.658777031	-7.690639012	-0.301029996	-1.552262523	-5.578914575
6.658777031	-7.690639012	-0.301029996	-1.552262523	-5.580640321
6.658777031	-7.690639012	-0.301029996	-1.552262523	-5.584059254
6.658777031	-7.690639012	-0.301029996	-1.552262523	-5.588565498
6.658777031	-7.690639012	-0.301029996	-1.552262523	-5.590487687
6.658777031	-7.690639012	-0.301029996	-1.552262523	-5.592128119
6.482685772	-7.690639012	-0.477121255	-1.728353782	-5.452193308
6.579595785	-7.690639012	-0.380211242	-1.631443769	-5.510435234
6.658777031	-7.690639012	-0.301029996	-1.552262523	-5.588565498
6.783715767	-7.690639012	-0.176091259	-1.427323786	-5.674003308
6.88062578	-7.690639012	-0.079181246	-1.330413773	-5.766935322
6.658777031	-7.690639012	-0.301029996	-1.278753601	-5.884389488
6.658777031	-7.690639012	-0.301029996	-1.462397998	-5.665707128
6.658777031	-7.690639012	-0.301029996	-1.552262523	-5.568700581
6.658777031	-7.690639012	-0.301029996	-1.69019608	-5.431024279
6.658777031	-7.690639012	-0.301029996	-1.853292519	-5.315837124
6.658777031	-7.690639012	-0.301029996	-1.915575699	-5.236269603
6.658777031	-7.690639012	-0.124938737	-1.552262523	-4.809846304
6.658777031	-7.690639012	-0.301029996	-1.552262523	-5.588558762
6.658777031	-7.690639012	-0.425968732	-1.552262523	-4.581958153
6.658777031	-7.690639012	-0.301029996	-1.552262523	-5.611419278
6.658777031	-7.690639012	-0.301029996	-1.552262523	-5.605898698
6.658777031	-7.690639012	-0.301029996	-1.552262523	-5.600443952
6.658777031	-7.690639012	-0.301029996	-1.552262523	-5.595073963

Table 0-32 shows the regression statistics for the additive regression model

Table 0-32: Regression statistics for equation vii for the 6mm hole

-0.975275985	-0.105576038	1.126782901	0.396993308	-1.072353722
0.408966138	0.750915765	0.226568715	0.474834089	1.960187401
0.77420976	0.241058559	#N/A	#N/A	#N/A
29.14555984	34	#N/A	#N/A	#N/A
6.774504005	1.975713775	#N/A	#N/A	#N/A

R2=77.42%	df=34	FDIST=4.844×10^{-12}

The regression statistics shown in Table 0-32 leads to the following equation:

$$\Delta A = 0.08465 \cdot \left(\frac{t\sqrt{\rho E}}{\mu}\right)^{0.397} \cdot \left(\frac{P}{E}\right)^{1.127} \cdot \left(\frac{t}{d}\right)^{-0.106} \cdot \left(\frac{t}{D}\right)^{-0.975}$$

A.2.3 Discussion on the 6mm hole regression models

Based on the additive and multiplicative regression models for the 6mm holes, it was found that the best fit model was given by equation iii. The best fit was chosen based on the R^2 and FDIST results, the regression model presented by equation iii portrayed the best results when compared to the other models.

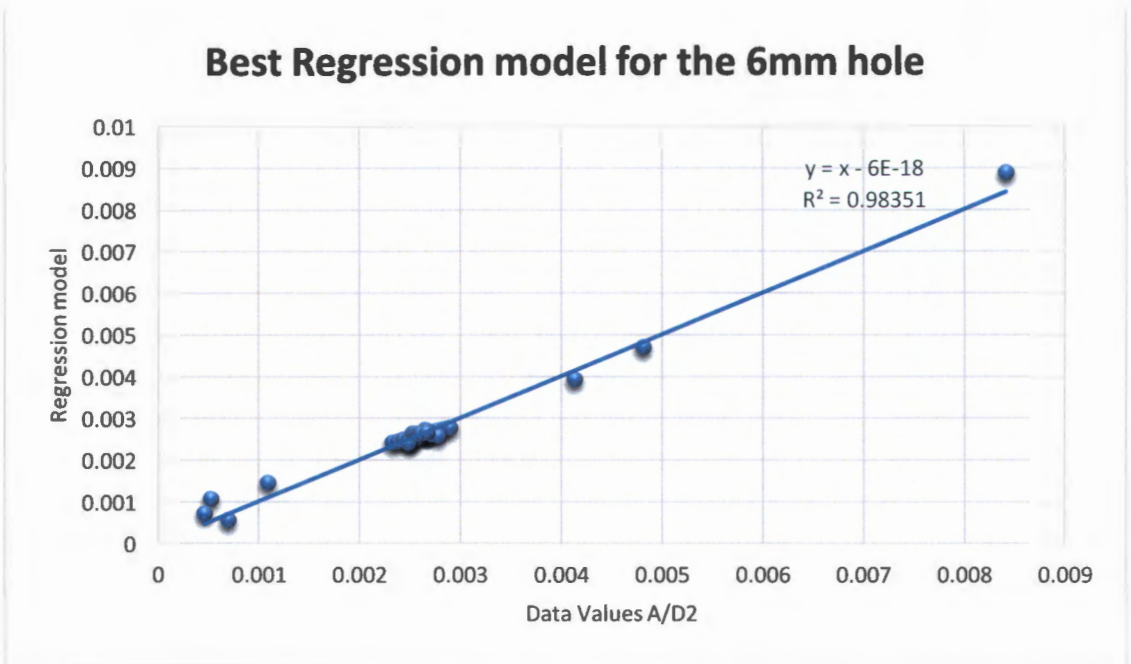

Figure 0-2: Correlation between the regression model and the FEA data values

A.3 Regression analysis for the 8mm hole

This section contains the full regression analyses carried out for the 8mm hole. The regression models used here are similar to those used for the 4mm and 6mm hole.This section will illustrates the full tables with all the FEA data points used for the 8mm hole. Also, other tables that are needed to set up each model are shown. The equations that have been modeled along with their results and additional statistics appear after each regression. Both the additive and multiplicative regression models are carried out for the 8mm hole. The values of ρ and μ are 1000kg/m^3 and 0.00114kg/m.s respectively.

A.3.1 Additive Regression models for the 8mm hole

This section starts with Table 0-33 that shows the input values to be used for the additive models of the 6mm hole

Table 0-33: Shows the input values to be used for the additive models.

Pressure	E(Gpa)	v	t(m)	D(m)	d0	Longitudinal stress	A	
0	3.00E+09	0.4	0.003	0.107	0.008	0.00E+00	4.970E-05	
10.19367992	3.00E+09	0.4	0.003	0.107	0.008	8.92E+05	5.038E-05	
20.38735984	3.00E+09	0.4	0.003	0.107	0.008	1.78E+06	5.073E-05	
30.58103976	3.00E+09	0.4	0.003	0.107	0.008	2.68E+06	5.159E-05	
40.77471967	3.00E+09	0.4	0.003	0.107	0.008	3.57E+06	5.231E-05	
50.96839959	3.00E+09	0.4	0.003	0.107	0.008	4.46E+06	5.299E-05	Change in Pressure
61.16207951	3.00E+09	0.4	0.003	0.107	0.008	5.35E+06	5.370E-05	
71.35575943	3.00E+09	0.4	0.003	0.107	0.008	6.24E+06	5.425E-05	
81.54943935	3.00E+09	0.4	0.003	0.107	0.008	7.13E+06	5.482E-05	
91.74311927	3.00E+09	0.4	0.003	0.107	0.008	8.03E+06	5.537E-05	
101.9367992	3.00E+09	0.4	0.003	0.107	0.008	8.92E+06	5.587E-05	
61.16207951	3.00E+09	0.4	0.003	0.107	0.008	5.20E+06	5.370E-05	
61.16207951	1.00E+10	0.4	0.003	0.107	0.008	5.20E+06	5.071E-05	Change in Elastic Modulus
61.16207951	3.00E+10	0.4	0.003	0.107	0.008	5.20E+06	4.975E-05	
61.16207951	9.00E+10	0.4	0.003	0.107	0.008	5.20E+06	4.942E-05	
61.16207951	2.00E+11	0.4	0.003	0.107	0.008	5.20E+06	4.932E-05	
61.16207951	3.00E+09	0.17	0.003	0.107	0.008	5.20E+06	5.390E-05	
61.16207951	3.00E+09	0.21	0.003	0.107	0.008	5.20E+06	5.386E-05	
61.16207951	3.00E+09	0.29	0.003	0.107	0.008	5.20E+06	5.379E-05	Change in poisson ratio
61.16207951	3.00E+09	0.4	0.003	0.107	0.008	5.20E+06	5.370E-05	
61.16207951	3.00E+09	0.45	0.003	0.107	0.008	5.20E+06	5.367E-05	
61.16207951	3.00E+09	0.495	0.003	0.107	0.008	5.20E+06	5.364E-05	
61.16207951	3.00E+09	0.4	0.002	0.107	0.008	7.95E+06	5.464E-05	
61.16207951	3.00E+09	0.4	0.0025	0.107	0.008	6.30E+06	5.396E-05	
61.16207951	3.00E+09	0.4	0.003	0.107	0.008	5.20E+06	5.330E-05	Change in thickness
61.16207951	3.00E+09	0.4	0.004	0.107	0.008	3.83E+06	5.255E-05	
61.16207951	3.00E+09	0.4	0.005	0.107	0.008	3.00E+06	5.185E-05	
61.16207951	3.00E+09	0.4	0.003	0.057	0.008	2.70E+06	5.143E-05	
61.16207951	3.00E+09	0.4	0.003	0.087	0.008	4.20E+06	5.279E-05	
61.16207951	3.00E+09	0.4	0.003	0.107	0.008	5.20E+06	5.370E-05	Change in
61.16207951	3.00E+09	0.4	0.003	0.147	0.008	7.20E+06	5.541E-05	Internal diameter
61.16207951	3.00E+09	0.4	0.003	0.214	0.008	1.07E+07	5.731E-05	
61.16207951	3.00E+09	0.4	0.003	0.247	0.008	1.22E+07	5.893E-05	
61.16207951	3.00E+09	0.4	0.003	0.107	0.004	5.35E+06	1.203E-05	
61.16207951	3.00E+09	0.4	0.003	0.107	0.006	5.35E+06	3.010E-05	Change in hole diameter
61.16207951	3.00E+09	0.4	0.003	0.107	0.008	5.35E+06	5.370E-05	
61.16207951	3.00E+09	0.4	0.003	0.107	0.008	0.00E+00	5.339E-05	
61.16207951	3.00E+09	0.4	0.003	0.107	0.008	1.04E+06	5.345E-05	
61.16207951	3.00E+09	0.4	0.003	0.107	0.008	2.08E+06	5.351E-05	Change in longitudinal stress
61.16207951	3.00E+09	0.4	0.003	0.107	0.008	3.12E+06	5.357E-05	
61.16207951	3.00E+09	0.4	0.003	0.107	0.008	5.20E+06	5.362E-05	

Similar to the other holes, the first regression model was taken from the dimensional analysis set shown in chapter 4. The form of the model is:

$$\frac{A}{t^2} = a_1 \frac{\mu}{t\sqrt{\rho E}} + a_2 \frac{\sigma_l}{E} + a_3 \frac{D}{t} + a_4 \frac{d}{t} + a_5 \frac{P}{E} + b \qquad \textbf{equation i}$$

Table 0-34 that follows shows how the independent and the dependent variables were setup in Excel for each FEA data point.

Table 0-34: Input FEA data values of equation i regression analysis for the 8mm hole

x1	x2	x3	x4	x5	y
μ/(ρE)0.5	σ/E	D/t	d/t	P/E	A/t2
2.19E-07	0.00E+00	3.57E+01	2.67E+00	0.00E+00	5.52E+00
2.19E-07	2.97E-04	3.57E+01	2.67E+00	3.40E-09	5.60E+00
2.19E-07	5.94E-04	3.57E+01	2.67E+00	6.80E-09	5.64E+00
2.19E-07	8.92E-04	3.57E+01	2.67E+00	1.02E-08	5.73E+00
2.19E-07	1.19E-03	3.57E+01	2.67E+00	1.36E-08	5.81E+00
2.19E-07	1.49E-03	3.57E+01	2.67E+00	1.70E-08	5.89E+00
2.19E-07	1.78E-03	3.57E+01	2.67E+00	2.04E-08	5.97E+00
2.19E-07	2.08E-03	3.57E+01	2.67E+00	2.38E-08	6.03E+00
2.19E-07	2.38E-03	3.57E+01	2.67E+00	2.72E-08	6.09E+00
2.19E-07	2.68E-03	3.57E+01	2.67E+00	3.06E-08	6.15E+00
2.19E-07	2.97E-03	3.57E+01	2.67E+00	3.40E-08	6.21E+00
2.19E-07	1.73E-03	3.57E+01	2.67E+00	2.04E-08	5.97E+00
1.20E-07	5.20E-04	3.57E+01	2.67E+00	6.12E-09	5.63E+00
6.94E-08	1.73E-04	3.57E+01	2.67E+00	2.04E-09	5.53E+00
4.01E-08	5.78E-05	3.57E+01	2.67E+00	6.80E-10	5.49E+00
2.69E-08	2.60E-05	3.57E+01	2.67E+00	3.06E-10	5.48E+00
2.19E-07	1.73E-03	3.57E+01	2.67E+00	2.04E-08	5.99E+00
2.19E-07	1.73E-03	3.57E+01	2.67E+00	2.04E-08	5.98E+00
2.19E-07	1.73E-03	3.57E+01	2.67E+00	2.04E-08	5.98E+00
2.19E-07	1.73E-03	3.57E+01	2.67E+00	2.04E-08	5.97E+00
2.19E-07	1.73E-03	3.57E+01	2.67E+00	2.04E-08	5.96E+00
2.19E-07	1.73E-03	3.57E+01	2.67E+00	2.04E-08	5.96E+00
3.29E-07	2.65E-03	5.35E+01	4.00E+00	2.04E-08	1.37E+01
2.63E-07	2.10E-03	4.28E+01	3.20E+00	2.04E-08	8.63E+00
2.19E-07	1.73E-03	3.57E+01	2.67E+00	2.04E-08	5.92E+00
1.65E-07	1.28E-03	2.68E+01	2.00E+00	2.04E-08	3.28E+00
1.32E-07	1.00E-03	2.14E+01	1.60E+00	2.04E-08	2.07E+00
2.19E-07	9.00E-04	1.90E+01	2.67E+00	2.04E-08	5.71E+00
2.19E-07	1.40E-03	2.90E+01	2.67E+00	2.04E-08	5.87E+00
2.19E-07	1.73E-03	3.57E+01	2.67E+00	2.04E-08	5.97E+00
2.19E-07	2.40E-03	4.90E+01	2.67E+00	2.04E-08	6.16E+00
2.19E-07	3.57E-03	7.13E+01	2.67E+00	2.04E-08	6.37E+00
2.19E-07	4.07E-03	8.23E+01	2.67E+00	2.04E-08	6.55E+00
2.19E-07	1.78E-03	3.57E+01	1.33E+00	2.04E-08	1.34E+00
2.19E-07	1.78E-03	3.57E+01	2.00E+00	2.04E-08	3.34E+00
2.19E-07	1.78E-03	3.57E+01	2.67E+00	2.04E-08	5.97E+00
2.19E-07	0.00E+00	3.57E+01	2.67E+00	2.04E-08	5.93E+00
2.19E-07	3.47E-04	3.57E+01	2.67E+00	2.04E-08	5.94E+00
2.19E-07	6.93E-04	3.57E+01	2.67E+00	2.04E-08	5.95E+00
2.19E-07	1.04E-03	3.57E+01	2.67E+00	2.04E-08	5.95E+00
2.19E-07	1.73E-03	3.57E+01	2.67E+00	2.04E-08	5.96E+00

Table 0-35shows the regression statistics for the additive regression model

Table 0-35: Regression statistics for equation I for the 8mm hole

8213805.645	4.159826979	0.008157864	109.536135	2358314.442	-6.167835
14946284.46	0.169403764	0.009524359	143.9047447	1426393.208	0.488584
0.963191651	0.352616828	#N/A	#N/A	#N/A	#N/A
183.1742459	35	#N/A	#N/A	#N/A	#N/A
113.8781718	4.351851967	#N/A	#N/A	#N/A	#N/A

R^2=96.32%	df=35	FDIST=4.642x10^{-24}

The regression statistics shown in Table 0-35 leads to the following equation:

$$\frac{A}{t^2} = 2358314.44\frac{\mu}{t\sqrt{\rho E}} + 109.54\frac{\sigma_l}{E} + 0.00816\frac{D}{t} + 4.1598\frac{d}{t} + 8213805.65\frac{P}{E} - 6.168$$

The next model is also a set from the dimensionless analysis conducted in Capter 4. The equation has the basic form:

$$\frac{A}{t^2} = a_1\frac{t\sqrt{\rho E}}{\mu} + a_2\frac{P}{E} + a_3\frac{t}{d} + a_4\frac{t}{D} + a_5\frac{\sigma_l}{E} + b \qquad \textbf{equation ii}$$

Table 0-36 shows the dependent and the independent variables set up on Excel for each FEA data point.

Table 0-36: Input FEA data values of equation ii for the regression analysis of the 8mm hole.

x1	x3	x4	x5	y
t(ρE)0.5/μ	t/d	t/D	σ/E	A/l2
4.56E+06	3.75E-01	0.028037383	0.00E+00	5.52E+00
4.56E+06	3.75E-01	0.028037383	2.97E-04	5.60E+00
4.56E+06	3.75E-01	0.028037383	5.94E-04	5.64E+00
4.56E+06	3.75E-01	0.028037383	8.92E-04	5.73E+00
4.56E+06	3.75E-01	0.028037383	1.19E-03	5.81E+00
4.56E+06	3.75E-01	0.028037383	1.49E-03	5.89E+00
4.56E+06	3.75E-01	0.028037383	1.78E-03	5.97E+00
4.56E+06	3.75E-01	0.028037383	2.08E-03	6.03E+00
4.56E+06	3.75E-01	0.028037383	2.38E-03	6.09E+00
4.56E+06	3.75E-01	0.028037383	2.68E-03	6.15E+00
4.56E+06	3.75E-01	0.028037383	2.97E-03	6.21E+00
4.56E+06	3.75E-01	0.028037383	1.73E-03	5.97E+00
8.32E+06	3.75E-01	0.028037383	5.20E-04	5.63E+00
1.44E+07	3.75E-01	0.028037383	1.73E-04	5.53E+00
2.50E+07	3.75E-01	0.028037383	5.78E-05	5.49E+00
3.72E+07	3.75E-01	0.028037383	2.60E-05	5.48E+00
4.56E+06	3.75E-01	0.028037383	1.73E-03	5.99E+00
4.56E+06	3.75E-01	0.028037383	1.73E-03	5.98E+00
4.56E+06	3.75E-01	0.028037383	1.73E-03	5.98E+00
4.56E+06	3.75E-01	0.028037383	1.73E-03	5.97E+00
4.56E+06	3.75E-01	0.028037383	1.73E-03	5.96E+00
4.56E+06	3.75E-01	0.028037383	1.73E-03	5.96E+00
3.04E+06	2.50E-01	0.018691589	2.65E-03	1.37E+01
3.80E+06	3.13E-01	0.023364486	2.10E-03	8.63E+00
4.56E+06	3.75E-01	0.028037383	1.73E-03	5.92E+00
6.08E+06	5.00E-01	0.037383178	1.28E-03	3.28E+00
7.60E+06	6.25E-01	0.046728972	1.00E-03	2.07E+00
4.56E+06	3.75E-01	0.052631579	9.00E-04	5.71E+00
4.56E+06	3.75E-01	0.034482759	1.40E-03	5.87E+00
4.56E+06	3.75E-01	0.028037383	1.73E-03	5.97E+00
4.56E+06	3.75E-01	0.020408163	2.40E-03	6.16E+00
4.56E+06	3.75E-01	0.014018692	3.57E-03	6.37E+00
4.56E+06	3.75E-01	0.012145749	4.07E-03	6.55E+00
4.56E+06	7.50E-01	0.028037383	1.78E-03	1.34E+00
4.56E+06	5.00E-01	0.028037383	1.78E-03	3.34E+00
4.56E+06	3.75E-01	0.028037383	1.78E-03	5.97E+00
4.56E+06	3.75E-01	0.028037383	0.00E+00	5.93E+00
4.56E+06	3.75E-01	0.028037383	3.47E-04	5.94E+00
4.56E+06	3.75E-01	0.028037383	6.93E-04	5.95E+00
4.56E+06	3.75E-01	0.028037383	1.04E-03	5.95E+00
4.56E+06	3.75E-01	0.028037383	1.73E-03	5.96E+00

Table 0-37 shows the regression statistics for the additive regression model

Table 0-37: Regression statistics for equation ii of the 8mm hole

267.6987443	-28.89712913	-17.15680308	4255743.01	-1.19842E-08	12.96926528
299.2574748	32.79607782	2.06183297	34886271.92	3.00065E-08	1.111017953
0.738042072	0.940688077	#N/A	#N/A	#N/A	#N/A
19.72184828	35	#N/A	#N/A	#N/A	#N/A
87.25873171	30.97129201	#N/A	#N/A	#N/A	#N/A

R^2=73.84%	df=35	FDIST=2.6264x10^{-9}

The regression statistics shown in Table 0-21 leads to the following equation:

$$\frac{A}{D^2} = -1.198\times10^{-8}\frac{\rho\sigma_l D^2}{\mu^2} + 4255743.01\frac{\sigma_l}{E} - 17.157\frac{t}{D} - 28.897\frac{d}{D} + 267.69\frac{P}{E} + 12.97$$

The next additive model shown is based on the dimensionless analysis, the parameters are interchanged such that the unit dimensions are still maintained. The following equation was developed:

$$\frac{A}{D^2} = a_1\frac{\rho\sigma_l D^2}{\mu^2} + a_2\frac{\sigma_l}{E} + a_3\frac{t}{D} + a_4\frac{d}{D} + a_5\frac{P}{E} + b \qquad \textbf{equation iii}$$

Table 0-38 that follows shows how the independent and the dependent variables were set up in Excel.

Table 0-38: Input FEA data values of equation iii for the regression analysis of the 8mm hole

x1	x2	x3	x4	x5	y
ρσlD2/μ2	σl /E	t/D	d/D	P/E	A/D2
0.00E+00	0.00E+00	2.80E-02	7.48E-02	0.00E+00	4.34E-03
7.86E+12	2.97E-04	2.80E-02	7.48E-02	3.40E-09	4.40E-03
1.57E+13	5.94E-04	2.80E-02	7.48E-02	6.80E-09	4.43E-03
2.36E+13	8.92E-04	2.80E-02	7.48E-02	1.02E-08	4.51E-03
3.14E+13	1.19E-03	2.80E-02	7.48E-02	1.36E-08	4.57E-03
3.93E+13	1.49E-03	2.80E-02	7.48E-02	1.70E-08	4.63E-03
4.71E+13	1.78E-03	2.80E-02	7.48E-02	2.04E-08	4.69E-03
5.50E+13	2.08E-03	2.80E-02	7.48E-02	2.38E-08	4.74E-03
6.28E+13	2.38E-03	2.80E-02	7.48E-02	2.72E-08	4.79E-03
7.07E+13	2.68E-03	2.80E-02	7.48E-02	3.06E-08	4.84E-03
7.86E+13	2.97E-03	2.80E-02	7.48E-02	3.40E-08	4.88E-03
4.58E+13	1.73E-03	2.80E-02	7.48E-02	2.04E-08	4.69E-03
4.58E+13	5.20E-04	2.80E-02	7.48E-02	6.12E-09	4.43E-03
4.58E+13	1.73E-04	2.80E-02	7.48E-02	2.04E-09	4.35E-03
4.58E+13	5.78E-05	2.80E-02	7.48E-02	6.80E-10	4.32E-03
4.58E+13	2.60E-05	2.80E-02	7.48E-02	3.06E-10	4.31E-03
4.58E+13	1.73E-03	2.80E-02	7.48E-02	2.04E-08	4.71E-03
4.58E+13	1.73E-03	2.80E-02	7.48E-02	2.04E-08	4.70E-03
4.58E+13	1.73E-03	2.80E-02	7.48E-02	2.04E-08	4.70E-03
4.58E+13	1.73E-03	2.80E-02	7.48E-02	2.04E-08	4.69E-03
4.58E+13	1.73E-03	2.80E-02	7.48E-02	2.04E-08	4.69E-03
4.58E+13	1.73E-03	2.80E-02	7.48E-02	2.04E-08	4.68E-03
7.00E+13	2.65E-03	1.87E-02	7.48E-02	2.04E-08	4.77E-03
5.55E+13	2.10E-03	2.34E-02	7.48E-02	2.04E-08	4.71E-03
4.58E+13	1.73E-03	2.80E-02	7.48E-02	2.04E-08	4.66E-03
3.37E+13	1.28E-03	3.74E-02	7.48E-02	2.04E-08	4.59E-03
2.64E+13	1.00E-03	4.67E-02	7.48E-02	2.04E-08	4.53E-03
6.75E+12	9.00E-04	5.26E-02	1.40E-01	2.04E-08	1.58E-02
2.45E+13	1.40E-03	3.45E-02	9.20E-02	2.04E-08	6.97E-03
4.58E+13	1.73E-03	2.80E-02	7.48E-02	2.04E-08	4.69E-03
1.20E+14	2.40E-03	2.04E-02	5.44E-02	2.04E-08	2.56E-03
3.77E+14	3.57E-03	1.40E-02	3.74E-02	2.04E-08	1.25E-03
5.73E+14	4.07E-03	1.21E-02	3.24E-02	2.04E-08	9.66E-04
4.71E+13	1.78E-03	2.80E-02	3.74E-02	2.04E-08	1.05E-03
4.71E+13	1.78E-03	2.80E-02	5.61E-02	2.04E-08	2.63E-03
4.71E+13	1.78E-03	2.80E-02	7.48E-02	2.04E-08	4.69E-03
0.00E+00	0.00E+00	2.80E-02	7.48E-02	2.04E-08	4.66E-03
9.16E+12	3.47E-04	2.80E-02	7.48E-02	2.04E-08	4.67E-03
1.83E+13	6.93E-04	2.80E-02	7.48E-02	2.04E-08	4.67E-03
2.75E+13	1.04E-03	2.80E-02	7.48E-02	2.04E-08	4.68E-03
4.58E+13	1.73E-03	2.80E-02	7.48E-02	2.04E-08	4.68E-03

Table 0-39 shows the regression statistics for the additive regression model

Table 0-39: Regression ststaistics of equation iii for the 8mm hole

10831.85817	0.138133975	0.040202572	0.058093883	5.16512E-18	-0.00722179
15891.50738	0.006587413	0.016852779	0.17636592	1.16953E-18	0.000466689
0.96748386	0.00040614	#N/A	#N/A	#N/A	#N/A
208.2777064	35	#N/A	#N/A	#N/A	#N/A
0.000171777	5.77325E-06	#N/A	#N/A	#N/A	#N/A

R2=96.75%	df=35	FDIST=5.3352×10^{-25}

The regression statistics shown in Table 0-23 leads to the following equation:

$$\frac{A}{D^2} = 5.1651\times10^{-18}\frac{\rho\sigma_l D^2}{\mu^2} + 0.05809\frac{\sigma_l}{E} + 0.04020\frac{t}{D} + 0.1381\frac{d}{D} + 10831.86\frac{P}{E} - 0.007222$$

The final additive regression model was also based on the dimensional analysis results. The parameters are interchanged and the unit dimension is maintained. This model was of the form:

$$\frac{A}{d^2} = a_1 \frac{\rho \sigma_l D^2}{\mu^2} + a_2 \frac{\sigma_l}{E} + a_3 \frac{D}{t} + a_4 \frac{D}{d} + a_5 \frac{P}{E} + b \qquad \textbf{equation iv}$$

Table 0-40 is the set up that contains all dependent and independent variables.

Table 0-40: Input FEA data values of equation iv for the regression analysis of the 8mm hole

x1	x2	x3	x4	x5	y
ρσlD2/μ2	σl /E	D/t	D/d	P/E	A/d2
0.00E+00	0.00E+00	35.66666667	1.34E+01	0.00E+00	7.77E-01
7.86E+12	2.97E-04	35.66666667	1.34E+01	3.40E-09	7.87E-01
1.57E+13	5.94E-04	35.66666667	1.34E+01	6.80E-09	7.93E-01
2.36E+13	8.92E-04	35.66666667	1.34E+01	1.02E-08	8.06E-01
3.14E+13	1.19E-03	35.66666667	1.34E+01	1.36E-08	8.17E-01
3.93E+13	1.49E-03	35.66666667	1.34E+01	1.70E-08	8.28E-01
4.71E+13	1.78E-03	35.66666667	1.34E+01	2.04E-08	8.39E-01
5.50E+13	2.08E-03	35.66666667	1.34E+01	2.38E-08	8.48E-01
6.28E+13	2.38E-03	35.66666667	1.34E+01	2.72E-08	8.57E-01
7.07E+13	2.68E-03	35.66666667	1.34E+01	3.06E-08	8.65E-01
7.86E+13	2.97E-03	35.66666667	1.34E+01	3.40E-08	8.73E-01
4.58E+13	1.73E-03	35.66666667	1.34E+01	2.04E-08	8.39E-01
4.58E+13	5.20E-04	35.66666667	1.34E+01	6.12E-09	7.92E-01
4.58E+13	1.73E-04	35.66666667	1.34E+01	2.04E-09	7.77E-01
4.58E+13	5.78E-05	35.66666667	1.34E+01	6.80E-10	7.72E-01
4.58E+13	2.60E-05	35.66666667	1.34E+01	3.06E-10	7.71E-01
4.58E+13	1.73E-03	35.66666667	1.34E+01	2.04E-08	8.42E-01
4.58E+13	1.73E-03	35.66666667	1.34E+01	2.04E-08	8.42E-01
4.58E+13	1.73E-03	35.66666667	1.34E+01	2.04E-08	8.41E-01
4.58E+13	1.73E-03	35.66666667	1.34E+01	2.04E-08	8.39E-01
4.58E+13	1.73E-03	35.66666667	1.34E+01	2.04E-08	8.39E-01
4.58E+13	1.73E-03	35.66666667	1.34E+01	2.04E-08	8.38E-01
7.00E+13	2.65E-03	53.5	1.34E+01	2.04E-08	8.54E-01
5.55E+13	2.10E-03	42.8	1.34E+01	2.04E-08	8.43E-01
4.58E+13	1.73E-03	35.66666667	1.34E+01	2.04E-08	8.33E-01
3.37E+13	1.28E-03	26.75	1.34E+01	2.04E-08	8.21E-01
2.64E+13	1.00E-03	21.4	1.34E+01	2.04E-08	8.10E-01
6.75E+12	9.00E-04	19	7.13E+00	2.04E-08	8.04E-01
2.45E+13	1.40E-03	29	1.09E+01	2.04E-08	8.25E-01
4.58E+13	1.73E-03	35.66666667	1.34E+01	2.04E-08	8.39E-01
1.20E+14	2.40E-03	49	1.84E+01	2.04E-08	8.66E-01
3.77E+14	3.57E-03	71.33333333	2.68E+01	2.04E-08	8.95E-01
5.73E+14	4.07E-03	82.33333333	3.09E+01	2.04E-08	9.21E-01
4.71E+13	1.78E-03	35.66666667	2.68E+01	2.04E-08	7.52E-01
4.71E+13	1.78E-03	35.66666667	1.78E+01	2.04E-08	8.36E-01
4.71E+13	1.78E-03	35.66666667	1.34E+01	2.04E-08	8.39E-01
0.00E+00	0.00E+00	35.66666667	1.34E+01	2.04E-08	8.34E-01
9.16E+12	3.47E-04	35.66666667	1.34E+01	2.04E-08	8.35E-01
1.83E+13	6.93E-04	35.66666667	1.34E+01	2.04E-08	8.36E-01
2.75E+13	1.04E-03	35.66666667	1.34E+01	2.04E-08	8.37E-01
4.58E+13	1.73E-03	35.66666667	1.34E+01	2.04E-08	8.38E-01

Table 0-41 shows the regression statistics for the additive regression model

Table 0-41: Regression ststistics for equation iv for the 8mm hole

3179140.171	-0.004551013	0.002211611	-3.495084444	1.37102E-16	0.752588804
346564.2469	0.000591853	0.000338273	3.786190354	3.74987E-17	0.01285013
0.938404878	0.008897637	#N/A	#N/A	#N/A	#N/A
106.6453633	35	#N/A	#N/A	#N/A	#N/A
0.042214474	0.002770878	#N/A	#N/A	#N/A	#N/A

R^2=93.84%	df=35	FDIST=3.6621x10^{-20}

The regression statistics shown in Table 0-41 leads to the following equation:

$$\frac{A}{d^2} = 1.3710\times10^{-16}\frac{\rho\sigma_l D^2}{\mu^2} - 3.4951\frac{\sigma_l}{E} + 0.00221\frac{D}{t} - 0.00455\frac{D}{d} + 3179140.17\frac{P}{E} + 0.7526$$

A.3.2 Multiplicative regression models for the 8mm hole

The following section will show the full regression analyses of the multiplicative regression models that appear for the 4mm round holes. It will include the table of all the models that were set up for each multiplicative model. The final equations modelled along with the results after each regression are also illustrated. Table 0-42 shows the input values to be used for the multiplicative models for the 8mm hole.

Table 0-42: shows the input values to be used for the multiplicative models for the 8mm hole

Pressure	E(Gpa)	v	t(m)	D(m)	d0	Longitudinal stress	A	ΔA	
0	3.00E+09	0.4	0.003	0.107	0.008	0.00E+00	4.970E-05	0.00E+00	Change in Pressure
10.19367992	3.00E+09	0.4	0.003	0.107	0.008	8.92E+05	5.038E-05	6.82E-07	
20.38735984	3.00E+09	0.4	0.003	0.107	0.008	1.78E+06	5.073E-05	1.03E-06	
30.58103976	3.00E+09	0.4	0.003	0.107	0.008	2.68E+06	5.159E-05	1.89E-06	
40.77471967	3.00E+09	0.4	0.003	0.107	0.008	3.57E+06	5.231E-05	2.61E-06	
50.96839959	3.00E+09	0.4	0.003	0.107	0.008	4.46E+06	5.299E-05	3.29E-06	
61.16207951	3.00E+09	0.4	0.003	0.107	0.008	5.35E+06	5.370E-05	4.00E-06	
71.35575943	3.00E+09	0.4	0.003	0.107	0.008	6.24E+06	5.425E-05	4.55E-06	
81.54943935	3.00E+09	0.4	0.003	0.107	0.008	7.13E+06	5.482E-05	5.12E-06	
91.74311927	3.00E+09	0.4	0.003	0.107	0.008	8.03E+06	5.537E-05	5.67E-06	
101.9367992	3.00E+09	0.4	0.003	0.107	0.008	8.92E+06	5.587E-05	6.17E-06	
61.16207951	3.00E+09	0.4	0.003	0.107	0.008	5.20E+06	5.370E-05	4.00E-06	Change in Elastic Modulus
61.16207951	1.00E+10	0.4	0.003	0.107	0.008	5.20E+06	5.071E-05	1.01E-06	
61.16207951	3.00E+10	0.4	0.003	0.107	0.008	5.20E+06	4.975E-05	4.76E-08	
61.16207951	9.00E+10	0.4	0.003	0.107	0.008	5.20E+06	4.942E-05	-2.84E-07	
61.16207951	2.00E+11	0.4	0.003	0.107	0.008	5.20E+06	4.932E-05	-3.76E-07	
61.16207951	3.00E+09	0.17	0.003	0.107	0.008	5.20E+06	5.390E-05	4.20E-06	Change in poisson ratio
61.16207951	3.00E+09	0.21	0.003	0.107	0.008	5.20E+06	5.386E-05	4.16E-06	
61.16207951	3.00E+09	0.29	0.003	0.107	0.008	5.20E+06	5.379E-05	4.09E-06	
61.16207951	3.00E+09	0.4	0.003	0.107	0.008	5.20E+06	5.370E-05	4.00E-06	
61.16207951	3.00E+09	0.45	0.003	0.107	0.008	5.20E+06	5.367E-05	3.97E-06	
61.16207951	3.00E+09	0.495	0.003	0.107	0.008	5.20E+06	5.364E-05	3.94E-06	
61.16207951	3.00E+09	0.4	0.002	0.107	0.008	7.95E+06	5.464E-05	4.94E-06	Change in thickness
61.16207951	3.00E+09	0.4	0.0025	0.107	0.008	6.30E+06	5.396E-05	4.26E-06	
61.16207951	3.00E+09	0.4	0.003	0.107	0.008	5.20E+06	5.330E-05	3.60E-06	
61.16207951	3.00E+09	0.4	0.004	0.107	0.008	3.83E+06	5.255E-05	2.85E-06	
61.16207951	3.00E+09	0.4	0.005	0.107	0.008	3.00E+06	5.185E-05	2.15E-06	
61.16207951	3.00E+09	0.4	0.003	0.057	0.008	2.70E+06	5.143E-05	1.73E-06	Change in Internal diameter
61.16207951	3.00E+09	0.4	0.003	0.087	0.008	4.20E+06	5.279E-05	3.09E-06	
61.16207951	3.00E+09	0.4	0.003	0.107	0.008	5.20E+06	5.370E-05	4.00E-06	
61.16207951	3.00E+09	0.4	0.003	0.147	0.008	7.20E+06	5.541E-05	5.71E-06	
61.16207951	3.00E+09	0.4	0.003	0.214	0.008	1.07E+07	5.731E-05	7.61E-06	
61.16207951	3.00E+09	0.4	0.003	0.247	0.008	1.22E+07	5.893E-05	9.23E-06	
61.16207951	3.00E+09	0.4	0.003	0.107	0.004	5.35E+06	1.203E-05	1.46E-07	Change in hole diameter
61.16207951	3.00E+09	0.4	0.003	0.107	0.006	5.35E+06	3.010E-05	2.58E-06	
61.16207951	3.00E+09	0.4	0.003	0.107	0.008	5.35E+06	5.370E-05	4.00E-06	
61.16207951	3.00E+09	0.4	0.003	0.107	0.008	0.00E+00	5.339E-05	3.69E-06	Change in longitudinal stress
61.16207951	3.00E+09	0.4	0.003	0.107	0.008	1.04E+06	5.345E-05	3.75E-06	
61.16207951	3.00E+09	0.4	0.003	0.107	0.008	2.08E+06	5.351E-05	3.81E-06	
61.16207951	3.00E+09	0.4	0.003	0.107	0.008	3.12E+06	5.357E-05	3.87E-06	
61.16207951	3.00E+09	0.4	0.003	0.107	0.008	5.20E+06	5.362E-05	3.92E-06	

The first multiplicative regression that was performed had all the parameters except the longitudinal stress because the longitudinal stress has a FEA data point with 0MPa which is

undefined when the logarithmic transformation is applied. The basic form of the first model was therefore:

$$\Delta A = b \cdot P^{a_1} \cdot E^{a_2} \cdot \upsilon^{a_3} \cdot t^{a_4} \cdot d^{a_5} \cdot D^{a_6} \qquad \textbf{Equation v}$$

Table 0-43shows the set up that contains all dependent and independent variables.

Table 0-43: Input FEA data values of equation v for the regression analysis of the 8mm hole

x1	x2	x3	x4	x5	x6	y
log P	log E	log v	log t	log d	log D	log ΔA
1.008330993	9.477121	-0.397940	-2.522878745	-2.096910013	-0.970616222	-6.165960982
1.309360988	9.477121	-0.397940	-2.522878745	-2.096910013	-0.970616222	-5.985101613
1.485452247	9.477121	-0.397940	-2.522878745	-2.096910013	-0.970616222	-5.72263837
1.610390984	9.477121	-0.397940	-2.522878745	-2.096910013	-0.970616222	-5.583367813
1.707300997	9.477121	-0.397940	-2.522878745	-2.096910013	-0.970616222	-5.482790902
1.786482243	9.477121	-0.397940	-2.522878745	-2.096910013	-0.970616222	-5.397467645
1.853429033	9.477121	-0.397940	-2.522878745	-2.096910013	-0.970616222	-5.342281732
1.91142098	9.477121	-0.397940	-2.522878745	-2.096910013	-0.970616222	-5.290370029
1.962573502	9.477121	-0.397940	-2.522878745	-2.096910013	-0.970616222	-5.24664632
2.008330993	9.477121	-0.397940	-2.522878745	-2.096910013	-0.970616222	-5.209883448
1.786482243	9.477121	-0.397940	-2.522878745	-2.096910013	-0.970616222	-5.397467645
1.786482243	10.000000	-0.397940	-2.522878745	-2.096910013	-0.970616222	-5.995231834
1.786482243	10.477121	-0.397940	-2.522878745	-2.096910013	-0.970616222	-7.32254818
1.786482243	10.954243	-0.397940	-2.522878745	-2.096910013	-0.970616222	-6.54626897
1.786482243	11.301030	-0.397940	-2.522878745	-2.096910013	-0.970616222	-6.424295813
1.786482243	9.477121	-0.769551	-2.522878745	-2.096910013	-0.970616222	-5.376807585
1.786482243	9.477121	-0.677781	-2.522878745	-2.096910013	-0.970616222	-5.380517911
1.786482243	9.477121	-0.537602	-2.522878745	-2.096910013	-0.970616222	-5.387845479
1.786482243	9.477121	-0.397940	-2.522878745	-2.096910013	-0.970616222	-5.397467645
1.786482243	9.477121	-0.346787	-2.522878745	-2.096910013	-0.970616222	-5.40155317
1.786482243	9.477121	-0.305395	-2.522878745	-2.096910013	-0.970616222	-5.404989255
1.786482243	9.477121	-0.397940	-2.698970004	-2.096910013	-0.970616222	-5.306571384
1.786482243	9.477121	-0.397940	-2.602059991	-2.096910013	-0.970616222	-5.370993381
1.786482243	9.477121	-0.397940	-2.522878745	-2.096910013	-0.970616222	-5.443172682
1.786482243	9.477121	-0.397940	-2.397940009	-2.096910013	-0.970616222	-5.544671438
1.786482243	9.477121	-0.397940	-2.301029996	-2.096910013	-0.970616222	-5.667541555
1.786482243	9.477121	-0.397940	-2.522878745	-2.096910013	-1.244125144	-5.761878592
1.786482243	9.477121	-0.397940	-2.522878745	-2.096910013	-1.060480747	-5.510071037
1.786482243	9.477121	-0.397940	-2.522878745	-2.096910013	-0.970616222	-5.397505931
1.786482243	9.477121	-0.397940	-2.522878745	-2.096910013	-0.832682665	-5.243668233
1.786482243	9.477121	-0.397940	-2.522878745	-2.096910013	-0.669586227	-5.118843679
1.786482243	9.477121	-0.397940	-2.522878745	-2.096910013	-0.607303047	-5.034854295
1.786482243	9.477121	-0.397940	-2.522878745	-2.397940009	-0.970616222	-6.834602525
1.786482243	9.477121	-0.397940	-2.522878745	-2.22184875	-0.970616222	-5.588558762
1.786482243	9.477121	-0.397940	-2.522878745	-2.096910013	-0.970616222	-5.397467645
1.786482243	9.477121	-0.397940	-2.522878745	-2.096910013	-0.970616222	-5.432491823
1.786482243	9.477121	-0.397940	-2.522878745	-2.096910013	-0.970616222	-5.425821676
1.786482243	9.477121	-0.397940	-2.522878745	-2.096910013	-0.970616222	-5.419251742
1.786482243	9.477121	-0.397940	-2.522878745	-2.096910013	-0.970616222	-5.41279994
1.786482243	9.477121	-0.397940	-2.522878745	-2.096910013	-0.970616222	-5.406441875

Table 0-44 shows the regression statistics for the additive regression model

Table 0-44: Additional regression statistics of equation 5 for the 8mm hole

1.11473886	4.158961742	-0.913305223	-0.149752718	-0.831767975	0.997626137	8.107762421
0.391049563	0.695413365	0.691508398	0.455886207	0.08929114	0.218988662	2.494905315
0.813801294	0.220672044	#N/A	#N/A	#N/A	#N/A	#N/A
24.03833625	33	#N/A	#N/A	#N/A	#N/A	#N/A
7.023446713	1.606972984	#N/A	#N/A	#N/A	#N/A	#N/A

R^2=81.38%	df=33	FDIST=3.103×10^{-11}

The regression statistics shown in Table 0-44 leads to the following equation:

$$\Delta A = 128.16\times10^{6}\cdot P^{0.9976}\cdot E^{-0.8318}\cdot \upsilon^{-0.1498}\cdot t^{-0.9133}\cdot d^{4.159}\cdot D^{1.1147}$$

Once again an observation that can be made from the equation above is that the pressure and the elastic modulus are inverse of each, thus the next form of equation to be regressed has the following form:

$$\Delta A = b\cdot\left(\frac{\mu}{t\sqrt{\rho E}}\right)^{a_1}\cdot\left(\frac{D}{t}\right)^{a_2}\cdot\left(\frac{d}{t}\right)^{a_3}\cdot\left(\frac{P}{E}\right)^{a_4} \qquad \textbf{Equation vi}$$

Table **0-45** shows the set up that contains all dependent and independent variables.

Table 0-45: Input FEA data values of equation vi for the regression analysis of the 8mm hole

x1	x3	x4	x5	x5
log(μ/t(ρE)0.5)	log(D/t)	log(d/t)	log(P/E)	log ΔA
-6.658777031	1.552262523	0.425969	-8.468790	-6.165960982
-6.658777031	1.552262523	0.425969	-8.167760	-5.985101613
-6.658777031	1.552262523	0.425969	-7.991669	-5.72263837
-6.658777031	1.552262523	0.425969	-7.866730	-5.583367813
-6.658777031	1.552262523	0.425969	-7.769820	-5.482790902
-6.658777031	1.552262523	0.425969	-7.690639	-5.397467645
-6.658777031	1.552262523	0.425969	-7.623692	-5.342281732
-6.658777031	1.552262523	0.425969	-7.565700	-5.290370029
-6.658777031	1.552262523	0.425969	-7.514548	-5.24664632
-6.658777031	1.552262523	0.425969	-7.468790	-5.209883448
-6.658777031	1.552262523	0.425969	-7.690639	-5.397467645
-6.920216403	1.552262523	0.425969	-8.213518	-5.995231834
-7.158777031	1.552262523	0.425969	-8.690639	-7.32254818
-7.397337658	1.552262523	0.425969	-9.167760	-6.54626897
-7.570731401	1.552262523	0.425969	-9.514548	-6.424295813
-6.658777031	1.552262523	0.425969	-7.690639	-5.376807585
-6.658777031	1.552262523	0.425969	-7.690639	-5.380517911
-6.658777031	1.552262523	0.425969	-7.690639	-5.387845479
-6.658777031	1.552262523	0.425969	-7.690639	-5.397467645
-6.658777031	1.552262523	0.425969	-7.690639	-5.40155317
-6.658777031	1.552262523	0.425969	-7.690639	-5.404989255
-6.482685772	1.728353782	0.602060	-7.690639	-5.306571384
-6.579595785	1.631443769	0.505150	-7.690639	-5.370993381
-6.658777031	1.552262523	0.425969	-7.690639	-5.443172682
-6.783715767	1.427323786	0.301030	-7.690639	-5.544671438
-6.88062578	1.330413773	0.204120	-7.690639	-5.667541555
-6.658777031	1.278753601	0.425969	-7.690639	-5.761878592
-6.658777031	1.462397998	0.425969	-7.690639	-5.510071037
-6.658777031	1.552262523	0.425969	-7.690639	-5.397505931
-6.658777031	1.69019608	0.425969	-7.690639	-5.243668233
-6.658777031	1.853292519	0.425969	-7.690639	-5.118843679
-6.658777031	1.915575699	0.425969	-7.690639	-5.034854295
-6.658777031	1.552262523	0.124939	-7.690639	-6.834602525
-6.658777031	1.552262523	0.301030	-7.690639	-5.588558762
-6.658777031	1.552262523	0.425969	-7.690639	-5.397467645
-6.658777031	1.552262523	0.425969	-7.690639	-5.432491823
-6.658777031	1.552262523	0.425969	-7.690639	-5.425821676
-6.658777031	1.552262523	0.425969	-7.690639	-5.419251742
-6.658777031	1.552262523	0.425969	-7.690639	-5.41279994

Table 0-46 shows the regression statistics for the additive regression model

Table 0-46: Regression statistics for equation vi for the 8mm hole

1.280149867	2.72857499	0.651702029	-0.988660731	-4.345908882
0.236349234	0.652498761	0.427015962	0.490180408	2.051513881
0.741590141	0.255574067	#N/A	#N/A	#N/A
24.39348187	34	#N/A	#N/A	#N/A
6.373343926	2.22081553	#N/A	#N/A	#N/A

R^2=74.16%	df=34	FDIST=5.5397x10^{-11}

The regression statistics shown in Table 0-28 leads to the following equation:

$$\Delta A = 4.509\times10^{-5}\cdot\left(\frac{\mu}{t\sqrt{\rho E}}\right)^{-0.989}\cdot\left(\frac{D}{t}\right)^{0.652}\cdot\left(\frac{d}{t}\right)^{2.73}\cdot\left(\frac{P}{E}\right)^{1.280}$$

The final multiplicative model that was investigated had the following form:

$$\Delta A = b\cdot\left(\frac{t\sqrt{\rho E}}{\mu}\right)^{a_1}\cdot\left(\frac{P}{E}\right)^{a_2}\cdot\left(\frac{t}{d}\right)^{a_3}\cdot\left(\frac{t}{D}\right)^{a_4}$$

Table 0-47 shows the set up that contains all the dependent and independent variables.

Table 0-47: Input FEA data values of equation vii for the regression analysis of the 8mm hole

x1	x2	x3	x4	x5
log(t(ρE)0.5/μ)	log(P/E)	log(t/d)	log(t/D)	log ΔA
6.658777	-8.46879	-0.4259687	-1.552263	-6.16596
6.658777	-8.16776	-0.4259687	-1.552263	-5.98510
6.658777	-7.99167	-0.4259687	-1.552263	-5.72264
6.658777	-7.86673	-0.4259687	-1.552263	-5.58337
6.658777	-7.76982	-0.4259687	-1.552263	-5.48279
6.658777	-7.69064	-0.4259687	-1.552263	-5.39747
6.658777	-7.62369	-0.4259687	-1.552263	-5.34228
6.658777	-7.56570	-0.4259687	-1.552263	-5.29037
6.658777	-7.51455	-0.4259687	-1.552263	-5.24665
6.658777	-7.46879	-0.4259687	-1.552263	-5.20988
6.658777	-7.69064	-0.4259687	-1.552263	-5.39747
6.920216	-8.21352	-0.4259687	-1.552263	-5.99523
7.158777	-8.69064	-0.4259687	-1.552263	-7.32255
7.397338	-9.16776	-0.4259687	-1.552263	-6.54627
7.570731	-9.51455	-0.4259687	-1.552263	-6.42430
6.658777	-7.69064	-0.4259687	-1.552263	-5.37681
6.658777	-7.69064	-0.4259687	-1.552263	-5.38052
6.658777	-7.69064	-0.4259687	-1.552263	-5.38785
6.658777	-7.69064	-0.4259687	-1.552263	-5.39747
6.658777	-7.69064	-0.4259687	-1.552263	-5.40155
6.658777	-7.69064	-0.4259687	-1.552263	-5.40499
6.482686	-7.69064	-0.6020600	-1.728354	-5.30657
6.579596	-7.69064	-0.5051500	-1.631444	-5.37099
6.658777	-7.69064	-0.4259687	-1.552263	-5.44317
6.783716	-7.69064	-0.3010300	-1.427324	-5.54467
6.880626	-7.69064	-0.2041200	-1.330414	-5.66754
6.658777	-7.69064	-0.4259687	-1.278754	-5.76188
6.658777	-7.69064	-0.4259687	-1.462398	-5.51007
6.658777	-7.69064	-0.4259687	-1.552263	-5.39751
6.658777	-7.69064	-0.4259687	-1.690196	-5.24367
6.658777	-7.69064	-0.4259687	-1.853293	-5.11884
6.658777	-7.69064	-0.4259687	-1.915576	-5.03485
6.658777	-7.69064	-0.1249387	-1.552263	-6.83460
6.658777	-7.69064	-0.3010300	-1.552263	-5.58856
6.658777	-7.69064	-0.4259687	-1.552263	-5.39747
6.658777	-7.69064	-0.4259687	-1.552263	-5.43249
6.658777	-7.69064	-0.4259687	-1.552263	-5.42582
6.658777	-7.69064	-0.4259687	-1.552263	-5.41925
6.658777	-7.69064	-0.4259687	-1.552263	-5.41280

Table 0-48 shows the regression statistics for the additive regression model

Table 0-48: Regresion statistics of equation vii for the 8mm hole

-0.651702029	-2.72857499	1.280149867	0.988660731	-4.345908882
0.427015962	0.652498761	0.236349234	0.490180408	2.051513881
0.741590141	0.255574067	#N/A	#N/A	#N/A
24.39348187	34	#N/A	#N/A	#N/A
6.373343926	2.22081553	#N/A	#N/A	#N/A

R^2=74.16%	df=34	FDIST=5.53967×10^{-11}

The regression statistics shown in Table 0-32 leads to the following equation:

$$\Delta A = 4.509\times10^{-5}\cdot\left(\frac{t\sqrt{\rho E}}{\mu}\right)^{0.989}\cdot\left(\frac{P}{E}\right)^{1.280}\cdot\left(\frac{t}{d}\right)^{-2.729}\cdot\left(\frac{t}{D}\right)^{-0.652}$$

A.3.3 Discussion on the 8mm hole regression models

Similar regression models were used to those used for the 4mm and the 6mm hole. Based on the above additive and multiplicative regression models once again the best fit model was that presented by equation iii. It is possible to see how good this relationship actually is by comparing the regression model to the FEA data values. Simply plotting the model against the dependent variable's values does this. Figure 0-3 shows the correlation between the regression model and the FEA data values for the 8mm hole.

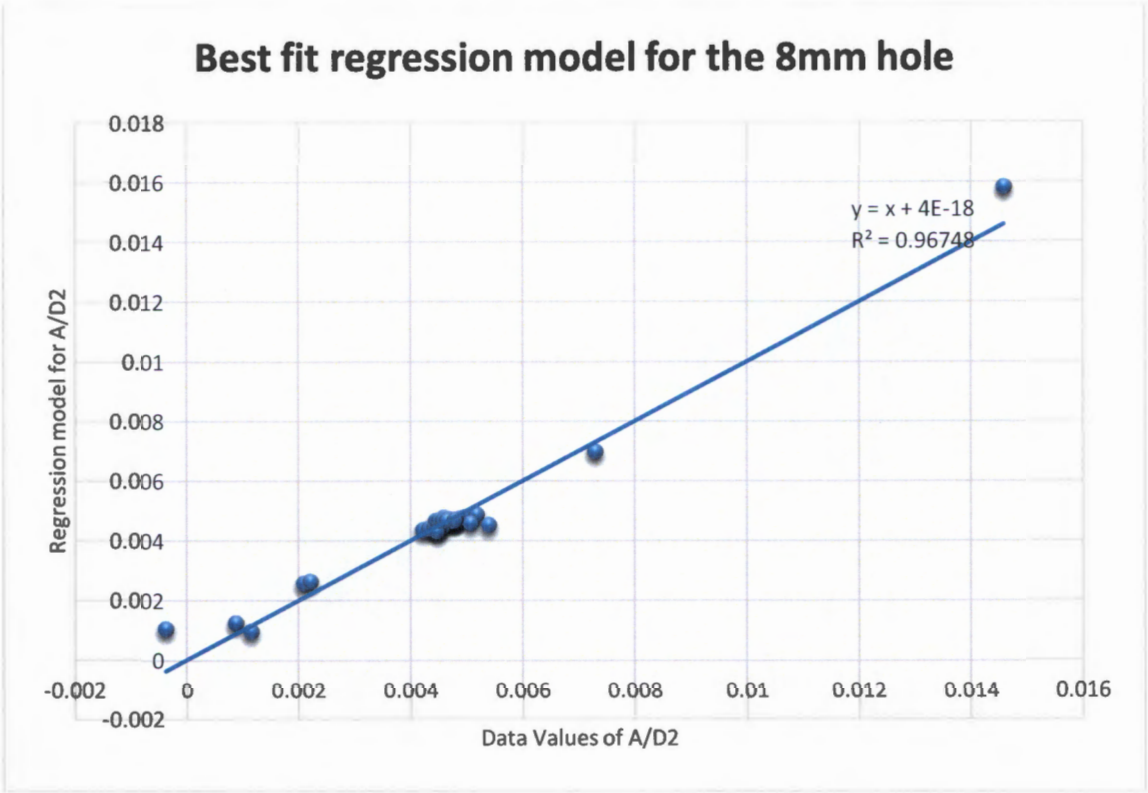

Figure 0-3: Correlation between the FEA data values and the best fit regression model for the 8mm hole

B. Appendix B Sensitivity analysis

B.1 Sensitivity analysis for the internal diamter

Table 0-49 shows the element sizes and the corresponding von mises stress that were obtained for each elenment size.

Table 0-49: Showing the von mises stresses obtained

	Stresses for various Internal diameters (Mpa)					
Element size (mm)	Stress for 54mm	stress for 84mm	Stress for 104mm	Stress for 144mm	Stress for 214mm	Stress for 244mm
3	86.9854	142.87	180	254.952	386.162	442.41
2	84.2031	135.345	171.545	244.5	372.451	427.319
1	75.463	128.412	163.806	235.278	360.927	414.847
0.6	71.3081	123.31	158.806	228.633	362.797	406.118
0.5	70.2773	122.073	158.149	227.023	350.827	405.258
0.4	69.056	120.541	156.987	224.21	348.235	403.2658
0.3	68.521	119.836	156.776	223.884	346.258	402.1236

Figure 0-4 shows the sensitivity analysis for the change in internal diameter

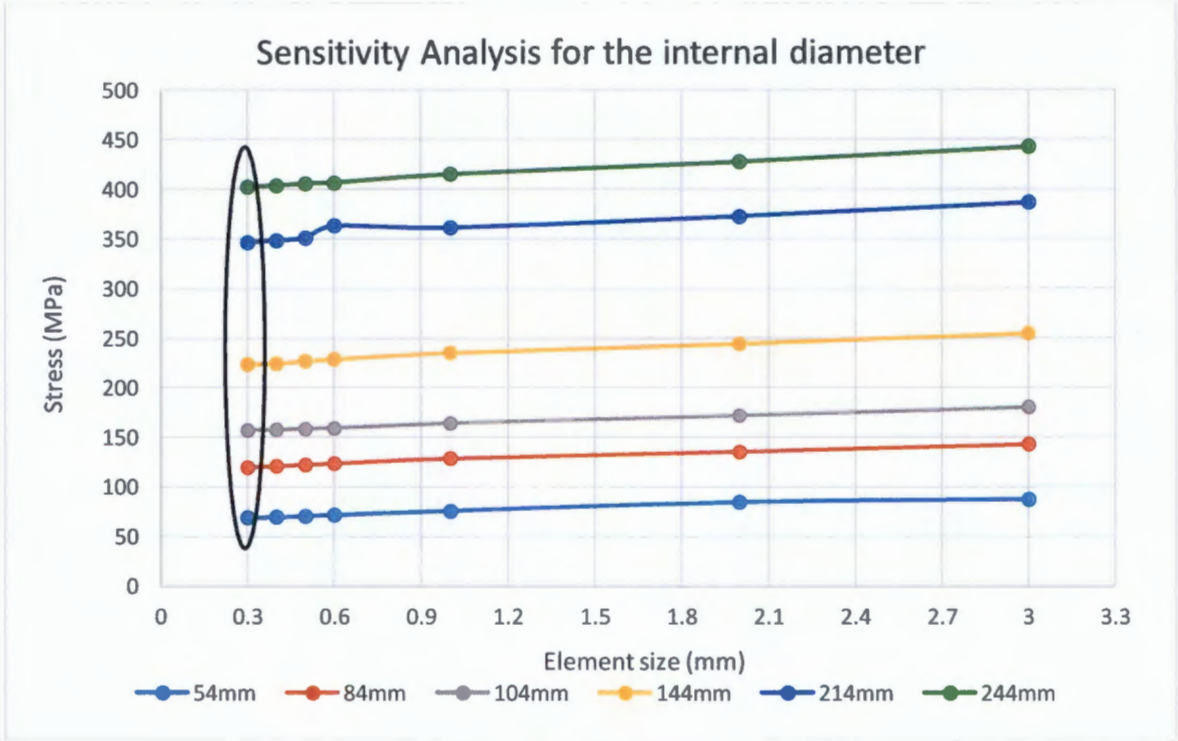

Figure 0-4: SENSITIVITY ANALYSIS FOR CHANGE IN INTERNAL DIAMETER FOR A PIPE WITH A 8 MM round hole

Based on Figure 0-4it can be seen that convergence occurred at 0.3mm element size. All internal diamers used 0.3mm as the standard element size for the local seeding.

B.2 Sensitivity analysis for the wall thickness

Table 0-50 shows the von mises stress distribution for the various wall thicknes' and element sizes investigated.

Table 0-50: Von mises stress distribution for the various wall thickness'

Element size(mm)	Von mises stress for various wall thickness' (MPa)				
	Stress for 2mm	Stress for 2.5mm	Stress for 3mm	Stress for 4mm	Stress for 5mm
3	232.99	212.99	198.68	185.36	175.98
2	224.535	201.485	171.545	147.94	134
1	216.796	192.946	163.806	143.28	125.461
0.5	205.36	175.584	158.149	138.42	119.604
0.3	202.36	169.25	156.776	133.56	118.031

Figure 0-5 that follows shows the sensitivity analysisfor a change in wall thickness for a pipe with a 8mm round hole.

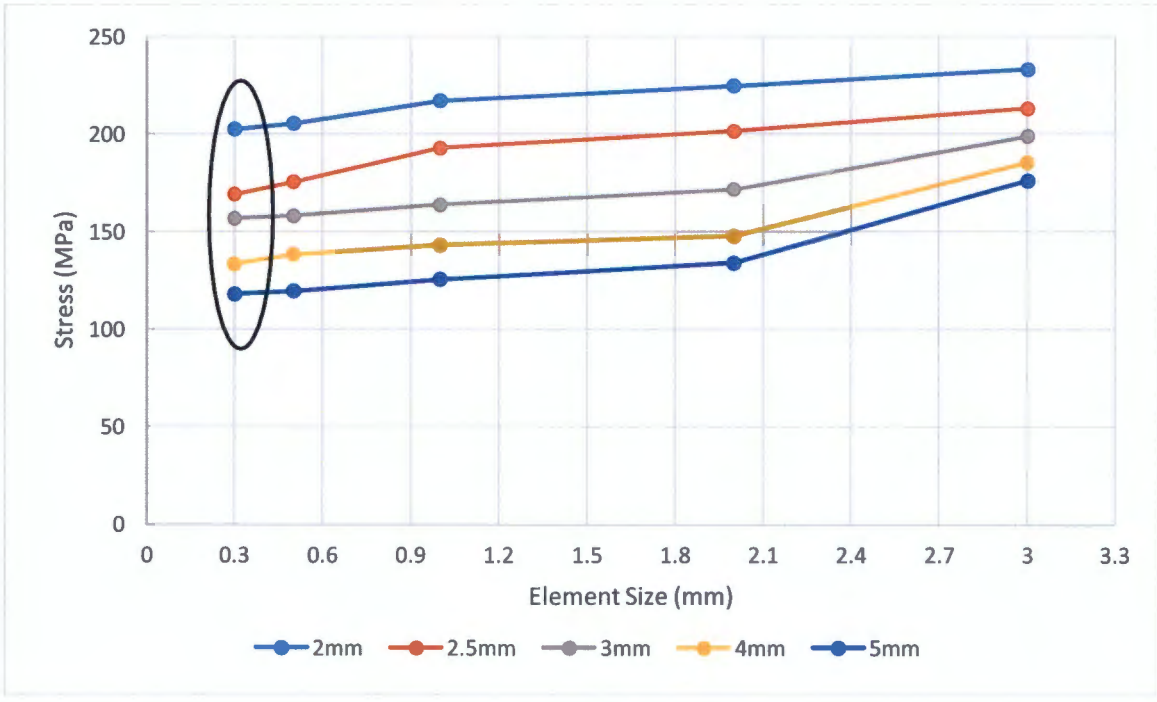

Figure 0-5: Sensetivity Analysis For Change In Wall Thickness For A ipe With A 8mm round hole

Based on Figure 0-5, once again iot can be seen that convergence occurs at the smallest element size of 0.3mm. All the wall thickness were investigated using a 0.3mm element size for the local seeding.

C. Calculation of the head-area slope of the derived equation

This section shows the calculations done for the derived head-area slope equation.

Parameter change	Trial No	t (m)	E (Pa)	v	Internal Diameter	α	σ	Diameter of pipe (m)	1/E	K	ϕ (m)	A_p		m_{FEM}	m_{FEM} x10^3
change in thickness	1	0.002	3.00E+09	0.4	0.106	5.00E-01	7.95E+06	0.108	3.33E-10	3	0.004	1.25664E-05	1.09E-09	1.8494E-08	18.4
	2	0.0025	3.00E+09	0.4	0.105	5.00E-01	6.30E+06	0.1075	3.33E-10	3	0.004	1.25664E-05	8.63E-10	1.38849E-08	13.8
	3	0.003	3.00E+09	0.4	0.104	5.00E-01	5.20E+06	0.11	3.33E-10	3	0.004	1.25664E-05	7.12E-10	1.03713E-08	10.3
	4	0.004	3.00E+09	0.4	0.102	5.00E-01	3.83E+06	0.11	3.33E-10	3	0.004	1.25664E-05	5.24E-10	5.44863E-09	5.4
	5	0.005	3.00E+09	0.4	0.1	5.00E-01	3.00E+06	0.11	3.33E-10	3	0.004	1.25664E-05	4.11E-10	2.21518E-09	2.2
Change in elastic modulus	6	0.003	3.00E+09	0.4	0.104	5.00E-01	5.20E+06	0.11	3.33E-10	3	0.004	1.25664E-05	7.12E-10	1.03E-08	10.3
	7	0.003	1.00E+10	0.4	0.104	5.00E-01	5.20E+06	0.11	1.00E-10	3	0.004	1.25664E-05	2.14E-10	-4.24003E-09	-4.2
	8	0.003	3.00E+10	0.4	0.104	5.00E-01	5.20E+06	0.11	3.33E-11	3	0.004	1.25664E-05	7.12E-11	-8.76654E-09	-8.7
	9	0.003	9.00E+10	0.4	0.104	5.00E-01	5.20E+06	0.11	1.11E-11	3	0.004	1.25664E-05	2.37E-11	-1.03123E-08	-10.3
	10	0.003	2.00E+11	0.4	0.104	5.00E-01	5.20E+06	0.11	5.00E-12	3	0.004	1.25664E-05	1.07E-11	-1.07401E-08	-10.7
Change in poisson ratio	11	0.003	3.00E+09	0.17	0.104	5.00E-01	5.20E+06	0.11	3.33E-10	3	0.004	1.25664E-05	7.12E-10	1.04147E-08	10.4
	12	0.003	3.00E+09	0.21	0.104	5.00E-01	5.20E+06	0.11	3.33E-10	3	0.004	1.25664E-05	7.12E-10	1.04068E-08	10.4
	13	0.003	3.00E+09	0.29	0.104	5.00E-01	5.20E+06	0.11	3.33E-10	3	0.004	1.25664E-05	7.12E-10	1.03915E-08	10.3
	14	0.003	3.00E+09	0.4	0.104	5.00E-01	5.20E+06	0.11	3.33E-10	3	0.004	1.25664E-05	7.12E-10	1.03728E-08	10.3
	15	0.003	3.00E+09	0.45	0.104	5.00E-01	5.20E+06	0.11	3.33E-10	3	0.004	1.25664E-05	7.12E-10	1.03662E-08	10.3
	16	0.003	3.00E+09	0.495	0.104	5.00E-01	5.20E+06	0.11	3.33E-10	3	0.004	1.25664E-05	7.12E-10	1.03618E-08	10.3
Change in internal diameter	17	0.003	3.00E+09	0.4	0.054	5.00E-01	2.70E+06	0.06	3.33E-10	3	0.004	1.25664E-05	3.70E-10	6.35082E-09	6.3
	18	0.003	3.00E+09	0.4	0.084	5.00E-01	4.20E+06	0.09	3.33E-10	3	0.004	1.25664E-05	5.75E-10	7.05501E-09	7.0
	19	0.003	3.00E+09	0.4	0.104	5.00E-01	5.20E+06	0.11	3.33E-10	3	0.004	1.25664E-05	7.12E-10	7.52148E-09	7.5
	20	0.003	3.00E+09	0.4	0.144	5.00E-01	7.20E+06	0.15	3.33E-10	3	0.004	1.25664E-05	9.86E-10	8.44526E-09	8.4
	21	0.003	3.00E+09	0.4	0.214	5.00E-01	1.07E+07	0.22	3.33E-10	3	0.004	1.25664E-05	1.47E-09	9.59074E-09	9.5
	22	0.003	3.00E+09	0.4	0.244	5.00E-01	1.22E+07	0.25	3.33E-10	3	0.004	1.25664E-05	1.67E-09	1.07218E-08	10.7
Change in longitudinal stress	23	0.003	3.00E+09	0.4	0.104	0.00E+00	0.00E+00	0.11	3.33E-10	3	0.004	1.25664E-05	7.12E-10	9.44159E-09	9.4
	24	0.003	3.00E+09	0.4	0.104	1.00E-01	1.04E+06	0.11	3.33E-10	3	0.004	1.25664E-05	7.12E-10	9.65979E-09	9.6
	25	0.003	3.00E+09	0.4	0.104	2.00E-01	2.08E+06	0.11	3.33E-10	3	0.004	1.25664E-05	7.12E-10	9.87867E-09	9.8
	26	0.003	3.00E+09	0.4	0.104	3.00E-01	3.12E+06	0.11	3.33E-10	3	0.004	1.25664E-05	7.12E-10	1.00971E-08	10.1
	27	0.003	3.00E+09	0.4	0.104	5.00E-01	5.20E+06	0.11	3.33E-10	3	0.004	1.25664E-05	7.12E-10	1.03152E-08	10.3
change in thickness	28	0.002	3.00E+09	0.4	0.106	5.00E-01	7.95E+06	0.11	3.33E-10	3	0.006	2.82743E-05	2.45E-09	4.53864E-08	45.3
	29	0.0025	3.00E+09	0.4	0.105	5.00E-01	6.30E+06	0.11	3.33E-10	3	0.006	2.82743E-05	1.94E-09	3.81424E-08	38.1
	30	0.003	3.00E+09	0.4	0.104	5.00E-01	5.20E+06	0.11	3.33E-10	3	0.006	2.82743E-05	1.60E-09	2.98317E-08	29.8
	31	0.004	3.00E+09	0.4	0.102	5.00E-01	3.83E+06	0.11	3.33E-10	3	0.006	2.82743E-05	1.18E-09	2.23016E-08	22.3
	32	0.005	3.00E+09	0.4	0.1	5.00E-01	3.00E+06	0.11	3.33E-10	3	0.006	2.82743E-05	9.25E-10	1.56296E-08	15.6
Change in elastic modulus	33	0.003	3.00E+09	0.4	0.104	5.00E-01	5.20E+06	0.11	3.33E-10	3	0.006	2.82743E-05	1.60E-09	2.96196E-08	29.6
	34	0.003	1.00E+10	0.4	0.104	5.00E-01	5.20E+06	0.11	1.00E-10	3	0.006	2.82743E-05	4.81E-10	-8.10047E-10	-0.8
	35	0.003	3.00E+10	0.4	0.104	5.00E-01	5.20E+06	0.11	3.33E-11	3	0.006	2.82743E-05	1.60E-10	-1.04194E-08	-10.4
	36	0.003	9.00E+10	0.4	0.104	5.00E-01	5.20E+06	0.11	1.11E-11	3	0.006	2.82743E-05	5.34E-11	-1.37132E-08	-13.7
	37	0.003	2.00E+11	0.4	0.104	5.00E-01	5.20E+06	0.11	5.00E-12	3	0.006	2.82743E-05	2.40E-11	-1.46263E-08	-14.6
Change in poisson ratio	38	0.003	3.00E+09	0.17	0.104	5.00E-01	5.20E+06	0.11	3.33E-10	3	0.006	2.82743E-05	1.60E-09	3.07802E-08	30.7
	39	0.003	3.00E+09	0.21	0.104	5.00E-01	5.20E+06	0.11	3.33E-10	3	0.006	2.82743E-05	1.60E-09	3.06092E-08	30.6
	40	0.003	3.00E+09	0.29	0.104	5.00E-01	5.20E+06	0.11	3.33E-10	3	0.006	2.82743E-05	1.60E-09	3.02725E-08	30.2
	41	0.003	3.00E+09	0.4	0.104	5.00E-01	5.20E+06	0.11	3.33E-10	3	0.006	2.82743E-05	1.60E-09	2.98327E-08	29.8
	42	0.003	3.00E+09	0.45	0.104	5.00E-01	5.20E+06	0.11	3.33E-10	3	0.006	2.82743E-05	1.60E-09	2.96465E-08	29.6
	43	0.003	3.00E+09	0.495	0.104	5.00E-01	5.20E+06	0.11	3.33E-10	3	0.006	2.82743E-05	1.60E-09	2.94882E-08	29.4
Change in internal diameter	44	0.003	3.00E+09	0.4	0.054	5.00E-01	2.70E+06	0.06	3.33E-10	3	0.006	2.82743E-05	8.32E-10	9.00339E-09	9.0
	45	0.003	3.00E+09	0.4	0.084	5.00E-01	4.20E+06	0.09	3.33E-10	3	0.006	2.82743E-05	1.29E-09	2.29696E-08	22.9
	46	0.003	3.00E+09	0.4	0.104	5.00E-01	5.20E+06	0.11	3.33E-10	3	0.006	2.82743E-05	1.60E-09	3.18051E-08	31.8
	47	0.003	3.00E+09	0.4	0.144	5.00E-01	7.20E+06	0.15	3.33E-10	3	0.006	2.82743E-05	2.22E-09	4.82696E-08	48.2
	48	0.003	3.00E+09	0.4	0.214	5.00E-01	1.07E+07	0.22	3.33E-10	3	0.006	2.82743E-05	3.30E-09	6.66764E-08	66.6
	49	0.003	3.00E+09	0.4	0.244	5.00E-01	1.22E+07	0.25	3.33E-10	3	0.006	2.82743E-05	3.76E-09	8.25627E-08	82.5
Change in longitudinal stress	50	0.003	3.00E+09	0.4	0.104	0.00E+00	0.00E+00	0.11	3.33E-10	3	0.006	2.82743E-05	1.60E-09	2.7653E-08	27.6
	51	0.003	3.00E+09	0.4	0.104	1.00E-01	1.04E+06	0.11	3.33E-10	3	0.006	2.82743E-05	1.60E-09	2.81645E-08	28.1
	52	0.003	3.00E+09	0.4	0.104	2.00E-01	2.08E+06	0.11	3.33E-10	3	0.006	2.82743E-05	1.60E-09	2.86762E-08	28.6
	53	0.003	3.00E+09	0.4	0.104	3.00E-01	3.12E+06	0.11	3.33E-10	3	0.006	2.82743E-05	1.60E-09	2.91864E-08	29.1
	54	0.003	3.00E+09	0.4	0.104	5.00E-01	5.20E+06	0.11	3.33E-10	3	0.006	2.82743E-05	1.60E-09	2.96967E-08	29.7
change in thickness	55	0.002	3.00E+09	0.4	0.106	5.00E-01	7.95E+06	0.11	3.33E-10	3	0.008	5.02655E-05	4.36E-09	7.14679E-08	71.4
	56	0.0025	3.00E+09	0.4	0.105	5.00E-01	6.30E+06	0.11	3.33E-10	3	0.008	5.02655E-05	3.45E-09	6.03408E-08	60.3
	57	0.003	3.00E+09	0.4	0.104	5.00E-01	5.20E+06	0.11	3.33E-10	3	0.008	5.02655E-05	2.85E-09	4.96855E-08	49.6
	58	0.004	3.00E+09	0.4	0.102	5.00E-01	3.83E+06	0.11	3.33E-10	3	0.008	5.02655E-05	2.10E-09	3.74038E-08	37.4
	59	0.005	3.00E+09	0.4	0.1	5.00E-01	3.00E+06	0.11	3.33E-10	3	0.008	5.02655E-05	1.64E-09	2.59085E-08	25.9
Change in elastic modulus	60	0.003	3.00E+09	0.4	0.104	5.00E-01	5.20E+06	0.11	3.33E-10	3	0.008	5.02655E-05	2.85E-09	5.58258E-08	55.8
	61	0.003	1.00E+10	0.4	0.104	5.00E-01	5.20E+06	0.11	1.00E-10	3	0.008	5.02655E-05	8.55E-10	7.23307E-09	7.2
	62	0.003	3.00E+10	0.4	0.104	5.00E-01	5.20E+06	0.11	3.33E-11	3	0.008	5.02655E-05	2.85E-10	-8.40746E-09	-8.4
	63	0.003	9.00E+10	0.4	0.104	5.00E-01	5.20E+06	0.11	1.11E-11	3	0.008	5.02655E-05	9.50E-11	-1.37947E-08	-13.7
	64	0.003	2.00E+11	0.4	0.104	5.00E-01	5.20E+06	0.11	5.00E-12	3	0.008	5.02655E-05	4.27E-11	-1.52911E-08	-15.2
Change in poisson ratio	65	0.003	3.00E+09	0.17	0.104	5.00E-01	5.20E+06	0.11	3.33E-10	3	0.008	5.02655E-05	2.85E-09	5.94174E-08	59.4
	66	0.003	3.00E+09	0.21	0.104	5.00E-01	5.20E+06	0.11	3.33E-10	3	0.008	5.02655E-05	2.85E-09	5.88333E-08	58.8
	67	0.003	3.00E+09	0.29	0.104	5.00E-01	5.20E+06	0.11	3.33E-10	3	0.008	5.02655E-05	2.85E-09	5.76943E-08	57.6
	68	0.003	3.00E+09	0.4	0.104	5.00E-01	5.20E+06	0.11	3.33E-10	3	0.008	5.02655E-05	2.85E-09	5.62274E-08	56.2
	69	0.003	3.00E+09	0.45	0.104	5.00E-01	5.20E+06	0.11	3.33E-10	3	0.008	5.02655E-05	2.85E-09	5.56144E-08	55.6
	70	0.003	3.00E+09	0.495	0.104	5.00E-01	5.20E+06	0.11	3.33E-10	3	0.008	5.02655E-05	2.85E-09	5.51033E-08	55.1
Change in internal diameter	71	0.003	3.00E+09	0.4	0.054	5.00E-01	2.70E+06	0.06	3.33E-10	3	0.008	5.02655E-05	1.48E-09	1.90448E-08	19.0
	72	0.003	3.00E+09	0.4	0.084	5.00E-01	4.20E+06	0.09	3.33E-10	3	0.008	5.02655E-05	2.30E-09	4.12724E-08	41.2
	73	0.003	3.00E+09	0.4	0.104	5.00E-01	5.20E+06	0.11	3.33E-10	3	0.008	5.02655E-05	2.85E-09	5.62198E-08	56.2
	74	0.003	3.00E+09	0.4	0.144	5.00E-01	7.20E+06	0.15	3.33E-10	3	0.008	5.02655E-05	3.94E-09	8.40475E-08	84.0
	75	0.003	3.00E+09	0.4	0.214	5.00E-01	1.07E+07	0.22	3.33E-10	3	0.008	5.02655E-05	5.86E-09	1.15112E-07	115.1
	76	0.003	3.00E+09	0.4	0.244	5.00E-01	1.22E+07	0.25	3.33E-10	3	0.008	5.02655E-05	6.68E-09	1.41645E-07	141.6
Change in longitudinal stress	77	0.003	3.00E+09	0.4	0.104	0.00E+00	0.00E+00	0.11	3.33E-10	3	0.008	5.02655E-05	2.85E-09	5.11211E-08	51.1
	78	0.003	3.00E+09	0.4	0.104	1.00E-01	1.04E+06	0.11	3.33E-10	3	0.008	5.02655E-05	2.85E-09	5.20554E-08	52.0
	79	0.003	3.00E+09	0.4	0.104	2.00E-01	2.08E+06	0.11	3.33E-10	3	0.008	5.02655E-05	2.85E-09	5.29897E-08	52.9
	80	0.003	3.00E+09	0.4	0.104	3.00E-01	3.12E+06	0.11	3.33E-10	3	0.008	5.02655E-05	2.85E-09	5.3921E-08	53.9
	81	0.003	3.00E+09	0.4	0.104	5.00E-01	5.20E+06	0.11	3.33E-10	3	0.008	5.02655E-05	2.85E-09	5.48525E-08	54.8

Parameter change	m_1	m_2	$m_1+m_2=m_{calculated}$	m1 contribution	m2 contribution	m1 x 10^9	$m_{1\ modified}$	$m_{1\ modified}$ x 10^9
change in thickness	2.99256E-09	4.31E-12	2.99686E-09	99.86%	0.14%	2.992555498	1.59E-08	15.94
	2.38296E-09	2.73E-12	2.38569E-09	99.89%	0.11%	2.38296086	1.11E-08	11.06
	2.03198E-09	1.99E-12	2.03397E-09	99.90%	0.10%	2.031982128	8.26E-09	8.26
	1.52399E-09	1.12E-12	1.52510E-09	99.93%	0.07%	1.523986596	4.19E-09	4.19
	1.21919E-09	7.15E-13	1.21990E-09	99.94%	0.06%	1.219189277	1.75E-09	1.75
Change in elastic modulus	2.03198E-09	1.99E-12	2.03397E-09	99.90%	0.10%	2.031982128	8.26E-09	8.26
	6.09595E-10	1.79E-13	6.09773E-10	99.97%	0.03%	0.609594639	-3.12E-09	-3.12
	2.03198E-10	1.99E-14	2.03218E-10	99.99%	0.01%	0.203198213	-6.37E-09	-6.37
	6.77327E-11	2.21E-15	6.77349E-11	100.00%	0.00%	0.067732738	-7.46E-09	-7.46
	3.04797E-11	4.47E-16	3.04802E-11	100.00%	0.00%	0.030479732	-7.76E-09	-7.76
Change in poisson ratio	2.81091E-09	7.50E-12	2.81841E-09	99.73%	0.27%	2.810908611	1.45E-08	14.49
	2.67544E-09	6.45E-12	2.68189E-09	99.76%	0.24%	2.675443136	1.34E-08	13.40
	2.40451E-09	4.46E-12	2.40897E-09	99.81%	0.19%	2.404512185	1.12E-08	11.24
	2.03198E-09	1.99E-12	2.03397E-09	99.90%	0.10%	2.031982128	8.26E-09	8.26
	1.86265E-09	9.62E-13	1.86361E-09	99.95%	0.05%	1.862650284	6.90E-09	6.90
	1.71025E-09	9.34E-14	1.71035E-09	99.99%	0.01%	1.710251625	5.68E-09	5.68
Change in internal diameter	1.10835E-09	5.91E-13	1.10895E-09	99.95%	0.05%	1.108353888	8.67E-10	0.87
	1.66253E-09	1.33E-12	1.66386E-09	99.92%	0.08%	1.662530832	5.30E-09	5.30
	2.03198E-09	1.99E-12	2.03397E-09	99.90%	0.10%	2.031982128	8.26E-09	8.26
	2.77088E-09	3.69E-12	2.77458E-09	99.87%	0.13%	2.77088472	1.42E-08	14.17
	4.06396E-09	7.95E-12	4.07191E-09	99.80%	0.20%	4.063964257	2.45E-08	24.51
	4.61814E-09	1.03E-11	4.62840E-09	99.78%	0.22%	4.618141201	2.89E-08	28.95
Change in longitudinal stress	1.35465E-09	-9.93E-12	1.34472E-09	100.74%	-0.74%	1.354654752	2.84E-09	2.84
	1.49012E-09	-7.15E-12	1.48297E-09	100.48%	-0.48%	1.490120227	3.92E-09	3.92
	1.62559E-09	-4.57E-12	1.62102E-09	100.28%	-0.28%	1.625585703	5.00E-09	5.00
	1.76105E-09	-2.19E-12	1.75887E-09	100.12%	-0.12%	1.761051178	6.09E-09	6.09
	2.03198E-09	1.99E-12	2.03397E-09	99.90%	0.10%	2.031982128	8.26E-09	8.26
change in thickness	6.85794E-09	1.01E-11	6.86800E-09	99.85%	0.15%	6.857939683	4.69E-08	46.86
	5.48635E-09	6.44E-12	5.49279E-09	99.88%	0.12%	5.486351747	3.59E-08	35.89
	4.57196E-09	4.47E-12	4.57643E-09	99.90%	0.10%	4.571959789	2.86E-08	28.58
	3.42897E-09	2.51E-12	3.43148E-09	99.93%	0.07%	3.428969842	1.94E-08	19.43
	2.74318E-09	1.61E-12	2.74479E-09	99.94%	0.06%	2.743175873	1.39E-08	13.95
Change in elastic modulus	4.57196E-09	4.47E-12	4.57643E-09	99.90%	0.10%	4.571959789	2.86E-08	28.58
	1.37159E-09	4.02E-13	1.37199E-09	99.97%	0.03%	1.371587937	2.97E-09	2.97
	4.57196E-10	4.47E-14	4.57241E-10	99.99%	0.01%	0.457195979	-4.34E-09	-4.34
	1.52399E-10	4.97E-15	1.52404E-10	100.00%	0.00%	0.15239866	-6.78E-09	-6.78
	6.85794E-11	1.01E-15	6.85804E-11	100.00%	0.00%	0.068579397	-7.45E-09	-7.45
Change in poisson ratio	6.32454E-09	1.69E-11	6.34142E-09	99.73%	0.27%	6.324544374	4.26E-08	42.60
	6.01975E-09	1.45E-11	6.03425E-09	99.76%	0.24%	6.019747055	4.02E-08	40.16
	5.41015E-09	1.00E-11	5.42019E-09	99.81%	0.19%	5.410152417	3.53E-08	35.28
	4.57196E-09	4.47E-12	4.57643E-09	99.90%	0.10%	4.571959789	2.86E-08	28.58
	4.19096E-09	2.17E-12	4.19313E-09	99.95%	0.05%	4.19096314	2.55E-08	25.53
	3.84807E-09	2.10E-13	3.84828E-09	99.99%	0.01%	3.848066156	2.28E-08	22.78
Change in internal diameter	2.4938E-09	1.33E-12	2.49513E-09	99.95%	0.05%	2.493796248	1.20E-08	11.95
	3.74069E-09	2.99E-12	3.74369E-09	99.92%	0.08%	3.740694373	2.19E-08	21.93
	4.57196E-09	4.47E-12	4.57643E-09	99.90%	0.10%	4.571959789	2.86E-08	28.58
	6.23449E-09	8.31E-12	6.24280E-09	99.87%	0.13%	6.234490621	4.19E-08	41.88
	9.14392E-09	1.79E-11	9.16180E-09	99.80%	0.20%	9.143919578	6.52E-08	65.15
	1.03908E-08	2.31E-11	1.04139E-08	99.78%	0.22%	10.3908177	7.51E-08	75.13
Change in longitudinal stress	3.04797E-09	-2.24E-11	3.02562E-09	100.74%	-0.74%	3.047973193	1.64E-08	16.38
	3.35277E-09	-1.61E-11	3.33668E-09	100.48%	-0.48%	3.352770512	1.88E-08	18.82
	3.65757E-09	-1.03E-11	3.64729E-09	100.28%	-0.28%	3.657567831	2.13E-08	21.26
	3.96237E-09	-4.92E-12	3.95745E-09	100.12%	-0.12%	3.96236515	2.37E-08	23.70
	4.57196E-09	4.47E-12	4.57643E-09	99.90%	0.10%	4.571959789	2.86E-08	28.58
change in thickness	1.21919E-08	1.79E-11	1.22098E-08	99.85%	0.15%	12.19189277	8.95E-08	89.54
	9.75351E-09	1.14E-11	9.76496E-09	99.88%	0.12%	9.753514216	7.00E-08	70.03
	8.12793E-09	7.95E-12	8.13588E-09	99.90%	0.10%	8.127928513	5.70E-08	57.02
	6.09595E-09	4.47E-12	6.10042E-09	99.93%	0.07%	6.095946385	4.08E-08	40.77
	4.87676E-09	2.86E-12	4.87962E-09	99.94%	0.06%	4.876757108	3.10E-08	31.01
Change in elastic modulus	8.12793E-09	7.95E-12	8.13588E-09	99.90%	0.10%	8.127928513	5.70E-08	57.02
	2.43838E-09	7.15E-13	2.43909E-09	99.97%	0.03%	2.438378554	1.15E-08	11.51
	8.12793E-10	7.95E-14	8.12872E-10	99.99%	0.01%	0.812792851	-1.50E-09	-1.50
	2.70931E-10	8.83E-15	2.70940E-10	100.00%	0.00%	0.27093095	-5.83E-09	-5.83
	1.21919E-10	1.79E-15	1.21921E-10	100.00%	0.00%	0.121918928	-7.02E-09	-7.02
Change in poisson ratio	1.12436E-08	3.00E-11	1.12736E-08	99.73%	0.27%	11.24363444	8.19E-08	81.95
	1.07018E-08	2.58E-11	1.07276E-08	99.76%	0.24%	10.70177254	7.76E-08	77.61
	9.61805E-09	1.78E-11	9.63589E-09	99.81%	0.19%	9.618048741	6.89E-08	68.94
	8.12793E-09	7.95E-12	8.13588E-09	99.90%	0.10%	8.127928513	5.70E-08	57.02
	7.4506E-09	3.85E-12	7.45445E-09	99.95%	0.05%	7.450601137	5.16E-08	51.60
	6.84101E-09	3.74E-13	6.84138E-09	99.99%	0.01%	6.841006499	4.67E-08	46.73
Change in internal diameter	4.43342E-09	2.36E-12	4.43578E-09	99.95%	0.05%	4.433415553	2.75E-08	27.47
	6.65012E-09	5.32E-12	6.65544E-09	99.92%	0.08%	6.650123329	4.52E-08	45.20
	8.12793E-09	7.95E-12	8.13588E-09	99.90%	0.10%	8.127928513	5.70E-08	57.02
	1.10835E-08	1.48E-11	1.10983E-08	99.87%	0.13%	11.08353888	8.07E-08	80.67
	1.62559E-08	3.18E-11	1.62876E-08	99.80%	0.20%	16.25585703	1.22E-07	122.05
	1.84726E-08	4.11E-11	1.85136E-08	99.78%	0.22%	18.4725648	1.40E-07	139.78
Change in longitudinal stress	5.41862E-09	-3.97E-11	5.37888E-09	100.74%	-0.74%	5.418619009	3.53E-08	35.35
	5.96048E-09	-2.86E-11	5.93187E-09	100.48%	-0.48%	5.96048091	3.97E-08	39.68
	6.50234E-09	-1.83E-11	6.48406E-09	100.28%	-0.28%	6.502342811	4.40E-08	44.02
	7.0442E-09	-8.74E-12	7.03546E-09	100.12%	-0.12%	7.044204712	4.84E-08	48.35
	8.12793E-09	7.95E-12	8.13588E-09	99.90%	0.10%	8.127928513	5.70E-08	57.02

D. Mathematical models

D.1 Mathematical Model For The 4mm Hole

		Original		Deformed	
Degrees	radians	Rx	Ry	Rx	Ry
0	0	0	4	0	4.58666667
5	0.08726646	0.34862297	3.98477879	0.35075344	4.56921302
10	0.17453293	0.69459271	3.93923101	0.69883744	4.51698489
15	0.26179939	1.03527618	3.86370331	1.04160287	4.43037979
20	0.34906585	1.36808057	3.75877048	1.37644107	4.31005682
25	0.43633231	1.69047305	3.62523115	1.70080372	4.15693172
30	0.52359878	2	3.46410162	2.01222222	3.97216985
35	0.61086524	2.29430575	3.27660818	2.3083265	3.75717738
40	0.6981317	2.57115044	3.06417777	2.58686302	3.51359051
45	0.78539816	2.82842712	2.82842712	2.84571196	3.2432631
50	0.87266463	3.06417777	2.57115044	3.0829033	2.9482525
55	0.95993109	3.27660818	2.29430575	3.29663189	2.63080392
60	1.04719755	3.46410162	2	3.48527113	2.29333333
65	1.13446401	3.62523115	1.69047305	3.64738534	1.93840909
70	1.22173048	3.75877048	1.36808057	3.78174075	1.56873239
75	1.30899694	3.86370331	1.03527618	3.88731483	1.18711669
80	1.3962634	3.93923101	0.69459271	3.96330409	0.79646631
85	1.48352986	3.98477879	0.34862297	4.00913022	0.39975434
90	1.57079633	4	2.4503E-16	4.02444444	2.8097E-16
95	1.65806279	3.98477879	-0.348623	4.00913022	-0.3997543
100	1.74532925	3.93923101	-0.6945927	3.96330409	-0.7964663
105	1.83259571	3.86370331	-1.0352762	3.88731483	-1.1871167
110	1.91986218	3.75877048	-1.3680806	3.78174075	-1.5687324
115	2.00712864	3.62523115	-1.690473	3.64738534	-1.9384091
120	2.0943951	3.46410162	-2	3.48527113	-2.2933333
125	2.18166156	3.27660818	-2.2943057	3.29663189	-2.6308039
130	2.26892803	3.06417777	-2.5711504	3.0829033	-2.9482525
135	2.35619449	2.82842712	-2.8284271	2.84571196	-3.2432631
140	2.44346095	2.57115044	-3.0641778	2.58686302	-3.5135905
145	2.53072742	2.29430575	-3.2766082	2.3083265	-3.7571774
150	2.61799388	2	-3.4641016	2.01222222	-3.9721699
155	2.70526034	1.69047305	-3.6252311	1.70080372	-4.1569317
160	2.7925268	1.36808057	-3.7587705	1.37644107	-4.3100568
165	2.87979327	1.03527618	-3.8637033	1.04160287	-4.4303798
170	2.96705973	0.69459271	-3.939231	0.69883744	-4.5169849
175	3.05432619	0.34862297	-3.9847788	0.35075344	-4.569213
180	3.14159265	4.9006E-16	-4	4.9305E-16	-4.5866667
185	3.22885912	-0.348623	-3.9847788	-0.3507534	-4.569213
190	3.31612558	-0.6945927	-3.939231	-0.6988374	-4.5169849
195	3.40339204	-1.0352762	-3.8637033	-1.0416029	-4.4303798
200	3.4906585	-1.3680806	-3.7587705	-1.3764411	-4.3100568
205	3.57792497	-1.690473	-3.6252311	-1.7008037	-4.1569317
210	3.66519143	-2	-3.4641016	-2.0122222	-3.9721699
215	3.75245789	-2.2943057	-3.2766082	-2.3083265	-3.7571774
220	3.83972435	-2.5711504	-3.0641778	-2.586863	-3.5135905
225	3.92699082	-2.8284271	-2.8284271	-2.845712	-3.2432631
230	4.01425728	-3.0641778	-2.5711504	-3.0829033	-2.9482525
235	4.10152374	-3.2766082	-2.2943057	-3.2966319	-2.6308039
240	4.1887902	-3.4641016	-2	-3.4852711	-2.2933333
245	4.27605667	-3.6252311	-1.690473	-3.6473853	-1.9384091
250	4.36332313	-3.7587705	-1.3680806	-3.7817407	-1.5687324
255	4.45058959	-3.8637033	-1.0352762	-3.8873148	-1.1871167
260	4.53785606	-3.939231	-0.6945927	-3.9633041	-0.7964663
265	4.62512252	-3.9847788	-0.348623	-4.0091302	-0.3997543
270	4.71238898	-4	-7.351E-16	-4.0244444	-8.429E-16
275	4.79965544	-3.9847788	0.34862297	-4.0091302	0.39975434
280	4.88692191	-3.939231	0.69459271	-3.9633041	0.79646631
285	4.97418837	-3.8637033	1.03527618	-3.8873148	1.18711669
290	5.06145483	-3.7587705	1.36808057	-3.7817407	1.56873239
295	5.14872129	-3.6252311	1.69047305	-3.6473853	1.93840909
300	5.23598776	-3.4641016	2	-3.4852711	2.29333333
305	5.32325422	-3.2766082	2.29430575	-3.2966319	2.63080392
310	5.41052068	-3.0641778	2.57115044	-3.0829033	2.9482525
315	5.49778714	-2.8284271	2.82842712	-2.845712	3.2432631
320	5.58505361	-2.5711504	3.06417777	-2.586863	3.51359051
325	5.67232007	-2.2943057	3.27660818	-2.3083265	3.75717738
330	5.75958653	-2	3.46410162	-2.0122222	3.97216985
335	5.84685299	-1.690473	3.62523115	-1.7008037	4.15693172
340	5.93411946	-1.3680806	3.75877048	-1.3764411	4.31005682
345	6.02138592	-1.0352762	3.86370331	-1.0416029	4.43037979
350	6.10865238	-0.6945927	3.93923101	-0.6988374	4.51698489
355	6.19591884	-0.348623	3.98477879	-0.3507534	4.56921302
360	6.28318531	-9.801E-16	4	-9.861E-16	4.58666667

Riemman Sum Calculation for original hole area			
Y	X1	X2	original Area
0.01522121	0	0.348622971	0.002653231
0.04554778	0.34862297	0.694592711	0.023758079
0.07552771	0.69459271	1.03527618	0.065326515
0.10493282	1.03527618	1.368080573	0.126095503
0.13353933	1.36808057	1.690473047	0.204218608
0.16112953	1.69047305	2	0.297322099
0.18749344	2	2.294305745	0.402577074
0.2124304	2.29430575	2.571150439	0.516785413
0.23575065	2.57115044	2.828427125	0.636476954
0.25727669	2.82842712	3.064177772	0.75801493
0.27684469	3.06417777	3.276608177	0.877706471
0.29430575	3.27660818	3.464101615	0.99191481
0.30952695	3.46410162	3.625231148	1.097169785
0.32239247	3.62523115	3.758770483	1.190273276
0.33280439	3.75877048	3.863703305	1.268396381
0.34068347	3.86370331	3.939231012	1.329165369
0.34596974	3.93923101	3.984778792	1.370733805
0.34862297	3.98477879	4	1.391838653
0.34862297	4	3.984778792	1.391838653
0.34596974	3.98477879	3.939231012	1.370733805
0.34068347	3.93923101	3.863703305	1.329165369
0.33280439	3.86370331	3.758770483	1.268396381
0.32239247	3.75877048	3.625231148	1.190273276
0.30952695	3.62523115	3.464101615	1.097169785
0.29430575	3.46410162	3.276608177	0.99191481
0.27684469	3.27660818	3.064177772	0.877706471
0.25727669	3.06417777	2.828427125	0.75801493
0.23575065	2.82842712	2.571150439	0.636476954
0.2124304	2.57115044	2.294305745	0.516785413
0.18749344	2.29430575	2	0.402577074
0.16112953	2	1.690473047	0.297322099
0.13353933	1.69047305	1.368080573	0.204218608
0.10493282	1.36808057	1.03527618	0.126095503
0.07552771	1.03527618	0.694592711	0.065326515
0.04554778	0.69459271	0.348622971	0.023758079
0.01522121	0.34862297	4.90059E-16	0.002653231
0.01522121	4.9006E-16	0.348622971	0.002653231
0.04554778	0.34862297	0.694592711	0.023758079
0.07552771	0.69459271	1.03527618	0.065326515
0.10493282	1.03527618	1.368080573	0.126095503
0.13353933	1.36808057	1.690473047	0.204218608
0.16112953	1.69047305	2	0.297322099
0.18749344	2	2.294305745	0.402577074
0.2124304	2.29430575	2.571150439	0.516785413
0.23575065	2.57115044	2.828427125	0.636476954
0.25727669	2.82842712	3.064177772	0.75801493
0.27684469	3.06417777	3.276608177	0.877706471
0.29430575	3.27660818	3.464101615	0.99191481
0.30952695	3.46410162	3.625231148	1.097169785
0.32239247	3.62523115	3.758770483	1.190273276
0.33280439	3.75877048	3.863703305	1.268396381
0.34068347	3.86370331	3.939231012	1.329165369
0.34596974	3.93923101	3.984778792	1.370733805
0.34862297	3.98477879	4	1.391838653
0.34862297	4	3.984778792	1.391838653
0.34596974	3.98477879	3.939231012	1.370733805
0.34068347	3.93923101	3.863703305	1.329165369
0.33280439	3.86370331	3.758770483	1.268396381
0.32239247	3.75877048	3.625231148	1.190273276
0.30952695	3.62523115	3.464101615	1.097169785
0.29430575	3.46410162	3.276608177	0.99191481
0.27684469	3.27660818	3.064177772	0.877706471
0.25727669	3.06417777	2.828427125	0.75801493
0.23575065	2.82842712	2.571150439	0.636476954
0.2124304	2.57115044	2.294305745	0.516785413
0.18749344	2.29430575	2	0.402577074
0.16112953	2	1.690473047	0.297322099
0.13353933	1.69047305	1.368080573	0.204218608
0.10493282	1.36808057	1.03527618	0.126095503
0.07552771	1.03527618	0.694592711	0.065326515
0.04554778	0.69459271	0.348622971	0.023758079
0.01522121	0.34862297	9.80119E-16	0.002653231
4	9.8012E-16	0	1.96024E-15
		Estimated original Area	50.20170782
		Actual Area	50.26548246
		%error	0.001268756

Riemman Sum Calculation for deformed hole area			
Y	X1	X2	Deformed Area
0.01745365	0	0.350753445	0.003060964
0.05222812	0.35075344	0.698837444	0.02740908
0.0866051	0.69883744	1.041602868	0.075365507
0.12032297	1.04160287	1.376441066	0.145473113
0.1531251	1.37644107	1.700803716	0.235601714
0.18476186	1.70080372	2.012222222	0.343012798
0.21499248	2.01222222	2.308326503	0.464442733
0.24358686	2.3083265	2.586863025	0.596201933
0.27032741	2.58686302	2.845711957	0.734286961
0.2950106	2.84571196	3.082903303	0.874502172
0.31744858	3.0829033	3.296631894	1.0125872
0.33747059	3.29663189	3.485271125	1.1443464
0.35492424	3.48527113	3.647385338	1.265776335
0.3696767	3.64738534	3.781740747	1.373187419
0.3816157	3.78174075	3.887314825	1.46331602
0.39065038	3.88731483	3.96330409	1.533423626
0.39671197	3.96330409	4.009130218	1.581380053
0.39975434	4.00913022	4.024444444	1.605728169
0.39975434	4.02444444	4.009130218	1.605728169
0.39671197	4.00913022	3.96330409	1.581380053
0.39065038	3.96330409	3.887314825	1.533423626
0.3816157	3.88731483	3.781740747	1.46331602
0.3696767	3.78174075	3.647385338	1.373187419
0.35492424	3.64738534	3.485271125	1.265776335
0.33747059	3.48527113	3.296631894	1.1443464
0.31744858	3.29663189	3.082903303	1.0125872
0.2950106	3.0829033	2.845711957	0.874502172
0.27032741	2.84571196	2.586863025	0.734286961
0.24358686	2.58686302	2.308326503	0.596201933
0.21499248	2.3083265	2.012222222	0.464442733
0.18476186	2.01222222	1.700803716	0.343012798
0.1531251	1.70080372	1.376441066	0.235601714
0.12032297	1.37644107	1.041602868	0.145473113
0.0866051	1.04160287	0.698837444	0.075365507
0.05222812	0.69883744	0.350753445	0.02740908
0.01745365	0.35075344	4.93054E-16	0.003060964
0.01745365	4.9305E-16	0.350753445	0.003060964
0.05222812	0.35075344	0.698837444	0.02740908
0.0866051	0.69883744	1.041602868	0.075365507
0.12032297	1.04160287	1.376441066	0.145473113
0.1531251	1.37644107	1.700803716	0.235601714
0.18476186	1.70080372	2.012222222	0.343012798
0.21499248	2.01222222	2.308326503	0.464442733
0.24358686	2.3083265	2.586863025	0.596201933
0.27032741	2.58686302	2.845711957	0.734286961
0.2950106	2.84571196	3.082903303	0.874502172
0.31744858	3.0829033	3.296631894	1.0125872
0.33747059	3.29663189	3.485271125	1.1443464
0.35492424	3.48527113	3.647385338	1.265776335
0.3696767	3.64738534	3.781740747	1.373187419
0.3816157	3.78174075	3.887314825	1.46331602
0.39065038	3.88731483	3.96330409	1.533423626
0.39671197	3.96330409	4.009130218	1.581380053
0.39975434	4.00913022	4.024444444	1.605728169
0.39975434	4.02444444	4.009130218	1.605728169
0.39671197	4.00913022	3.96330409	1.581380053
0.39065038	3.96330409	3.887314825	1.533423626
0.3816157	3.88731483	3.781740747	1.46331602
0.3696767	3.78174075	3.647385338	1.373187419
0.35492424	3.64738534	3.485271125	1.265776335
0.33747059	3.48527113	3.296631894	1.1443464
0.31744858	3.29663189	3.082903303	1.0125872
0.2950106	3.0829033	2.845711957	0.874502172
0.27032741	2.84571196	2.586863025	0.734286961
0.24358686	2.58686302	2.308326503	0.596201933
0.21499248	2.3083265	2.012222222	0.464442733
0.18476186	2.01222222	1.700803716	0.343012798
0.1531251	1.70080372	1.376441066	0.235601714
0.12032297	1.37644107	1.041602868	0.145473113
0.0866051	1.04160287	0.698837444	0.075365507
0.05222812	0.69883744	0.350753445	0.02740908
0.01745365	0.35075344	9.86108E-16	0.003060964
4.58666667	9.8611E-16	0	2.26148E-15
		Estimated deformed Area	57.91640879
		Actual Area	57.98998393
		Calculated Area of ellipse	57.98998393
		% error	0.001268756

D2. Mathematical Model For The 6mm Hole

		Original		Deformed	
Degrees	radians	R_{x0}	R_{y0}	$R_{x\ new}$	$R_{y\ new}$
0	0	0	6	0	6.176
5	0.087266463	0.522934456	5.9771682	0.523574	6.1524985
10	0.174532925	1.041889066	5.9088465	1.043162	6.0821727
15	0.261799388	1.552914271	5.795555	1.554812	5.9655579
20	0.34906585	2.05212086	5.6381557	2.054629	5.8035416
25	0.436332313	2.53570957	5.4378467	2.538809	5.5973569
30	0.523598776	3	5.1961524	3.003667	5.3485729
35	0.610865238	3.441458618	4.9149123	3.445665	5.059083
40	0.698131701	3.856725658	4.5962667	3.861439	4.7310905
45	0.785398163	4.242640687	4.2426407	4.247826	4.3670915
50	0.872664626	4.596266659	3.8567257	4.601884	3.9698563
55	0.959931089	4.914912266	3.4414586	4.920919	3.5424081
60	1.047197551	5.196152423	3	5.202503	3.088
65	1.134464014	5.437846722	2.5357096	5.444493	2.6100904
70	1.221730476	5.638155725	2.0521209	5.645047	2.1123164
75	1.308996939	5.795554958	1.5529143	5.802638	1.5984664
80	1.396263402	5.908846518	1.0418891	5.916068	1.0724511
85	1.483529864	5.977168189	0.5229345	5.984474	0.5382739
90	1.570796327	6	3.675E-16	6.007333	3.783E-16
95	1.658062789	5.977168189	-0.522934	5.984474	-0.538274
100	1.745329252	5.908846518	-1.041889	5.916068	-1.072451
105	1.832595715	5.795554958	-1.552914	5.802638	-1.598466
110	1.919862177	5.638155725	-2.052121	5.645047	-2.112316
115	2.00712864	5.437846722	-2.53571	5.444493	-2.61009
120	2.094395102	5.196152423	-3	5.202503	-3.088
125	2.181661565	4.914912266	-3.441459	4.920919	-3.542408
130	2.268928028	4.596266659	-3.856726	4.601884	-3.969856
135	2.35619449	4.242640687	-4.242641	4.247826	-4.367091
140	2.443460953	3.856725658	-4.596267	3.861439	-4.73109
145	2.530727415	3.441458618	-4.914912	3.445665	-5.059083
150	2.617993878	3	-5.196152	3.003667	-5.348573
155	2.705260341	2.53570957	-5.437847	2.538809	-5.597357
160	2.792526803	2.05212086	-5.638156	2.054629	-5.803542
165	2.879793266	1.552914271	-5.795555	1.554812	-5.965558
170	2.967059728	1.041889066	-5.908847	1.043162	-6.082173
175	3.054326191	0.522934456	-5.977168	0.523574	-6.152498
180	3.141592654	7.35089E-16	-6	7.36E-16	-6.176
185	3.228859116	-0.522934456	-5.977168	-0.52357	-6.152498
190	3.316125579	-1.041889066	-5.908847	-1.04316	-6.082173
195	3.403392041	-1.552914271	-5.795555	-1.55481	-5.965558
200	3.490658504	-2.05212086	-5.638156	-2.05463	-5.803542
205	3.577924967	-2.53570957	-5.437847	-2.53881	-5.597357
210	3.665191429	-3	-5.196152	-3.00367	-5.348573
215	3.752457892	-3.441458618	-4.914912	-3.44566	-5.059083
220	3.839724354	-3.856725658	-4.596267	-3.86144	-4.73109
225	3.926990817	-4.242640687	-4.242641	-4.24783	-4.367091
230	4.01425728	-4.596266659	-3.856726	-4.60188	-3.969856
235	4.101523742	-4.914912266	-3.441459	-4.92092	-3.542408
240	4.188790205	-5.196152423	-3	-5.2025	-3.088
245	4.276056667	-5.437846722	-2.53571	-5.44449	-2.61009
250	4.36332313	-5.638155725	-2.052121	-5.64505	-2.112316
255	4.450589593	-5.795554958	-1.552914	-5.80264	-1.598466
260	4.537856055	-5.908846518	-1.041889	-5.91607	-1.072451
265	4.625122518	-5.977168189	-0.522934	-5.98447	-0.538274
270	4.71238898	-6	-1.1E-15	-6.00733	-1.13E-15
275	4.799655443	-5.977168189	0.5229345	-5.98447	0.5382739
280	4.886921906	-5.908846518	1.0418891	-5.91607	1.0724511
285	4.974188368	-5.795554958	1.5529143	-5.80264	1.5984664
290	5.061454831	-5.638155725	2.0521209	-5.64505	2.1123164
295	5.148721293	-5.437846722	2.5357096	-5.44449	2.6100904
300	5.235987756	-5.196152423	3	-5.2025	3.088
305	5.323254219	-4.914912266	3.4414586	-4.92092	3.5424081
310	5.410520681	-4.596266659	3.8567257	-4.60188	3.9698563
315	5.497787144	-4.242640687	4.2426407	-4.24783	4.3670915
320	5.585053606	-3.856725658	4.5962667	-3.86144	4.7310905
325	5.672320069	-3.441458618	4.9149123	-3.44566	5.059083
330	5.759586532	-3	5.1961524	-3.00367	5.3485729
335	5.846852994	-2.53570957	5.4378467	-2.53881	5.5973569
340	5.934119457	-2.05212086	5.6381557	-2.05463	5.8035416
345	6.021385919	-1.552914271	5.795555	-1.55481	5.9655579
350	6.108652382	-1.041889066	5.9088465	-1.04316	6.0821727
355	6.195918845	-0.522934456	5.9771682	-0.52357	6.1524985
360	6.283185307	-1.47018E-15	6	-1.5E-15	6.176

Riemman Sum Calculation for original hole area			
Y	X1	X2	original Area
0.02283181	0	0.522934456	0.00596977
0.06832167	0.52293446	1.041889066	0.053455679
0.11329156	1.04188907	1.552914271	0.146984659
0.15739923	1.55291427	2.05212086	0.283714882
0.200309	2.05212086	2.53570957	0.459491869
0.2416943	2.53570957	3	0.668974723
0.28124016	3	3.441458618	0.905798416
0.31864561	3.44145862	3.856725658	1.162767179
0.35362597	3.85672566	4.242640687	1.432073147
0.38591503	4.24264069	4.596266659	1.705533592
0.41526704	4.59626666	4.914912266	1.974839559
0.44145862	4.91491227	5.196152423	2.231808322
0.46429043	5.19615242	5.437846722	2.468632015
0.48358871	5.43784672	5.638155725	2.67811487
0.49920659	5.63815572	5.795554958	2.853891857
0.5110252	5.79555496	5.908846518	2.99062208
0.51895461	5.90884652	5.977168189	3.08415106
0.52293446	5.97716819	6	3.131636968
0.52293446	6	5.977168189	3.131636968
0.51895461	5.97716819	5.908846518	3.08415106
0.5110252	5.90884652	5.795554958	2.99062208
0.49920659	5.79555496	5.638155725	2.853891857
0.48358871	5.63815572	5.437846722	2.67811487
0.46429043	5.43784672	5.196152423	2.468632015
0.44145862	5.19615242	4.914912266	2.231808322
0.41526704	4.91491227	4.596266659	1.974839559
0.38591503	4.59626666	4.242640687	1.705533592
0.35362597	4.24264069	3.856725658	1.432073147
0.31864561	3.85672566	3.441458618	1.162767179
0.28124016	3.44145862	3	0.905798416
0.2416943	3	2.53570957	0.668974723
0.200309	2.53570957	2.05212086	0.459491869
0.15739923	2.05212086	1.552914271	0.283714882
0.11329156	1.55291427	1.041889066	0.146984659
0.06832167	1.04188907	0.522934456	0.053455679
0.02283181	0.52293446	7.35089E-16	0.00596977
0.02283181	7.3509E-16	0.522934456	0.00596977
0.06832167	0.52293446	1.041889066	0.053455679
0.11329156	1.04188907	1.552914271	0.146984659
0.15739923	1.55291427	2.05212086	0.283714882
0.200309	2.05212086	2.53570957	0.459491869
0.2416943	2.53570957	3	0.668974723
0.28124016	3	3.441458618	0.905798416
0.31864561	3.44145862	3.856725658	1.162767179
0.35362597	3.85672566	4.242640687	1.432073147
0.38591503	4.24264069	4.596266659	1.705533592
0.41526704	4.59626666	4.914912266	1.974839559
0.44145862	4.91491227	5.196152423	2.231808322
0.46429043	5.19615242	5.437846722	2.468632015
0.48358871	5.43784672	5.638155725	2.67811487
0.49920659	5.63815572	5.795554958	2.853891857
0.5110252	5.79555496	5.908846518	2.99062208
0.51895461	5.90884652	5.977168189	3.08415106
0.52293446	5.97716819	6	3.131636968
0.52293446	6	5.977168189	3.131636968
0.51895461	5.97716819	5.908846518	3.08415106
0.5110252	5.90884652	5.795554958	2.99062208
0.49920659	5.79555496	5.638155725	2.853891857
0.48358871	5.63815572	5.437846722	2.67811487
0.46429043	5.43784672	5.196152423	2.468632015
0.44145862	5.19615242	4.914912266	2.231808322
0.41526704	4.91491227	4.596266659	1.974839559
0.38591503	4.59626666	4.242640687	1.705533592
0.35362597	4.24264069	3.856725658	1.432073147
0.31864561	3.85672566	3.441458618	1.162767179
0.28124016	3.44145862	3	0.905798416
0.2416943	3	2.53570957	0.668974723
0.200309	2.53570957	2.05212086	0.459491869
0.15739923	2.05212086	1.552914271	0.283714882
0.11329156	1.55291427	1.041889066	0.146984659
0.06832167	1.04188907	0.522934456	0.053455679
0.02283181	0.52293446	1.47018E-15	0.00596977
6	1.4702E-15	0	4.41053E-15
		Estimated original Area	112.9538426
		Actual Area	113.0973355
		%error	0.001268756

Riemman Sum Calculation for deformed hole area			
Y	X1	X2	Deformed Area
0.02350154	0	0.523573599	0.006152394
0.07032577	0.5235736	1.043162486	0.055090963
0.11661478	1.04316249	1.554812277	0.151481127
0.16201628	1.55481228	2.054629008	0.29239412
0.20618473	2.05462901	2.538808771	0.473548372
0.248784	2.53880877	3.003666667	0.689439602
0.28948987	3.00366667	3.445664845	0.933508065
0.32799254	3.44566485	3.861439434	1.198337864
0.363999	3.86143943	4.247826137	1.47588228
0.3972352	4.24782614	4.601884318	1.757708265
0.42744821	4.60188432	4.920919381	2.035252681
0.45440807	4.92091938	5.202503276	2.30008248
0.47790962	5.20250328	5.444492979	2.544150943
0.49777398	5.44449298	5.645046804	2.760042173
0.51384998	5.6450468	5.802638414	2.941196425
0.52601528	5.80263841	5.916068442	3.082109418
0.53417728	5.91606844	5.984473616	3.178499582
0.53827387	5.98447362	6.007333333	3.227438151
0.53827387	6.00733333	5.984473616	3.227438151
0.53417728	5.98447362	5.916068442	3.178499582
0.52601528	5.91606844	5.802638414	3.082109418
0.51384998	5.80263841	5.645046804	2.941196425
0.49777398	5.6450468	5.444492979	2.760042173
0.47790962	5.44449298	5.202503276	2.544150943
0.45440807	5.20250328	4.920919381	2.30008248
0.42744821	4.92091938	4.601884318	2.035252681
0.3972352	4.60188432	4.247826137	1.757708265
0.363999	4.24782614	3.861439434	1.47588228
0.32799254	3.86143943	3.445664845	1.198337864
0.28948987	3.44566485	3.003666667	0.933508065
0.248784	3.00366667	2.538808771	0.689439602
0.20618473	2.53880877	2.054629008	0.473548372
0.16201628	2.05462901	1.554812277	0.29239412
0.11661478	1.55481228	1.043162486	0.151481127
0.07032577	1.04316249	0.523573599	0.055090963
0.02350154	0.5235736	7.35988E-16	0.006152394
0.02350154	7.3599E-16	0.523573599	0.006152394
0.07032577	0.5235736	1.043162486	0.055090963
0.11661478	1.04316249	1.554812277	0.151481127
0.16201628	1.55481228	2.054629008	0.29239412
0.20618473	2.05462901	2.538808771	0.473548372
0.248784	2.53880877	3.003666667	0.689439602
0.28948987	3.00366667	3.445664845	0.933508065
0.32799254	3.44566485	3.861439434	1.198337864
0.363999	3.86143943	4.247826137	1.47588228
0.3972352	4.24782614	4.601884318	1.757708265
0.42744821	4.60188432	4.920919381	2.035252681
0.45440807	4.92091938	5.202503276	2.30008248
0.47790962	5.20250328	5.444492979	2.544150943
0.49777398	5.44449298	5.645046804	2.760042173
0.51384998	5.6450468	5.802638414	2.941196425
0.52601528	5.80263841	5.916068442	3.082109418
0.53417728	5.91606844	5.984473616	3.178499582
0.53827387	5.98447362	6.007333333	3.227438151
0.53827387	6.00733333	5.984473616	3.227438151
0.53417728	5.98447362	5.916068442	3.178499582
0.52601528	5.91606844	5.802638414	3.082109418
0.51384998	5.80263841	5.645046804	2.941196425
0.49777398	5.6450468	5.444492979	2.760042173
0.47790962	5.44449298	5.202503276	2.544150943
0.45440807	5.20250328	4.920919381	2.30008248
0.42744821	4.92091938	4.601884318	2.035252681
0.3972352	4.60188432	4.247826137	1.757708265
0.363999	4.24782614	3.861439434	1.47588228
0.32799254	3.86143943	3.445664845	1.198337864
0.28948987	3.44566485	3.003666667	0.933508065
0.248784	3.00366667	2.538808771	0.689439602
0.20618473	2.53880877	2.054629008	0.473548372
0.16201628	2.05462901	1.554812277	0.29239412
0.11661478	1.55481228	1.043162486	0.151481127
0.07032577	1.04316249	0.523573599	0.055090963
0.02350154	0.5235736	1.47198E-15	0.006152394
6.176	1.472E-15	0	4.54546E-15
		Estimated deformed Area	116.4092596
		Actual Area	116.5571422
		Calculated Area of ellipse	116.5571422
		% error	0.001268756

D3. Mathematical Model For The 8mm Hole

		Original		Deformed	
Degrees	radians	Rx	Ry	Rx	Ry
0	0	0	8	0	8.23466667
5	0.08726646	0.69724594	7.96955758	0.69809813	8.20333127
10	0.17453293	1.38918542	7.87846202	1.39088331	8.10956358
15	0.26179939	2.07055236	7.72740661	2.07308304	7.9540772
20	0.34906585	2.73616115	7.51754097	2.73950534	7.7380555
25	0.43633231	3.38094609	7.2504623	3.38507836	7.46314252
30	0.52359878	4	6.92820323	4.00488889	7.13143053
35	0.61086524	4.58861149	6.55321635	4.59421979	6.74544403
40	0.6981317	5.14230088	6.12835554	5.14858591	6.30812064
45	0.78539816	5.65685425	5.65685425	5.66376818	5.82278864
50	0.87266463	6.12835554	5.14230088	6.13584576	5.2931417
55	0.95993109	6.55321635	4.58861149	6.56122584	4.72321076
60	1.04719755	6.92820323	4	6.93667103	4.11733333
65	1.13446401	7.2504623	3.38094609	7.25932397	3.48012051
70	1.22173048	7.51754097	2.73616115	7.52672907	2.81642187
75	1.30899694	7.72740661	2.07055236	7.73685122	2.13128856
80	1.3962634	7.87846202	1.38918542	7.88809126	1.42993486
85	1.48352986	7.96955758	0.69724594	7.97929816	0.71769849
90	1.57079633	8	4.9006E-16	8.00977778	5.0443E-16
95	1.65806279	7.96955758	-0.6972459	7.97929816	-0.7176985
100	1.74532925	7.87846202	-1.3891854	7.88809126	-1.4299349
105	1.83259571	7.72740661	-2.0705524	7.73685122	-2.1312886
110	1.91986218	7.51754097	-2.7361611	7.52672907	-2.8164219
115	2.00712864	7.2504623	-3.3809461	7.25932397	-3.4801205
120	2.0943951	6.92820323	-4	6.93667103	-4.1173333
125	2.18166156	6.55321635	-4.5886115	6.56122584	-4.7232108
130	2.26892803	6.12835554	-5.1423009	6.13584576	-5.2931417
135	2.35619449	5.65685425	-5.6568542	5.66376818	-5.8227886
140	2.44346095	5.14230088	-6.1283555	5.14858591	-6.3081206
145	2.53072742	4.58861149	-6.5532164	4.59421979	-6.745444
150	2.61799388	4	-6.9282032	4.00488889	-7.1314305
155	2.70526034	3.38094609	-7.2504623	3.38507836	-7.4631425
160	2.7925268	2.73616115	-7.517541	2.73950534	-7.7380555
165	2.87979327	2.07055236	-7.7274066	2.07308304	-7.9540772
170	2.96705973	1.38918542	-7.878462	1.39088331	-8.1095636
175	3.05432619	0.69724594	-7.9695576	0.69809813	-8.2033313
180	3.14159265	9.8012E-16	-8	9.8132E-16	-8.2346667
185	3.22885912	-0.6972459	-7.9695576	-0.6980981	-8.2033313
190	3.31612558	-1.3891854	-7.878462	-1.3908833	-8.1095636
195	3.40339204	-2.0705524	-7.7274066	-2.073083	-7.9540772
200	3.4906585	-2.7361611	-7.517541	-2.7395053	-7.7380555
205	3.57792497	-3.3809461	-7.2504623	-3.3850784	-7.4631425
210	3.66519143	-4	-6.9282032	-4.0048889	-7.1314305
215	3.75245789	-4.5886115	-6.5532164	-4.5942198	-6.745444
220	3.83972435	-5.1423009	-6.1283555	-5.1485859	-6.3081206
225	3.92699082	-5.6568542	-5.6568542	-5.6637682	-5.8227886
230	4.01425728	-6.1283555	-5.1423009	-6.1358458	-5.2931417
235	4.10152374	-6.5532164	-4.5886115	-6.5612258	-4.7232108
240	4.1887902	-6.9282032	-4	-6.936671	-4.1173333
245	4.27605667	-7.2504623	-3.3809461	-7.259324	-3.4801205
250	4.36332313	-7.517541	-2.7361611	-7.5267291	-2.8164219
255	4.45058959	-7.7274066	-2.0705524	-7.7368512	-2.1312886
260	4.53785606	-7.878462	-1.3891854	-7.8880913	-1.4299349
265	4.62512252	-7.9695576	-0.6972459	-7.9792982	-0.7176985
270	4.71238898	-8	-1.47E-15	-8.0097778	-1.513E-15
275	4.79965544	-7.9695576	0.69724594	-7.9792982	0.71769849
280	4.88692191	-7.878462	1.38918542	-7.8880913	1.42993486
285	4.97418837	-7.7274066	2.07055236	-7.7368512	2.13128856
290	5.06145483	-7.517541	2.73616115	-7.5267291	2.81642187
295	5.14872129	-7.2504623	3.38094609	-7.259324	3.48012051
300	5.23598776	-6.9282032	4	-6.936671	4.11733333
305	5.32325422	-6.5532164	4.58861149	-6.5612258	4.72321076
310	5.41052068	-6.1283555	5.14230088	-6.1358458	5.2931417
315	5.49778714	-5.6568542	5.65685425	-5.6637682	5.82278864
320	5.58505361	-5.1423009	6.12835554	-5.1485859	6.30812064
325	5.67232007	-4.5886115	6.55321635	-4.5942198	6.74544403
330	5.75958653	-4	6.92820323	-4.0048889	7.13143053
335	5.84685299	-3.3809461	7.2504623	-3.3850784	7.46314252
340	5.93411946	-2.7361611	7.51754097	-2.7395053	7.7380555
345	6.02138592	-2.0705524	7.72740661	-2.073083	7.9540772
350	6.10865238	-1.3891854	7.87846202	-1.3908833	8.10956358
355	6.19591884	-0.6972459	7.96955758	-0.6980981	8.20333127
360	6.28318531	-1.96E-15	8	-1.963E-15	8.23466667

Riemman Sum Calculation for original hole area			
Y	X1	X2	original Area
0.03044242	0	0.697245942	0.010612925
0.09109556	0.69724594	1.389185421	0.095032317
0.15105541	1.38918542	2.070552361	0.261306061
0.20986564	2.07055236	2.736161147	0.504382013
0.26707867	2.73616115	3.380946094	0.816874433
0.32225907	3.38094609	4	1.189288397
0.37498688	4	4.588611491	1.610308296
0.42486081	4.58861149	5.142300877	2.067141652
0.4715013	5.14230088	5.656854249	2.545907816
0.51455337	5.65685425	6.128355545	3.03205972
0.55368939	6.12835554	6.553216354	3.510825884
0.58861149	6.55321635	6.92820323	3.96765924
0.61905391	6.92820323	7.250462296	4.388679139
0.64478495	7.2504623	7.517540966	4.761093103
0.66560879	7.51754097	7.72740661	5.073585523
0.68136694	7.72740661	7.878462024	5.316661475
0.69193948	7.87846202	7.969557585	5.482935218
0.69724594	7.96955758	8	5.567354611
0.69724594	8	7.969557585	5.567354611
0.69193948	7.96955758	7.878462024	5.482935218
0.68136694	7.87846202	7.72740661	5.316661475
0.66560879	7.72740661	7.517540966	5.073585523
0.64478495	7.51754097	7.250462296	4.761093103
0.61905391	7.2504623	6.92820323	4.388679139
0.58861149	6.92820323	6.553216354	3.96765924
0.55368939	6.55321635	6.128355545	3.510825884
0.51455337	6.12835554	5.656854249	3.03205972
0.4715013	5.65685425	5.142300877	2.545907816
0.42486081	5.14230088	4.588611491	2.067141652
0.37498688	4.58861149	4	1.610308296
0.32225907	4	3.380946094	1.189288397
0.26707867	3.38094609	2.736161147	0.816874433
0.20986564	2.73616115	2.070552361	0.504382013
0.15105541	2.07055236	1.389185421	0.261306061
0.09109556	1.38918542	0.697245942	0.095032317
0.03044242	0.69724594	9.80119E-16	0.010612925
0.03044242	9.8012E-16	0.697245942	0.010612925
0.09109556	0.69724594	1.389185421	0.095032317
0.15105541	1.38918542	2.070552361	0.261306061
0.20986564	2.07055236	2.736161147	0.504382013
0.26707867	2.73616115	3.380946094	0.816874433
0.32225907	3.38094609	4	1.189288397
0.37498688	4	4.588611491	1.610308296
0.42486081	4.58861149	5.142300877	2.067141652
0.4715013	5.14230088	5.656854249	2.545907816
0.51455337	5.65685425	6.128355545	3.03205972
0.55368939	6.12835554	6.553216354	3.510825884
0.58861149	6.55321635	6.92820323	3.96765924
0.61905391	6.92820323	7.250462296	4.388679139
0.64478495	7.2504623	7.517540966	4.761093103
0.66560879	7.51754097	7.72740661	5.073585523
0.68136694	7.72740661	7.878462024	5.316661475
0.69193948	7.87846202	7.969557585	5.482935218
0.69724594	7.96955758	8	5.567354611
0.69724594	8	7.969557585	5.567354611
0.69193948	7.96955758	7.878462024	5.482935218
0.68136694	7.87846202	7.72740661	5.316661475
0.66560879	7.72740661	7.517540966	5.073585523
0.64478495	7.51754097	7.250462296	4.761093103
0.61905391	7.2504623	6.92820323	4.388679139
0.58861149	6.92820323	6.553216354	3.96765924
0.55368939	6.55321635	6.128355545	3.510825884
0.51455337	6.12835554	5.656854249	3.03205972
0.4715013	5.65685425	5.142300877	2.545907816
0.42486081	5.14230088	4.588611491	2.067141652
0.37498688	4.58861149	4	1.610308296
0.32225907	4	3.380946094	1.189288397
0.26707867	3.38094609	2.736161147	0.816874433
0.20986564	2.73616115	2.070552361	0.504382013
0.15105541	2.07055236	1.389185421	0.261306061
0.09109556	1.38918542	0.697245942	0.095032317
0.03044242	0.69724594	1.96024E-15	0.010612925
8	1.9602E-15	0	7.84095E-15
		Estimated original Area	200.8068313
		Actual Area	201.0619298
		%error	0.001268756

Riemman Sum Calculation for deformed hole area			
Y	X1	X2	Deformed Area
0.03133539	0	0.698098131	0.01093759
0.0937677	0.69809813	1.390883315	0.09793949
0.15548637	1.39088331	2.073083036	0.269299781
0.2160217	2.07308304	2.739505344	0.519811769
0.27491298	2.73950534	3.385078361	0.841863772
0.331712	3.38507836	4.004888889	1.225670403
0.38598649	4.00488889	4.594219794	1.659569893
0.43732339	4.59421979	5.148585912	2.130378425
0.485332	5.14858591	5.663768182	2.623790719
0.52964694	5.66376818	6.135845757	3.124814694
0.56993094	6.13584576	6.561225841	3.618226988
0.60587743	6.56122584	6.936671034	4.08903552
0.63721282	6.93667103	7.259323972	4.52293501
0.66369864	7.25932397	7.526729072	4.906741642
0.68513331	7.52672907	7.736851218	5.228793645
0.7013537	7.73685122	7.888091255	5.479305632
0.71223637	7.88809126	7.979298155	5.650665924
0.71769849	7.97929816	8.009777778	5.737667824
0.71769849	8.00977778	7.979298155	5.737667824
0.71223637	7.97929816	7.888091255	5.650665924
0.7013537	7.88809126	7.736851218	5.479305632
0.68513331	7.73685122	7.526729072	5.228793645
0.66369864	7.52672907	7.259323972	4.906741642
0.63721282	7.25932397	6.936671034	4.52293501
0.60587743	6.93667103	6.561225841	4.08903552
0.56993094	6.56122584	6.135845757	3.618226988
0.52964694	6.13584576	5.663768182	3.124814694
0.485332	5.66376818	5.148585912	2.623790719
0.43732339	5.14858591	4.594219794	2.130378425
0.38598649	4.59421979	4.004888889	1.659569893
0.331712	4.00488889	3.385078361	1.225670403
0.27491298	3.38507836	2.739505344	0.841863772
0.2160217	2.73950534	2.073083036	0.519811769
0.15548637	2.07308304	1.390883315	0.269299781
0.0937677	1.39088331	0.698098131	0.09793949
0.03133539	0.69809813	9.81317E-16	0.01093759
0.03133539	9.8132E-16	0.698098131	0.01093759
0.0937677	0.69809813	1.390883315	0.09793949
0.15548637	1.39088331	2.073083036	0.269299781
0.2160217	2.07308304	2.739505344	0.519811769
0.27491298	2.73950534	3.385078361	0.841863772
0.331712	3.38507836	4.004888889	1.225670403
0.38598649	4.00488889	4.594219794	1.659569893
0.43732339	4.59421979	5.148585912	2.130378425
0.485332	5.14858591	5.663768182	2.623790719
0.52964694	5.66376818	6.135845757	3.124814694
0.56993094	6.13584576	6.561225841	3.618226988
0.60587743	6.56122584	6.936671034	4.08903552
0.63721282	6.93667103	7.259323972	4.52293501
0.66369864	7.25932397	7.526729072	4.906741642
0.68513331	7.52672907	7.736851218	5.228793645
0.7013537	7.73685122	7.888091255	5.479305632
0.71223637	7.88809126	7.979298155	5.650665924
0.71769849	7.97929816	8.009777778	5.737667824
0.71769849	8.00977778	7.979298155	5.737667824
0.71223637	7.97929816	7.888091255	5.650665924
0.7013537	7.88809126	7.736851218	5.479305632
0.68513331	7.73685122	7.526729072	5.228793645
0.66369864	7.52672907	7.259323972	4.906741642
0.63721282	7.25932397	6.936671034	4.52293501
0.60587743	6.93667103	6.561225841	4.08903552
0.56993094	6.56122584	6.135845757	3.618226988
0.52964694	6.13584576	5.663768182	3.124814694
0.485332	5.66376818	5.148585912	2.623790719
0.43732339	5.14858591	4.594219794	2.130378425
0.38598649	4.59421979	4.004888889	1.659569893
0.331712	4.00488889	3.385078361	1.225670403
0.27491298	3.38507836	2.739505344	0.841863772
0.2160217	2.73950534	2.073083036	0.519811769
0.15548637	2.07308304	1.390883315	0.269299781
0.0937677	1.39088331	0.698098131	0.09793949
0.03133539	0.69809813	1.96263E-15	0.01093759
8.23466667	1.9626E-15	0	8.08082E-15
		Estimated deformed Area	206.9497949
		Actual Area	207.2126972
		Calculated Area of ellipse	207.2126972
		% error	0.001268756